NASA
Technical
Paper
1962

March 1982

Static Internal Performance of Single Expansion-Ramp Nozzles With Thrust Vectoring and Reversing

Richard J. Re
and Bobby L. Berrier

NASA

NASA Technical Paper 1962

1982

Static Internal Performance of Single Expansion-Ramp Nozzles With Thrust Vectoring and Reversing

Richard J. Re
and Bobby L. Berrier
Langley Research Center
Hampton, Virginia

NASA
National Aeronautics
and Space Administration

Scientific and Technical Information Branch

SUMMARY

An investigation has been conducted at static conditions (wind off) in the static-test facility of the Langley 16-Foot Transonic Tunnel. The effects of geometric design parameters on the internal performance of nonaxisymmetric single expansion-ramp nozzles were investigated at nozzle pressure ratios up to approximately 10. Forward-flight (cruise), vectored-thrust, and reversed-thrust nozzle operating modes were investigated.

The results of this investigation indicate that single expansion-ramp nozzle peak (on design) performance is not as high as peak performance for comparable nonaxisymmetric convergent-divergent nozzles. However, at off-design nozzle pressure ratios, single expansion-ramp nozzle performance is significantly higher than nonaxisymmetric convergent-divergent nozzle performance. Test results also show that a thrust-vectoring concept utilizing upper and lower nozzle flaps was a much more effective flow-turning device than a thrust-vectoring concept utilizing only a single flap near the trailing edge of the upper expansion ramp. All thrust-reverser configurations investigated produced significant levels of reverse thrust, however, only one exhaust-flow blocker position provided a minimal normal-force component of thrust.

INTRODUCTION

Since the advent of the turbojet engine, exhaust nozzles have traditionally been circular in cross section to facilitate integration with the engine. Extensive development of the "round" nozzle concept has resulted in structurally and thermally efficient exhaust systems with high internal performance. However, experimental investigations (refs. 1 to 3) on current twin-engine fighter aircraft have shown that sizable airplane performance penalties are associated with the installation of the exhaust system into the airframe. Most of the external installation penalty, for multiengine aircraft, probably results from the integration of "round" nozzles into a "rectangular" afterbody. (See ref. 4.) These configurations inherently have boattailed "gutter" interfairings or base regions on the afterbody.

Recent studies on twin-engine fighter airplanes (refs. 5 to 13) have identified potential benefits of nonaxisymmetric or two-dimensional nozzles. This nozzle concept is geometrically amenable to improved capability in the areas of improved integration for installed drag reduction; thrust vectoring for maneuver enhancement and short-field take-off and landing (STOL); and thrust reversing for improved agility, ground handling, and reduced landing ground roll. One of the most promising types of nonaxisymmetric nozzles identified in recent years is the single expansion-ramp nozzle (SERN) (refs. 8 and 13 to 23). The SERN was originally developed with a jet deflector to provide high vector angles (up to 110°) for vertical take-off and landing (VTOL) operations (refs. 15 to 18 and 20). However, system studies and wind tunnel tests have shown that the SERN is also competitive with other nozzle types during cruise and combat operating modes (refs. 8, 13, and 21 to 23). If conventional or moderate STOL performance is desired, the jet deflector can be removed from the SERN design to reduce nozzle weight and low vector angles can be achieved by deflection of the nozzle expansion surfaces. Most of the experimental investigations conducted on the SERN have concentrated on quantifying the uninstalled and installed

performance of a specific nozzle design at various nozzle power settings during cruise and vectored-thrust operating modes. These investigations did not include a reverse-thrust operating mode for the SERN. Until now, little effort has been expended on providing parametric data on the geometric variables of internal nozzle design which could lead to improved SERN designs with higher performance and/or lower structural weight. The effect of sidewall geometry on SERN performance is reported in reference 19 and a limited amount of data on the effect of nozzle aspect ratio on SERN performance is contained in reference 21.

This paper presents static internal performance of single expansion-ramp nozzles with geometries representative of cruise, vectored-thrust, and reversed-thrust operating modes. The effects of nozzle expansion ratio, lower-flap length, lower-flap divergence angle, and sidewall cutback on internal performance are presented for the cruise or forward-flight operating mode. Two thrust-vectoring schemes were investigated at design thrust-vector angles from -10° to 20°. The effect of sidewall length is presented at a design thrust-vector angle equal to 20°. For the reverse-thrust operating mode, the effect of exhaust-flow blocker position on thrust and normal force is presented. This investigation was conducted in the static-test facility of the Langley 16-Foot Transonic Tunnel at a Mach number of 0 and at nozzle pressure ratios up to approximately 10.

SYMBOLS AND ABBREVIATION

All forces (with the exception of resultant gross thrust) and angles are referred to the model center line (body axis). A detailed discussion of the data-reduction and calibration procedures as well as definitions of forces, angles, and propulsion relationships used herein can be found in reference 14.

AR	nozzle-throat aspect ratio, w_t/h_t
A_e	nozzle-exit area, cm^2
$(A_e/A_t)_e$	external expansion ratio for fully expanded flow (A_e measured at end of nozzle expansion ramp)
$(A_e/A_t)_i$	internal expansion ratio (A_e measured at end of nozzle lower flap)
A_p	geometric area of reverser-port minimum, cm^2
A_t	nozzle geometric throat area, cm^2
F	measured thrust along body axis, N
F_i	ideal isentropic gross thrust, $w_p\sqrt{RT_{t,j}\left(\frac{2\gamma}{\gamma-1}\right)\left[1-\left(\frac{p_\infty}{p_{t,j}}\right)^{\frac{\gamma-1}{\gamma}}\right]}$, N
F_r	resultant gross thrust, $\sqrt{F^2+N^2}$, N
h_e	nozzle-exit height, cm
h_t	nozzle-throat height, cm
l_f	axial length of nozzle flap, cm

l_{vf}	axial length of upper vectoring flap, cm
N	measured normal force, N
p	local static pressure, Pa
$p_{t,j}$	jet total pressure, Pa
p_∞	ambient pressure, Pa
pt or Pt	point number
R	gas constant, 287.3 J/kg-K
Sta.	model station, cm
$T_{t,j}$	jet total temperature, K
w_i	ideal mass-flow rate, kg/sec
w_p	measured mass-flow rate, kg/sec
w_t	nozzle-throat width, 10.157 cm
x	axial distance measured from nozzle connect station (positive downstream), cm
x_t	length from nozzle connect station to nozzle-throat station, cm
y	lateral distance measured from model center line (positive to left looking upstream), cm
z	vertical distance measured from model center line (positive up), cm
z_e	vertical distance of nozzle-flap trailing edge from model center line (positive up), cm
α	nozzle-flap terminal divergence angle, deg
γ	ratio of specific heats, 1.3997 for air
δ_{static}	resultant thrust-vector angle, $\tan^{-1} \frac{N}{F}$, deg
δ_v	design thrust-vector angle measured from horizontal reference line (positive for downward deflection angles), deg

Subscripts:

e	external
i	internal
l	lower
u	upper

Configuration designations:

SERN	single expansion-ramp nozzle
F1,...,F6	forward-flight (cruise) SERN configurations
VF1(δ_v),VF2(δ_v),VF3(δ_v)	vectored upper-flap SERN configurations where δ_v = Design thrust-vector angle
V1(δ_v),V2(δ_v),V3(δ_v)	vectored upper- and lower-flap SERN configurations where δ_v = Design thrust-vector angle
R1,...,R5	reversed-thrust SERN configurations

APPARATUS AND METHODS

Static-Test Facility

This investigation was conducted in the static-test facility of the Langley 16-Foot Transonic Tunnel. The testing was done in a room with a high ceiling where the jet could exhaust to atmosphere through a large open doorway. This facility utilizes the same clean, dry-air supply as that used in the 16-Foot Transonic Tunnel and a similar air-control system, including valving, filters, and a heat exchanger (to operate the jet flow at constant stagnation temperature). Data were recorded on a 96-channel, magnetic-tape data acquisition system.

Single-Engine Propulsion-Simulation System

A sketch of the single-engine air-powered nacelle model on which various nozzles were mounted is presented in figure 1 with a typical nozzle configuration attached. The body shell forward of station (Sta.) 52.07 was removed for this investigation.

An external high-pressure air system provided a continuous flow of clean, dry air at a controlled temperature of about 300 K. This high-pressure air was varied up to approximately 10 atm (1 atm = 101.3 kPa) and was brought through the dolly-mounted support strut by six tubes which connect to a high-pressure plenum chamber. As shown in figure 1, the air was then discharged perpendicularly into the model low-pressure plenum through eight multiholed sonic nozzles equally spaced around the high-pressure plenum. This method was designed to minimize any forces imposed by the transfer of axial momentum as the air is passed from the nonmetric high-pressure plenum to the metric (mounted to the force balance) low-pressure plenum. Two flexible metal bellows are used as seals and serve to compensate for axial forces caused by pressurization.

The air was then passed from the model low-pressure plenum (circular in cross section) through a transition section, choke plate, and instrumentation section which were common for all nonaxisymmetric nozzles investigated. The transition section provided a smooth flow path for the airflow from the round low-pressure plenum to the rectangular choke plate and instrumentation section. The instrumentation section had a flow-path width-to-height ratio of 1.437 and was identical in geometry to the nozzle airflow entrance. All nozzle configurations were attached to the instrumentation section at model station 104.47.

Nozzle Design

The single expansion-ramp nozzle (SERN) is a nonaxisymmetric, variable-area, internal/external expansion exhaust system. A photograph showing a typical SERN test nozzle installed on the single-engine propulsion-simulation system is shown in figure 2. Basic nozzle components consist of (1) a 2-D variable-geometry convergent-divergent upper-flap assembly used to vary nozzle power setting (throat area), (2) a 2-D variable lower flap used to vary nozzle expansion ratio A_e/A_t, and (3) a 2-D upper external expansion ramp. Note that the throat is forward of the variable lower flap so that the power setting A_t is independent of the lower-flap position or expansion ratio A_e/A_t. Additional details on nozzle operation and construction can be found in references 15 and 16. All test nozzles had a nominally constant exhaust-flow path width of 10.16 cm. Parametric geometry changes were achieved by using interchangeable upper and lower nozzle flaps and sidewalls.

Figure 3 presents sketches showing the geometry of the six cruise or forward-flight SERN configurations tested. Important geometric parameters for these six configurations are summarized in table I. Simulation of a variable lower flap (variable expansion ratio A_e/A_t) at a constant power setting A_t was achieved by testing configurations F1, F2, and F3. The internal expansion ratio $(A_e/A_t)_i$ varied from 1.097 to 1.391 for these configurations. Configurations F4 and F5 were used to study the effect of lower-flap geometry changes and configuration F6 was used to investigate the effect of sidewall cutback. Configurations F2 and F6 have been previously tested and data are reported in reference 19 as configurations SR4 and SR2, respectively.

Two thrust-vectoring concepts for SERN were studied during the current investigation. The first concept incorporates a variable flap in the trailing edge of the 2-D upper external expansion surface. This thrust-vectoring concept results in external turning of the supersonic exhaust stream. Figure 4 presents a sketch showing the geometry of nozzle configuration VF1(δ_v), where δ_v equals the design thrust-vector angle (which was varied from -10° (up) to 20° (down)). It should be noted that the unvectored or cruise nozzle configuration VF1(0) is nozzle configuration F6 shown previously in figure 3. Also shown in figure 4 is the geometry for configurations VF2(20) and VF3(20) which were used to investigate the effect of sidewall length during vectored-thrust operation (δ_v = 20°). The second thrust-vectoring concept incorporates a variable full-length upper expansion surface used in conjunction with the existing variable lower flap. This thrust-vectoring concept results in internal turning of the supersonic exhaust stream. Figure 5 presents a sketch of configuration V1(δ_v) which simulates this thrust-vectoring concept at design thrust-vector angles from -10° to 20°. The unvectored or cruise nozzle configuration V1(0) is again configuration F6 shown previously in figure 3. The geometry for configurations V2(20) and V3(20), which were used to study the effect of sidewall length during vectored-thrust operation, is also shown in figure 5.

Sketches of SERN configurations in reverse-thrust operating modes are shown in figure 6. These configurations simulate a SERN reverse-thrust concept in which the upper expansion ramp forms an exhaust-flow blocker while simultaneously opening a reverse-port exit on the nozzle upper surface. A parametric study of the exhaust-flow blocker position, illustrated by the sketches of figure 6(b), was conducted to determine thrust-reverser efficiency (50-percent reverse thrust suggested as a goal in ref. 14) and potential impact on aircraft stability and control by examining normal force generated by each blocker position. The minimum open area of each port

for each blocker position is shown in figure 6(b). For all blocker positions, the sum of the minimum port areas was greater than the upstream forward-flight (cruise) geometric throat area. The included angle of the blocker face was 88.75° for all configurations. The geometry of the blocker aft of the blocker face is not intended to represent the geometry of actual flight hardware but was designed as shown for ease of static-test hardware fabrication.

Instrumentation

A three-component strain-gage balance was used to measure the forces and moments on the model downstream of station 52.07 cm. (See fig. 1.) Jet total pressure was measured at a fixed station in the instrumentation section (see fig. 1) by means of a four-probe rake through the upper surface, a three-probe rake through the side, and a three-probe rake through the corner. A thermocouple, also located in the instrumentation section, was used to measure jet total temperature. Mass flow of the high-pressure air supplied to the nozzle was determined from pressure and temperature measurements in the high-pressure plenum (see fig. 1) calibrated with standard axisymmetric nozzles. Internal static-pressure orifices were located on the nozzle upper and lower flaps and on the blocker of reverse-thrust configuration R1. Typical internal static-pressure instrumentation is illustrated in the sketches of figure 7. Coordinates of the static-pressure orifices for each configuration are given in table II.

Data Reduction

All data were recorded simultaneously on magnetic tape. Approximately 11 frames of data, taken at a rate of 2 frames per second, were used for each data point; average values were used in computations. Data were recorded in an ascending order of $p_{t,j}$ with several repeat points being recorded as $p_{t,j}$ was decreased from the maximum value obtained. With the exception of resultant gross thrust F_r, all force data in this report are referenced to the model center line.

The basic performance parameter used for the presentation of results is the internal thrust ratio F/F_i, which is the ratio of the actual nozzle thrust (along the body axis) to the ideal nozzle thrust. Actual nozzle thrust was obtained from the balance axial-force measurement corrected for weight tares and balance interactions. Although the bellows arrangement was designed to eliminate pressure and momentum interactions with the balance, small bellows tares on axial, normal, and pitch balance components still exist. These tares result from a small pressure difference between the ends of the bellows when internal velocities are high and also small differences in the forward and aft bellows spring constants when the bellows are pressurized. As discussed in reference 14, these bellows tares were determined by running calibration nozzles with known performance over a range of expected normal forces and pitching moments. The balance data were then corrected in a manner similar to that discussed in reference 14.

RESULTS AND DISCUSSION

Basic Data

Basic data for the SERN configurations investigated are presented in figures 8 to 11. Forward-flight (cruise) nozzle data are presented in figure 8, vectored-

thrust nozzle data are presented in figures 9 and 10, and reversed-thrust data are presented in figure 11. Nozzle internal thrust ratio F/F_i, resultant thrust ratio F_r/F_i, and discharge coefficient w_p/w_i are presented as a function of nozzle pressure ratio $p_{t,j}/p_\infty$ for each configuration investigated.

For single expansion-ramp nozzles, the exhaust-flow expansion process occurs both internally and externally. Internal expansion occurs from the throat up the lower-flap exit. External expansion occurs downstream of the lower-flap exit and between the fixed upper boundary and the free (free stream/exhaust) lower boundary. Thus, performance is influenced by internal and external expansion ratios and is generally characterized by some indication of two performance peaks. Values of the nozzle pressure ratio required for fully expanded flow (design) are listed in the following table for each cruise-nozzle expansion ratio. Generally, for nozzles with

Configuration	$(A_e/A_t)_i$	$(A_e/A_t)_e$	Design $p_{t,j}/p_\infty$
F1	1.097		3.03
		1.407	5.49
F2 and F6	1.215		3.98
		1.510	6.34
F3	1.391		5.39
		1.665	7.65
F4	1.091		2.99
		1.476	6.02
F5	1.389		5.35
		1.558	6.71

internal and external expansion ratios, the first peak occurs near the design pressure ratio corresponding to $(A_e/A_t)_i$ and is lower in magnitude than the second peak, which occurs near the design pressure ratio corresponding to $(A_e/A_t)_e$ (see ref. 19). For the nozzles of the current investigation, the performance peaks are relatively flat over a large range of nozzle pressure ratios when compared to typical convergent-divergent nozzles. As expected, thrust vectoring decreases the internal thrust ratio F/F_i (compare figs. 9 and 10 to fig. 8(f)) since the thrust vector is being turned away from the axial direction and all reverse-thrust configurations produce negative values of internal thrust ratio (see fig. 11).

The resultant thrust ratio, shown by dashed lines in figures 8 to 11, is equal to the internal thrust ratio when the thrust vector is aligned with the thrust or body axis. Significant differences can be noted between the internal and resultant thrust ratios shown in figures 8 to 11, not only for the vectored-thrust SERN but also for the forward-flight (unvectored) configurations shown in figure 8. This effect is caused by changing wave patterns impinging on the expansion surfaces as nozzle pressure ratio varies and the unequal normal projected areas of the upper and lower flaps. Wave patterns (and resulting inclination of the exhaust stream) for underexpanded and overexpanded SERN type nozzles are illustrated in reference 24. Resultant thrust-vector angle characteristics for SERN configurations will be discussed in a later section of this report.

Measured values of discharge coefficient w_p/w_i are, as expected, less than 1.0 for all nozzles tested and, except for the reverse-thrust configurations shown in figure 11, are relatively independent of nozzle pressure ratio above the value for choked flow ($p_{t,j}/p_\infty = 1.89$). Discharge coefficients less than 1.0 are caused by viscous effects (momentum and vena contracta losses) which reduce the amount of flow passing through the throat. Therefore, the sonic-flow area is proportionately less than the geometric throat area A_t by the ratio of measured mass-flow rate to ideal mass-flow rate w_p/w_i. As shown in figure 11, the measured discharge coefficients for the reverse-thrust nozzles are substantially lower (particularly configurations R1, R3, and R4) than those measured for the forward-flight and vectored SERN configurations and are not independent of nozzle pressure ratio. The low values of discharge coefficient indicate a sonic-flow area which is substantially less than the geometric throat area used to compute ideal mass-flow rate w_i. The variation of discharge coefficient with nozzle pressure ratio indicates a change in the sonic-flow area with increasing nozzle pressure ratio. The minimum geometric flow-passage area (throat) for the reverse-thrust configurations occurs at the same location as for the forward-flight and vectored SERN (i.e., the geometric throat area is less than the sum of the upper and lower reverser exit ports (see fig. 6(b)). However, a possible cause for the trends of the discharge coefficient, shown in figure 11, is the formation of separation bubbles on the forward surfaces of the reverser exit ports as the exhaust flow turns through a sharp corner. The existence of separation bubbles at these locations could result in smaller flow areas in the exit ports and cause these configurations to choke in the exit ports rather than at the geometric throat. The size of such separation bubbles would probably be dependent on nozzle pressure ratio.

Internal Static-Pressure Distributions

Internal static-pressure data are presented in tabulated form in tables III, IV, and V for the forward-flight, vectored, and reversed SERN configurations, respectively. Typical internal static-pressure distributions are presented in figures 12 to 15. The effects of expansion ratio and lower-flap length on internal flap static-pressure distributions are shown in figure 12. Pressure distribution levels on both flaps (upper-flap geometry fixed for all configurations shown) appear to be a function of lower-flap divergence angle rather than expansion ratio. Flap static pressure generally decreases with increasing lower-flap divergence angle. Static pressures near the trailing edge of the upper expansion ramp (aft of $x/x_{t,u} \approx 1.4$) on configuration F3 ($\alpha_l = 13.5°$) actually produce a force component in the drag direction as indicated by lower values of $p/p_{t,j}$ than $p_\infty/p_{t,j}$. This fact leads one to expect increasing internal performance with decreasing lower-flap divergence angle. Almost identical pressure distributions were measured on the lower flap for SERN configurations with a lower-flap divergence angle of approximately 4° (configurations F2, F4, and F5) even though the internal expansion ratio varied from 1.091 to 1.389; the expansion ratio for these configurations was set by lower-flap length. Similarly, pressure distributions on the upper expansion ramp were nearly identical for these configurations up to $x/x_{t,u} \approx 1.4$ on the upper flap. Aft of this location, expansion-ramp static pressures for configuration F4 (short lower flap) are lower than those measured on configurations F2 and F5 (longer lower flaps). This trend indicates that internal performance might increase with increasing lower-flap length. The Mach line (nozzle assumed to be operating at the design internal expansion ratio) originating from the short lower-flap trailing edge of configuration F4 intersects the upper expansion ramp at $x/x_{t,u} \approx 1.4$. From the rule of "forbidden

signals" (see ref. 25), the pressure distribution upstream of the Mach line on the upper expansion ramp is a function of internal geometry and flow conditions only; downstream of the Mach line, static pressures on the upper expansion ramp are also a function of external ambient pressure because of the lower free-jet boundary. The Mach line originating from the longer lower-flap lips (configurations F2 and F5) passes downstream of the upper expansion-ramp trailing edge; pressure distributions on the upper expansion ramps of these two configurations are nearly identical except at $x/x_{t,u} = 1.449$.

The effect of the thrust-vector concept on internal static-pressure distributions is presented in figure 13. Thrust vectoring with an aft flap on the upper expansion ramp had no effect on lower-flap static pressures. Static pressures on the upper expansion ramp aft of $x/x_{t,u} = 1.4$ (vector-flap hinge line at $x/x_{t,u} = 1.461$) increase with increasing design thrust-vector angle; positive normal force and negative pitching moment would result from these increased upper-flap static pressures. It should be noted that the upper-flap static-pressure distributions indicate the formation of a shock at the vector-flap hinge line for positive design thrust-vector angles. The use of both the upper and lower flaps for thrust vectoring affects the static-pressure distributions on both flaps (see fig. 13(b)). Increasing the design thrust-vector angle increases the static pressure on the upper expansion ramp upstream of $x/x_{t,u} = 1.4$ and decreases static pressure on the lower flap. From examination of figure 13, one might expect more effective flow turning with the use of a thrust-vectoring concept which utilizes the upper and lower flaps. Figure 14 presents the effect of sidewall length on flap spanwise static-pressure distributions during vectored operation ($\delta_v = 20°$) with deflected upper and lower flaps. For this thrust-vectoring concept, sidewall length generally had little effect on nozzle internal static pressure. At $x/x_{t,u} = 1.250$ on the upper flap, static pressure measured near the extreme edge of the flap indicates possible side venting of the exhaust flow with the cutback sidewall (configuration V2(20)). At $x/x_{t,u} = 1.691$ on the upper flap, there is an unexplained reduction in static pressure near the flap quarter-span $\left(\frac{y}{w_t/2} = 0 = \text{Flap center line}\right)$ with the cutback sidewall configuration. Both of these effects, although small, would tend to reduce normal force and thus reduce the resultant vector angle for the cutback sidewall configuration. Internal static pressures were not measured on sidewall variation configurations VF2(20) and VF3(20) which simulated a thrust-vectoring concept utilizing an aft, upper flap only. The effect of sidewall length on forward-flight SERN performance is reported in reference 19.

The effect of thrust reversing on SERN internal static-pressure distributions is presented in figure 15. Configuration R1 had one of the lowest measured discharge coefficients w_p/w_i (see fig. 11(a)) and configuration R2 had one of the highest measured discharge coefficients (see fig. 11(b)). The flap pressure distributions shown in figure 15 for configuration R1 indicate that the exhaust flow does not choke at the geometric throat ($x/x_{t,u} = x/x_{t,l} = 1.0$). The pressure distribution on the exhaust-flow blocker of configuration R1 shows a rapid decrease in static pressure near the exit of the upper and lower reverser ports; it is probable that the exhaust flow is choked at the reverser port exits on configuration R1. Flap pressure distributions for configuration R2 indicate choked exhaust flow on the upper flap but unchoked flow on the lower flap. Unfortunately, blocker pressures were measured only on configuration R1. In general, the pressure distributions shown in figure 15 support the previous discussion on reverse-thrust SERN discharge coefficient.

Forward-Flight (Cruise) Performance

The effects of expansion ratio (lower-flap position), lower-flap length, and sidewall length on static internal performance of forward-flight SERN configurations were studied during the current investigation. A more detailed study of sidewall containment for SERN configurations is reported in reference 19. Data on configurations F2 and F6 are reported in reference 19 as configurations SR4 and SR2, respectively. Figure 16 presents a comparison of data obtained for configuration F2 during the current investigation with data obtained for the same configuration (SR4) during the investigation reported in reference 19. Except at the highest nozzle pressure ratios investigated, thrust ratio and discharge coefficient data from the two tests agree to within 1/2 percent.

Effect of expansion ratio.- The effect of expansion ratio on static internal performance is presented in figure 17. At nozzle pressure ratios below 7.0, thrust ratio decreases with increasing expansion ratio. Similar to other nozzle types, SERN overexpansion losses are greater at low nozzle pressure ratios for nozzles having large expansion ratios. The results shown in figure 17 at $p_{t,j}/p_\infty = 5.98$ are consistent with the internal pressure distributions shown in figure 12. At nozzle pressure ratios above 7.0, the medium expansion ratio SERN (configuration F2) produced the highest thrust ratio. At nozzle pressure ratios above those tested, the higher expansion ratio SERN configurations (configurations F2 and F3) would be expected to exhibit significantly higher performance than the low expansion ratio SERN (configuration F1) because of smaller underexpansion losses. Figure 18 presents the effect of expansion ratio on resultant thrust-vector angle δ_{static}. As is obvious from the figure, single expansion-ramp nozzles produce significant resultant thrust-vector angles which are dependent on nozzle pressure ratio, even for nozzles designed for unvectored ($\delta_v = 0°$) operation (see refs. 14 and 19). A resultant thrust-vector angle of 0° occurs at only one nozzle pressure ratio for each configuration tested. It can be deduced from the wave patterns shown in reference 24, that this nozzle pressure ratio should correspond closely to the design nozzle pressure ratio for the nozzle external expansion ratio. At all other nozzle pressure ratios, a thrust performance penalty would be associated with the nonzero values of measured resultant thrust-vector angle, since the thrust vector is turned away from the thrust (body) axis. The magnitude of this penalty can be assessed by comparing internal thrust ratios with the resultant thrust ratios shown in figure 8. Thrust losses from 0 to 1.5 percent are shown in figure 8 for the resultant thrust-vector angles shown in figure 18. In addition to the thrust losses discussed above, nonzero values of resultant thrust-vector angle would also cause a thrust induced pitching moment which may have to be trimmed out with aerodynamic control surfaces, or conversely be used to augment aerodynamic control surfaces for airplane trim, depending on the flight conditions. These data suggest a need for integration of a SERN thrust-vectoring mechanism into an integrated flight/propulsion control system to eliminate unwanted resultant thrust-vector angles or to optimize thrust-vector angle for a particular airplane flight condition.

Effect of lower-flap geometry.- Figure 19 presents the effect of lower-flap geometry on SERN static internal performance and figure 20 presents the effect of lower-flap length on resultant thrust-vector angle. Data are shown for two nominally constant internal expansion ratios $(A_e/A_{t,i})$ = 1.1 and 1.39. For a constant internal expansion ratio, increasing lower-flap length (decreasing lower-flap divergence angle) increased the thrust ratio across the nozzle pressure ratio range shown. The effect of lower-flap geometry on resultant thrust-vector angle was generally small.

Effect of sidewall length.- The effect of sidewall length on static internal performance is presented in figure 21 and on resultant thrust-vector angle in figure 22. For the amount of sidewall cutback employed in the current investigation, only small effects on F/F_i and δ_{static} were measured. Consistent with results reported in reference 19, which examined a broader range of sidewall geometry, the nozzle pressure ratio for peak F/F_i tends to shift to a lower value with sidewall cutback. This effect probably results from an effective reduction in external expansion ratio $(A_e/A_t)_e$ when sidewall containment of the exhaust flow is reduced.

Performance comparison with nonaxisymmetric convergent-divergent nozzles.- A comparison of SERN configuration F1, which has high internal performance, with two nonaxisymmetric convergent-divergent nozzles reported in reference 19 (configurations C1 and C9), is presented in figure 23. Unlike the SERN, nonaxisymmetric convergent-divergent nozzles do not have a free-jet boundary and have only one performance peak related to an internal expansion ratio A_e/A_t. Configuration C1 (ref. 19) has an expansion ratio close to the internal expansion ratio $(A_e/A_t)_i$ of SERN configuration F1. Configuration C9 (ref. 19) has an expansion ratio close to the external expansion ratio $(A_e/A_t)_e$ of SERN configuration F1. The data in figure 23 indicate that SERN internal performance is slightly lower, generally less than 1/2 percent, than nonaxisymmetric convergent-divergent nozzle internal performance (with similar expansion ratios), when operating near the design nozzle pressure ratio (2.97 and 5.41 for configurations C1 and C9, respectively). However, at off-design nozzle pressure ratios, the SERN configuration has significantly lower overexpansion losses than configuration C9 (ref. 19) at low nozzle pressure ratios, and significantly lower underexpansion losses than configuration C1 (ref. 19) at high nozzle pressure ratios. These data indicate that single expansion-ramp nozzles have high static internal performance over a broader range of operating nozzle pressure ratios than comparable nonaxisymmetric convergent-divergent nozzles. This result suggests that one might consider the use of a fixed SERN or one with limited variable geometry in place of a variable-geometry convergent-divergent nozzle in order to reduce weight and provide simplicity. For example, if one considers the nonaxisymmetric convergent-divergent nozzle configurations shown in figure 23 to represent a variable-geometry nozzle design with an expansion ratio range from 1.089 to 1.397 (performance envelope obtained by fairing a line between two performance peaks), and the SERN configuration to represent a fixed-geometry nozzle design, it is apparent that SERN performance is only 0.2 to 1.6 percent lower than the convergent-divergent nozzle performance throughout the nozzle pressure ratio range. This performance penalty could be traded for simplicity and reduced weight.

Vectored-Thrust Performance

Aft-flap thrust vectoring.- The effect on thrust ratio of thrust vectoring by deflection of an upper, aft flap on the SERN expansion ramp is presented in figure 24. As expected, the highest internal performance was obtained on the unvectored ($\delta_v = 0°$) or forward-flight SERN configuration. Thrust ratio was decreased by either negative or positive flap deflections (positive deflection defined as trailing edge down in order to produce positive thrust-vector component in the normal-force direction). The loss in thrust ratio during vectored-thrust operation results from two sources. First, during vectored-thrust operation, the thrust vector is turned away from the body or thrust axis. This loss is merely a trigonometric function of the resultant thrust-vector angle. An appreciation of the magnitude of this loss can be

obtained by comparing thrust ratio with the resultant thrust-ratio data in figure 9. The second source for thrust loss during vectored-thrust operation is exhaust-flow turning losses. For negative flap deflections, turning losses result from flow separation and/or lower pressures on the flap. For positive flap deflections, turning losses result from a shock originating at the flap hinge line. An appreciation of the magnitude of this loss can be obtained by comparing the resultant thrust-ratio data in figures 9(c) and 9(d) with resultant thrust-ratio data for the unvectored ($\delta_v = 0°$) configuration F6 in figure 8(f). The effect of design thrust-vector angle on resultant thrust-vector angle is shown in figure 25. As expected, resultant thrust-vector angle increases with increasing design thrust-vector angle.

Upper- and lower-flap thrust vectoring.- Figures 26 and 27 present the effect of upper- and lower-flap thrust vectoring (deflection) on thrust ratio and resultant thrust-vector angle, respectively. The data trends for this thrust-vectoring concept are similar to those discussed previously for the upper, aft-flap thrust-vectoring concept. However, a comparison of the vectored resultant thrust ratios shown in figure 10 with the unvectored (configurations V1(0) and F6 are identical) resultant thrust ratios shown in figure 8(f) indicates that most of the thrust ratio loss during vectored operation for this concept (upper- and lower-flap deflection) results from turning the thrust vector away from the thrust axis; exhaust-flow turning losses with this vectoring concept are small. The difference in exhaust-flow turning losses between the two thrust-vectoring concepts is indicated by comparison of the resultant thrust ratios for each vectored concept (compare fig. 9 with fig. 10).

Effect of sidewall length on vectored-thrust performance.- The effect of sidewall length on nozzle internal performance and resultant thrust-vector angle during vectored-thrust operation ($\delta_v = 20°$) is presented in figures 28 and 29, respectively. Results on both thrust-vectoring concepts are shown. Sidewall length generally had only a small effect (less than 1 percent over the nozzle pressure-ratio range tested) on thrust ratio for either thrust-vectoring concept (see fig. 28). At nozzle pressure ratios greater than 4.0, the cutback-sidewall nozzles generally produced the highest thrust ratios and the extended-sidewall nozzles generally produced the lowest thrust ratios. However, an examination of the resultant thrust ratios shown in figures 9(e) and 10(c) indicates that the highest resultant thrust ratios are obtained with the baseline and extended-sidewall nozzles. These trends could only occur if the longer-sidewall nozzles produced higher values of resultant thrust-vector angle. This result, an increase in resultant thrust-vector angle with increasing sidewall length, is clearly indicated in figure 29, particularly for the aft, upper-flap thrust-vectoring concept. This trend on the upper- and lower-flap thrust-vectoring concept was indicated by the internal static-pressure distributions shown in figure 14 and discussed previously. Thus, although higher values of thrust ratio can be obtained with cutback sidewalls at a given value of design thrust-vector angle, a lower resultant thrust-vector angle (and thus normal force or lift) is also obtained. To achieve a given level of resultant thrust-vector angle with cutback sidewalls, a larger value of geometric vector angle must be used and, as discussed previously, large thrust-ratio losses will occur.

Effect of thrust-vectoring concept.- A comparison of thrust ratio and resultant thrust ratio for the two thrust-vectoring concepts investigated is presented in figure 30. Comparisons are made at constant design thrust-vector angles of -10° (up) and 20° (down). As expected, large losses in axial thrust (see fig. 30(a)) occur at both negative and positive values of design thrust-vector angle since the thrust vector is turned away from the thrust (body) axis during vectored-thrust operation. Resultant thrust-ratio data (see fig. 30(b)) indicate that most of the axial thrust loss for the upper- and lower-flap thrust-vectoring concept results from this

effect. For the upper- and lower-flap thrust-vectoring concept, the resultant thrust ratio during vectored operation (configurations V1(-10) and V1(20)) is generally within 1 percent of the unvectored (configuration V1(0)) resultant thrust ratio, thus indicating only small internal thrust losses associated with turning the exhaust flow. Larger internal thrust losses, particularly at $\delta_v = 20°$, are indicated by the resultant thrust ratios for the upper, aft-flap thrust-vectoring concept. For example, at $\delta_v = 20°$ and $p_{t,j}/p_\infty = 5$, the upper, aft-flap thrust-vectoring concept suffers a 5-percent internal thrust loss as compared to an 0.8-percent internal thrust loss for the upper- and lower-flap thrust-vectoring concept. The large thrust loss for the upper, aft-flap thrust-vectoring concept at positive design thrust-vector angles is probably caused by a shock which originates at the flap hinge line and causes static-pressure changes on the aft flap.

Figure 31 presents a comparison at constant design thrust-vector angles of resultant thrust-vector angle as a function of nozzle pressure ratio for the two thrust-vectoring concepts investigated. Figure 32 presents a similar comparison at constant nozzle pressure ratios for varying design thrust-vector angle. Data shown in both figures indicate that the upper- and lower-flap thrust-vectoring concept is a much more effective flow-turning device at both positive and negative design thrust-vector angles than the upper, aft-flap thrust-vectoring concept. This result was also indicated by the pressure distributions shown in figure 13. At $\delta_v = 20°$, the upper aft-flap thrust-vectoring concept never realizes the design goal of a 20° resultant thrust-vector angle for the nozzle pressure ratio range tested. The data of figure 32 can be used to indicate the design thrust-vector angle required by each thrust-vectoring concept to produce a desired resultant thrust-vector angle. For example, at $p_{t,j}/p_\infty = 6.0$, a design thrust-vector angle of 20° is required by the upper, aft-flap thrust-vectoring concept to produce the same resultant thrust-vector angle (11°) as a design thrust-vector angle of 11° for the upper- and lower-flap thrust-vectoring concept. These design thrust-vector angles would produce a thrust ratio of 0.974 (see fig. 10(b)) for the upper- and lower-flap thrust-vectoring concept and a thrust ratio of 0.940 (see fig. 30(a)) for the upper, aft-flap thrust-vectoring concept at $p_{t,j}/p_\infty = 6.0$. Thus, the upper, aft-flap thrust-vectoring concept would suffer a 3.4-percent axial thrust loss to achieve the same resultant thrust-vector angle as the upper- and lower-flap thrust-vectoring concept at the test conditions cited.

Effect of a programmed vector flap.- As discussed previously, a thrust penalty would be associated with the nonzero values of resultant thrust-vector angle measured on the forward-flight nozzle configurations. If a thrust-vectoring concept is included as part of the SERN design, it can be used in conjunction with a flight computer to eliminate or null nonzero values of resultant thrust-vector angle during cruise flight. Figure 33 presents a comparison of design thrust-vector angle, resultant thrust-vector angle, and thrust ratio for SERN cruise configuration F6 (or VF1(0)) with a fixed ($\delta_v = 0°$) vector flap and with a variable vector flap programmed to null out nonzero resultant thrust-vector angles. The upper, aft-flap thrust-vectoring concept was selected for this comparison because data were obtained at more design thrust-vector angles for this thrust-vectoring concept than for the concept utilizing upper and lower flaps. A similar comparison can be made with the upper- and lower-flap thrust-vectoring concept but more data interpolation will be required. Figure 33(a) shows design and resultant thrust-vector angles for nozzle configurations with fixed and programmed vector flaps. The fixed vector-flap nozzle had a constant design thrust-vector angle of 0° and produced resultant thrust-vector angles from -8° to about 5° over the nozzle pressure ratio range investigated; these data were shown previously in figure 21 (configuration F6) and figure 25 (configuration VF1(0)). The programmed vector-flap configuration (dashed line in fig. 33) had a design thrust-

vector-flap schedule which varied from -10° to 9° and produced a constant resultant thrust-vector angle equal to 0° over the nozzle pressure ratio range investigated; these data were obtained by interpolation of the data shown in figure 25. A comparison of thrust ratios for these nozzle configurations is shown in figure 33(b); data for the fixed vector flap are shown in figure 8(f) (configuration F6) and figure 24 (configuration VF1(0)); data for the programmed vector flap were obtained by interpolation of data from figure 24. Thrust ratios for the programmed vector-flap configuration ranged from 0 to 0.9 percent lower than the fixed vector-flap configuration. This result was expected since the data of figure 24 show that the highest thrust ratios were always obtained with a design thrust-vector angle equal to 0°. The axial thrust gain achieved by eliminating nonzero values of resultant thrust-vector angle is more than offset by the internal thrust loss associated with turning the exhaust flow when the upper, aft-flap thrust-vectoring concept is utilized to trim out resultant thrust-vector angle. The inefficient thrust-vectoring performance of the upper, aft-flap thrust-vectoring concept was discussed previously. It should be noted that although the use of a programmed upper, aft vector-flap results in a small thrust penalty (less than 1 percent), the normal thrust-vector component has been entirely eliminated and could result in a reduction of airplane trim drag.

Data from reference 14 indicate that it is possible to achieve higher thrust performance by utilizing a programmed vectored-thrust mechanism on SERN nozzles; maximum resultant thrust ratio was achieved at resultant thrust-vector angles from -5° to -7.5°. Examination of figure 26 indicates that the use of the upper- and lower-flap thrust-vectoring concept to trim out nonzero resultant thrust-vector angles could result in a thrust-ratio gain in addition to elimination of the normal thrust-vector component. At $p_{t,j}/p_\infty$ less than 4.5, a design thrust-vector angle equal to -10° generally produced higher thrust ratios than the unvectored configuration. Unfortunately, a design thrust-vector angle of -5° was not tested with this thrust-vectoring concept. The more efficient thrust-vectoring performance of this concept relative to the upper, aft vector-flap concept has been discussed previously. Interpolation of the limited data shown in figures 26 and 27 indicates design thrust-vector angles from about -5° to 6° would be required to trim out the resultant thrust-vector angles shown for the unvectored configuration and that small thrust-ratio improvements do occur at nozzle pressure ratios less than 4.5.

Reversed-Thrust Performance

The effect of external exhaust-flow blocker position on the internal performance of a reversed-thrust nozzle is presented in figure 34. The exhaust-flow blocker would be deployed from the aft portion of the upper ramp of the SERN downstream of the forward-flight geometric throat. The resulting upper and lower ports differed in area and passage angle, and the total port area was greater than the forward-flight geometric throat (see fig. 6).

All exhaust-flow blocker positions produced useful amounts of reverse thrust (where an F/F_i value of -0.5 is considered desirable at low nozzle pressure ratios). However, due to the difference between upper and lower port areas and passage angles, consideration must be given to the magnitude of the normal-force component of the resultant thrust with the deployed blocker in each position. Figure 35 presents the effect of blocker position on measured normal force. Configuration R5 (blocker lowered) had the least impact on normal force and R4 (blocker raised) had the largest impact on normal force. In fact, configurations R2 and R4 produced enough normal force to cause the nozzle pressure ratio test range to be truncated due

to force balance limitations in pitching moment. In some applications it could be beneficial to generate normal force during thrust reversal for aerodynamic trim purposes, however, generation of a large, uncontrolled normal-force component would probably be undesirable.

The smallest amount of reverse thrust was produced by configurations R2 and R4 (fig. 34). These configurations are the only ones that gave any indication of choking (sonic flow on upper ramp only) at the forward-flight geometric throat (see fig. 15). In addition, configurations R2 and R4 had the largest normal-force thrust components. The largest amount of reverse thrust was produced by configuration R3 and this configuration was the furthest from choking at the forward-flight geometric throat (see fig. 15). These results tend to indicate that improved reverse-thrust performance can be accomplished by blocking and turning a low velocity exhaust stream and allowing choked conditions to occur at the reverser port exits.

During the thrust-reverser investigation, considerable nozzle vibration was encountered and is probably attributable to flow unsteadiness caused by separation at the entrance corners of the reverser passages as discussed in the section on internal static-pressure distributions. For practical application of this type of thrust-reverser arrangement, vibration would have to be eliminated.

The practicality of a thrust reverser is dependent on possible effects on engine (and airplane) stability and not solely on the efficient production of reverse thrust. A change in back pressure due to deployment of a reverser can result in engine stall or overspeed if the reverser port area is not properly sized (see ref. 26).

The likelihood of back pressure effects affecting engine stability can be assessed by examining the discharge coefficient which is a measure of nozzle normalized flow rate at a particular nozzle pressure ratio. Therefore, a change in discharge coefficient, when based on a constant geometric throat area, is the same as a change in flow rate unless a compensating change in throat area is made. The reversed-thrust discharge coefficients presented in figure 34 are based on the forward-flight throat area and range from 0.66 to 0.94. Configurations R2 and R4, which gave an indication of some sonic flow at the forward-flight geometric throat, have the highest discharge coefficients. Even at the highest discharge coefficient of 0.945, these configurations have about a 3 to 4 percent lower flow rate than a typical forward-flight SERN. This indicates that a 3- to 4-percent increase in reverser throat (sonic) area would be necessary to eliminate an increase in back pressure on the engine in the reversed-thrust mode.

The other reversed-thrust configurations, which as indicated by the internal pressures are unchoked at the forward-flight geometric throat, have much lower discharge coefficients. This indicates that the flow is probably choked at the reverser ports at a significantly smaller effective throat area than the forward-flight geometric throat and that a significant increase in reverser port area would be required to prevent driving the engine toward stall (see ref. 26).

CONCLUSIONS

An investigation has been conducted at static conditions (wind off) in the static-test facility of the Langley 16-Foot Transonic Tunnel. The effects of geometric design parameters on the internal performance of nonaxisymmetric single

expansion-ramp nozzles were investigated at nozzle pressure ratios up to approximately 10. Forward-flight (cruise), vectored-thrust, and reversed-thrust operating modes were investigated. Results of this study indicate the following conclusions:

1. Single expansion-ramp nozzles have high static internal performance over a broader range of operating nozzle pressure ratios than nonaxisymmetric convergent-divergent nozzles with comparable expansion ratios.

2. Sidewall length has little effect on nozzle thrust performance or resultant thrust-vector angle for the forward-flight (cruise) nozzle geometry.

3. Thrust ratio was increased by increasing lower-flap length and decreasing lower-flap divergence angle.

4. A thrust-vectoring concept utilizing upper and lower nozzle flaps was a much more effective flow-turning device than a thrust-vectoring concept utilizing only a single flap near the trailing edge of the upper expansion ramp.

5. For vectored-thrust operation, reduced sidewall containment tended to reduce resultant thrust-vector angle.

6. Use of a programmed thrust-vectoring mechanism can eliminate undesired resultant thrust-vector angles during cruise flight. The effect of the programmed vector flap on thrust ratio depends on the efficiency of the thrust-vectoring mechanism. During the current investigation, small thrust-ratio losses (less than 1 percent) occurred when the upper, aft flap was utilized for this purpose. However, the data indicate that small thrust-ratio gains may be possible with the more efficient upper- and lower-flap thrust-vectoring concept.

7. During reverse-thrust operation, all blocker positions tested produced useful amounts of reverse thrust. However, only the lowered blocker position had little or no effect on normal force. In addition, all exhaust-flow blocker positions tested produced lower discharge coefficients than the forward-flight configurations and would require an increase in reverser port area to prevent driving the engine toward stall.

Langley Research Center
National Aeronautics and Space Administration
Hampton, VA 23665
January 20, 1982

REFERENCES

1. Schmeer, James W.; Lauer, Rodney F., Jr.; and Berrier, Bobby L.: Performance of Blow-in-Door Ejector Nozzles Installed on a Twin-Jet Variable-Wing-Sweep Fighter Airplane Model. NASA TM X-1383, 1967.

2. Reubush, David E.; and Mercer, Charles E.: Effects of Nozzle Interfairing Modifications on Longitudinal Aerodynamic Characteristics of a Twin-Jet, Variable-Wing-Sweep Fighter Model. NASA TN D-7817, 1975.

3. Maiden, Donald L.; and Berrier, Bobby L.: Effect of Airframe Modifications on Longitudinal Aerodynamic Characteristics of a Fixed-Wing, Twin-Jet Fighter Airplane Model. NASA TM X-2523, 1972.

4. Maiden, Donald L.; and Petit, John E.: Investigation of Two-Dimensional Wedge Exhaust Nozzles for Advanced Aircraft. J. Aircr., vol. 13, no. 10, Oct. 1976, pp. 809-816.

5. Martens, Richard E.: F-15 Nozzle/Afterbody Integration. J. Aircr., vol. 13, no. 5, May 1976, pp. 327-333.

6. Capone, Francis J.: Summary of Propulsive-Lift Research in the Langley 16-Ft. Transonic Tunnel. J. Aircr., vol. 13, no. 10, Oct. 1976, pp. 803-808.

7. Hiley, P. E.; Wallace, H. W.; and Booz, D. E.: Nonaxisymmetric Nozzles Installed in Advanced Fighter Aircraft. J. Aircr., vol. 13, no. 12, Dec. 1976, pp. 1000-1006.

8. Sedgwick, T. A.: Investigation of Non-Symmetric Two-Dimensional Nozzles Installed in Twin-Engine Tactical Aircraft. AIAA Paper No. 75-1319, Sept.-Oct. 1975.

9. Berrier, Bobby L.; Palcza, J. Lawrence; and Richey, G. Keith: Nonaxisymmetric Nozzle Technology Program - An Overview. AIAA Paper 77-1225, Aug. 1977.

10. F-15 2-D Nozzle System Integration Study. Volume I - Technical Report. NASA CR-145295, 1978.

11. Stevens, H. L.: F-15/Nonaxisymmetric Nozzle System Integration Study Support Program. NASA CR-135252, 1978.

12. Bergman, D.; Mace, J. L.; and Thayer, E. B.: Non-Axisymmetric Nozzle Concepts for an F-111 Test Bed. AIAA Paper No. 77-841, July 1977.

13. Wasson, H. R.; Hall, G. R.; and Palcza, J. L.: Results of a Feasibility Study to Add Canards and ADEN Nozzle to the YF-17. AIAA Paper 77-1227, Aug. 1977.

14. Capone, Francis J.: Static Performance of Five Twin-Engine Nonaxisymmetric Nozzles With Vectoring and Reversing Capability. NASA TP-1224, 1978.

15. Lander, J. A.; and Palcza, J. Lawrence: Exhaust Nozzle Deflector Systems for V/STOL Fighter Aircraft. AIAA Paper No. 74-1169, Oct. 1974.

16. Lander, J. A.; Nash D. O.; and Palcza, J. Lawrence: Augmented Deflector Exhaust Nozzle (ADEN) Design for Future Fighters. AIAA Paper No. 75-1318, Sept.-Oct. 1975.

17. Nash, D. O.; Wakeman, T. G.; and Palcza, J. L.: Structural and Cooling Aspects of the ADEN Nonaxisymmetric Exhaust Nozzle. Paper No. 77-GT-110, American Soc. Mech. Eng., Mar. 1977.

18. Schnell, W. C.; Grossman, R. L.; and Hoff, G. E.: Comparison of Non-Axisymmetric and Axisymmetric Nozzles Installed on a V/STOL Fighter Model. [Preprint] 770983, Soc. Automot. Eng., Nov. 1977.

19. Berrier, Bobby L.; and Re, Richard J.: Effect of Several Geometric Parameters on the Static Internal Performance of Three Nonaxisymmetric Nozzle Concepts. NASA TP-1468, 1979.

20. Schnell, W. C.; and Grossman, R. L.: Vectoring Non-Axisymmetric Nozzle Jet Induced Effects on a V/STOL Fighter Model. AIAA Paper 78-1080, July 1978.

21. Hutchinson, R. A.; Petit, J. E.; Capone, F. J.; and Whittaker, R. W.: Investigation of Advanced Thrust Vectoring Exhaust Systems for High Speed Propulsive Lift. AIAA-80-1159, June/July 1980.

22. Hiley, P. E.; and Bowers, D. L.: Advanced Nozzle Integration for Supersonic Strike Fighter Application. AIAA-81-1441, July 1981.

23. Capone, Francis J.; Hunt, Brian L.; and Poth, Greg E.: Subsonic/Supersonic Nonvectored Aeropropulsive Characteristics of Nonaxisymmetric Nozzles Installed on an F-18 Model. AIAA-81-1445, July 1981.

24. Ferri, Antonio: Elements of Aerodynamics of Supersonic Flows. Macmillan Co., 1949, p. 171.

25. Von Karman, Theodore: Supersonic Aerodynamics - Principles and Applications. J. Aeronaut. Sci., vol. 14, no. 7, July 1947, pp. 373-409.

26. Willard, C. M.; Capone, F. J.; Konarski, M.; and Stevens, H. L.: Static Performance of Vectoring/Reversing Non-Axisymmetric Nozzles. AIAA Paper 77-840, July 1977.

TABLE I.- SUMMARY OF FORWARD-FLIGHT NOZZLE GEOMETRY

Configuration	A_t, cm^2	$(A_e/A_t)_i$	$(A_e/A_t)_e$	$l_{f,u}$, cm	$l_{f,l}$, cm	α_u, deg	α_l, deg	AR	Sidewall
F1	26.168	1.097	1.407	8.32	2.36	2.5	-3.0	3.94	baseline
F2	26.111	1.215	1.510	8.32	2.36	2.5	4.0	3.95	baseline
F3	26.111	1.391	1.665	8.32	2.36	2.5	13.5	3.95	baseline
F4	26.168	1.091	1.476	8.32	1.09	2.5	4.4	3.94	baseline
F5	26.168	1.389	1.558	8.32	4.01	2.5	4.5	3.94	baseline
F6	26.111	1.215	1.510	8.32	2.36	2.5	4.0	3.95	cutback

TABLE II.- INTERNAL STATIC-PRESSURE

ORIFICE LOCATIONS

(a) Configurations F1 and F3

Upper flap			
$x/x_{t,u}$	$y/(w_t/2)$		
	0.000	0.450	0.875
0.888	X		
0.954	X		
1.008	X	X	X
1.063	X		
1.129	X	X	X
1.184	X		
1.250	X	X	X
1.316	X	X	X
1.383	X		
1.449	X		
1.522	X		
1.606	X	X	X
1.691	X	X	X

Lower flap						
$x/x_{t,l}$	$y/(w_t/2)$					
	0.000	0.250	0.500	0.750	0.875	0.950
0.881	X					
.941	X					
1.001	X	X	X	X	X	X
1.019	X					
1.049	X					
1.079	X					
1.121	X	X	X	X	X	X
1.157	X					
1.199	X					

TABLE II.- Continued

(b) Configurations F2, F6, VF1(0), and V1(0)

Upper flap			
$x/x_{t,u}$	$y/(w_t/2)$		
	0.000	0.450	0.875
0.888	X	X	X
.954	X	X	X
1.008	X	X	X
1.063	X	X	
1.129	X	X	X
1.184	X	X	X
1.250	X	X	X
1.316	X	X	X
1.383	X	X	X
1.449	X	X	X
1.522	X	X	X
1.606	X	X	X
1.691	X	X	X

Lower flap			
$x/x_{t,l}$	$y/(w_t/2)$		
	0.000	0.450	0.875
0.881	X	X	X
.947	X	X	X
1.001	X	X	X
1.043	X	X	X
1.079	X	X	X
1.127	X	X	X
1.168	X	X	X

TABLE II.- Continued

(c) Configuration F4

Upper flap			
$x/x_{t,u}$	$y/(w_t/2)$		
	0.000	0.450	0.875
0.888	X		
.954	X		
1.008	X	X	X
1.063	X		
1.129	X	X	X
1.184	X		
1.250	X	X	X
1.316	X	X	X
1.383	X		
1.449	X		
1.522	X		
1.606	X	X	X
1.691	X	X	X

Lower flap						
$x/x_{t,l}$	$y/(w_t/2)$					
	0.000	0.250	0.500	0.750	0.875	0.950
0.881	X					
.941	X					
1.001	X	X	X	X	X	X
1.019	X					
1.049	X					
1.079	X					

TABLE II.- Continued

(d) Configuration F5

Upper flap			
$x/x_{t,u}$	$y/(w_t/2)$		
	0.000	0.450	0.875
0.888	X		
.954	X		
1.008	X	X	X
1.063	X		
1.129	X	X	X
1.184	X		
1.250	X	X	X
1.316	X	X	X
1.383	X		
1.449	X		
1.522	X		
1.606	X	X	X
1.691	X	X	X

Lower flap						
$x/x_{t,l}$	$y/(w_t/2)$					
	0.000	0.250	0.5000	0.750	0.875	0.950
0.881	X					
.941	X					
1.001	X	X	X	X	X	X
1.019	X					
1.049	X					
1.079	X					
1.121	X	X	X	X	X	
1.157	X					
1.199	X					
1.259	X					
1.319	X	X	X	X	X	X

TABLE II.- Continued

(e) Configurations VF1(-10), VF1(-5), VF1(5), VF1(10), and VF1(20)

Upper flap						
$x/x_{t,u}$	$y/(w_t/2)$					
	0.000	0.250	0.500	0.750	0.875	0.950
0.888	X					
.924	X					
.966	X					
1.008	X	X	X	X	X	X
1.051	X					
1.087	X					
1.129	X					
1.190	X					
1.250	X	X	X	X	X	X
1.322	X					
1.389	X					
1.449	X					
1.510	X					
1.570	X					
1.630	X					
1.691	X	X	X	X	X	X
1.751	X					

Lower flap			
$x/x_{t,l}$	$y/(w_t/2)$		
	0.000	0.450	0.875
0.881	X		
.947	X		
1.001	X		
1.043	X	X	X
1.079	X	X	X
1.127	X	X	X
1.168	X	X	

TABLE II.- Continued

(f) Configurations V1(-10), V1(11), V1(20), V2(20), and V3(20)

Upper flap						
$x/x_{t,u}$	$y/(w_t/2)$					
	0.000	0.250	0.500	0.750	0.875	0.950
0.888	X					
0.924	X					
0.966	X					
1.008	X	X	X	X	X	X
1.051	X					
1.087	X					
1.129	X					
1.190	X					
1.250	X	X	X	X	X	X
1.322	X					
1.389	X					
1.449	X					
1.510	X					
1.570	X					
1.630	X					
1.691	X	X	X	X	X	X
1.751	X*					

Lower flap						
$x/x_{t,l}$	$y/(w_t/2)$					
	0.000	0.250	0.500	0.750	0.875	0.950
0.881	X					
0.941	X					
1.001	X	X	X	X	X	X
1.019	X					
1.049	X					
1.079	X					
1.121	X	X	X	X	X	X
1.157	X					
1.199	X					

* Configurations V1(20), V2(20), and V3(20) do not have orifice on upper flap at $x/x_{t,u} = 1.751$.

TABLE II.- Concluded

(g) Configurations R1, R2, R3, R4, and R5

Upper flap	
$x/x_{t,u}$	$y/(w_t/2)$
	0.000
0.954	X
0.978	X
1.002	X
1.027	X
1.051	X

Lower flap	
$x/x_{t,l}$	$y/(w_t/2)$
	0.000
0.959	X
0.983	X
1.007	X
1.031	X
1.055	X

Blocker surface*	
z/h_t	$y/(w_t/2)$
	0.000
0.745	X
0.345	X
0.000	X
-0.498	X
-0.996	X
-1.345	X
-1.745	X

*Blocker orifices on configuration R1 only.

TABLE III.- COMPUTER PRINTOUT OF RATIO OF INTERNAL STATIC PRESSURE TO JET TOTAL PRESSURE FOR FORWARD-FLIGHT SINGLE EXPANSION-RAMP NOZZLES

(a) Configuration F1

Upper-flap static-pressure ratio, $p/p_{t,j}$

$y/(w_t/2) = 0.000$

$x/x_{t,u}$

pt	$p_{t,j}/p_\infty$	0.888	0.954	1.008	1.063	1.129	1.184	1.250	1.316	1.383	1.449	1.522	1.606	1.691
1	1.001	.996	.999	.999	1.001	1.000	.999	.998	.997	.999	.999	.998	.999	.999
2	1.993	.792	.572	.246	.238	.284	.319	.506	.600	.609	.536	.562	.561	.549
3	2.994	.794	.570	.247	.237	.289	.317	.328	.332	.314	.392	.532	.495	.427
4	2.988	.794	.570	.247	.237	.289	.317	.328	.332	.314	.395	.532	.496	.425
5	3.994	.793	.569	.247	.237	.290	.315	.327	.331	.314	.259	.269	.214	.400
6	4.983	.793	.570	.246	.237	.291	.314	.326	.331	.313	.228	.268	.214	.175
7	5.983	.793	.569	.245	.235	.291	.313	.326	.331	.313	.209	.268	.215	.175
8	5.963	.793	.569	.245	.235	.291	.314	.326	.331	.313	.210	.268	.215	.175
9	6.955	.792	.570	.245	.234	.291	.313	.325	.331	.313	.199	.268	.215	.176
10	7.972	.792	.570	.244	.233	.290	.313	.325	.330	.313	.191	.268	.215	.176
11	7.951	.792	.570	.244	.233	.290	.313	.325	.330	.313	.191	.268	.215	.176
12	8.955	.792	.571	.244	.233	.291	.312	.325	.330	.313	.186	.268	.215	.176
13	9.957	.792	.571	.244	.233	.291	.311	.325	.330	.313	.184	.268	.215	.176
14	9.876	.792	.571	.244	.233	.291	.311	.325	.330	.313	.185	.268	.215	.176
15	9.951	.791	.571	.244	.233	.291	.311	.325	.330	.313	.185	.268	.215	.176
16	.998	1.002	1.002	1.002	1.001	1.001	1.002	1.002	1.004	1.002	1.003	1.003	1.002	.999

Upper-flap static-pressure ratio, $p/p_{t,j}$

$y/(w_t/2) = 0.450$ | $y/(w_t/2) = 0.875$

$x/x_{t,u}$ | $x/x_{t,u}$

pt	$p_{t,j}/p_\infty$	1.008	1.129	1.250	1.316	1.606	1.691	1.008	1.129	1.250	1.316	1.606	1.691
1	1.001	.999	.999	.999	1.000	1.000	.999	.999	.999	.998	.998	.998	.998
2	1.993	.245	.289	.508	.605	.561	.546	.248	.289	.533	.579	.553	.501
3	2.994	.245	.288	.327	.341	.485	.432	.247	.291	.322	.326	.457	.334
4	2.988	.246	.288	.327	.341	.486	.430	.247	.291	.322	.327	.457	.334
5	3.994	.245	.289	.326	.339	.212	.394	.246	.290	.320	.325	.216	.250
6	4.983	.244	.288	.324	.338	.210	.171	.244	.288	.318	.323	.211	.201
7	5.983	.243	.287	.324	.337	.211	.172	.243	.287	.318	.322	.211	.167
8	5.963	.243	.288	.324	.337	.211	.172	.243	.287	.318	.322	.211	.168
9	6.955	.242	.287	.324	.337	.211	.172	.242	.286	.317	.321	.211	.144
10	7.972	.241	.286	.323	.337	.211	.172	.241	.285	.317	.320	.210	.125
11	7.951	.241	.286	.324	.337	.211	.172	.241	.285	.317	.320	.210	.126
12	8.955	.241	.286	.323	.337	.211	.172	.241	.284	.317	.320	.205	.112
13	9.957	.240	.286	.323	.337	.211	.172	.242	.283	.317	.319	.199	.100
14	9.876	.240	.286	.323	.337	.212	.172	.242	.283	.317	.319	.200	.101
15	9.951	.240	.286	.323	.337	.211	.172	.242	.284	.317	.319	.200	.100
16	.998	1.001	1.002	1.002	1.003	1.004	1.001	1.001	1.002	1.003	1.002	1.001	.999

TABLE III.- Continued

(a) Concluded

		Lower-flap static-pressure ratio, $p/p_{t,j}$								
		$y/(w_t/2) = 0.000$								
		$x/x_{t,1}$								
pt	$p_{t,j}/p_\infty$	0.881	0.941	1.001	1.019	1.049	1.079	1.121	1.157	1.199
1	1.001	.999	1.001	.996	1.001	1.000	1.000	.999	1.000	.998
2	1.993	.846	.740	.614	.599	.567	.530	.468	.411	.409
3	2.994	.844	.739	.613	.597	.563	.528	.468	.412	.363
4	2.988	.844	.739	.613	.597	.564	.528	.468	.412	.363
5	3.994	.844	.739	.611	.597	.563	.527	.468	.411	.361
6	4.983	.844	.739	.611	.597	.562	.528	.468	.410	.361
7	5.983	.844	.738	.611	.597	.563	.528	.468	.410	.360
8	5.963	.844	.738	.611	.597	.563	.528	.468	.409	.360
9	6.955	.844	.738	.611	.597	.563	.529	.469	.410	.360
10	7.972	.844	.738	.611	.597	.564	.530	.469	.410	.360
11	7.951	.844	.738	.611	.597	.564	.530	.469	.410	.360
12	8.955	.844	.738	.611	.596	.565	.531	.469	.410	.360
13	9.957	.845	.738	.611	.596	.566	.531	.469	.410	.360
14	9.876	.845	.738	.611	.596	.566	.531	.469	.410	.360
15	9.951	.845	.738	.611	.596	.566	.531	.469	.410	.360
16	.998	1.001	1.001	1.006	1.001	1.000	1.001	1.002	1.001	1.002

		Lower-flap static-pressure ratio, $p/p_{t,j}$									
		$x/x_{t,1} = 1.001$					$x/x_{t,1} = 1.121$				
		$y/(w_t/2)$					$y/(w_t/2)$				
pt	$p_{t,j}/p_\infty$	0.250	0.500	0.750	0.875	0.950	0.250	0.500	0.750	0.875	0.950
1	1.001	.999	1.005	1.000	.999	.999	.999	1.000	.999	.997	1.001
2	1.993	.620	.619	.614	.614	.623	.470	.467	.470	.460	.469
3	2.994	.617	.615	.610	.606	.619	.468	.466	.467	.456	.466
4	2.988	.617	.615	.611	.606	.619	.468	.466	.468	.457	.466
5	3.994	.615	.614	.610	.602	.618	.468	.464	.466	.455	.465
6	4.983	.615	.613	.610	.601	.618	.468	.464	.466	.455	.465
7	5.983	.615	.613	.610	.600	.619	.468	.464	.466	.455	.465
8	5.963	.615	.613	.610	.600	.619	.468	.464	.466	.455	.465
9	6.955	.615	.613	.610	.599	.619	.469	.465	.467	.455	.465
10	7.972	.615	.613	.611	.599	.618	.469	.465	.468	.455	.463
11	7.951	.615	.613	.611	.599	.618	.469	.465	.468	.455	.463
12	8.955	.615	.613	.611	.599	.619	.470	.465	.469	.456	.463
13	9.957	.616	.613	.612	.599	.619	.470	.466	.469	.457	.463
14	9.876	.615	.612	.612	.599	.619	.470	.465	.469	.457	.463
15	9.951	.615	.612	.612	.599	.619	.470	.465	.469	.457	.463
16	.998	1.001	.996	1.001	1.001	1.002	1.001	1.000	1.001	1.004	1.000

TABLE III.- Continued

(b) Configuration F2

Upper-flap static-pressure ratio, $p/p_{t,j}$

$y/(w_t/2) = 0.000$

$x/x_{t,u}$

Pt	$p_{t,j}/p_\infty$	0.888	0.954	1.008	1.063	1.129	1.184	1.250	1.316	1.383	1.449	1.522	1.606	1.691
1	.999	1.001	1.000	1.000	1.001	1.001	1.000	1.000	1.001	1.001	1.001	1.001	1.000	1.006
2	1.990	.793	.570	.243	.229	.256	.281	.423	.463	.551	.595	.585	.569	.552
3	2.999	.794	.568	.244	.228	.261	.263	.242	.229	.237	.389	.428	.494	.469
4	4.001	.792	.567	.244	.228	.263	.264	.241	.228	.233	.227	.217	.205	.335
5	4.992	.792	.566	.243	.228	.263	.263	.240	.226	.232	.227	.217	.205	.192
6	5.990	.791	.566	.242	.227	.263	.262	.240	.225	.231	.226	.216	.205	.192
7	5.995	.791	.566	.242	.227	.263	.262	.240	.225	.231	.226	.216	.205	.192
8	6.955	.790	.566	.241	.226	.263	.262	.239	.225	.230	.226	.216	.205	.192
9	6.962	.790	.566	.241	.226	.263	.262	.240	.225	.230	.226	.216	.205	.192
10	7.988	.790	.566	.241	.225	.263	.262	.239	.224	.230	.225	.216	.205	.192
11	9.010	.790	.566	.240	.224	.263	.262	.239	.224	.229	.225	.216	.206	.192
12	8.994	.790	.566	.240	.224	.263	.262	.239	.224	.229	.225	.216	.206	.192
13	9.996	.790	.567	.240	.224	.263	.262	.239	.224	.229	.225	.216	.206	.193
14	1.000	1.001	1.000	1.000	1.000	.999	.999	1.000	1.001	1.001	1.001	1.000	1.001	.997

Upper-flap static-pressure ratio, $p/p_{t,j}$

$y/(w_t/2) = 0.450$

$x/x_{t,u}$

Pt	$p_{t,j}/p_\infty$	0.888	0.954	1.008	1.063	1.129	1.184	1.250	1.316	1.383	1.449	1.522	1.606	1.691
1	.999	1.000	1.004	1.000	1.001	1.001	1.000	1.000	1.000	1.001	1.000	1.001	1.001	1.001
2	1.990	.793	.580	.242	.229	.262	.265	.421	.475	.577	.593	.575	.565	.546
3	2.999	.793	.578	.241	.229	.262	.263	.244	.234	.238	.385	.440	.506	.456
4	4.001	.793	.577	.240	.229	.262	.262	.243	.233	.238	.234	.217	.205	.351
5	4.992	.792	.576	.239	.229	.261	.260	.242	.233	.237	.233	.216	.204	.186
6	5.990	.792	.576	.238	.228	.260	.259	.241	.232	.237	.233	.216	.203	.186
7	5.995	.792	.576	.238	.228	.260	.259	.241	.232	.237	.233	.216	.203	.185
8	6.955	.792	.576	.237	.227	.260	.259	.241	.232	.237	.233	.215	.203	.185
9	6.962	.792	.576	.237	.227	.260	.259	.241	.232	.237	.233	.216	.203	.185
10	7.988	.792	.576	.237	.227	.259	.258	.240	.232	.237	.233	.215	.202	.185
11	9.010	.791	.576	.236	.227	.259	.258	.240	.232	.236	.233	.215	.202	.185
12	8.994	.791	.576	.236	.226	.259	.258	.240	.232	.237	.233	.215	.202	.185
13	9.996	.791	.576	.236	.226	.259	.258	.240	.232	.237	.233	.215	.202	.186
14	1.000	1.000	1.001	1.000	1.001	1.000	1.000	1.000	1.001	1.000	1.000	1.001	1.001	1.000

TABLE III.- Continued

(b) Continued

Upper-flap static-pressure ratio, $p/p_{t,j}$

$y/(w_t/2) = 0.875$

$x/x_{t,u}$

Pt	$p_{t,j}/p_\infty$	0.888	0.954	1.008	1.129	1.184	1.250	1.316	1.383	1.449	1.522	1.606	1.691
1	.999	.999	1.001	1.000	1.001	1.001	1.001	1.000	1.001	1.001	1.000	1.001	1.000
2	1.990	.790	.568	.247	.258	.266	.433	.498	.533	.560	.562	.556	.537
3	2.999	.789	.564	.246	.258	.262	.240	.234	.234	.380	.445	.459	.434
4	4.001	.788	.562	.245	.257	.261	.239	.233	.233	.230	.215	.264	.345
5	4.992	.787	.561	.242	.256	.261	.238	.232	.232	.230	.214	.203	.196
6	5.990	.787	.560	.241	.255	.260	.237	.231	.231	.229	.214	.202	.188
7	5.995	.787	.560	.241	.255	.260	.237	.231	.231	.229	.214	.202	.188
8	6.955	.787	.559	.240	.254	.260	.237	.230	.231	.229	.213	.202	.187
9	6.962	.787	.559	.240	.255	.260	.237	.230	.231	.229	.213	.202	.187
10	7.988	.786	.559	.240	.254	.259	.237	.230	.230	.229	.213	.202	.187
11	9.010	.786	.558	.239	.253	.259	.236	.230	.230	.229	.213	.202	.187
12	8.994	.786	.558	.239	.253	.259	.236	.230	.230	.229	.213	.202	.187
13	9.996	.786	.558	.239	.253	.259	.236	.229	.229	.228	.212	.202	.187
14	1.000	1.001	1.000	1.000	1.000	1.000	1.001	1.001	1.000	1.001	.999	1.000	1.001

Lower-flap static-pressure ratio, $p/p_{t,j}$

$y/(w_t/2) = 0.000$

$x/x_{t,l}$

Pt	$p_{t,j}/p_\infty$	0.881	0.947	1.001	1.043	1.079	1.127	1.168
1	.999	.998	1.004	.998	1.001	1.001	1.000	1.000
2	1.990	.842	.695	.529	.434	.423	.376	.334
3	2.999	.840	.693	.528	.433	.423	.374	.334
4	4.001	.840	.692	.527	.433	.421	.372	.333
5	4.992	.840	.690	.527	.433	.420	.370	.333
6	5.990	.840	.689	.527	.433	.420	.370	.333
7	5.995	.840	.689	.527	.433	.420	.370	.333
8	6.955	.840	.689	.527	.433	.420	.370	.333
9	6.962	.840	.689	.527	.433	.420	.370	.333
10	7.988	.841	.688	.527	.432	.421	.370	.333
11	9.010	.841	.688	.527	.432	.421	.370	.333
12	8.994	.841	.688	.527	.432	.421	.370	.333
13	9.996	.841	.687	.527	.432	.421	.370	.334
14	1.000	1.004	.998	1.003	1.000	1.001	1.000	1.000

TABLE III.- Continued

(b) Concluded

		Lower-flap static-pressure ratio, $p/p_{t,j}$						
		$y/(w_t/2) = 0.450$						
		$x/x_{t,l}$						
Pt	$p_{t,j}/p_\infty$	0.881	0.947	1.001	1.043	1.079	1.127	1.168
1	.999	1.000	.999	1.001	1.002	1.000	1.000	1.001
2	1.990	.832	.703	.533	.432	.423	.382	.335
3	2.999	.833	.702	.530	.430	.420	.381	.336
4	4.001	.833	.702	.528	.426	.418	.381	.334
5	4.992	.834	.701	.527	.424	.417	.380	.333
6	5.990	.833	.700	.526	.424	.416	.380	.333
7	5.995	.833	.700	.526	.424	.416	.380	.333
8	6.955	.833	.700	.526	.423	.416	.380	.333
9	6.962	.833	.700	.526	.423	.416	.380	.333
10	7.988	.833	.699	.526	.423	.416	.380	.333
11	9.010	.833	.699	.526	.423	.416	.380	.333
12	8.994	.833	.699	.526	.423	.416	.380	.333
13	9.996	.832	.699	.525	.424	.416	.381	.334
14	1.000	1.000	1.001	1.001	1.000	1.000	1.001	1.000

		Lower-flap static-pressure ratio, $p/p_{t,j}$						
		$y/(w_t/2) = 0.875$						
		$x/x_{t,l}$						
Pt	$p_{t,j}/p_\infty$	0.881	0.947	1.001	1.043	1.079	1.127	1.168
1	.999	1.000	1.002	.998	1.002	1.001	1.001	1.000
2	1.990	.844	.698	.533	.438	.428	.378	.338
3	2.999	.844	.695	.523	.436	.426	.376	.337
4	4.001	.844	.693	.519	.434	.424	.374	.335
5	4.992	.844	.692	.516	.433	.424	.372	.334
6	5.990	.844	.692	.514	.433	.423	.372	.334
7	5.995	.844	.691	.514	.433	.423	.372	.334
8	6.955	.844	.692	.513	.433	.423	.371	.334
9	6.962	.844	.692	.513	.433	.423	.371	.334
10	7.988	.844	.691	.513	.433	.423	.371	.333
11	9.010	.844	.689	.512	.433	.423	.371	.334
12	8.994	.844	.689	.512	.433	.423	.371	.334
13	9.996	.844	.687	.512	.433	.423	.371	.334
14	1.000	1.002	1.000	1.004	1.000	.999	.999	1.000

TABLE III.- Continued

(c) Configuration F3

Upper-flap static-pressure ratio, $p/p_{t,j}$

$y/(w_t/2) = 0.000$

$x/x_{t,u}$

pt	$p_{t,j}/p_\infty$	0.888	0.954	1.008	1.063	1.129	1.184	1.25	1.316	1.383	1.449	1.522	1.606	1.691
1	1.000	1.002	.997	.999	1.000	1.001	.997	.998	1.000	.999	.995	1.000	1.000	1.002
2	1.991	.793	.565	.240	.225	.250	.253	.404	.438	.545	.543	.576	.560	.545
3	2.979	.793	.564	.241	.224	.255	.254	.224	.199	.171	.327	.311	.330	.376
4	3.974	.792	.564	.241	.224	.256	.253	.224	.199	.171	.242	.130	.141	.224
5	4.941	.791	.566	.241	.225	.257	.254	.225	.199	.171	.200	.129	.113	.108
6	5.958	.791	.565	.239	.224	.257	.252	.224	.198	.171	.168	.129	.113	.108
7	6.976	.790	.565	.239	.223	.257	.251	.224	.198	.171	.144	.129	.113	.108
8	6.967	.790	.565	.239	.223	.257	.251	.224	.198	.171	.143	.129	.113	.108
9	7.926	.789	.565	.238	.222	.257	.251	.223	.198	.170	.129	.129	.113	.107
10	8.896	.789	.566	.238	.221	.257	.251	.223	.199	.171	.120	.129	.113	.107
11	9.909	.788	.567	.238	.221	.257	.251	.224	.199	.171	.115	.129	.115	.107
12	1.000	.998	1.002	1.001	1.000	1.000	1.003	1.002	1.000	1.000	1.005	.999	1.001	.995

Upper-flap static-pressure ratio, $p/p_{t,j}$

$y/(w_t/2) = 0.450$ | $y/(w_t/2) = 0.875$

$x/x_{t,u}$ | $x/x_{t,u}$

pt	$p_{t,j}/p_\infty$	1.008	1.129	1.250	1.316	1.606	1.691	1.008	1.129	1.250	1.316	1.606	1.691
1	1.000	1.000	1.000	.999	.998	.999	.998	1.000	1.000	.998	1.000	1.001	1.000
2	1.991	.241	.254	.405	.468	.557	.542	.241	.255	.440	.516	.546	.502
3	2.979	.241	.254	.224	.201	.347	.435	.240	.256	.224	.201	.396	.335
4	3.974	.239	.255	.224	.200	.118	.221	.240	.256	.224	.200	.206	.251
5	4.941	.238	.254	.224	.201	.119	.110	.238	.254	.224	.200	.121	.202
6	5.958	.237	.253	.224	.200	.118	.109	.236	.253	.222	.199	.123	.168
7	6.976	.236	.253	.223	.199	.118	.109	.235	.252	.222	.198	.125	.143
8	6.967	.236	.253	.223	.199	.118	.109	.235	.252	.221	.198	.116	.144
9	7.926	.235	.252	.223	.199	.118	.109	.235	.251	.221	.198	.115	.126
10	8.896	.235	.252	.223	.199	.116	.109	.234	.251	.221	.198	.114	.112
11	9.909	.234	.252	.223	.200	.117	.109	.234	.251	.222	.198	.114	.101
12	1.000	1.000	1.000	1.002	1.002	.999	.999	1.000	1.000	1.003	1.000	.998	1.000

TABLE III.- Continued

(c) Concluded

		Lower-flap static-pressure ratio, $p/p_{t,j}$								
		$y/(w_t/2) = 0.000$								
		$x/x_{t,1}$								
pt	$p_{t,j}/p_\infty$	0.881	0.941	1.001	1.019	1.049	1.079	1.121	1.157	1.199
1	1.000	.997	1.002	.997	.998	1.007	.999	1.000	1.000	1.000
2	1.991	.837	.732	.482	.356	.271	.268	.426	.441	.461
3	2.979	.838	.729	.487	.357	.270	.267	.255	.235	.212
4	3.974	.837	.730	.487	.356	.269	.267	.254	.236	.209
5	4.941	.837	.730	.488	.357	.265	.266	.254	.235	.209
6	5.958	.837	.730	.487	.357	.264	.266	.253	.234	.208
7	6.976	.837	.729	.487	.357	.264	.265	.253	.233	.208
8	6.967	.837	.729	.487	.356	.264	.265	.253	.233	.208
9	7.926	.837	.729	.486	.356	.264	.265	.253	.233	.208
10	8.896	.838	.729	.486	.356	.264	.265	.253	.232	.208
11	9.909	.838	.729	.486	.357	.264	.265	.253	.232	.208
12	1.000	1.003	.998	1.003	1.001	.993	1.001	1.000	.999	1.000

		Lower-flap static-pressure ratio, $p/p_{t,j}$									
		$x/x_{t,1} = 1.001$					$x/x_{t,1} = 1.121$				
		$y/(w_t/2)$					$y/(w_t/2)$				
pt	$p_{t,j}/p_\infty$	0.250	0.500	0.750	0.875	0.950	0.250	0.500	0.750	0.875	0.950
1	1.000	.998	.998	.997	1.013	.999	.999	1.000	1.000	1.000	1.001
2	1.991	.494	.490	.490	.503	.496	.272	.362	.353	.439	.445
3	2.979	.491	.486	.485	.485	.489	.259	.257	.264	.243	.248
4	3.974	.490	.485	.485	.476	.488	.257	.256	.262	.246	.249
5	4.941	.491	.487	.486	.469	.488	.256	.255	.258	.252	.244
6	5.958	.490	.486	.485	.446	.485	.255	.255	.256	.260	.245
7	6.976	.490	.485	.484	.463	.485	.255	.254	.255	.267	.234
8	6.967	.490	.485	.484	.467	.485	.255	.254	.253	.254	.257
9	7.926	.490	.485	.484	.465	.485	.255	.254	.253	.254	.257
10	8.896	.490	.485	.485	.453	.485	.255	.254	.253	.254	.257
11	9.909	.491	.486	.487	.440	.486	.255	.254	.253	.255	.257
12	1.000	1.002	1.001	1.005	.989	1.002	1.001	1.000	1.001	1.000	1.000

TABLE III.- Continued

(d) Configuration F4

		Upper-flap static-pressure ratio, $p/p_{t,j}$												
		$y/(w_t/2) = 0.000$												
		$x/x_{t,u}$												
Pt	$p_{t,j}/p_\infty$	0.888	0.954	1.008	1.063	1.129	1.184	1.250	1.316	1.383	1.449	1.522	1.606	1.691
1	1.000	1.000	.998	1.000	1.000	1.000	.998	.999	.999	.999	.997	.999	1.001	.996
2	1.995	.792	.568	.241	.229	.257	.429	.455	.577	.609	.542	.568	.562	.542
3	2.989	.793	.566	.242	.228	.262	.266	.241	.226	.231	.354	.424	.493	.460
4	3.988	.792	.566	.242	.228	.264	.265	.241	.226	.229	.248	.174	.145	.273
5	4.980	.791	.566	.241	.227	.264	.264	.241	.225	.229	.200	.173	.145	.126
6	5.972	.791	.566	.240	.226	.264	.263	.240	.224	.228	.174	.173	.145	.127
7	6.947	.791	.566	.239	.225	.264	.263	.240	.224	.228	.161	.173	.145	.128
8	7.943	.790	.568	.239	.224	.265	.264	.241	.224	.228	.153	.174	.147	.126
9	7.962	.790	.569	.239	.225	.265	.264	.241	.224	.228	.153	.174	.147	.126
10	8.951	.790	.569	.239	.224	.265	.263	.241	.224	.228	.147	.174	.147	.126
11	9.938	.789	.569	.239	.224	.265	.263	.241	.224	.228	.141	.174	.147	.126
12	9.943	.789	.569	.239	.224	.265	.263	.241	.224	.228	.141	.174	.147	.127
13	1.000	1.002	1.002	1.001	1.000	1.001	1.001	1.002	1.001	1.000	1.002	1.002	1.001	.989

		Upper-flap static-pressure ratio, $p/p_{t,j}$											
		$y/(w_t/2) = 0.450$						$y/(w_t/2) = 0.875$					
		$x/x_{t,u}$						$x/x_{t,u}$					
Pt	$p_{t,j}/p_\infty$	1.008	1.129	1.250	1.316	1.606	1.691	1.008	1.129	1.250	1.316	1.606	1.691
1	1.000	.999	1.000	1.000	.999	.998	1.001	.999	1.000	.999	1.000	1.000	.999
2	1.995	.241	.263	.459	.582	.558	.544	.242	.259	.513	.546	.554	.500
3	2.989	.241	.262	.240	.227	.506	.452	.242	.259	.242	.234	.461	.334
4	3.988	.240	.263	.240	.226	.145	.274	.241	.259	.241	.233	.250	.250
5	4.980	.239	.262	.239	.225	.146	.125	.239	.258	.240	.232	.143	.200
6	5.972	.238	.262	.239	.224	.146	.126	.238	.257	.239	.230	.145	.167
7	6.947	.237	.261	.238	.223	.145	.126	.236	.256	.239	.230	.143	.143
8	7.943	.237	.261	.240	.227	.145	.126	.236	.259	.240	.220	.141	.125
9	7.962	.237	.261	.240	.227	.145	.126	.236	.259	.240	.220	.141	.125
10	8.951	.237	.261	.240	.227	.145	.126	.236	.259	.240	.220	.136	.111
11	9.938	.236	.261	.240	.227	.146	.126	.236	.258	.239	.220	.131	.100
12	9.943	.236	.261	.240	.227	.145	.126	.236	.258	.239	.220	.132	.100
13	1.000	1.000	1.001	1.000	1.002	.999	1.001	1.001	1.001	1.001	1.001	1.000	.998

TABLE III.- Continued

(d) Concluded

		Lower-flap static-pressure ratio, $p/p_{t,j}$										
		$y/(w_t/2) = 0.000$						$x/x_{t,l} = 1.001$				
		$x/x_{t,l}$						$y/(w_t/2)$				
Pt	$p_{t,j}/p_\infty$	0.881	0.941	1.001	1.019	1.049	1.079	0.250	0.500	0.750	0.875	0.950
1	1.000	.996	.999	.995	.999	1.016	.999	.999	1.006	.996	.995	.997
2	1.995	.840	.729	.554	.471	.423	.423	.559	.562	.554	.540	.479
3	2.989	.840	.729	.553	.468	.424	.421	.559	.558	.551	.532	.476
4	3.988	.840	.730	.553	.469	.424	.419	.558	.557	.551	.515	.472
5	4.980	.840	.730	.553	.470	.425	.418	.558	.556	.552	.512	.469
6	5.972	.840	.730	.553	.471	.425	.418	.558	.556	.552	.520	.471
7	6.947	.841	.730	.554	.471	.426	.418	.558	.556	.553	.520	.478
8	7.943	.841	.730	.554	.472	.427	.418	.559	.557	.558	.536	.573
9	7.962	.841	.730	.555	.472	.427	.419	.559	.557	.559	.535	.573
10	8.951	.842	.730	.555	.472	.428	.419	.559	.557	.560	.525	.573
11	9.938	.842	.730	.555	.471	.428	.419	.559	.557	.560	.517	.573
12	9.943	.842	.730	.555	.471	.428	.419	.559	.557	.560	.517	.573
13	1.000	1.003	.998	1.002	1.001	.982	1.002	1.002	.994	1.004	.998	1.002

TABLE III.- Continued

(e) Configuration F5

Upper-flap static-pressure ratio, $p/p_{t,j}$

$y/(w_t/2) = 0.000$

$x/x_{t,u}$

Pt	$p_{t,j}/p_\infty$	0.888	0.954	1.008	1.063	1.129	1.184	1.250	1.316	1.383	1.449	1.522	1.606	1.691
1	1.000	1.000	1.000	1.000	1.001	1.001	1.000	1.000	1.000	1.000	.999	.995	1.000	1.001
2	1.996	.793	.567	.241	.228	.257	.264	.420	.433	.526	.552	.586	.571	.551
3	3.005	.793	.566	.242	.227	.262	.265	.242	.224	.232	.329	.345	.410	.482
4	3.986	.792	.566	.242	.227	.263	.265	.242	.224	.231	.251	.213	.209	.198
5	4.985	.792	.566	.242	.227	.264	.264	.242	.223	.230	.204	.212	.210	.197
6	5.999	.791	.566	.240	.226	.264	.263	.240	.223	.229	.182	.213	.209	.197
7	6.962	.790	.566	.240	.225	.264	.262	.240	.223	.229	.169	.213	.209	.197
8	7.982	.790	.566	.239	.224	.264	.262	.240	.222	.228	.160	.212	.209	.196
9	8.980	.789	.567	.238	.223	.264	.262	.240	.222	.228	.154	.213	.209	.196
10	9.973	.789	.567	.238	.223	.264	.261	.240	.222	.227	.149	.212	.209	.198
11	.998	1.001	1.001	1.001	1.001	1.001	1.002	1.002	1.003	1.002	1.002	.996	1.003	.999

Upper-flap static-pressure ratio, $p/p_{t,j}$

$y/(w_t/2) = 0.450$ | $y/(w_t/2) = 0.875$

$x/x_{t,u}$ | $x/x_{t,u}$

Pt	$p_{t,j}/p_\infty$	1.008	1.129	1.250	1.316	1.606	1.691	1.008	1.129	1.250	1.316	1.606	1.691
1	1.000	1.000	1.001	1.000	1.000	.998	.999	1.000	1.000	1.000	1.000	1.000	1.000
2	1.996	.242	.262	.417	.439	.567	.548	.243	.262	.390	.482	.566	.501
3	3.005	.241	.262	.241	.229	.426	.490	.242	.264	.244	.229	.424	.333
4	3.986	.240	.262	.241	.229	.210	.190	.241	.262	.244	.228	.203	.250
5	4.985	.239	.261	.241	.227	.206	.190	.240	.261	.243	.227	.207	.200
6	5.999	.238	.261	.239	.227	.207	.190	.238	.260	.241	.226	.207	.167
7	6.962	.237	.260	.239	.226	.207	.189	.237	.259	.240	.226	.207	.144
8	7.982	.236	.260	.239	.226	.207	.189	.236	.258	.240	.226	.207	.125
9	8.980	.236	.259	.239	.226	.207	.190	.236	.258	.241	.227	.207	.112
10	9.973	.235	.259	.239	.226	.207	.190	.235	.256	.240	.227	.207	.101
11	.998	1.003	1.002	1.002	1.002	1.000	1.001	1.002	1.002	1.001	1.002	1.002	1.001

TABLE III.- Continued

(e) Continued

Lower-flap static-pressure ratio, $p/p_{t,j}$

$y/(w_t/2) = 0.000$

Pt	$p_{t,j}/p_\infty$	$x/x_{t,l}$ = 0.881	0.941	1.001	1.019	1.049	1.079	1.121	1.157	1.199	1.259	1.319
1	1.000	.998	1.000	.998	1.000	1.000	1.000	1.000	1.001	.999	1.000	1.000
2	1.996	.843	.735	.542	.471	.425	.420	.393	.349	.315	.480	.485
3	3.005	.844	.733	.541	.470	.425	.419	.392	.350	.302	.228	.186
4	3.986	.844	.734	.541	.471	.423	.417	.392	.347	.300	.229	.186
5	4.985	.843	.734	.540	.472	.423	.416	.391	.346	.301	.228	.186
6	5.999	.844	.734	.540	.472	.422	.415	.391	.344	.300	.228	.186
7	6.962	.844	.734	.539	.472	.422	.415	.392	.345	.300	.228	.185
8	7.982	.844	.733	.538	.472	.422	.416	.392	.345	.300	.228	.185
9	8.980	.844	.733	.538	.472	.422	.416	.392	.345	.300	.228	.184
10	9.973	.844	.733	.538	.472	.422	.416	.392	.345	.301	.228	.184
11	.998	1.005	1.000	1.003	1.001	1.002	1.002	1.002	1.002	1.004	1.002	1.003

TABLE III.- Continued

(e) Concluded

		Lower-flap static-pressure ratio, $p/p_{t,j}$									
		$x/x_{t,l}$ = 1.001					$x/x_{t,l}$ = 1.121				
		$y/(w_t/2)$					$y/(w_t/2)$				
Pt	$p_{t,j}/p_\infty$	0.250	0.500	0.750	0.875	0.950	0.250	0.500	0.750	0.875	0.950
1	1.000	1.000	1.013	1.001	1.000	1.000	.999	1.000	1.000	.999	1.000
2	1.996	.549	.552	.552	.544	.530	.391	.389	.391	.391	.391
3	3.005	.546	.546	.550	.541	.527	.389	.389	.388	.390	.391
4	3.986	.545	.544	.550	.540	.528	.387	.387	.386	.388	.389
5	4.985	.545	.542	.550	.541	.529	.387	.386	.386	.388	.389
6	5.999	.544	.541	.549	.540	.528	.387	.387	.385	.389	.389
7	6.962	.544	.540	.549	.541	.527	.387	.387	.385	.389	.389
8	7.982	.544	.539	.549	.541	.527	.387	.387	.385	.389	.389
9	8.980	.545	.539	.549	.542	.537	.387	.388	.386	.385	.388
10	9.973	.545	.538	.548	.539	.528	.387	.387	.389	.391	.386
11	.998	1.001	.989	1.003	1.002	1.002	1.001	1.001	1.002	1.003	1.002

		Lower-flap static-pressure ratio, $p/p_{t,j}$				
		$x/x_{t,l}$ = 1.319				
		$y/(w_t/2)$				
Pt	$p_{t,j}/p_\infty$	0.250	0.500	0.750	0.875	0.950
1	1.000	.998	.999	.999	1.000	.999
2	1.996	.484	.479	.478	.471	.469
3	3.005	.189	.187	.213	.198	.194
4	3.986	.188	.187	.189	.192	.192
5	4.985	.187	.187	.189	.191	.193
6	5.999	.187	.187	.188	.191	.192
7	6.962	.186	.187	.187	.191	.192
8	7.982	.186	.187	.187	.190	.191
9	8.980	.186	.186	.187	.191	.191
10	9.973	.186	.187	.187	.190	.191
11	.998	1.002	1.002	1.002	1.003	1.002

TABLE III.- Continued

(f) Configurations F6, VF1(0), and V1(0)

Upper-flap static-pressure ratio, $p/p_{t,j}$

$y/(w_t/2) = 0.000$

$x/x_{t,u}$

Pt	$p_{t,j}/p_\infty$	0.888	0.954	1.008	1.063	1.129	1.184	1.250	1.316	1.383	1.449	1.522	1.606	1.691
1	1.002	.999	1.000	1.000	.999	1.002	1.000	.998	.998	.998	.998	.997	.998	.991
2	1.507	.791	.573	.386	.465	.492	.512	.543	.576	.607	.633	.654	.673	.676
3	1.759	.791	.571	.244	.228	.272	.434	.507	.603	.628	.625	.616	.614	.602
4	2.014	.792	.569	.245	.228	.258	.266	.421	.451	.549	.593	.578	.562	.542
5	2.515	.792	.568	.245	.228	.260	.262	.241	.368	.412	.456	.515	.524	.492
6	2.518	.792	.568	.245	.228	.260	.262	.241	.367	.411	.456	.515	.524	.493
7	3.027	.794	.568	.246	.228	.262	.264	.241	.229	.236	.388	.427	.491	.466
8	3.538	.792	.567	.246	.228	.263	.264	.241	.229	.234	.227	.256	.389	.451
9	4.047	.792	.567	.246	.228	.263	.264	.241	.228	.234	.227	.216	.206	.326
10	5.044	.792	.567	.245	.228	.263	.263	.240	.227	.233	.227	.215	.207	.192
11	5.059	.791	.566	.245	.228	.263	.263	.240	.227	.233	.227	.215	.207	.192
12	6.068	.791	.567	.244	.227	.263	.262	.240	.226	.232	.227	.216	.205	.193
13	7.093	.790	.567	.243	.226	.263	.262	.240	.225	.231	.226	.216	.205	.193
14	7.071	.791	.567	.243	.226	.263	.262	.240	.225	.231	.226	.216	.205	.193
15	8.081	.790	.567	.243	.225	.263	.262	.239	.225	.230	.226	.215	.205	.193
16	8.100	.790	.567	.243	.225	.263	.262	.239	.225	.230	.226	.215	.205	.194
17	9.115	.790	.567	.243	.225	.263	.262	.239	.224	.229	.226	.215	.205	.193
18	10.138	.790	.568	.242	.224	.263	.262	.239	.224	.227	.226	.215	.205	.194
19	.998	1.002	1.000	1.001	1.001	.999	1.000	1.003	1.002	1.002	1.002	1.003	1.002	1.012

Upper-flap static-pressure ratio, $p/p_{t,j}$

$y/(w_t/2) = 0.450$

$x/x_{t,u}$

Pt	$p_{t,j}/p_\infty$	0.888	0.954	1.008	1.063	1.129	1.184	1.250	1.316	1.383	1.449	1.522	1.606	1.691
1	1.002	1.000	1.002	.998	.999	.999	.999	.999	.999	.999	.998	.999	.997	.997
2	1.507	.793	.582	.429	.471	.491	.508	.534	.571	.605	.635	.660	.677	.683
3	1.759	.795	.580	.241	.228	.277	.434	.503	.603	.627	.622	.614	.611	.599
4	2.014	.793	.579	.242	.229	.260	.262	.416	.465	.571	.588	.567	.555	.538
5	2.515	.793	.578	.242	.228	.259	.259	.239	.336	.415	.483	.524	.508	.479
6	2.518	.793	.578	.242	.229	.259	.259	.239	.332	.415	.482	.524	.508	.480
7	3.027	.793	.578	.243	.230	.263	.264	.243	.231	.238	.385	.443	.501	.443
8	3.538	.793	.577	.243	.229	.263	.264	.243	.231	.238	.235	.233	.395	.453
9	4.047	.793	.577	.242	.229	.263	.263	.242	.231	.238	.235	.216	.204	.346
10	5.044	.793	.577	.241	.229	.262	.262	.242	.232	.236	.234	.216	.203	.185
11	5.059	.793	.577	.241	.229	.262	.262	.242	.232	.236	.234	.216	.203	.185
12	6.068	.793	.577	.240	.228	.260	.260	.245	.227	.239	.235	.215	.203	.185
13	7.093	.792	.577	.239	.228	.259	.258	.240	.233	.237	.234	.214	.203	.185
14	7.071	.792	.577	.239	.228	.259	.259	.240	.233	.237	.235	.214	.203	.185
15	8.081	.792	.577	.238	.227	.259	.258	.239	.233	.237	.234	.214	.203	.185
16	8.100	.792	.577	.238	.227	.259	.258	.239	.233	.237	.234	.214	.203	.185
17	9.115	.792	.577	.238	.227	.259	.258	.239	.232	.237	.234	.213	.203	.185
18	10.138	.791	.577	.238	.227	.259	.258	.239	.232	.237	.235	.214	.203	.185
19	.998	.999	.997	1.002	1.000	1.001	1.001	1.001	1.002	1.002	1.002	1.001	1.001	1.004

TABLE III.- Continued

(f) Continued

Upper-flap static-pressure ratio, $p/p_{t,j}$

$y/(w_t/2) = 0.875$

Pt	$p_{t,j}/p_\infty$	$x/x_{t,u}$ = 0.888	0.954	1.008	1.129	1.184	1.250	1.316	1.383	1.449	1.522	1.606	1.691
1	1.002	1.000	.999	1.000	1.001	.999	.998	1.000	.998	.998	.999	.997	.999
2	1.507	.793	.559	.411	.487	.522	.562	.594	.620	.644	.666	.679	.683
3	1.759	.792	.556	.237	.304	.437	.512	.559	.591	.603	.597	.593	.591
4	2.014	.793	.556	.236	.265	.282	.426	.491	.521	.533	.530	.527	.525
5	2.515	.792	.554	.234	.265	.263	.239	.297	.431	.467	.452	.449	.446
6	2.518	.791	.553	.235	.265	.263	.239	.293	.430	.467	.452	.449	.446
7	3.027	.790	.571	.258	.255	.264	.242	.237	.234	.385	.433	.399	.392
8	3.538	.789	.569	.259	.254	.264	.241	.237	.234	.229	.308	.374	.370
9	4.047	.789	.568	.259	.253	.263	.241	.237	.234	.229	.215	.267	.303
10	5.044	.788	.565	.257	.249	.262	.240	.236	.233	.229	.214	.196	.206
11	5.059	.788	.564	.257	.248	.262	.240	.236	.233	.229	.214	.196	.206
12	6.068	.787	.561	.245	.258	.261	.238	.234	.232	.229	.213	.196	.161
13	7.093	.787	.560	.240	.254	.260	.238	.233	.231	.230	.211	.195	.132
14	7.071	.787	.560	.240	.254	.260	.238	.233	.231	.229	.210	.195	.132
15	8.081	.787	.559	.239	.253	.259	.237	.233	.230	.229	.211	.195	.131
16	8.100	.786	.559	.239	.253	.259	.237	.232	.230	.229	.211	.195	.131
17	9.115	.786	.559	.239	.252	.259	.237	.232	.230	.229	.211	.195	.131
18	10.138	.786	.558	.239	.254	.259	.237	.232	.230	.229	.211	.195	.131
19	.998	1.001	1.001	1.001	1.000	1.001	1.002	1.000	1.002	1.002	1.001	1.003	1.001

Lower-flap static-pressure ratio, $p/p_{t,j}$

$y/(w_t/2) = 0.000$

Pt	$p_{t,j}/p_\infty$	$x/x_{t,l}$ = 0.881	0.947	1.001	1.043	1.079	1.127	1.168
1	1.002	.997	.993	.995	.999	1.001	.999	.999
2	1.507	.841	.693	.534	.439	.433	.416	.581
3	1.759	.840	.693	.529	.434	.423	.375	.514
4	2.014	.841	.693	.529	.434	.425	.376	.334
5	2.515	.840	.694	.528	.434	.425	.375	.334
6	2.518	.840	.694	.528	.434	.425	.375	.334
7	3.027	.841	.693	.528	.434	.424	.374	.334
8	3.538	.841	.693	.528	.434	.423	.373	.334
9	4.047	.841	.693	.528	.433	.423	.372	.334
10	5.044	.841	.691	.528	.433	.422	.370	.333
11	5.059	.841	.691	.528	.433	.422	.370	.333
12	6.068	.841	.691	.527	.432	.422	.369	.333
13	7.093	.841	.690	.527	.432	.421	.369	.333
14	7.071	.841	.690	.528	.432	.421	.369	.333
15	8.081	.841	.689	.528	.432	.422	.369	.333
16	8.100	.842	.689	.528	.432	.422	.369	.333
17	9.115	.842	.689	.527	.431	.422	.369	.333
18	10.138	.842	.688	.527	.431	.422	.369	.333
19	.998	1.003	1.006	1.005	1.001	.999	1.002	1.001

TABLE III.- Concluded

(f) Concluded

Lower-flap static-pressure ratio, $p/p_{t,j}$

$y/(w_t/2) = 0.450$

Pt	$p_{t,j}/p_\infty$	$x/x_{t,l}$ = 0.881	0.947	1.001	1.043	1.079	1.127	1.168
1	1.002	.999	1.000	.999	1.002	.999	.998	.999
2	1.507	.834	.703	.536	.438	.432	.431	.589
3	1.759	.834	.702	.533	.433	.421	.372	.504
4	2.014	.834	.703	.532	.434	.423	.373	.336
5	2.515	.835	.701	.531	.432	.422	.372	.337
6	2.518	.835	.702	.531	.433	.423	.373	.337
7	3.027	.834	.702	.530	.431	.422	.374	.339
8	3.538	.834	.702	.529	.429	.421	.373	.338
9	4.047	.834	.701	.528	.428	.420	.373	.337
10	5.044	.833	.700	.528	.425	.419	.373	.336
11	5.059	.833	.700	.528	.425	.419	.373	.336
12	6.068	.833	.699	.527	.424	.418	.372	.336
13	7.093	.833	.699	.526	.423	.417	.371	.335
14	7.071	.833	.699	.527	.423	.417	.371	.335
15	8.081	.832	.698	.527	.423	.417	.371	.335
16	8.100	.832	.698	.527	.423	.417	.371	.335
17	9.115	.832	.698	.526	.423	.417	.371	.335
18	10.138	.832	.697	.526	.423	.417	.371	.335
19	.998	1.002	1.001	1.002	1.000	1.000	1.002	1.001

Lower-flap static-pressure ratio, $p/p_{t,j}$

$y/(w_t/2) = 0.875$

Pt	$p_{t,j}/p_\infty$	$x/x_{t,l}$ = 0.881	0.947	1.001	1.043	1.079	1.127	1.168
1	1.002	.999	1.000	1.004	1.000	1.001	.999	1.000
2	1.507	.843	.698	.550	.442	.442	.480	.598
3	1.759	.843	.696	.538	.436	.432	.377	.474
4	2.014	.844	.695	.530	.435	.433	.377	.328
5	2.515	.844	.694	.519	.434	.432	.376	.326
6	2.518	.844	.694	.519	.434	.432	.376	.327
7	3.027	.845	.693	.513	.438	.434	.377	.327
8	3.538	.845	.690	.509	.437	.433	.376	.326
9	4.047	.845	.682	.504	.436	.433	.374	.325
10	5.044	.846	.680	.501	.435	.432	.373	.325
11	5.059	.846	.679	.505	.435	.432	.372	.326
12	6.068	.845	.680	.495	.434	.432	.372	.326
13	7.093	.845	.676	.492	.432	.430	.370	.331
14	7.071	.845	.676	.492	.433	.430	.370	.331
15	8.081	.845	.673	.490	.432	.429	.369	.330
16	8.100	.845	.671	.490	.432	.429	.369	.330
17	9.115	.844	.664	.502	.432	.429	.368	.331
18	10.138	.844	.651	.487	.432	.429	.368	.331
19	.998	1.003	1.002	.995	1.001	1.000	1.001	1.000

TABLE IV.- COMPUTER PRINTOUT OF RATIO OF INTERNAL STATIC PRESSURE TO JET TOTAL PRESSURE FOR VECTORED-THRUST SINGLE EXPANSION-RAMP NOZZLES

(a) Configuration VF1(-10)

Upper-flap static-pressure ratio, $p/p_{t,j}$

$y/(w_t/2) = 0.000$

Pt	$p_{t,j}/p_\infty$	$x/x_{t,u}$ = 0.888	0.924	0.966	1.008	1.051	1.087	1.129	1.190	1.250	1.322	1.389	1.449
1	1.000	1.000	1.000	1.000	.999	1.000	1.000	1.000	1.000	.999	1.000	1.000	1.001
2	1.978	.802	.707	.546	.243	.221	.238	.260	.266	.420	.471	.553	.548
3	2.961	.807	.706	.544	.243	.221	.241	.262	.264	.243	.229	.233	.298
4	3.960	.805	.705	.544	.242	.220	.244	.263	.264	.242	.228	.232	.271
5	4.916	.805	.706	.545	.241	.221	.244	.262	.263	.242	.227	.232	.268
6	5.882	.805	.706	.545	.240	.219	.245	.262	.262	.241	.226	.231	.266
7	6.854	.804	.706	.545	.240	.219	.245	.262	.262	.241	.226	.231	.265
8	7.840	.805	.706	.546	.239	.218	.245	.262	.262	.241	.226	.230	.263
9	8.825	.804	.707	.546	.239	.218	.245	.262	.262	.241	.226	.230	.261
10	9.774	.804	.707	.546	.239	.217	.245	.262	.262	.241	.226	.230	.261
11	.999	1.002	1.000	1.002	1.001	1.001	1.001	1.001	1.001	1.001	1.002	1.001	1.003

Upper-flap static-pressure ratio, $p/p_{t,j}$

$y/(w_t/2) = 0.000$ | $x/x_{t,u} = 1.008$

Pt	$p_{t,j}/p_\infty$	$x/x_{t,u}$ = 1.510	1.570	1.630	1.691	1.751	$y/(w_t/2)$ = 0.250	0.500	0.750	0.875	0.950
1	1.000	1.001	1.000	.996	1.000	1.000	1.000	1.000	1.000	1.000	.999
2	1.978	.422	.524	.541	.542	.531	.243	.238	.238	.233	.245
3	2.961	.295	.321	.369	.406	.399	.243	.239	.238	.237	.246
4	3.960	.122	.125	.125	.213	.245	.242	.238	.236	.238	.246
5	4.916	.122	.125	.125	.122	.139	.241	.237	.234	.237	.246
6	5.882	.121	.125	.124	.122	.116	.240	.236	.234	.237	.246
7	6.854	.121	.124	.124	.122	.116	.239	.236	.234	.236	.246
8	7.840	.120	.124	.124	.122	.116	.239	.235	.233	.236	.246
9	8.825	.120	.124	.124	.122	.116	.238	.235	.233	.236	.245
10	9.774	.120	.124	.124	.122	.116	.238	.235	.233	.236	.245
11	.999	1.002	1.001	1.003	1.001	1.002	1.001	1.001	1.001	1.001	1.002

TABLE IV.- Continued

(a) Continued

		Upper-flap static-pressure ratio, $p/p_{t,j}$									
		$x/x_{t,u} = 1.250$					$x/x_{t,u} = 1.691$				
		$y/(w_t/2)$					$y/(w_t/2)$				
Pt	$p_{t,j}/p_\infty$	0.250	0.500	0.750	0.875	0.950	0.250	0.500	0.750	0.875	0.950
1	1.000	1.000	1.000	1.000	1.000	1.000	1.000	1.001	.998	1.002	.999
2	1.978	.418	.420	.422	.437	.427	.547	.545	.538	.526	.520
3	2.961	.242	.241	.247	.249	.246	.417	.415	.379	.361	.353
4	3.960	.242	.240	.248	.248	.246	.219	.229	.252	.260	.255
5	4.916	.241	.239	.247	.247	.246	.124	.123	.173	.205	.211
6	5.882	.241	.239	.246	.246	.245	.124	.123	.134	.167	.181
7	6.854	.241	.239	.246	.246	.245	.124	.123	.113	.142	.154
8	7.840	.241	.239	.247	.246	.245	.123	.123	.113	.120	.130
9	8.825	.241	.239	.247	.246	.245	.123	.123	.112	.100	.114
10	9.774	.241	.239	.247	.246	.245	.123	.123	.112	.089	.103
11	.999	1.001	1.002	1.001	1.001	1.001	1.002	1.002	1.003	1.002	1.001

TABLE IV.- Continued

(a) Concluded

		Lower-flap static-pressure ratio, $p/p_{t,j}$										
		$y/(w_t/2) = 0.000$							$y/(w_t/2) = 0.450$			
		$x/x_{t,l}$							$x/x_{t,l}$			
Pt	$p_{t,j}/p_\infty$	0.881	0.947	1.001	1.043	1.079	1.127	1.168	1.043	1.079	1.127	1.168
1	1.000	1.001	1.001	.998	.999	1.000	.999	.999	1.001	1.000	.999	1.000
2	1.978	.844	.696	.529	.433	.421	.375	.329	.429	.420	.380	.334
3	2.961	.842	.696	.528	.433	.421	.374	.329	.427	.419	.379	.335
4	3.960	.841	.694	.527	.433	.419	.372	.328	.424	.416	.379	.334
5	4.916	.841	.694	.527	.433	.419	.370	.328	.421	.415	.378	.332
6	5.882	.841	.694	.527	.433	.418	.370	.328	.420	.414	.378	.332
7	6.854	.841	.693	.527	.433	.418	.369	.328	.420	.414	.378	.332
8	7.840	.842	.693	.527	.433	.418	.369	.328	.420	.414	.378	.332
9	8.825	.842	.692	.527	.433	.419	.369	.329	.419	.414	.378	.332
10	9.774	.842	.692	.527	.433	.419	.369	.329	.420	.414	.378	.332
11	.999	1.001	1.000	1.002	1.001	1.001	1.001	1.001	1.002	1.001	1.001	1.001

		Lower-flap static-pressure ratio, $p/p_{t,j}$		
		$y/(w_t/2) = 0.875$		
		$x/x_{t,l}$		
Pt	$p_{t,j}/p_\infty$	1.043	1.079	1.127
1	1.000	1.000	1.000	.999
2	1.978	.435	.429	.383
3	2.961	.436	.428	.381
4	3.960	.435	.426	.378
5	4.916	.434	.425	.378
6	5.882	.436	.425	.377
7	6.854	.437	.425	.376
8	7.840	.437	.425	.376
9	8.825	.437	.425	.376
10	9.774	.437	.424	.376
11	.999	1.001	1.000	1.001

TABLE IV.- Continued

(b) Configuration VF1(-5)

Upper-flap static-pressure ratio, $p/p_{t,j}$

		$y/(w_t/2) = 0.000$											
		$x/x_{t,u}$											
Pt	$p_{t,j}/p_\infty$	0.888	0.924	0.966	1.008	1.051	1.087	1.129	1.190	1.250	1.322	1.389	1.449
1	1.000	1.001	1.000	1.001	1.000	1.000	1.001	1.000	1.001	1.001	1.001	1.000	1.002
2	1.970	.803	.707	.546	.243	.221	.238	.261	.276	.424	.470	.562	.565
3	2.941	.807	.706	.544	.243	.220	.241	.262	.265	.243	.228	.233	.336
4	3.928	.805	.706	.544	.243	.220	.244	.263	.264	.242	.227	.232	.224
5	4.919	.805	.706	.544	.241	.220	.245	.263	.264	.242	.226	.232	.223
6	5.889	.805	.706	.545	.240	.219	.245	.262	.263	.241	.226	.231	.222
7	6.933	.805	.706	.545	.239	.218	.245	.262	.263	.241	.225	.231	.222
8	6.858	.804	.706	.545	.239	.218	.245	.262	.263	.241	.225	.231	.222
9	7.832	.805	.707	.545	.239	.217	.245	.262	.262	.241	.225	.231	.222
10	8.795	.804	.707	.546	.239	.217	.245	.262	.262	.241	.225	.231	.222
11	9.770	.804	.707	.546	.239	.217	.245	.262	.262	.241	.225	.231	.222
12	.999	1.001	.999	1.000	1.000	1.000	1.000	1.001	1.001	1.001	1.002	1.002	.999

Upper-flap static-pressure ratio, $p/p_{t,j}$

		$y/(w_t/2) = 0.000$					$x/x_{t,u} = 1.008$				
		$x/x_{t,u}$					$y/(w_t/2)$				
Pt	$p_{t,j}/p_\infty$	1.510	1.570	1.630	1.691	1.751	0.250	0.500	0.750	0.875	0.950
1	1.000	.999	1.000	1.002	1.000	1.000	1.000	1.000	1.000	.999	.999
2	1.970	.532	.548	.551	.546	.531	.243	.238	.236	.235	.246
3	2.941	.391	.433	.467	.453	.400	.243	.239	.236	.238	.246
4	3.928	.170	.163	.161	.274	.309	.242	.238	.236	.239	.246
5	4.919	.168	.163	.161	.154	.140	.241	.237	.236	.239	.246
6	5.889	.167	.162	.160	.153	.140	.240	.236	.235	.238	.247
7	6.933	.167	.162	.160	.154	.140	.239	.236	.235	.238	.246
8	6.858	.167	.162	.160	.154	.140	.239	.236	.235	.238	.246
9	7.832	.166	.163	.160	.154	.140	.239	.235	.235	.237	.246
10	8.795	.166	.162	.160	.154	.140	.238	.235	.234	.236	.245
11	9.770	.166	.162	.160	.154	.140	.238	.235	.234	.236	.245
12	.999	.999	1.001	1.000	1.000	1.000	1.001	1.000	1.001	1.000	1.000

TABLE IV.- Continued

(b) Continued

Upper-flap static-pressure ratio, $p/p_{t,j}$

		$x/x_{t,u} = 1.250$					$x/x_{t,u} = 1.691$				
		$y/(w_t/2)$					$y/(w_t/2)$				
Pt	$p_{t,j}/p_\infty$	0.250	0.500	0.750	0.875	0.950	0.250	0.500	0.750	0.875	0.950
1	1.000	1.000	1.000	1.000	1.000	1.000	.999	1.001	1.000	.997	1.000
2	1.970	.421	.424	.426	.442	.435	.542	.546	.539	.531	.522
3	2.941	.242	.241	.247	.251	.250	.449	.434	.413	.387	.364
4	3.928	.242	.240	.248	.250	.251	.279	.300	.312	.293	.277
5	4.919	.241	.239	.247	.248	.248	.152	.155	.173	.207	.214
6	5.889	.241	.238	.247	.248	.248	.152	.155	.137	.168	.177
7	6.933	.241	.238	.247	.247	.248	.151	.155	.136	.133	.146
8	6.858	.241	.238	.247	.247	.248	.151	.155	.136	.135	.148
9	7.832	.241	.238	.247	.247	.248	.151	.155	.136	.113	.130
10	8.795	.241	.238	.247	.248	.248	.151	.155	.137	.105	.115
11	9.770	.241	.238	.248	.247	.248	.151	.155	.136	.103	.102
12	.999	1.001	1.000	1.000	1.001	1.001	1.001	1.002	1.001	.998	1.002

TABLE IV.- Continued

(b) Concluded

Lower-flap static-pressure ratio, $p/p_{t,j}$

Pt	$p_{t,j}/p_\infty$	$y/(w_t/2) = 0.000$; $x/x_{t,l}$ = 0.881	0.947	1.001	1.043	1.079	1.127	1.168	$y/(w_t/2) = 0.450$; $x/x_{t,l}$ = 1.043	1.079	1.127	1.168
1	1.000	1.000	1.001	.999	1.000	1.001	1.001	1.000	1.001	1.000	.999	1.000
2	1.970	.843	.696	.529	.433	.421	.376	.329	.428	.421	.380	.334
3	2.941	.842	.696	.528	.433	.421	.374	.329	.427	.420	.379	.335
4	3.928	.841	.695	.527	.433	.419	.372	.328	.423	.417	.379	.333
5	4.919	.841	.694	.527	.433	.419	.370	.328	.421	.416	.378	.332
6	5.889	.841	.694	.527	.433	.418	.369	.328	.420	.415	.378	.331
7	6.933	.841	.693	.526	.433	.418	.369	.328	.419	.415	.378	.331
8	6.858	.841	.693	.527	.433	.418	.369	.328	.419	.415	.378	.331
9	7.832	.842	.693	.527	.433	.418	.369	.328	.419	.415	.378	.331
10	8.795	.842	.692	.527	.433	.419	.369	.329	.419	.415	.378	.331
11	9.770	.842	.692	.527	.433	.419	.369	.329	.419	.415	.378	.331
12	.999	.998	.999	1.002	1.000	1.001	1.000	1.001	1.000	1.000	1.001	1.000

Lower-flap static-pressure ratio, $p/p_{t,j}$

Pt	$p_{t,j}/p_\infty$	$y/(w_t/2) = 0.875$; $x/x_{t,l}$ = 1.043	1.079	1.127
1	1.000	1.001	1.001	1.001
2	1.970	.437	.429	.382
3	2.941	.438	.428	.381
4	3.928	.436	.426	.378
5	4.919	.436	.425	.377
6	5.889	.437	.425	.376
7	6.933	.437	.425	.376
8	6.858	.437	.425	.376
9	7.832	.437	.425	.376
10	8.795	.437	.425	.376
11	9.770	.437	.425	.376
12	.999	1.000	.999	1.000

TABLE IV.- Continued

(c) Configuration VF1(5)

Upper-flap static-pressure ratio, $p/p_{t,j}$

		$y/(w_t/2) = 0.000$											
		$x/x_{t,u}$											
Pt	$p_{t,j}/p_\infty$	0.888	0.924	0.966	1.008	1.051	1.087	1.129	1.190	1.250	1.322	1.389	1.449
1	.999	1.001	1.001	1.001	1.000	1.002	1.001	1.000	1.000	1.000	.998	1.000	1.000
2	1.977	.803	.709	.546	.243	.222	.239	.260	.359	.434	.505	.578	.618
3	2.972	.807	.708	.544	.243	.220	.242	.263	.265	.242	.230	.388	.412
4	3.955	.805	.707	.545	.242	.220	.245	.263	.264	.242	.227	.232	.238
5	4.924	.805	.707	.545	.241	.220	.245	.262	.264	.241	.226	.232	.237
6	5.904	.805	.708	.545	.240	.218	.245	.262	.263	.241	.226	.231	.236
7	6.905	.805	.708	.545	.240	.217	.245	.262	.263	.241	.226	.231	.235
8	6.888	.805	.708	.545	.240	.217	.245	.262	.263	.241	.226	.231	.236
9	7.871	.805	.708	.546	.239	.217	.245	.262	.263	.241	.226	.231	.236
10	8.841	.805	.708	.546	.239	.216	.245	.262	.263	.241	.226	.231	.235
11	8.860	.805	.708	.546	.239	.216	.245	.262	.263	.241	.226	.231	.235
12	9.909	.805	.709	.546	.239	.216	.245	.262	.262	.241	.225	.231	.235
13	9.842	.804	.708	.546	.238	.216	.245	.262	.262	.241	.225	.231	.235
14	1.000	1.001	.999	1.000	1.000	.999	1.000	1.001	1.002	1.001	1.003	1.000	1.002

Upper-flap static-pressure ratio, $p/p_{t,j}$

		$y/(w_t/2) = 0.000$					$x/x_{t,u} = 1.008$				
		$x/x_{t,u}$					$y/(w_t/2)$				
Pt	$p_{t,j}/p_\infty$	1.510	1.570	1.630	1.691	1.751	0.250	0.500	0.750	0.875	0.950
1	.999	.998	1.001	1.008	.999	1.001	1.000	1.000	.999	1.001	.998
2	1.977	.618	.606	.584	.567	.548	.243	.239	.237	.230	.285
3	2.972	.455	.503	.498	.462	.427	.244	.239	.237	.231	.285
4	3.955	.265	.260	.407	.473	.482	.242	.238	.236	.229	.282
5	4.924	.264	.259	.243	.225	.194	.241	.237	.235	.230	.282
6	5.904	.263	.259	.244	.225	.194	.240	.236	.233	.229	.282
7	6.905	.263	.258	.243	.225	.194	.240	.236	.233	.228	.278
8	6.888	.263	.258	.242	.225	.194	.240	.236	.233	.227	.277
9	7.871	.263	.259	.242	.225	.194	.239	.235	.233	.227	.277
10	8.841	.262	.259	.243	.226	.195	.239	.235	.233	.226	.275
11	8.860	.263	.259	.243	.226	.195	.239	.235	.233	.226	.274
12	9.909	.262	.259	.243	.226	.195	.239	.235	.233	.226	.274
13	9.842	.262	.259	.243	.226	.195	.239	.235	.232	.227	.273
14	1.000	1.001	1.002	.996	1.000	1.000	1.001	1.000	1.000	1.000	1.001

TABLE IV.- Continued

(c) Continued

		Upper-flap static-pressure ratio, $p/p_{t,j}$									
		$x/x_{t,u} = 1.250$					$x/x_{t,u} = 1.691$				
		$y/(w_t/2)$					$y/(w_t/2)$				
Pt	$p_{t,j}/p_\infty$	0.250	0.500	0.750	0.875	0.950	0.250	0.500	0.750	0.875	0.950
1	.999	1.000	.999	1.000	1.000	.999	1.002	.999	1.000	1.002	1.002
2	1.977	.435	.430	.448	.446	.442	.569	.564	.555	.541	.531
3	2.972	.242	.245	.247	.248	.246	.458	.434	.398	.371	.354
4	3.955	.242	.244	.247	.248	.246	.475	.467	.430	.380	.342
5	4.924	.241	.243	.247	.247	.247	.221	.218	.213	.218	.216
6	5.904	.241	.243	.247	.247	.247	.222	.217	.186	.176	.178
7	6.905	.241	.243	.247	.246	.247	.222	.217	.186	.137	.146
8	6.888	.241	.243	.247	.246	.247	.222	.218	.186	.137	.147
9	7.871	.241	.243	.248	.247	.247	.222	.218	.186	.137	.122
10	8.841	.241	.242	.248	.247	.247	.222	.218	.186	.137	.099
11	8.860	.241	.242	.248	.247	.247	.222	.218	.186	.137	.098
12	9.909	.241	.242	.248	.247	.247	.222	.218	.186	.137	.086
13	9.842	.241	.242	.248	.247	.247	.222	.218	.186	.137	.086
14	1.000	1.000	1.002	1.002	1.001	1.001	1.000	1.000	1.000	1.001	1.000

TABLE IV.- Continued

(c) Concluded

		Lower-flap static-pressure ratio, $p/p_{t,j}$										
		$y/(w_t/2) = 0.000$							$y/(w_t/2) = 0.450$			
		$x/x_{t,l}$							$x/x_{t,l}$			
Pt	$p_{t,j}/p_\infty$	0.881	0.947	1.001	1.043	1.079	1.127	1.168	1.043	1.079	1.127	1.168
1	.999	.996	1.002	.998	1.000	1.003	1.000	1.001	1.000	.998	1.000	.999
2	1.977	.841	.697	.529	.433	.423	.376	.330	.432	.422	.381	.334
3	2.972	.841	.697	.528	.433	.422	.374	.330	.430	.420	.380	.335
4	3.955	.841	.695	.528	.433	.419	.372	.329	.427	.418	.380	.334
5	4.924	.841	.694	.527	.433	.418	.371	.329	.425	.417	.380	.333
6	5.904	.841	.694	.527	.433	.418	.370	.328	.424	.417	.380	.332
7	6.905	.842	.693	.527	.433	.418	.370	.328	.423	.416	.379	.332
8	6.888	.842	.693	.527	.433	.418	.370	.328	.423	.416	.379	.332
9	7.871	.842	.692	.527	.433	.418	.369	.329	.423	.416	.379	.332
10	8.841	.842	.692	.527	.432	.419	.370	.329	.423	.416	.380	.332
11	8.860	.843	.692	.527	.432	.419	.370	.329	.423	.416	.380	.332
12	9.909	.843	.692	.527	.432	.419	.370	.329	.423	.416	.379	.332
13	9.842	.843	.691	.527	.432	.419	.369	.329	.423	.416	.380	.332
14	1.000	1.006	1.000	1.003	1.000	.997	1.001	1.000	1.002	1.001	1.001	1.002

		Lower-flap static-pressure ratio, $p/p_{t,j}$		
		$y/(w_t/2) = 0.875$		
		$x/x_{t,l}$		
Pt	$p_{t,j}/p_\infty$	1.043	1.079	1.127
1	.999	1.000	1.001	.999
2	1.977	.435	.428	.382
3	2.972	.434	.427	.381
4	3.955	.433	.425	.378
5	4.924	.432	.424	.377
6	5.904	.432	.425	.375
7	6.905	.431	.424	.378
8	6.888	.432	.423	.376
9	7.671	.431	.423	.376
10	8.841	.431	.423	.376
11	8.860	.431	.422	.376
12	9.909	.431	.423	.376
13	9.842	.431	.423	.376
14	1.000	1.001	.999	1.000

TABLE IV.- Continued

(d) Configuration VF1(10)

Upper-flap static-pressure ratio, $p/p_{t,j}$

		$y/(w_t/2) = 0.000$											
		$x/x_{t,u}$											
Pt	$p_{t,j}/p_\infty$	0.888	0.924	0.966	1.008	1.051	1.087	1.129	1.190	1.250	1.322	1.389	1.449
1	1.000	1.001	1.000	1.000	1.000	1.001	1.001	1.000	1.000	1.000	.999	1.000	1.000
2	2.314	.803	.707	.544	.243	.221	.239	.260	.266	.416	.441	.482	.533
3	1.966	.803	.707	.545	.243	.221	.238	.275	.434	.447	.505	.582	.630
4	2.934	.807	.706	.543	.242	.220	.241	.262	.265	.242	.379	.413	.434
5	2.956	.806	.706	.544	.242	.220	.241	.262	.265	.242	.375	.412	.433
6	3.931	.805	.705	.544	.242	.219	.244	.263	.264	.242	.227	.232	.288
7	4.906	.805	.706	.544	.241	.220	.245	.262	.263	.242	.226	.231	.284
8	5.854	.805	.706	.545	.240	.219	.245	.262	.263	.241	.226	.231	.283
9	5.859	.805	.706	.545	.240	.219	.245	.261	.263	.241	.226	.231	.283
10	6.837	.804	.706	.545	.239	.218	.245	.261	.263	.241	.225	.231	.283
11	7.801	.804	.706	.546	.239	.217	.245	.261	.262	.241	.225	.231	.282
12	7.805	.804	.706	.545	.239	.217	.245	.261	.262	.241	.225	.231	.282
13	8.834	.804	.707	.546	.239	.217	.245	.262	.262	.241	.225	.231	.282
14	8.799	.804	.707	.546	.239	.217	.245	.262	.262	.241	.225	.231	.281
15	8.764	.804	.707	.546	.239	.217	.245	.262	.262	.241	.225	.231	.281
16	9.712	.804	.707	.546	.239	.217	.245	.262	.262	.241	.225	.231	.281
17	9.726	.804	.707	.546	.239	.216	.245	.262	.262	.241	.225	.231	.281
18	9.734	.804	.707	.546	.239	.217	.245	.262	.262	.241	.225	.231	.281
19	.999	.998	1.000	1.001	1.000	1.000	1.000	1.001	1.001	1.002	1.002	1.002	1.002

Upper-flap static-pressure ratio, $p/p_{t,j}$

		$y/(w_t/2) = 0.000$					$x/x_{t,u} = 1.008$				
		$x/x_{t,u}$					$y/(w_t/2)$				
Pt	$p_{t,j}/p_\infty$	1.510	1.570	1.630	1.691	1.751	0.250	0.500	0.750	0.875	0.950
1	1.000	.999	.997	1.008	.998	.999	1.000	1.000	1.000	1.000	1.000
2	2.314	.581	.597	.578	.542	.503	.243	.239	.238	.236	.258
3	1.966	.643	.632	.612	.584	.556	.243	.239	.238	.235	.257
4	2.934	.488	.536	.532	.506	.484	.243	.239	.238	.237	.252
5	2.956	.486	.535	.529	.498	.482	.243	.239	.238	.237	.251
6	3.931	.367	.497	.550	.545	.492	.242	.238	.237	.238	.260
7	4.906	.325	.314	.303	.258	.224	.241	.237	.234	.238	.254
8	5.854	.325	.314	.303	.259	.224	.240	.236	.234	.237	.251
9	5.859	.325	.314	.303	.259	.224	.240	.236	.234	.238	.251
10	6.837	.325	.314	.303	.258	.224	.239	.236	.233	.238	.250
11	7.801	.325	.314	.303	.259	.224	.239	.235	.233	.237	.249
12	7.805	.324	.314	.303	.259	.224	.239	.235	.233	.237	.248
13	8.834	.325	.314	.303	.260	.225	.238	.235	.233	.237	.249
14	8.799	.325	.315	.303	.260	.225	.238	.235	.233	.237	.248
15	8.764	.325	.314	.303	.260	.225	.238	.235	.233	.237	.248
16	9.712	.325	.314	.303	.260	.225	.238	.235	.233	.237	.248
17	9.726	.325	.314	.303	.260	.225	.238	.235	.233	.237	.247
18	9.734	.325	.315	.303	.260	.225	.238	.235	.233	.237	.245
19	.999	1.002	1.001	.997	1.001	1.002	1.001	1.000	1.001	1.000	1.000

TABLE IV.- Continued

(d) Continued

		Upper-flap static-pressure ratio, $p/p_{t,j}$									
		$x/x_{t,u} = 1.250$					$x/x_{t,u} = 1.691$				
		$y/(w_t/2)$					$y/(w_t/2)$				
Pt	$p_{t,j}/p_\infty$	0.250	0.500	0.750	0.875	0.950	0.250	0.500	0.750	0.875	0.950
1	1.000	1.001	1.000	1.001	1.000	1.000	1.002	.999	1.000	1.001	1.002
2	2.314	.416	.412	.393	.378	.343	.542	.527	.510	.495	.474
3	1.966	.469	.444	.461	.467	.455	.584	.575	.567	.559	.544
4	2.934	.242	.243	.248	.246	.252	.501	.471	.431	.419	.402
5	2.956	.242	.243	.249	.246	.250	.494	.462	.415	.405	.391
6	3.931	.242	.242	.249	.246	.243	.545	.520	.463	.417	.362
7	4.906	.242	.241	.247	.245	.234	.259	.254	.241	.238	.235
8	5.854	.241	.240	.246	.246	.248	.259	.252	.206	.184	.189
9	5.859	.241	.240	.247	.246	.247	.259	.252	.207	.183	.189
10	6.837	.241	.240	.248	.247	.242	.259	.253	.207	.153	.150
11	7.801	.241	.240	.247	.247	.241	.258	.254	.207	.151	.110
12	7.805	.241	.239	.248	.247	.242	.258	.254	.207	.151	.109
13	8.834	.241	.239	.249	.248	.240	.259	.255	.207	.151	.098
14	8.799	.241	.239	.249	.248	.245	.259	.256	.208	.154	.099
15	8.764	.241	.239	.248	.248	.243	.259	.256	.207	.153	.098
16	9.712	.241	.240	.247	.247	.244	.260	.256	.207	.152	.098
17	9.726	.241	.239	.248	.247	.245	.260	.257	.207	.152	.097
18	9.734	.241	.239	.249	.247	.246	.260	.257	.207	.152	.096
19	.999	1.001	1.001	1.001	1.000	1.002	.998	1.000	1.000	1.003	1.000

TABLE IV.- Continued

(d) Concluded

Lower-flap static-pressure ratio, $p/p_{t,j}$

Pt	$p_{t,j}/p_\infty$	$y/(w_t/2) = 0.000$; $x/x_{t,1}$ = 0.881	0.947	1.001	1.043	1.079	1.127	1.168	$y(w_t/2) = 0.450$; $x/x_{t,1}$ = 1.043	1.079	1.127	1.168
1	1.000	.997	1.000	.999	1.001	1.001	1.001	1.001	1.000	.999	.999	1.000
2	2.314	.841	.696	.529	.434	.424	.376	.330	.427	.422	.379	.334
3	1.966	.842	.696	.530	.433	.422	.376	.330	.427	.422	.379	.334
4	2.934	.841	.696	.528	.433	.422	.375	.329	.425	.420	.379	.335
5	2.956	.841	.696	.528	.433	.422	.375	.329	.425	.420	.379	.335
6	3.931	.841	.694	.527	.433	.420	.373	.328	.422	.418	.378	.333
7	4.906	.841	.694	.527	.433	.419	.372	.328	.420	.418	.378	.332
8	5.854	.841	.693	.527	.433	.419	.371	.328	.418	.417	.378	.331
9	5.859	.841	.693	.527	.433	.419	.371	.328	.418	.417	.378	.332
10	6.837	.841	.693	.527	.433	.418	.371	.329	.418	.416	.378	.332
11	7.801	.842	.692	.527	.433	.419	.371	.329	.418	.416	.378	.332
12	7.805	.842	.692	.527	.433	.418	.371	.329	.418	.416	.378	.331
13	8.834	.842	.692	.527	.433	.419	.371	.329	.418	.416	.378	.332
14	8.799	.842	.692	.527	.433	.419	.371	.329	.418	.416	.378	.332
15	8.764	.842	.692	.527	.433	.419	.371	.329	.418	.416	.378	.332
16	9.712	.842	.692	.527	.433	.419	.371	.329	.418	.416	.378	.332
17	9.726	.842	.692	.527	.433	.419	.371	.329	.418	.416	.378	.332
18	9.734	.842	.692	.527	.433	.419	.371	.329	.418	.416	.378	.332
19	.999	1.006	1.002	1.003	1.001	1.001	1.000	1.000	1.000	1.001	1.001	1.000

Lower-flap static-pressure ratio, $p/p_{t,j}$

Pt	$p_{t,j}/p_\infty$	$y/(w_t/2) = 0.875$; $x/x_{t,1}$ = 1.043	1.079	1.127
1	1.000	1.000	1.000	1.001
2	2.314	.441	.429	.381
3	1.966	.440	.429	.381
4	2.934	.439	.427	.380
5	2.956	.439	.427	.380
6	3.931	.436	.426	.377
7	4.906	.434	.426	.376
8	5.854	.434	.424	.377
9	5.859	.434	.423	.376
10	6.837	.435	.424	.375
11	7.801	.434	.423	.375
12	7.805	.433	.423	.375
13	8.834	.434	.423	.375
14	8.799	.433	.424	.374
15	8.764	.434	.424	.376
16	9.712	.434	.424	.377
17	9.726	.434	.424	.376
18	9.734	.434	.425	.375
19	.999	1.001	1.001	1.000

TABLE IV.- Continued

(e) Configuration VF1(20)

Upper-flap static-pressure ratio, $p/p_{t,j}$

$y/(w_t/2) = 0.000$

$x/x_{t,u}$

Pt	$p_{t,j}/p_\infty$	0.888	0.924	0.966	1.008	1.051	1.087	1.129	1.190	1.250	1.322	1.389	1.449
1	1.000	1.001	1.000	1.000	.999	1.000	1.000	.999	1.000	1.000	.999	1.000	.999
2	1.971	.803	.706	.545	.243	.224	.259	.390	.448	.484	.538	.588	.626
3	2.933	.807	.705	.544	.242	.220	.241	.262	.265	.395	.429	.443	.465
4	3.930	.805	.705	.544	.241	.219	.244	.263	.264	.242	.349	.402	.421
5	4.918	.804	.705	.544	.241	.220	.244	.262	.263	.242	.226	.231	.382
6	4.908	.804	.705	.544	.241	.219	.244	.262	.263	.241	.226	.231	.382
7	5.886	.805	.706	.545	.240	.219	.244	.261	.263	.241	.225	.230	.380
8	5.862	.804	.706	.545	.240	.219	.244	.261	.263	.241	.225	.230	.380
9	6.824	.804	.706	.545	.239	.218	.244	.261	.263	.241	.225	.230	.381
10	6.844	.804	.706	.545	.239	.218	.244	.261	.263	.241	.225	.230	.381
11	7.814	.804	.706	.545	.239	.217	.244	.261	.262	.241	.225	.230	.382
12	7.811	.804	.706	.545	.239	.217	.244	.261	.262	.241	.225	.230	.382
13	8.803	.804	.706	.546	.239	.217	.245	.261	.262	.241	.225	.230	.383
14	1.000	.998	.999	1.000	1.000	1.000	1.000	1.000	1.001	1.000	1.000	1.000	.999

Upper-flap static-pressure ratio, $p/p_{t,j}$

$y/(w_t/2) = 0.000$ | $x/x_{t,u} = 1.008$

$x/x_{t,u}$ | $y/(w_t/2)$

Pt	$p_{t,j}/p_\infty$	1.510	1.570	1.630	1.691	1.751	0.250	0.500	0.750	0.875	0.950
1	1.000	.997	1.000	1.004	1.000	1.000	1.000	1.000	.999	1.000	.999
2	1.971	.655	.665	.646	.615	.569	.243	.239	.238	.234	.243
3	2.933	.516	.581	.592	.565	.502	.243	.239	.238	.236	.242
4	3.930	.470	.537	.566	.537	.464	.242	.238	.235	.236	.242
5	4.918	.470	.510	.555	.547	.494	.240	.237	.234	.236	.243
6	4.908	.471	.513	.556	.547	.493	.240	.237	.234	.236	.243
7	5.886	.467	.462	.397	.338	.280	.239	.236	.234	.236	.244
8	5.862	.467	.463	.397	.338	.280	.239	.236	.234	.236	.244
9	6.824	.468	.463	.397	.338	.280	.239	.236	.233	.235	.244
10	6.844	.468	.463	.397	.338	.281	.239	.236	.233	.235	.244
11	7.814	.470	.464	.398	.338	.280	.238	.235	.233	.235	.245
12	7.811	.470	.464	.398	.338	.280	.238	.235	.233	.235	.245
13	8.803	.471	.465	.398	.338	.281	.238	.235	.233	.235	.247
14	1.000	1.001	1.000	.999	1.000	1.001	.999	1.000	1.000	.999	1.000

TABLE IV.- Continued

(e) Continued

Upper-flap static-pressure ratio, $p/p_{t,j}$

		$x/x_{t,u} = 1.250$					$x/x_{t,u} = 1.691$				
		$y/(w_t/2)$					$y/(w_t/2)$				
Pt	$p_{t,j}/p_\infty$	0.250	0.500	0.750	0.875	0.950	0.250	0.500	0.750	0.875	0.950
1	1.000	1.000	.999	.996	.999	.999	1.002	.999	1.000	1.002	1.002
2	1.971	.501	.496	.495	.498	.501	.619	.609	.594	.580	.560
3	2.933	.395	.394	.356	.317	.282	.566	.549	.514	.473	.434
4	3.930	.242	.239	.247	.248	.248	.536	.519	.448	.373	.323
5	4.918	.241	.238	.247	.247	.248	.549	.534	.475	.431	.389
6	4.908	.241	.238	.247	.247	.248	.549	.534	.476	.431	.388
7	5.886	.241	.238	.246	.247	.247	.336	.321	.272	.216	.216
8	5.862	.241	.238	.247	.247	.247	.336	.322	.272	.216	.217
9	6.824	.240	.238	.246	.246	.247	.336	.322	.252	.195	.151
10	6.844	.241	.238	.247	.246	.247	.336	.322	.252	.195	.150
11	7.814	.241	.238	.247	.246	.247	.337	.322	.252	.184	.130
12	7.811	.241	.238	.247	.246	.247	.337	.322	.252	.184	.130
13	8.803	.241	.238	.247	.246	.246	.336	.322	.252	.185	.128
14	1.000	1.000	1.000	.999	1.000	1.000	.999	1.000	1.000	1.002	1.001

TABLE IV.- Continued

(e) Concluded

Lower-flap static-pressure ratio, $p/p_{t,j}$

Pt	$p_{t,j}/p_\infty$	$y/(w_t/2) = 0.000$; $x/x_{t,l}$ = 0.881	0.947	1.001	1.043	1.079	1.127	1.168	$y/(w_t/2) = 0.450$; $x/x_{t,l}$ = 1.043	1.079	1.127	1.168
1	1.000	.997	.999	1.000	.999	1.000	.999	1.000	1.001	.999	.999	1.000
2	1.971	.841	.695	.529	.432	.421	.375	.330	.429	.420	.380	.334
3	2.933	.841	.695	.528	.432	.421	.374	.329	.427	.418	.379	.335
4	3.930	.841	.694	.527	.432	.419	.372	.328	.424	.416	.379	.334
5	4.918	.841	.694	.527	.433	.418	.370	.328	.421	.415	.378	.333
6	4.908	.841	.694	.527	.432	.418	.370	.328	.422	.415	.378	.333
7	5.886	.841	.693	.527	.432	.418	.369	.328	.421	.415	.378	.332
8	5.862	.841	.693	.527	.432	.418	.369	.328	.421	.415	.378	.332
9	6.824	.841	.692	.527	.432	.418	.369	.328	.420	.414	.378	.332
10	6.844	.841	.693	.527	.433	.418	.369	.328	.420	.414	.378	.332
11	7.814	.842	.692	.527	.433	.418	.369	.329	.420	.414	.378	.332
12	7.811	.842	.692	.527	.433	.418	.369	.329	.420	.414	.378	.332
13	8.803	.842	.692	.527	.433	.419	.369	.329	.420	.414	.378	.332
14	1.000	1.002	1.000	1.000	.999	.999	.999	1.000	1.001	1.000	1.000	1.000

Lower-flap static-pressure ratio, $p/p_{t,j}$

Pt	$p_{t,j}/p_\infty$	$y/(w_t/2) = 0.875$; $x/x_{t,l}$ = 1.043	1.079	1.127
1	1.000	1.000	1.000	1.000
2	1.971	.439	.430	.383
3	2.933	.439	.428	.381
4	3.930	.438	.426	.379
5	4.918	.437	.426	.378
6	4.908	.437	.426	.378
7	5.886	.437	.425	.377
8	5.862	.437	.425	.377
9	6.824	.437	.425	.377
10	6.844	.437	.425	.377
11	7.814	.437	.425	.377
12	7.811	.436	.425	.377
13	8.803	.436	.425	.377
14	1.000	1.000	1.000	1.000

TABLE IV.- Continued

(f) Configuration V1(-10)

		Upper-flap static-pressure ratio, $p/p_{t,j}$											
		$y/(w_t/2) = 0.000$											
		$x/x_{t,u}$											
pt	$p_{t,j}/p_\infty$	0.888	0.924	0.966	1.008	1.051	1.087	1.129	1.190	1.250	1.322	1.389	1.449
1	.999	1.002	1.002	1.001	1.001	1.001	1.001	1.000	1.001	1.001	1.000	1.002	1.000
2	1.994	.781	.688	.519	.359	.194	.226	.271	.342	.403	.428	.454	.489
3	2.988	.779	.685	.514	.357	.151	.151	.173	.189	.207	.208	.342	.384
4	3.975	.774	.683	.511	.355	.151	.152	.174	.189	.204	.207	.202	.203
5	4.961	.773	.683	.508	.354	.151	.152	.175	.189	.200	.206	.201	.203
6	5.973	.772	.682	.507	.354	.151	.152	.175	.188	.197	.206	.201	.202
7	5.952	.772	.682	.506	.354	.151	.152	.175	.188	.197	.206	.201	.202
8	6.935	.771	.682	.505	.354	.151	.152	.174	.187	.196	.205	.200	.201
9	7.928	.771	.682	.504	.354	.150	.152	.174	.186	.195	.205	.200	.201
10	8.947	.770	.682	.503	.354	.149	.152	.173	.186	.194	.205	.199	.201
11	8.916	.770	.681	.503	.354	.149	.151	.173	.186	.194	.205	.199	.201
12	9.955	.770	.681	.503	.354	.149	.151	.173	.186	.194	.204	.199	.200
13	9.941	.769	.681	.503	.354	.149	.151	.173	.185	.193	.204	.199	.200
14	.999	1.001	1.000	.999	1.000	1.000	1.000	1.001	1.001	1.001	1.002	1.002	1.001

		Upper-flap static-pressure ratio, $p/p_{t,j}$									
		$y/(w_t/2) = 0.000$					$x/x_{t,u} = 1.008$				
		$x/x_{t,u}$					$y/(w_t/2)$				
pt	$p_{t,j}/p_\infty$	1.510	1.570	1.630	1.691	1.751	0.250	0.500	0.750	0.875	0.950
1	.999	1.001	1.000	1.001	1.001	1.001	1.001	1.001	1.002	1.002	1.001
2	1.994	.516	.534	.547	.544	.525	.355	.364	.344	.339	.349
3	2.988	.408	.445	.472	.452	.403	.350	.362	.336	.332	.344
4	3.975	.198	.180	.313	.348	.367	.346	.360	.332	.329	.343
5	4.961	.198	.179	.170	.149	.132	.345	.359	.330	.328	.341
6	5.973	.197	.179	.170	.149	.132	.344	.359	.329	.326	.340
7	5.952	.197	.179	.170	.149	.132	.344	.359	.329	.326	.340
8	6.935	.197	.178	.170	.149	.132	.344	.359	.328	.325	.340
9	7.928	.196	.178	.170	.149	.132	.344	.358	.328	.325	.339
10	8.947	.196	.178	.170	.149	.132	.343	.358	.327	.324	.338
11	8.916	.196	.178	.169	.149	.132	.343	.358	.327	.324	.338
12	9.955	.195	.178	.169	.149	.132	.343	.358	.327	.323	.338
13	9.941	.195	.178	.169	.149	.132	.343	.358	.327	.323	.338
14	.999	1.001	1.002	1.001	1.001	1.001	1.001	1.001	1.001	1.000	1.001

TABLE IV.- Continued

(f) Continued

		Upper-flap static-pressure ratio, $p/p_{t,j}$									
		$x/x_{t,u} = 1.250$					$x/x_{t,u} = 1.691$				
		$y/(w_t/2)$					$y/(w_t/2)$				
pt	$p_{t,j}/p_\infty$	0.250	0.500	0.750	0.875	0.950	0.250	0.500	0.750	0.875	0.950
1	.999	1.001	1.001	1.001	1.001	1.001	1.001	1.001	1.001	1.000	1.001
2	1.994	.394	.349	.360	.381	.399	.545	.554	.538	.529	.513
3	2.988	.197	.198	.191	.200	.202	.448	.429	.356	.350	.338
4	3.975	.197	.197	.189	.199	.201	.348	.395	.329	.289	.271
5	4.961	.197	.196	.188	.198	.201	.150	.146	.193	.213	.209
6	5.973	.196	.195	.187	.197	.200	.150	.149	.143	.156	.167
7	5.952	.196	.195	.187	.197	.200	.150	.149	.143	.157	.168
8	6.935	.196	.194	.186	.196	.199	.150	.151	.140	.136	.136
9	7.928	.195	.194	.186	.196	.199	.150	.153	.139	.134	.115
10	8.947	.195	.193	.185	.195	.198	.150	.154	.138	.134	.099
11	8.916	.195	.193	.185	.195	.198	.150	.154	.138	.134	.099
12	9.955	.195	.193	.185	.195	.198	.150	.155	.136	.133	.088
13	9.941	.195	.193	.185	.194	.198	.150	.155	.136	.133	.088
14	.999	1.002	1.001	1.002	1.001	1.001	1.001	1.001	1.002	1.002	1.001

TABLE IV.- Continued

(f) Concluded

		Lower-flap static-pressure ratio, $p/p_{t,j}$								
		$y/(w_t/2) = 0.000$								
		$x/x_{t,l}$								
pt	$p_{t,j}/p_\infty$	0.881	0.941	1.001	1.019	1.049	1.079	1.121	1.157	1.199
1	.999	1.003	1.002	.997	1.002	1.000	1.001	1.002	1.003	1.002
2	1.994	.847	.740	.615	.601	.571	.536	.478	.425	.390
3	2.988	.845	.739	.614	.599	.568	.534	.479	.424	.348
4	3.975	.844	.739	.612	.599	.566	.533	.478	.422	.346
5	4.961	.844	.738	.612	.599	.566	.534	.478	.421	.346
6	5.973	.844	.738	.612	.599	.566	.535	.478	.421	.346
7	5.952	.844	.738	.612	.598	.566	.535	.478	.421	.346
8	6.935	.844	.737	.611	.598	.567	.535	.478	.421	.347
9	7.928	.844	.737	.611	.598	.567	.536	.478	.421	.347
10	8.947	.844	.737	.611	.597	.568	.537	.478	.422	.348
11	8.916	.844	.737	.611	.597	.568	.537	.478	.422	.348
12	9.955	.844	.737	.611	.597	.569	.538	.478	.422	.349
13	9.941	.844	.736	.611	.597	.569	.538	.478	.422	.349
14	.999	1.000	1.002	1.003	.999	1.001	1.000	1.001	1.000	1.001

		Lower-flap static-pressure ratio, $p/p_{t,j}$									
		$x/x_{t,l} = 1.001$					$x/x_{t,l} = 1.121$				
		$y/(w_t/2)$					$y/(w_t/2)$				
pt	$p_{t,j}/p_\infty$	0.250	0.500	0.750	0.875	0.950	0.250	0.500	0.750	0.875	0.950
1	.999	1.001	1.002	1.003	1.001	1.002	1.001	1.002	1.000	1.001	1.002
2	1.994	.621	.616	.617	.617	.625	.480	.484	.480	.479	.490
3	2.988	.618	.614	.613	.614	.622	.479	.481	.476	.476	.486
4	3.975	.616	.614	.612	.613	.621	.478	.481	.474	.474	.484
5	4.961	.616	.613	.611	.612	.621	.478	.480	.474	.474	.484
6	5.973	.616	.614	.611	.613	.621	.478	.481	.474	.474	.484
7	5.952	.615	.613	.611	.613	.621	.478	.480	.474	.474	.484
8	6.935	.616	.613	.611	.613	.622	.479	.480	.474	.474	.485
9	7.928	.616	.613	.612	.614	.622	.479	.481	.475	.475	.485
10	8.947	.616	.613	.612	.614	.623	.480	.481	.476	.475	.485
11	8.916	.616	.613	.612	.614	.622	.480	.480	.475	.475	.485
12	9.955	.616	.614	.613	.615	.623	.480	.481	.476	.476	.486
13	9.941	.616	.613	.612	.615	.623	.480	.481	.476	.475	.485
14	.999	1.000	1.000	1.000	1.002	1.001	.999	.999	1.000	1.000	.999

TABLE IV.- Continued

(g) Configuration V1(11)

Upper-flap static-pressure ratio, $p/p_{t,j}$

$y/(w_t/2) = 0.000$

pt	$p_{t,j}/p_\infty$	$x/x_{t,u}$ = 0.888	0.924	0.966	1.008	1.051	1.087	1.129	1.190	1.250	1.322	1.389	1.449
1	.999	1.000	1.000	1.001	1.001	1.001	1.002	1.001	1.001	1.001	1.000	1.000	1.000
2	1.963	.793	.701	.476	.316	.390	.445	.449	.396	.357	.554	.593	.579
3	2.942	.796	.699	.472	.313	.390	.450	.447	.393	.332	.274	.234	.201
4	3.919	.793	.699	.470	.310	.389	.451	.445	.391	.324	.274	.233	.199
5	4.898	.793	.699	.470	.310	.388	.451	.445	.390	.323	.273	.232	.198
6	4.872	.793	.699	.470	.309	.388	.451	.445	.390	.322	.273	.232	.199
7	5.865	.793	.699	.469	.309	.388	.451	.446	.390	.322	.273	.232	.198
8	6.813	.792	.699	.469	.308	.387	.451	.447	.390	.321	.273	.233	.197
9	7.797	.792	.699	.469	.307	.387	.452	.448	.390	.321	.274	.233	.198
10	8.788	.791	.699	.469	.307	.387	.452	.448	.390	.321	.274	.233	.198
11	9.055	.792	.699	.469	.307	.387	.453	.449	.390	.321	.274	.233	.198
12	1.000	.999	.998	1.000	.999	.999	.998	.998	.999	1.000	1.000	1.000	1.001

Upper-flap static-pressure ratio, $p/p_{t,j}$

$y/(w_t/2) = 0.000$ | $x/x_{t,u} = 1.008$

pt	$p_{t,j}/p_\infty$	$x/x_{t,u}$ = 1.510	1.570	1.630	1.691	1.751	$y/(w_t/2)$ = 0.250	0.500	0.750	0.875	0.950
1	.999	1.000	1.000	1.000	1.000	1.000	1.001	1.001	1.001	1.001	1.001
2	1.963	.567	.569	.559	.541	.493	.312	.315	.312	.318	.331
3	2.942	.339	.364	.401	.435	.409	.311	.314	.312	.314	.331
4	3.919	.175	.171	.172	.242	.254	.311	.317	.313	.319	.331
5	4.898	.175	.170	.172	.172	.160	.313	.318	.316	.320	.330
6	4.872	.175	.170	.172	.172	.160	.313	.318	.316	.320	.331
7	5.865	.175	.170	.172	.172	.160	.312	.317	.315	.319	.330
8	6.813	.174	.169	.172	.171	.159	.312	.316	.314	.318	.329
9	7.797	.174	.169	.172	.171	.159	.311	.316	.314	.318	.329
10	8.788	.173	.169	.172	.171	.159	.310	.315	.313	.317	.329
11	9.055	.174	.168	.172	.171	.159	.310	.315	.313	.317	.329
12	1.000	1.000	1.000	1.000	1.001	1.001	1.000	1.000	1.000	.999	1.000

TABLE IV.- Continued

(g) Continued

		Upper-flap static-pressure ratio, $p/p_{t,j}$									
		$x/x_{t,u} = 1.250$					$x/x_{t,u} = 1.691$				
		$y/(w_t/2)$					$y/(w_t/2)$				
pt	$p_{t,j}/p_\infty$	0.250	0.500	0.750	0.875	0.950	0.250	0.500	0.750	0.875	0.950
1	.999	1.001	1.001	1.001	1.001	1.001	1.000	1.000	1.000	1.000	1.001
2	1.963	.333	.334	.331	.341	.385	.543	.543	.534	.532	.527
3	2.942	.327	.329	.330	.330	.328	.446	.489	.428	.390	.365
4	3.919	.325	.327	.328	.327	.327	.263	.310	.297	.284	.270
5	4.898	.324	.326	.327	.326	.326	.173	.170	.198	.211	.214
6	4.872	.324	.326	.327	.327	.325	.173	.170	.198	.212	.215
7	5.865	.323	.326	.327	.326	.326	.173	.173	.159	.168	.174
8	6.813	.323	.325	.326	.326	.326	.173	.174	.127	.147	.147
9	7.797	.323	.325	.327	.325	.326	.172	.176	.126	.127	.130
10	8.788	.323	.326	.327	.325	.327	.172	.177	.126	.107	.117
11	9.055	.323	.326	.327	.325	.327	.172	.177	.126	.101	.114
12	1.000	1.000	1.000	1.000	1.000	1.001	1.000	1.001	1.001	1.001	1.001

TABLE IV.- Continued

(g) Concluded

		Lower-flap static-pressure ratio, $p/p_{t,j}$								
		$y/(w_t/2) = 0.000$								
		$x/x_{t,l}$								
pt	$p_{t,j}/p_\infty$	0.881	0.941	1.001	1.019	1.049	1.079	1.121	1.157	1.199
1	.999	1.003	1.003	.999	1.002	1.011	1.001	1.001	1.001	1.000
2	1.963	.840	.726	.474	.352	.264	.263	.419	.445	.478
3	2.942	.839	.726	.477	.351	.263	.257	.243	.224	.235
4	3.919	.838	.725	.478	.351	.262	.257	.242	.224	.199
5	4.898	.838	.725	.477	.351	.255	.256	.242	.224	.199
6	4.872	.838	.725	.477	.351	.255	.256	.242	.224	.199
7	5.865	.839	.725	.477	.352	.254	.256	.242	.222	.199
8	6.813	.839	.724	.477	.352	.254	.255	.242	.222	.198
9	7.797	.839	.724	.477	.352	.254	.255	.242	.221	.198
10	8.788	.839	.724	.477	.352	.254	.255	.242	.221	.198
11	9.055	.840	.724	.477	.352	.255	.255	.242	.221	.199
12	1.000	1.000	.998	1.003	.999	.990	1.001	1.000	1.001	1.000

		Lower-flap static-pressure ratio, $p/p_{t,j}$									
		$x/x_{t,l} = 1.001$					$x/x_{t,l} = 1.121$				
		$y/(w_t/2)$					$y/(w_t/2)$				
pt	$p_{t,j}/p_\infty$	0.250	0.500	0.750	0.875	0.950	0.250	0.500	0.750	0.875	0.950
1	.999	1.001	1.005	1.001	1.000	1.001	1.000	1.000	1.000	1.000	1.000
2	1.963	.488	.485	.482	.491	.481	.426	.399	.381	.397	.410
3	2.942	.485	.480	.479	.486	.475	.247	.245	.246	.248	.243
4	3.919	.483	.479	.478	.485	.474	.246	.245	.246	.249	.245
5	4.898	.483	.479	.477	.485	.473	.245	.244	.245	.248	.242
6	4.872	.483	.479	.478	.485	.473	.245	.244	.245	.248	.242
7	5.865	.483	.478	.477	.485	.473	.245	.244	.244	.248	.242
8	6.813	.483	.478	.477	.485	.472	.244	.243	.244	.247	.242
9	7.797	.483	.478	.477	.485	.472	.244	.243	.244	.248	.241
10	8.788	.483	.478	.478	.485	.472	.244	.243	.244	.248	.241
11	9.055	.483	.478	.477	.485	.472	.244	.243	.244	.248	.239
12	1.000	1.000	.996	1.000	1.000	1.000	1.000	.999	1.000	1.000	1.000

TABLE IV.- Continued

(h) Configuration V1(20)

		Upper-flap static-pressure ratio, $p/p_{t,j}$											
		$y/(w_t/2) = 0.000$											
		$x/x_{t,u}$											
pt	$p_{t,j}/p_\infty$	0.888	0.924	0.966	1.008	1.051	1.087	1.129	1.190	1.250	1.322	1.389	1.449
1	1.000	.999	1.000	1.000	.999	.999	.999	.999	.999	.999	.999	1.000	.999
2	1.968	.795	.698	.515	.624	.611	.584	.539	.482	.532	.568	.559	.547
3	2.947	.796	.695	.503	.617	.603	.580	.524	.443	.367	.306	.248	.203
4	3.948	.793	.693	.500	.615	.601	.579	.522	.441	.350	.306	.248	.203
5	4.901	.793	.692	.498	.615	.601	.580	.522	.440	.344	.306	.248	.202
6	5.897	.792	.692	.496	.615	.602	.581	.523	.440	.340	.307	.248	.202
7	1.001	.998	1.000	1.000	.999	.999	.999	1.000	1.000	1.000	1.001	1.000	1.000

		Upper-flap static-pressure ratio, $p/p_{t,j}$								
		$y/(w_t/2) = 0.000$				$x/x_{t,u} = 1.008$				
		$x/x_{t,u}$				$y/(w_t/2)$				
pt	$p_{t,j}/p_\infty$	1.510	1.570	1.630	1.691	0.250	0.500	0.750	0.875	0.950
1	1.000	.999	1.000	.999	.998	.998	.999	.999	1.000	.998
2	1.968	.559	.564	.551	.525	.641	.644	.644	.648	.643
3	2.947	.251	.325	.339	.345	.627	.632	.634	.639	.638
4	3.948	.172	.152	.140	.215	.623	.629	.632	.636	.637
5	4.901	.172	.151	.138	.122	.623	.628	.631	.635	.636
6	5.897	.172	.151	.137	.123	.623	.628	.631	.635	.636
7	1.001	1.001	1.000	1.000	1.000	1.000	1.000	1.000	1.000	1.001

TABLE IV.- Continued

(h) Continued

		Upper-flap static-pressure ratio, $p/p_{t,j}$									
		$x/x_{t,u} = 1.250$					$x/x_{t,u} = 1.691$				
		$y/(w_t/2)$					$y/(w_t/2)$				
pt	$p_{t,j}/p_\infty$	0.250	0.500	0.750	0.875	0.950	0.250	0.500	0.750	0.875	0.950
1	1.000	1.000	.999	.999	.999	.999	.998	.999	.999	.999	.999
2	1.968	.540	.509	.477	.487	.494	.524	.531	.529	.531	.528
3	2.947	.381	.380	.382	.381	.381	.362	.503	.411	.369	.348
4	3.948	.380	.377	.380	.380	.379	.218	.206	.243	.263	.261
5	4.901	.380	.377	.380	.380	.377	.118	.110	.174	.203	.212
6	5.897	.380	.377	.380	.380	.380	.118	.114	.126	.159	.171
7	1.001	1.000	1.000	1.000	1.000	1.000	1.000	1.001	1.001	1.001	1.000

TABLE IV.- Continued

(h) Concluded

		Lower-flap static-pressure ratio, $p/p_{t,j}$								
		$y/(w_t/2) = 0.000$								
		$x/x_{t,l}$								
pt	$p_{t,j}/p_\infty$	0.881	0.941	1.001	1.019	1.049	1.079	1.121	1.157	1.199
1	1.000	1.000	1.001	.997	.998	.995	.999	1.000	.999	.998
2	1.968	.840	.706	.509	.395	.463	.467	.466	.467	.468
3	2.947	.839	.693	.502	.277	.160	.166	.179	.188	.207
4	3.948	.838	.688	.499	.276	.158	.166	.178	.188	.201
5	4.901	.837	.686	.497	.276	.156	.165	.177	.187	.202
6	5.897	.837	.685	.496	.276	.155	.165	.177	.187	.203
7	1.001	1.005	1.000	.999	1.000	1.005	1.001	1.000	1.001	1.000

		Lower-flap static-pressure ratio, $p/p_{t,j}$									
		$x/x_{t,l} = 1.001$					$x/x_{t,l} = 1.121$				
		$y/(w_t/2)$					$y/(w_t/2)$				
pt	$p_{t,j}/p_\infty$	0.250	0.500	0.750	0.875	0.950	0.250	0.500	0.750	0.875	0.950
1	1.000	1.000	1.003	1.000	.999	.999	.998	.998	.999	.998	.998
2	1.968	.539	.528	.529	.521	.520	.430	.415	.400	.440	.429
3	2.947	.536	.522	.524	.517	.519	.181	.183	.187	.190	.231
4	3.948	.534	.521	.523	.515	.515	.180	.183	.185	.191	.194
5	4.901	.533	.520	.522	.514	.514	.179	.183	.184	.192	.191
6	5.897	.533	.519	.521	.513	.510	.179	.183	.184	.191	.189
7	1.001	.999	.997	1.001	.999	1.000	1.000	1.000	1.000	1.000	.999

TABLE IV.- Continued

(i) Configuration V2(20)

Upper-flap static-pressure ratio, $p/p_{t,j}$

$y/(w_t/2) = 0.000$

$x/x_{t,u}$

pt	$p_{t,j}/p_\infty$	0.888	0.924	0.966	1.008	1.051	1.087	1.129	1.190	1.250	1.322	1.389	1.449
1	1.000	1.000	1.001	1.001	1.000	1.000	1.001	1.000	1.000	1.000	1.000	1.000	1.000
2	1.967	.796	.699	.516	.625	.612	.586	.540	.484	.522	.572	.561	.549
3	2.973	.797	.695	.504	.618	.604	.581	.524	.444	.367	.305	.248	.204
4	2.939	.797	.695	.504	.618	.604	.581	.524	.444	.368	.305	.248	.203
5	3.940	.794	.694	.501	.616	.602	.580	.523	.441	.350	.306	.248	.203
6	4.890	.793	.693	.499	.616	.602	.580	.523	.440	.344	.306	.248	.202
7	4.903	.793	.692	.499	.615	.602	.580	.522	.440	.344	.306	.248	.202
8	5.876	.792	.692	.497	.616	.602	.581	.523	.440	.340	.306	.248	.202
9	6.844	.792	.692	.496	.616	.603	.583	.524	.440	.338	.306	.248	.201
10	1.000	.999	1.001	1.001	1.000	1.000	.999	1.000	1.000	1.000	1.001	1.001	1.001

Upper-flap static-pressure ratio, $p/p_{t,j}$

$y/(w_t/2) = 0.000$ | $x/x_{t,u} = 1.008$

$x/x_{t,u}$ | $y/(w_t/2)$

pt	$p_{t,j}/p_\infty$	1.510	1.570	1.630	1.691	0.250	0.500	0.750	0.875	0.950
1	1.000	.999	1.000	.999	.999	.999	1.000	1.000	.999	.999
2	1.967	.560	.564	.552	.525	.643	.646	.644	.648	.643
3	2.973	.257	.326	.339	.346	.627	.632	.634	.638	.638
4	2.939	.295	.335	.347	.353	.627	.632	.634	.639	.638
5	3.940	.171	.151	.140	.217	.624	.629	.632	.635	.636
6	4.890	.171	.151	.138	.122	.623	.628	.631	.634	.636
7	4.903	.171	.151	.138	.122	.623	.628	.631	.634	.636
8	5.876	.171	.151	.137	.122	.623	.628	.631	.634	.636
9	6.844	.171	.151	.135	.122	.623	.628	.631	.634	.636
10	1.000	1.002	1.001	1.001	1.001	1.000	1.000	1.000	.999	1.000

TABLE IV.- Continued

(i) Continued

Upper-flap static-pressure ratio, $p/p_{t,j}$

		$x/x_{t,u} = 1.250$					$x/x_{t,u} = 1.691$				
		$y/(w_t/2)$					$y/(w_t/2)$				
pt	$p_{t,j}/p_\infty$	0.250	0.500	0.750	0.875	0.950	0.250	0.500	0.750	0.875	0.950
1	1.000	1.001	1.000	1.000	1.000	1.000	.999	.999	.999	.999	.999
2	1.967	.534	.517	.517	.529	.521	.524	.528	.527	.531	.525
3	2.973	.381	.379	.380	.379	.365	.383	.492	.408	.365	.343
4	2.939	.381	.380	.380	.380	.366	.398	.498	.413	.367	.347
5	3.940	.380	.378	.378	.378	.348	.224	.207	.258	.276	.275
6	4.890	.379	.377	.379	.377	.345	.117	.157	.179	.205	.214
7	4.903	.379	.377	.378	.377	.345	.117	.154	.180	.206	.213
8	5.876	.379	.377	.378	.377	.344	.117	.095	.130	.163	.169
9	6.844	.379	.377	.379	.378	.344	.117	.096	.081	.127	.140
10	1.000	1.000	1.001	1.000	1.000	1.001	1.001	1.001	1.002	1.001	1.000

TABLE IV.- Continued

(i) Concluded

Lower-flap static-pressure ratio, $p/p_{t,j}$

		$y/(w_t/2) = 0.000$								
		$x/x_{t,l}$								
pt	$p_{t,j}/p_\infty$	0.881	0.941	1.001	1.019	1.049	1.079	1.121	1.157	1.199
1	1.000	.998	1.000	.998	1.000	1.000	.999	1.000	.999	.999
2	1.967	.840	.706	.510	.398	.466	.468	.467	.469	.469
3	2.973	.838	.693	.502	.277	.156	.166	.178	.188	.205
4	2.939	.838	.693	.503	.277	.156	.166	.178	.188	.209
5	3.940	.838	.688	.499	.276	.154	.166	.178	.188	.202
6	4.890	.837	.686	.497	.276	.154	.165	.177	.187	.202
7	4.903	.837	.686	.497	.276	.154	.165	.177	.188	.202
8	5.876	.837	.685	.496	.276	.153	.165	.177	.187	.202
9	6.844	.837	.685	.495	.275	.152	.164	.177	.186	.202
10	1.000	1.004	1.001	1.000	1.001	1.001	1.001	1.000	1.002	1.001

Lower-flap static-pressure ratio, $p/p_{t,j}$

		$x/x_{t,l} = 1.001$					$x/x_{t,l} = 1.121$				
		$y/(w_t/2)$					$y/(w_t/2)$				
pt	$p_{t,j}/p_\infty$	0.250	0.500	0.750	0.875	0.950	0.250	0.500	0.750	0.875	0.950
1	1.000	1.000	1.001	1.000	1.000	1.001	1.000	.999	1.000	1.000	.999
2	1.967	.540	.527	.528	.523	.525	.408	.410	.414	.454	.443
3	2.973	.536	.521	.523	.517	.519	.181	.183	.189	.191	.238
4	2.939	.536	.520	.523	.517	.519	.181	.184	.190	.191	.244
5	3.940	.534	.520	.522	.515	.516	.180	.180	.188	.192	.189
6	4.890	.533	.519	.521	.514	.515	.179	.182	.189	.193	.189
7	4.903	.533	.519	.521	.514	.515	.179	.184	.189	.193	.189
8	5.876	.533	.518	.520	.513	.514	.179	.185	.189	.193	.188
9	6.844	.533	.518	.520	.513	.514	.179	.185	.187	.192	.187
10	1.000	1.001	.999	1.000	1.000	1.001	1.000	1.000	1.000	1.001	.999

TABLE IV.- Continued

(j) Configuration V3(20)

Upper-flap static-pressure ratio, $p/p_{t,j}$

$y/(w_t/2) = 0.000$

$x/x_{t,u}$

pt	$p_{t,j}/p_\infty$	0.888	0.924	0.966	1.008	1.051	1.087	1.129	1.190	1.250	1.322	1.389	1.449
1	1.001	1.001	.999	.999	.999	1.000	1.000	.999	.999	.999	.999	.999	.999
2	1.976	.797	.698	.514	.624	.612	.585	.540	.481	.527	.570	.560	.548
3	2.967	.796	.694	.503	.617	.604	.581	.524	.444	.368	.306	.248	.204
4	3.932	.794	.692	.500	.615	.602	.580	.523	.442	.351	.306	.248	.203
5	4.893	.793	.692	.498	.615	.602	.580	.523	.441	.344	.306	.249	.203
6	5.887	.792	.691	.496	.615	.602	.582	.523	.440	.341	.307	.248	.202
7	1.000	1.001	.999	1.000	1.000	1.000	1.000	1.000	1.000	1.000	1.001	1.001	1.001

Upper-flap static-pressure ratio, $p/p_{t,j}$

$y/(w_t/2) = 0.000$ | $x/x_{t,u} = 1.008$

$x/x_{t,u}$ | $y/(w_t/2)$

pt	$p_{t,j}/p_\infty$	1.510	1.570	1.630	1.691	0.250	0.500	0.750	0.875	0.950
1	1.001	.998	.999	.998	.998	.998	.999	.999	.999	.999
2	1.976	.558	.562	.549	.524	.642	.644	.640	.647	.643
3	2.967	.172	.294	.317	.330	.627	.632	.633	.638	.638
4	3.932	.172	.152	.141	.218	.623	.629	.631	.635	.636
5	4.893	.172	.152	.139	.123	.623	.628	.631	.634	.636
6	5.887	.172	.151	.137	.123	.623	.628	.631	.634	.635
7	1.000	1.001	1.000	1.001	1.001	1.001	1.000	1.000	1.000	1.001

TABLE IV.- Continued

(j) Continued

		Upper-flap static-pressure ratio, $p/p_{t,j}$									
		$x/x_{t,u} = 1.250$					$x/x_{t,u} = 1.691$				
		$y/(w_t/2)$					$y/(w_t/2)$				
pt	$p_{t,j}/p_\infty$	0.250	0.500	0.750	0.875	0.950	0.250	0.500	0.750	0.875	0.950
1	1.001	.999	.999	.999	.999	.999	.998	.999	.998	.998	.998
2	1.976	.538	.507	.492	.504	.507	.523	.533	.523	.523	.518
3	2.967	.382	.380	.381	.382	.383	.331	.414	.425	.384	.351
4	3.932	.380	.378	.379	.381	.382	.221	.221	.228	.271	.265
5	4.893	.380	.378	.379	.381	.382	.119	.114	.159	.200	.213
6	5.887	.380	.378	.380	.381	.381	.119	.117	.127	.161	.173
7	1.000	1.000	1.000	1.000	1.000	1.000	1.001	1.002	1.001	1.001	1.001

TABLE IV.- Concluded

(j) Concluded

		Lower-flap static-pressure ratio, $p/p_{t,j}$								
		$y/(w_t/2) = 0.000$								
		$x/x_{t,l}$								
pt	$p_{t,j}/p_\infty$	0.881	0.941	1.001	1.019	1.049	1.079	1.121	1.157	1.199
1	1.001	1.000	1.000	.998	.999	.999	.998	.999	1.000	.999
2	1.976	.840	.706	.509	.393	.464	.465	.464	.466	.466
3	2.967	.838	.692	.502	.277	.154	.165	.178	.188	.205
4	3.932	.837	.687	.499	.276	.153	.165	.177	.187	.201
5	4.893	.836	.686	.497	.275	.152	.165	.177	.187	.202
6	5.867	.836	.685	.495	.275	.152	.164	.176	.187	.202
7	1.000	1.003	1.001	1.000	1.000	1.000	1.000	1.000	1.002	1.001

		Lower-flap static-pressure ratio, $p/p_{t,j}$									
		$x/x_{t,l} = 1.001$					$x/x_{t,l} = 1.121$				
		$y/(w_t/2)$					$y/(w_t/2)$				
pt	$p_{t,j}/p_\infty$	0.250	0.500	0.750	0.875	0.950	0.250	0.500	0.750	0.875	0.950
1	1.001	.999	1.000	1.000	.999	.999	.999	.998	.999	.999	.999
2	1.976	.539	.527	.529	.520	.524	.425	.413	.410	.439	.427
3	2.967	.535	.522	.525	.515	.518	.181	.183	.188	.191	.228
4	3.932	.533	.520	.523	.513	.515	.180	.183	.187	.191	.188
5	4.893	.532	.520	.522	.511	.514	.179	.183	.186	.192	.187
6	5.887	.532	.519	.521	.511	.513	.179	.183	.186	.192	.187
7	1.000	1.000	1.000	1.001	1.000	1.001	1.001	1.000	1.001	1.001	1.000

TABLE V.- COMPUTER PRINTOUT OF RATIO OF INTERNAL STATIC PRESSURE TO JET TOTAL PRESSURE FOR SINGLE EXPANSION-RAMP NOZZLES WITH REVERSER DEPLOYED

(a) Configuration R1

		Upper-flap static-pressure ratio, $p/p_{t,j}$					Lower-flap static-pressure ratio, $p/p_{t,j}$				
		$y/(w_t/2) = 0.000$					$y/(w_t/2) = 0.000$				
		$x/x_{t,u}$					$x/x_{t,l}$				
pt	$p_{t,j}/p_\infty$	0.954	0.978	1.002	1.027	1.051	0.959	0.983	1.007	1.031	1.055
1	1.000	1.000	1.000	1.000	1.000	1.002	1.000	.999	1.000	1.000	1.001
2	1.627	.803	.760	.743	.796	.843	.860	.846	.831	.832	.841
3	1.996	.762	.704	.681	.747	.805	.831	.813	.793	.794	.805
4	3.013	.725	.643	.621	.694	.752	.797	.770	.743	.742	.757
5	3.493	.719	.636	.630	.697	.742	.786	.755	.725	.723	.738
6	4.002	.715	.633	.634	.698	.738	.780	.748	.716	.714	.729
7	4.475	.711	.627	.632	.694	.733	.776	.743	.710	.707	.723
8	4.919	.708	.623	.631	.694	.729	.772	.738	.705	.702	.718
9	5.466	.705	.619	.630	.691	.726	.770	.735	.702	.698	.714
10	5.939	.704	.617	.628	.689	.724	.768	.733	.700	.696	.712
11	6.436	.704	.617	.628	.690	.724	.769	.733	.700	.697	.712
12	5.968	.704	.618	.629	.690	.725	.769	.733	.700	.697	.713
13	3.967	.714	.632	.636	.698	.735	.777	.744	.714	.710	.727
14	1.996	.763	.704	.679	.745	.799	.832	.813	.794	.794	.807
15	1.000	1.000	.999	.999	.999	.999	1.001	1.001	1.000	.999	1.001

		Blocker surface static-pressure ratio, $p/p_{t,j}$						
		$y/(w_t/2) = 0.000$						
		z/h_t						
pt	$p_{t,j}/p_\infty$	0.745	0.345	0.000	-0.498	-0.996	-1.345	-1.745
1	1.000	1.000	1.001	1.000	1.003	.999	1.000	.998
2	1.627	.785	.948	.994	1.001	.989	.996	.908
3	1.996	.741	.938	.992	.999	.985	.996	.887
4	3.013	.674	.909	.980	.993	.976	.991	.857
5	3.493	.639	.874	.966	.988	.972	.990	.841
6	4.002	.629	.862	.958	.987	.968	.989	.835
7	4.475	.623	.855	.955	.986	.967	.989	.830
8	4.919	.619	.847	.950	.985	.966	.989	.827
9	5.466	.613	.842	.950	.985	.966	.989	.823
10	5.939	.613	.840	.948	.984	.965	.988	.820
11	6.436	.611	.839	.947	.983	.964	.988	.817
12	5.968	.611	.838	.947	.983	.965	.988	.820
13	3.967	.624	.855	.957	.987	.969	.990	.836
14	1.996	.745	.943	.992	.995	.985	.996	.887
15	1.000	1.001	1.001	1.000	.999	1.000	1.000	.998

TABLE V.- Continued

(b) Configuration R2

		Upper-flap static-pressure ratio, $p/p_{t,j}$					Lower-flap static-pressure ratio, $p/p_{t,j}$				
		$y/(w_t/2) = 0.000$					$y/(w_t/2) = 0.000$				
		$x/x_{t,u}$					$x/x_{t,l}$				
pt	$p_{t,j}/p_\infty$	0.954	0.978	1.002	1.027	1.051	0.959	0.983	1.007	1.031	1.055
1	1.000	.998	.999	1.000	1.002	1.000	1.001	1.000	.999	1.001	.999
2	1.986	.695	.613	.582	.659	.720	.780	.750	.722	.722	.740
3	2.484	.665	.562	.525	.598	.662	.749	.710	.671	.670	.689
4	2.981	.657	.546	.520	.585	.634	.731	.685	.638	.630	.651
5	3.488	.656	.544	.529	.590	.629	.725	.677	.627	.615	.634
6	3.986	.651	.537	.526	.585	.619	.719	.669	.616	.603	.623
7	4.473	.651	.535	.524	.581	.614	.718	.667	.614	.599	.618
8	4.957	.649	.532	.522	.578	.609	.716	.665	.610	.594	.613
9	5.468	.648	.530	.521	.577	.607	.716	.664	.609	.593	.611
10	5.947	.647	.528	.519	.576	.605	.714	.662	.607	.590	.608
11	3.966	.654	.540	.528	.586	.619	.721	.670	.619	.606	.626
12	1.991	.697	.615	.582	.656	.719	.781	.750	.723	.723	.743
13	.999	1.001	1.002	1.002	.999	1.000	1.001	1.001	1.000	1.000	1.001

TABLE V.- Continued

(c) Configuration R3

		Upper-flap static-pressure ratio, $p/p_{t,j}$					Lower-flap static-pressure ratio, $p/p_{t,j}$				
		$y/(w_t/2) = 0.000$					$y/(w_t/2) = 0.000$				
		$x/x_{t,u}$					$x/x_{t,l}$				
pt	$p_{t,j}/p_\infty$	0.954	0.978	1.002	1.027	1.051	0.959	0.983	1.007	1.031	1.055
1	1.000	.999	1.004	1.005	1.005	1.006	1.000	.998	1.002	1.003	1.001
2	2.000	.834	.798	.782	.828	.869	.882	.870	.857	.857	.863
3	2.487	.815	.772	.753	.806	.852	.869	.855	.840	.838	.845
4	2.968	.807	.758	.739	.794	.843	.861	.846	.829	.826	.834
5	3.441	.799	.746	.731	.787	.835	.852	.835	.817	.813	.822
6	3.934	.797	.743	.739	.794	.835	.846	.825	.808	.804	.813
7	3.976	.795	.742	.740	.794	.834	.843	.823	.805	.801	.811
8	4.467	.793	.741	.745	.798	.833	.841	.820	.800	.797	.806
9	4.979	.793	.739	.741	.795	.832	.841	.819	.800	.796	.805
10	5.498	.791	.736	.739	.793	.830	.839	.817	.797	.793	.801
11	5.995	.789	.735	.740		.830	.837	.815	.795	.791	.799
12	6.522	.790	.734	.738			.838	.814	.796	.792	.799
13	6.984	.788	.733	.741			.836	.813	.793	.789	.797
14	7.437	.786	.731	.740			.834	.811	.790	.787	.794
15	7.953	.787	.731				.835	.811	.792	.788	.795
16	8.526	.788	.733				.836	.812	.792	.789	
17	9.004	.787	.731				.835	.811	.791	.788	
18	7.929	.787	.732				.835	.811	.791	.787	.795
19	3.894	.795	.740	.739	.793	.830	.842	.824	.803	.798	.812
20	3.937	.796	.741	.738	.793	.830	.843	.824	.805	.799	.812
21	.999	1.001	.995	.996	.995	.994	1.000	1.002	.999	.998	.999

TABLE V.- Continued

(d) Configuration R4

		Upper-flap static-pressure ratio, $p/p_{t,j}$					Lower-flap static-pressure ratio, $p/p_{t,j}$				
		$y/(w_t/2) = 0.000$					$y/(w_t/2) = 0.000$				
		$x/x_{t,u}$					$x/x_{t,l}$				
pt	$p_{t,j}/p_\infty$	0.954	0.978	1.002	1.027	1.051	0.959	0.983	1.007	1.031	1.055
1	.999	1.001	1.001	1.002	1.002	1.002	1.002	1.001	1.001	1.001	1.001
2	1.990	.678	.584	.535	.647	.726	.772	.742	.716	.723	.744
3	2.489	.650	.536	.500	.587	.661	.739	.699	.663	.669	.694
4	2.970	.646	.527	.536	.598	.636	.723	.676	.631	.633	.659
5	3.463	.648	.535	.568	.623	.648	.718	.670	.620	.620	.645
6	3.970	.646	.533	.570	.623	.645	.715	.665	.614	.613	.638
7	4.395	.644	.530	.568	.620	.641	.712	.662	.609	.607	.633
8	3.972	.646	.533	.571	.624	.644	.715	.665	.614	.612	.638
9	1.992	.679	.585	.535	.647	.722	.773	.743	.717	.724	.746
10	.999	1.000	1.000	1.000	1.000	.999	1.001	1.001	1.000	1.000	1.001

TABLE V.- Concluded

(e) Configuration R5

		Upper-flap static-pressure ratio, $p/p_{t,j}$					Lower-flap static-pressure ratio, $p/p_{t,j}$				
		$y/(w_t/2) = 0.000$					$y/(w_t/2) = 0.000$				
		$x/x_{t,u}$					$x/x_{t,l}$				
pt	$p_{t,j}/p_\infty$	0.954	0.978	1.002	1.027	1.051	0.959	0.983	1.007	1.031	1.055
1	.999	1.000	1.001	1.002	1.001	1.002	1.001	1.000	1.001	1.001	1.001
2	1.991	.775	.721	.697	.762	.817	.843	.827	.808	.809	.820
3	2.482	.739	.669	.641	.716	.779	.816	.795	.772	.773	.786
4	2.990	.719	.637	.615	.686	.744	.795	.767	.740	.741	.755
5	3.999	.704	.622	.621	.677	.714	.772	.738	.704	.703	.719
6	4.475	.700	.616	.616	.671	.706	.768	.731	.697	.695	.711
7	4.987	.698	.612	.613	.666	.701	.765	.728	.692	.690	.706
8	5.470	.696	.610	.611	.663	.696	.763	.724	.688	.685	.700
9	5.974	.694	.608	.609	.660	.693	.761	.721	.684	.681	.697
10	5.950	.694	.608	.610	.660	.692	.761	.721	.684	.681	.696
11	6.445	.693	.607	.609	.658	.691	.760	.720	.682	.678	.693
12	6.947	.693	.606	.609		.691	.760	.719	.681	.678	.693
13	5.956	.695	.609	.610	.662	.694	.762	.722	.686	.683	.699
14	3.881	.708	.626	.622	.678	.715	.775	.741	.709	.707	.724
15	2.001	.777	.722	.696	.761	.813	.844	.826	.811	.809	.822
16	.999	1.002	1.001	1.001	1.001	1.000	1.002	1.002	1.002	1.001	1.001

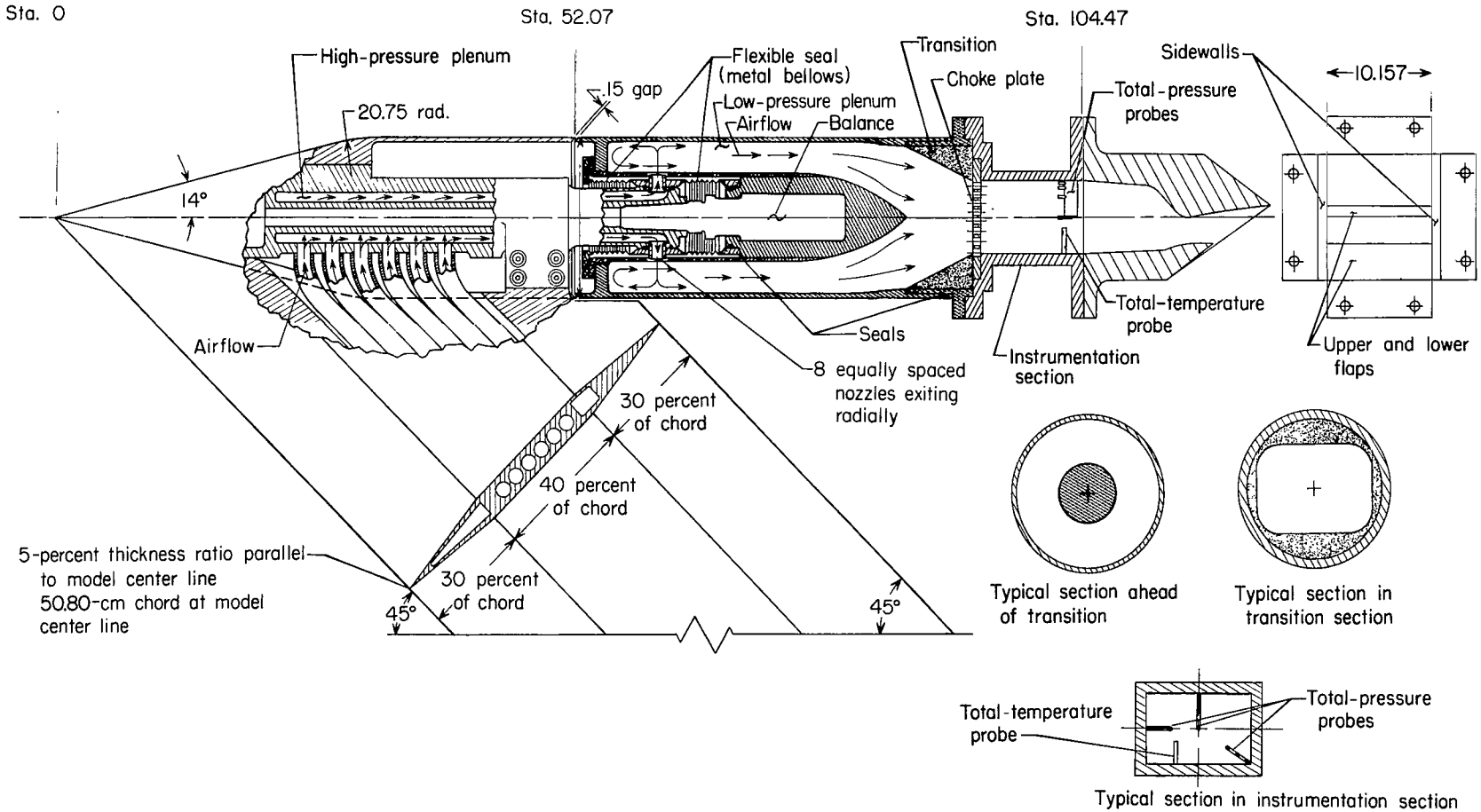

Figure 1.- Sketch of air powered nacelle model with typical nozzle configuration installed. All dimensions are in centimeters unless otherwise noted.

L-82-116

Figure 2.- Photograph of single expansion-ramp nozzle mounted on air-powered nacelle model. Configuration F6 shown with sidewall removed for clarity.

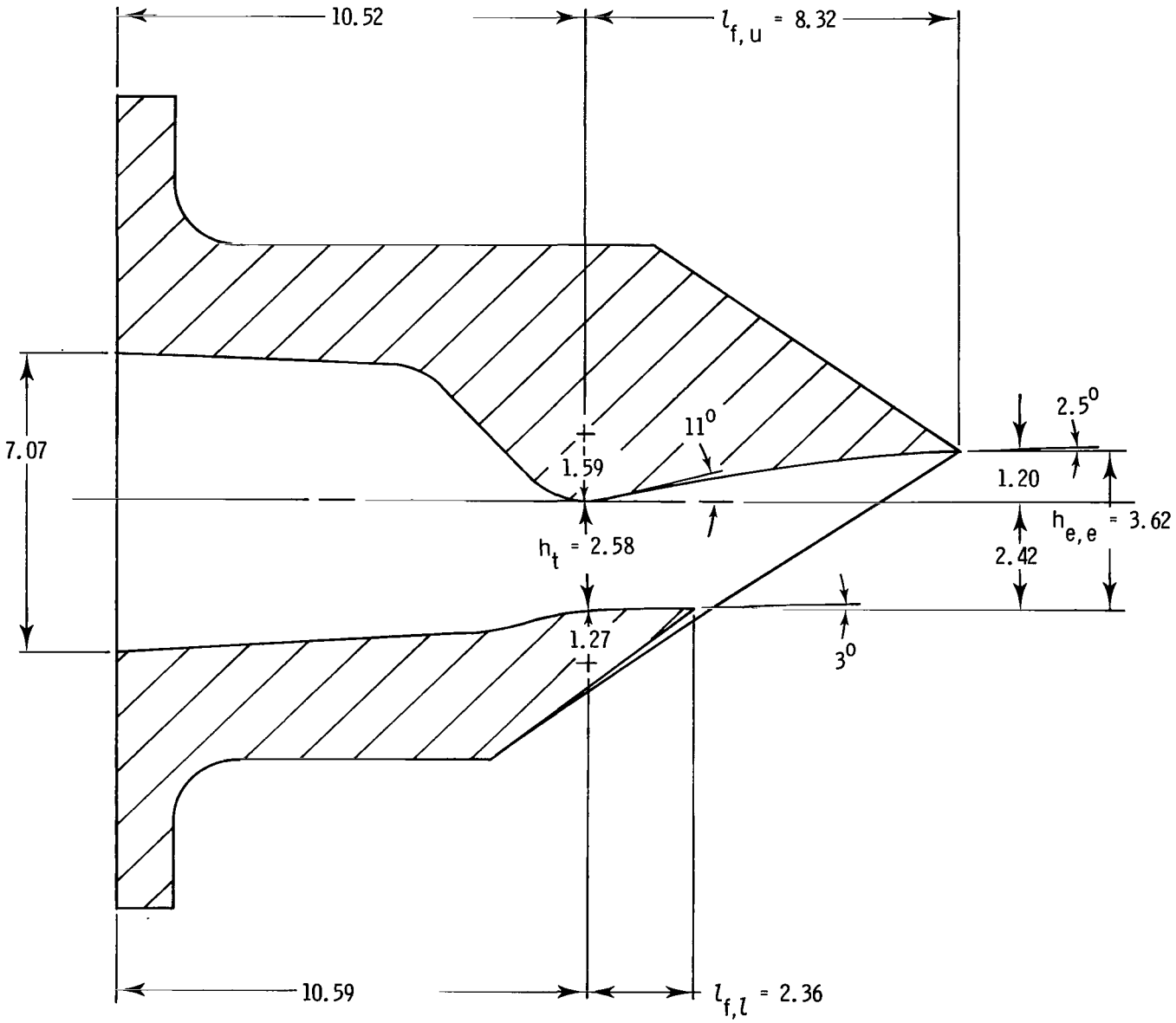

(a) Configuration F1. $(A_e/A_t)_i$ = 1.097; $l_{f,l}$ = 2.36 cm.

Figure 3.- Sketch of forward-flight (cruise) single expansion-ramp nozzle configurations showing important dimensions. All dimensions are in centimeters unless otherwise noted.

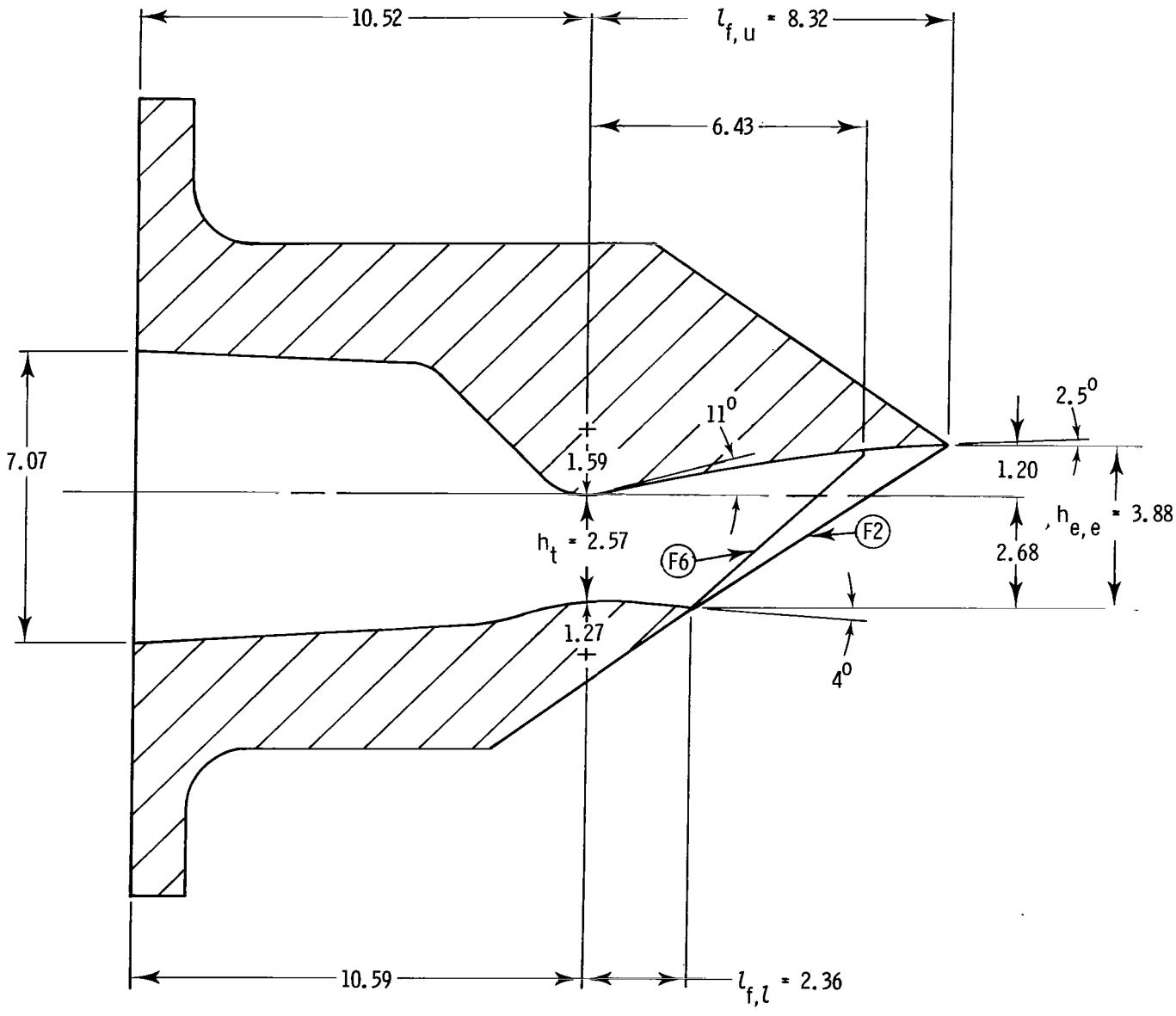

(b) Configurations F2 and F6. $(A_e/A_t)_i$ = 1.215; $l_{f,l}$ = 2.36 cm.

Figure 3.- Continued.

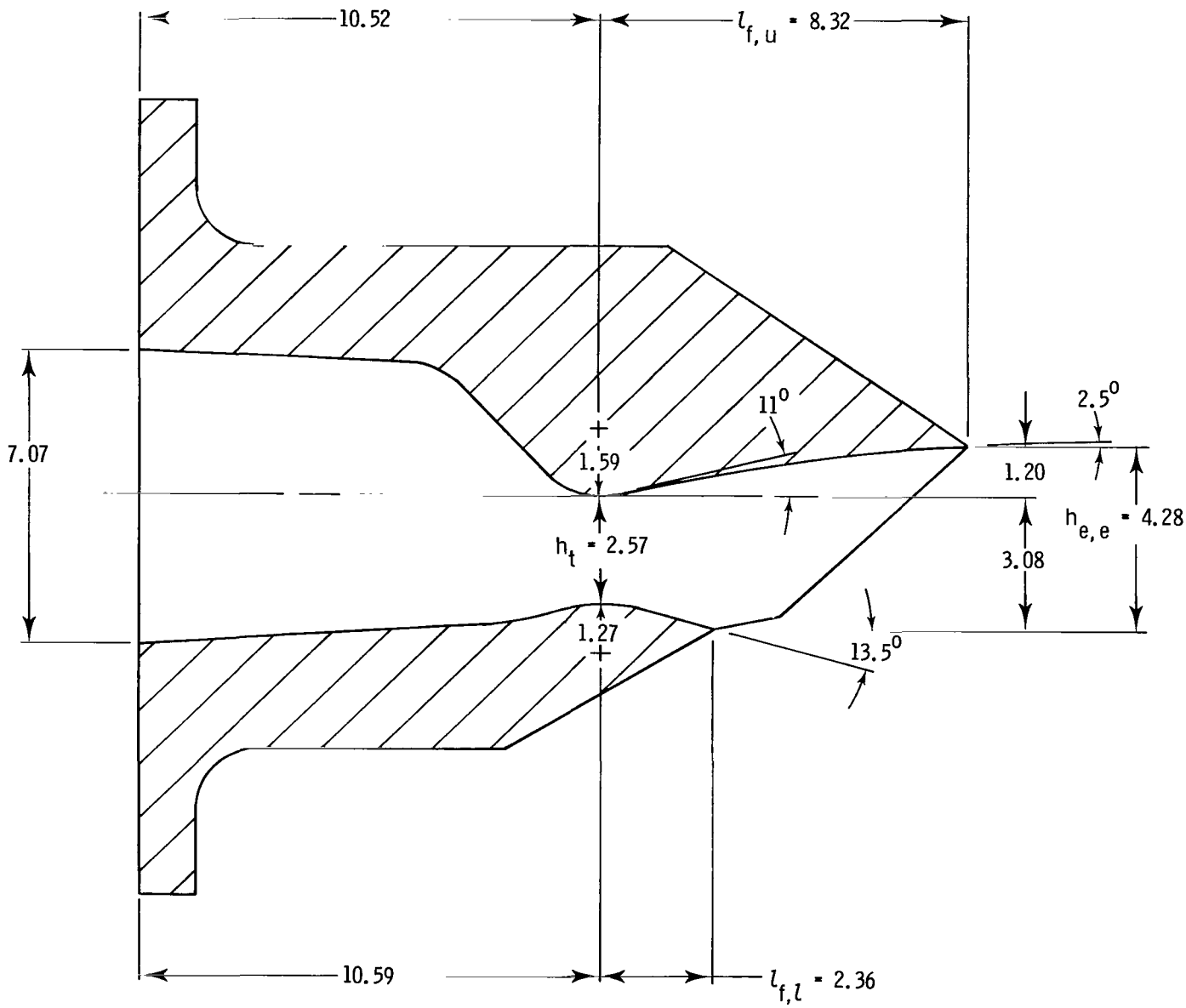

(c) Configuration F3. $(A_e/A_t)_i$ = 1.391; $l_{f,l}$ = 2.36 cm.

Figure 3.- Continued.

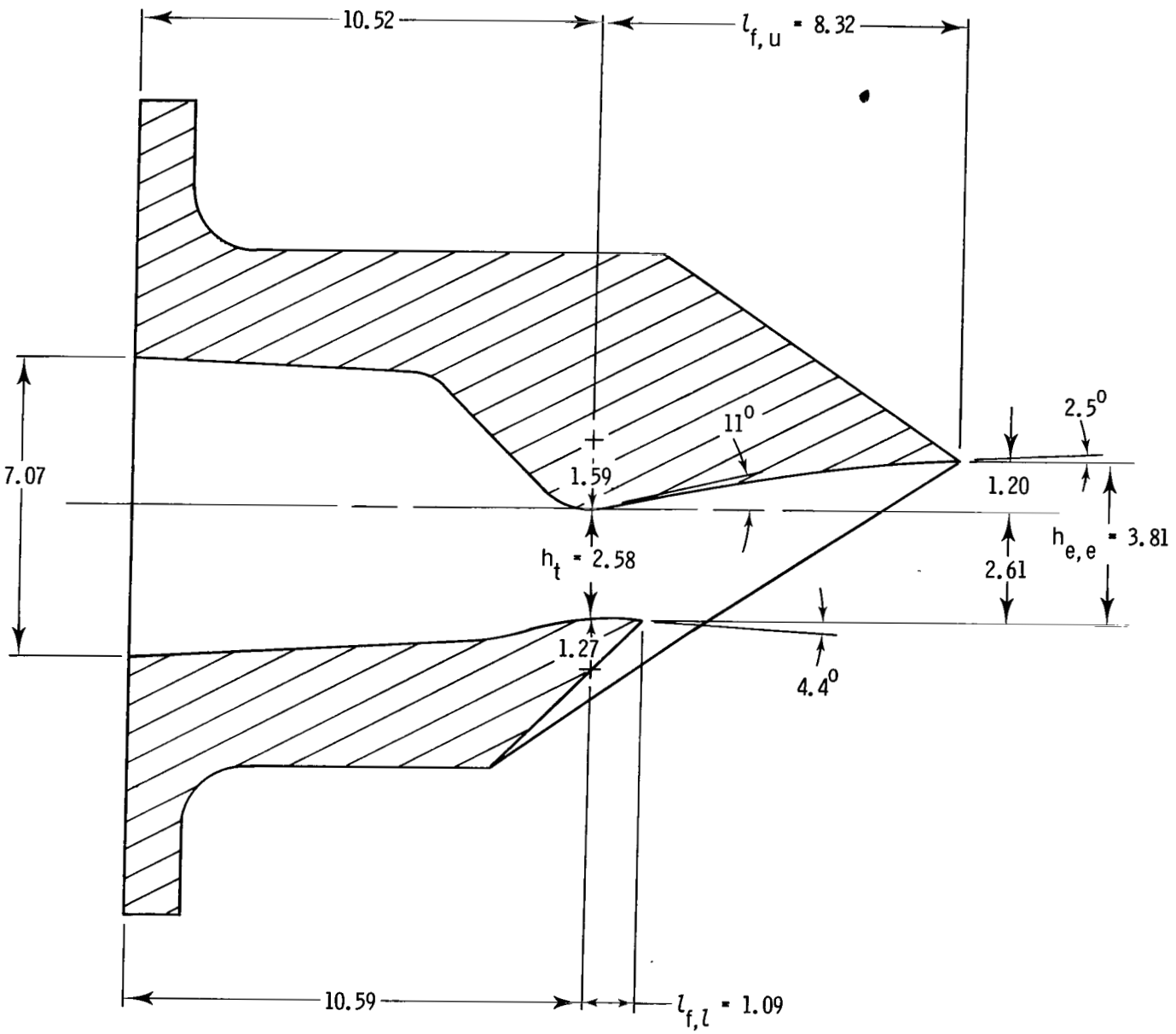

(d) Configuration F4. $(A_e/A_t)_i$ = 1.091; $l_{f,l}$ = 1.09 cm.

Figure 3.- Continued.

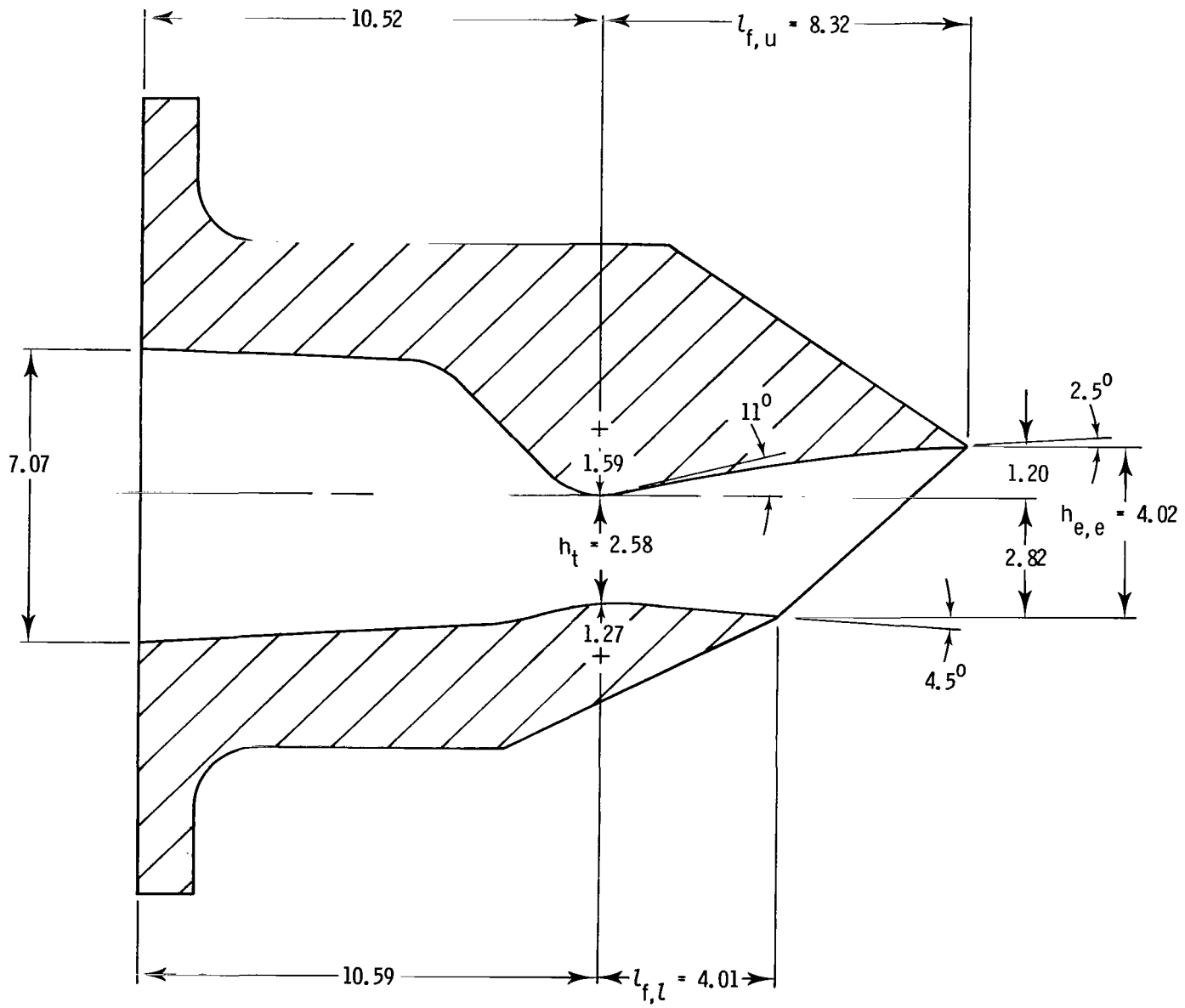

(e) Configuration F5. $(A_e/A_t)_i$ = 1.389; $l_{f,l}$ = 4.01 cm.

Figure 3.- Concluded.

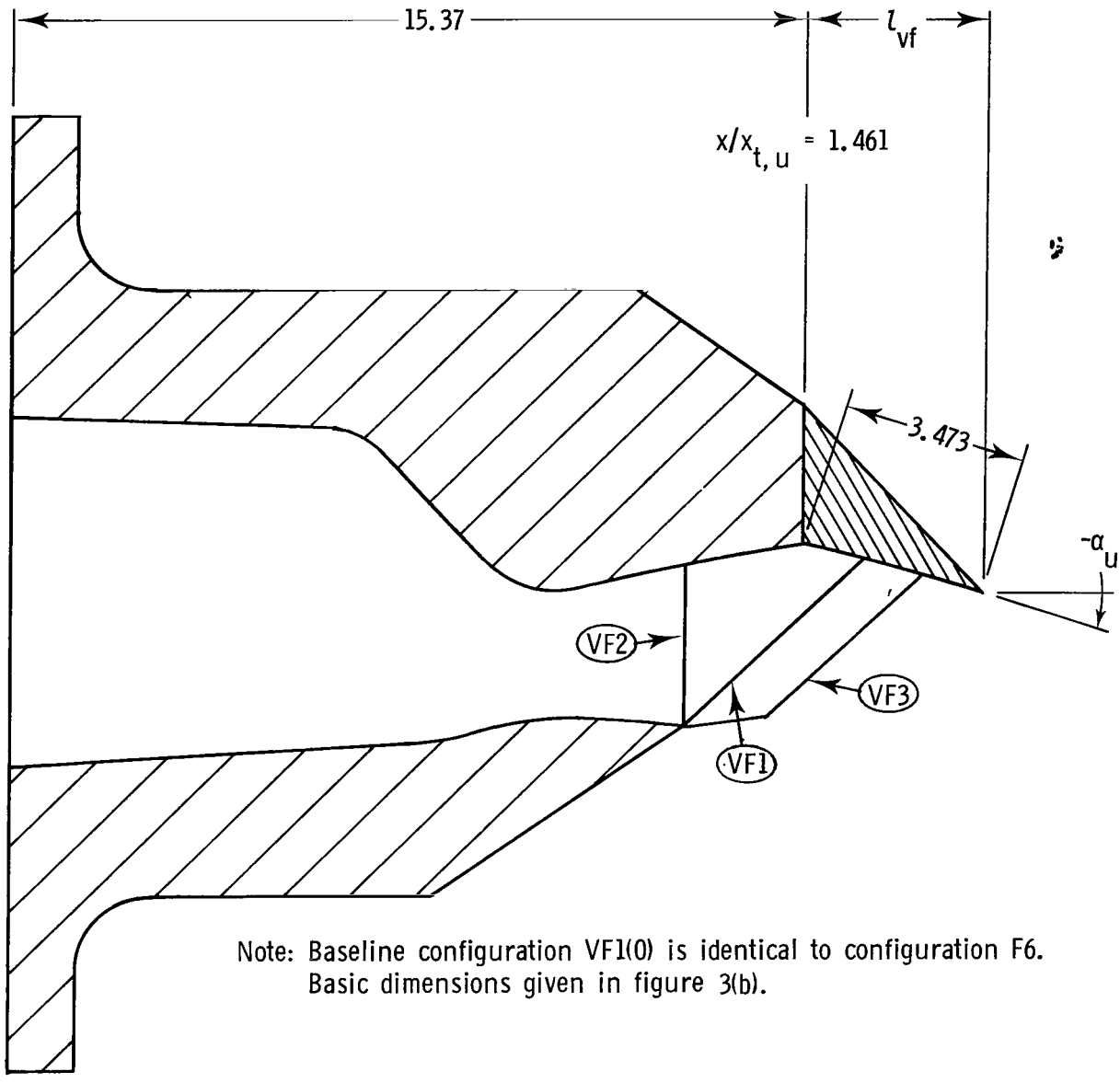

Note: Baseline configuration VF1(0) is identical to configuration F6.
Basic dimensions given in figure 3(b).

Configuration	δ_v, deg	α_u, deg	l_{vf}, cm	Sidewall
VF1(-10)	-10	12.5	3.39	Baseline
VF1(-5)	-5	7.5	3.44	↓
VF1(0) or F6	0	2.5	3.47	
VF1(5)	5	-2.5	3.47	
VF1(10)	10	-7.5	3.44	
VF1(20)	20	-17.5	3.31	
VF2(20)	↓	↓	↓	Cutback
VF3(20)				Extended

Figure 4.- Sketch of vectored-flap single expansion-ramp nozzle configurations showing important dimensions. All dimensions are in centimeters unless otherwise noted.

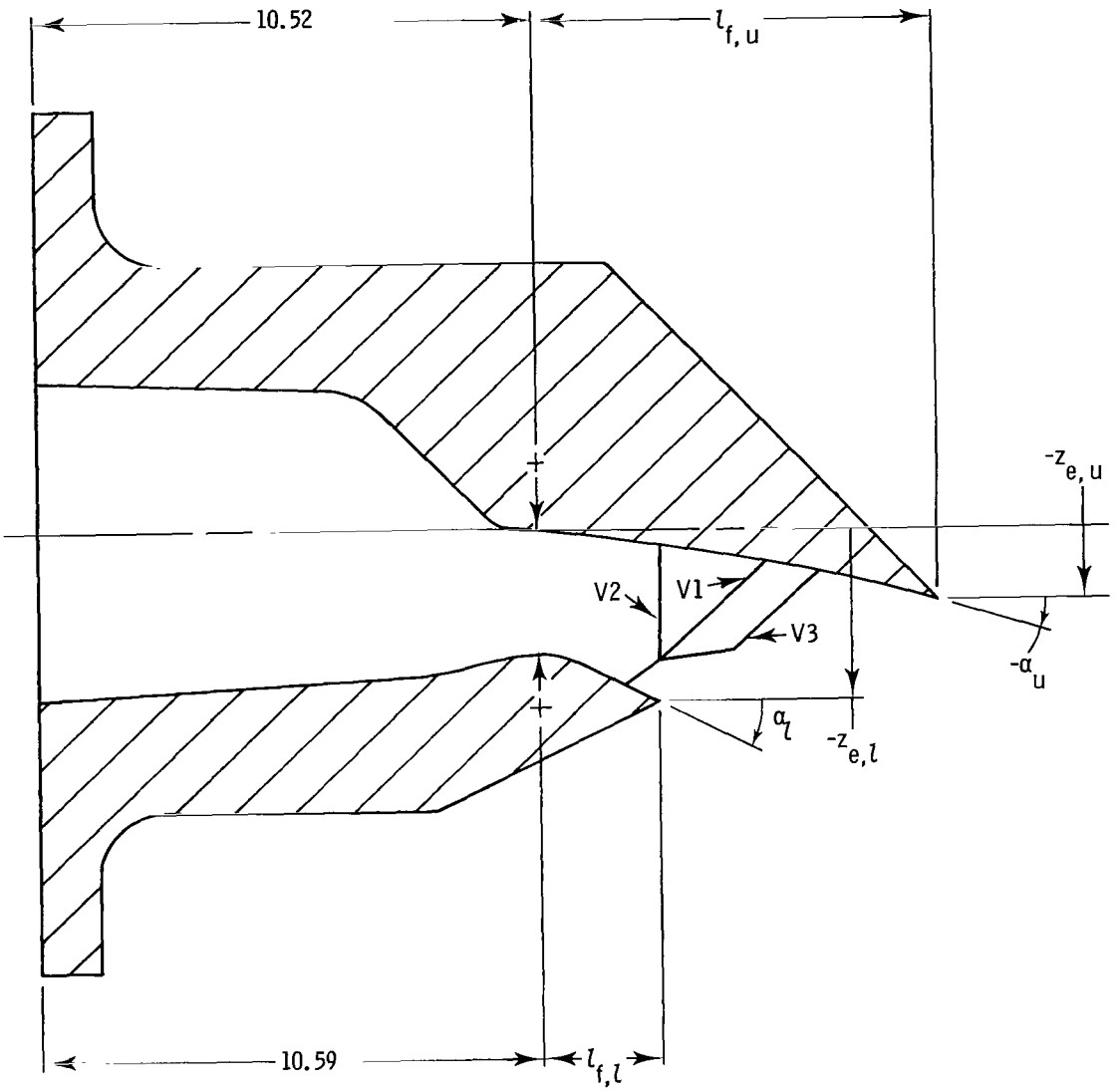

Note: Baseline configuration V1(0) identical to configuration F6.
Basic dimensions given on figure 3(b).

Configuration	δ_v, deg.	α_u, deg	α_l, deg	$l_{f,u}$, cm	$l_{f,l}$, cm	$z_{e,u}$, cm	$z_{e,l}$, cm	Sidewall
V1(-10)	-10	14.0	-3.0	8.27	2.36	2.65	-2.43	Baseline
V1(0)	0	2.5	4.0	8.32	2.36	1.20	-2.68	↓
V1(11)	11	-8.5	13.5	8.08	2.36	-0.38	-3.09	↓
V1(20)	20	-15.0	26.0	7.66	2.39	-1.62	-3.61	↓
V2(20)	↓	↓	↓	↓	↓	↓	↓	Cutback Extended
V3(20)								

Figure 5.- Sketch of vectored (upper and lower flaps) single expansion-ramp nozzle configurations showing important dimensions. All dimensions are in centimeters unless otherwise noted.

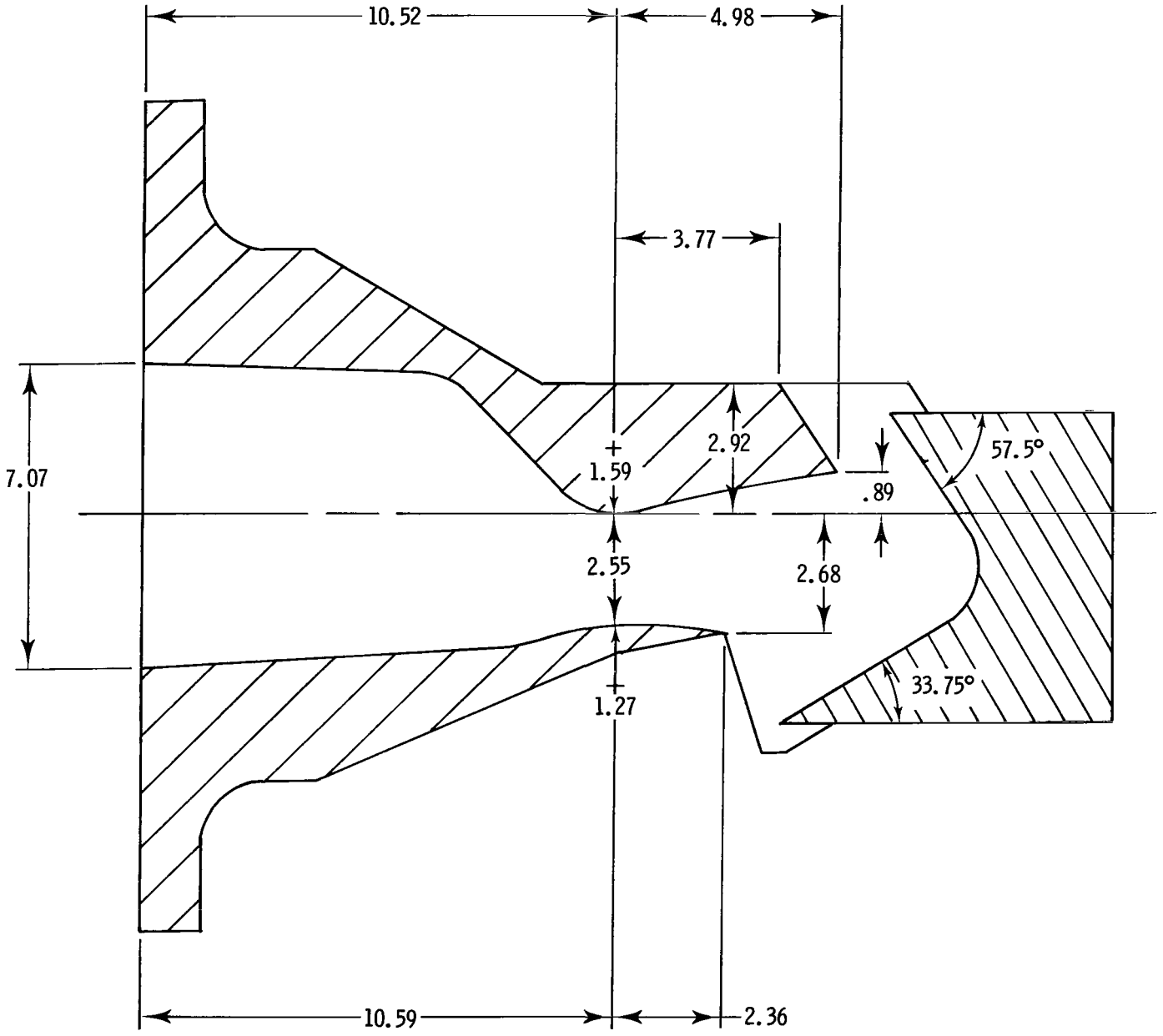

(a) Common dimensions for all reversed-thrust nozzle configurations.

Figure 6.- Sketch of reversed-thrust single expansion-ramp nozzle configurations showing important dimensions. All dimensions are in centimeters unless otherwise noted.

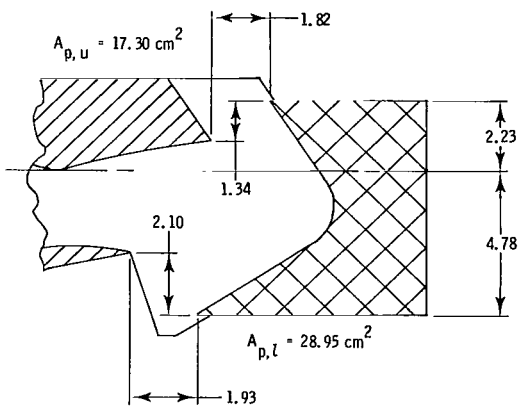

Configuration R2 (Aft blocker)

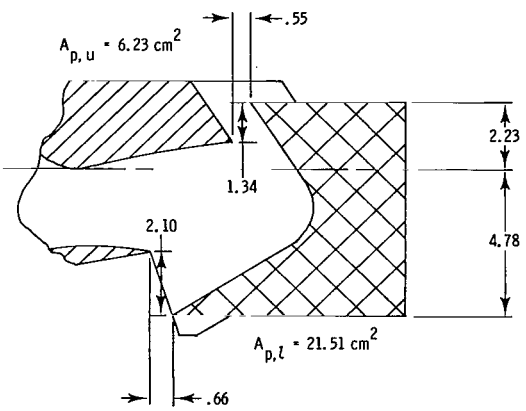

Configuration R3 (Forward blocker)

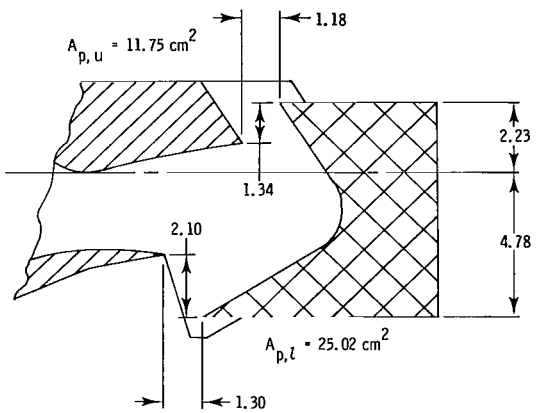

Configuration R1 (Baseline)

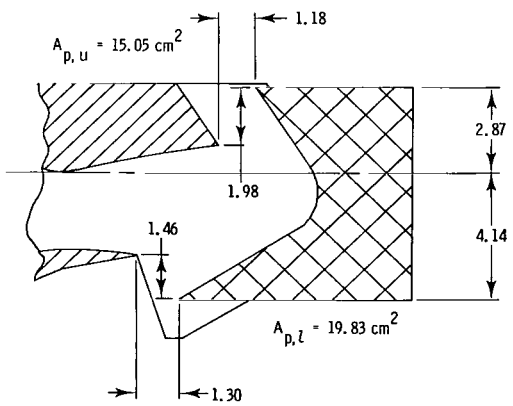

Configuration R4 (Raised blocker)

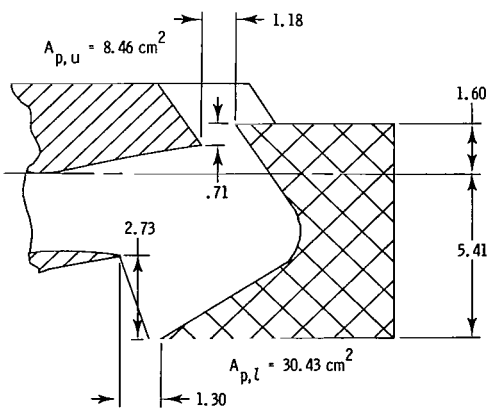

Configuration R5 (Lowered blocker)

(b) Blocker position geometry.

Figure 6.- Concluded.

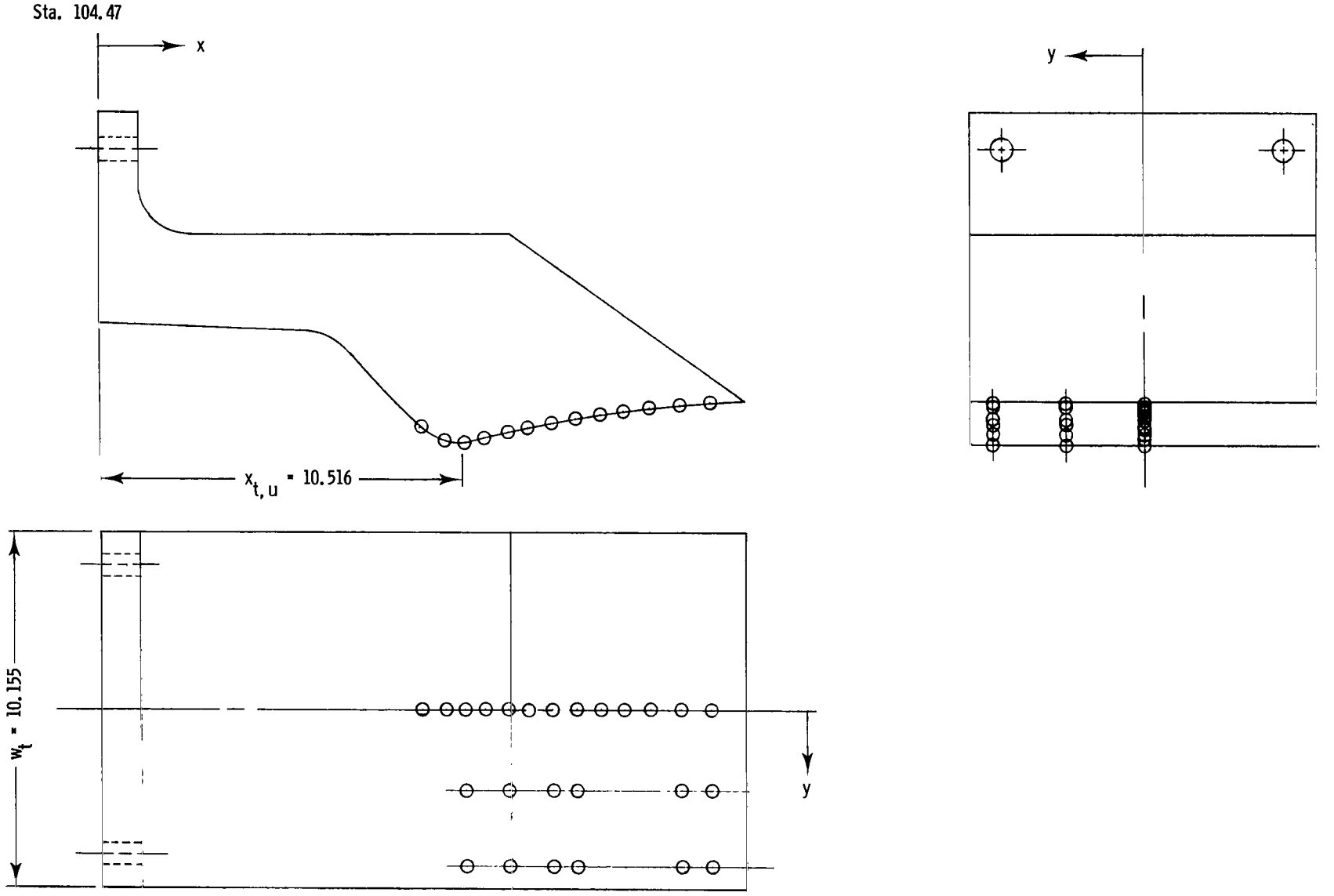

(a) Upper flap.

Figure 7.- Sketches showing typical nozzle internal static-pressure instrumentation. All dimensions given in centimeters unless otherwise noted. Exact orifice locations given for each configuration in table II.

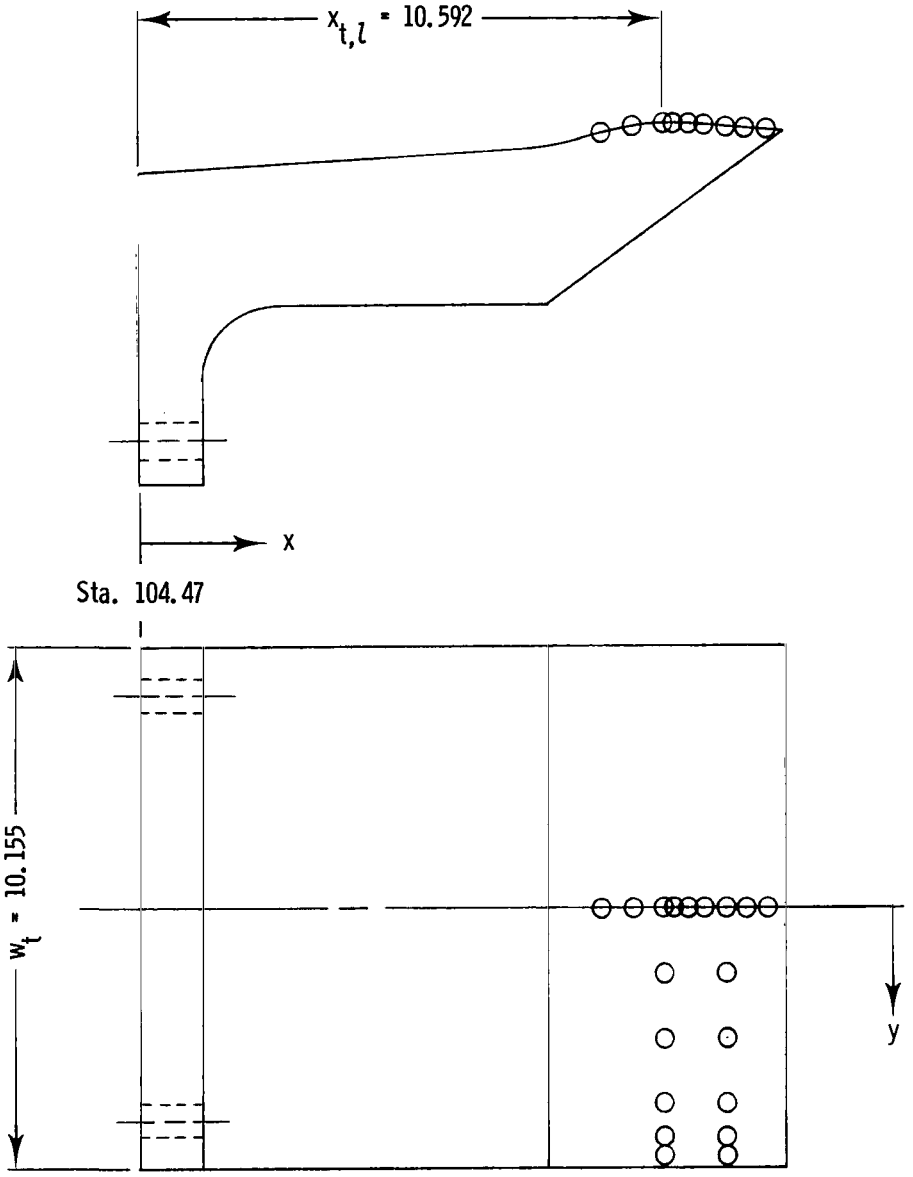

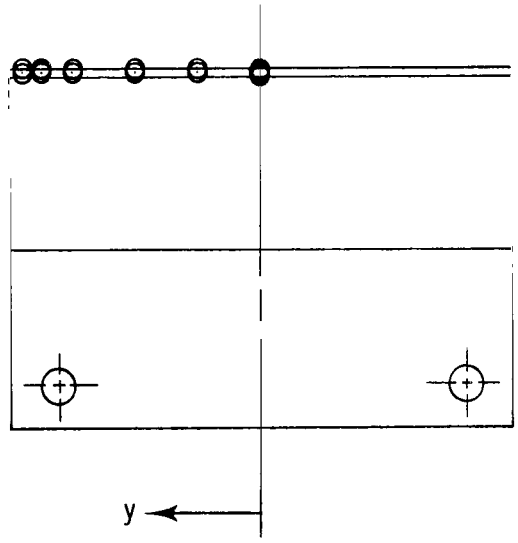

(b) Lower flap.

Figure 7.- Continued.

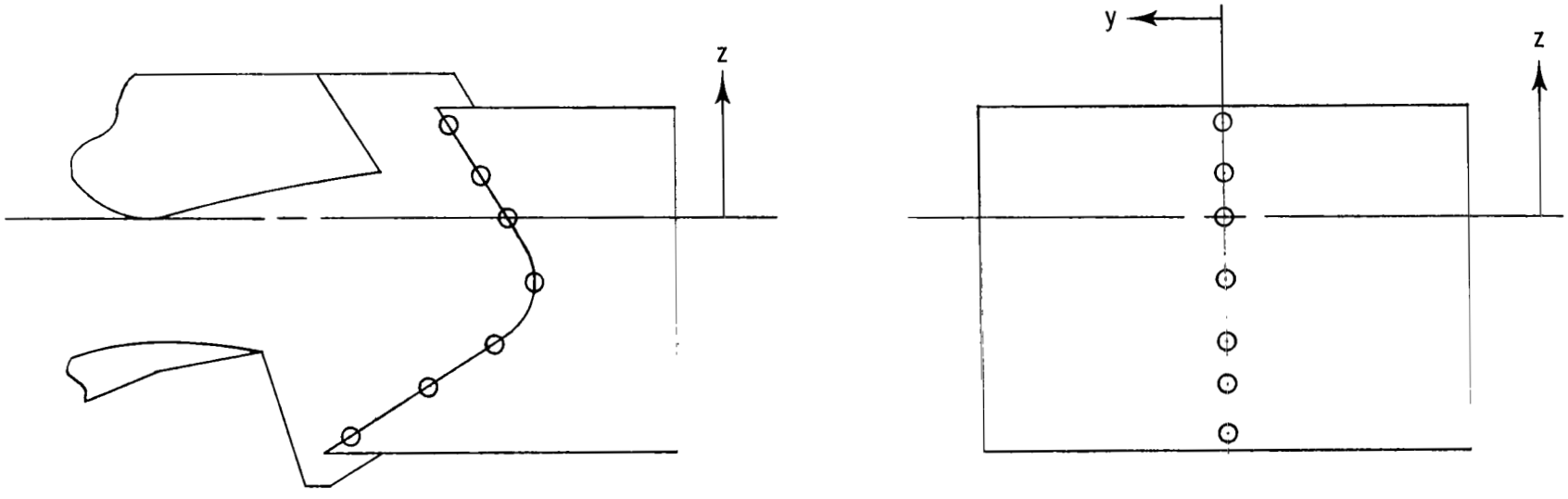

(c) Reverse-thrust blocker.

Figure 7.- Concluded.

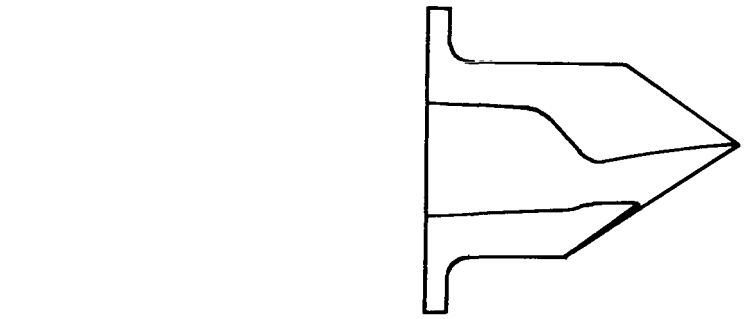

$(A_e/A_t)_i$ = 1.097, $(A_e/A_t)_e$ = 1.407, lower flap length = 2.36cm

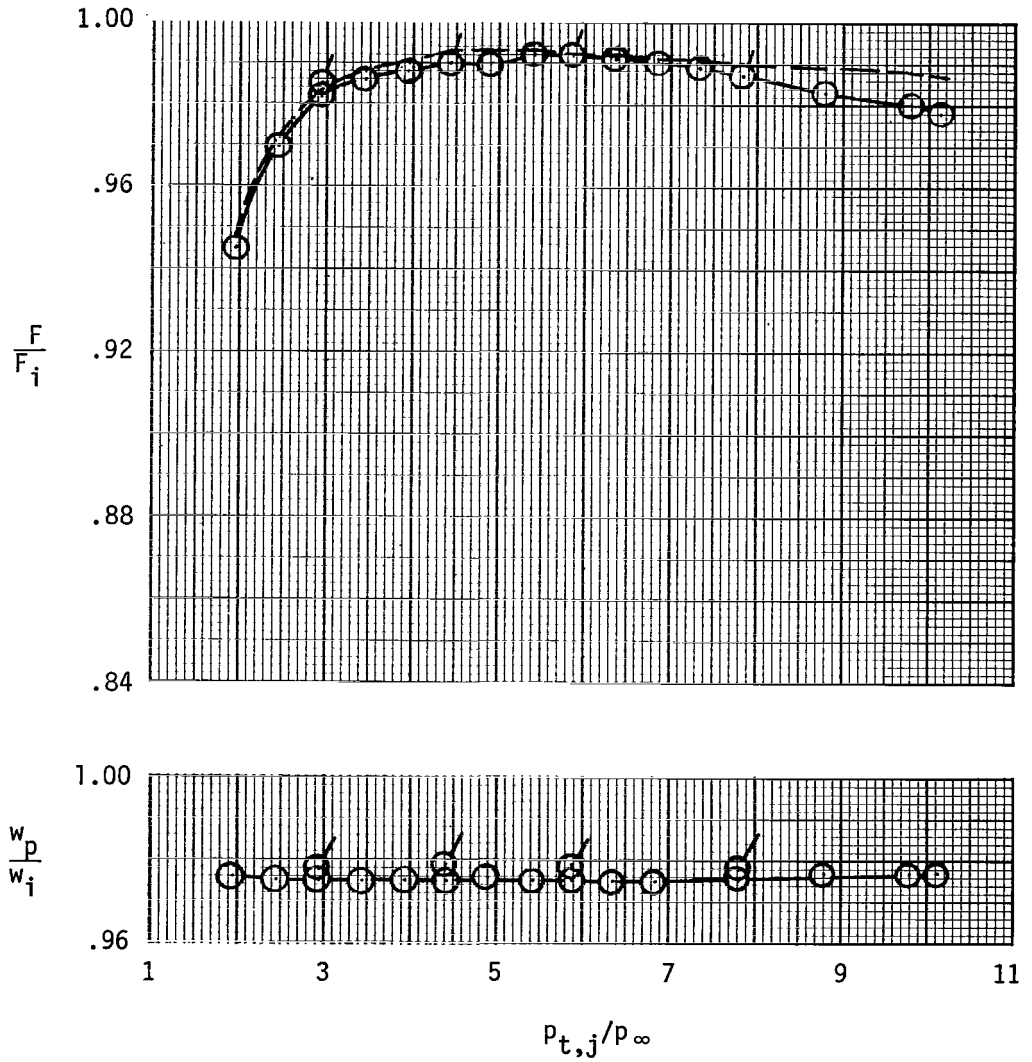

(a) Configuration F1.

Figure 8.- Variation of nozzle thrust ratio and discharge coefficient with nozzle pressure ratio for single expansion-ramp nozzles. Flagged symbols indicate data taken as nozzle pressure ratio was decreasing. Dashed line indicates values of resultant thrust ratio F_r/F_i.

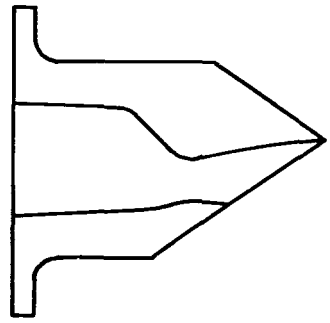

$(A_e/A_t)_i$ = 1.215, $(A_e/A_t)_e$ = 1.510, lower-flap length = 2.36cm

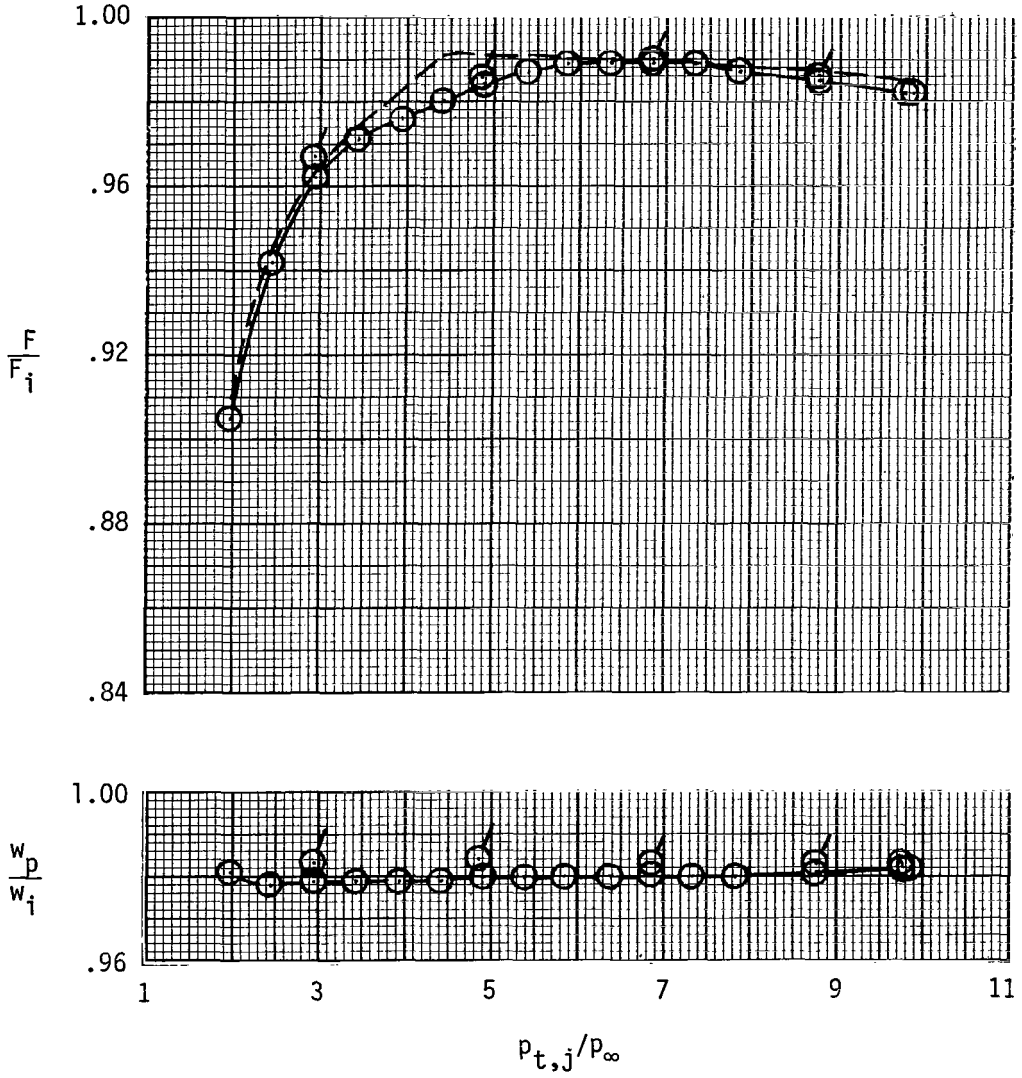

(b) Configuration F2.

Figure 8.- Continued.

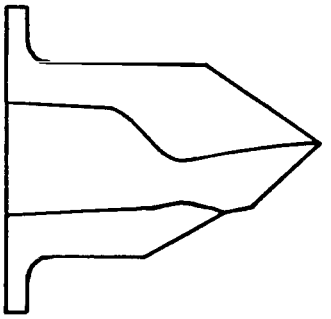

$(A_e/A_t)_i$ = 1.391, $(A_e/A_t)_e$ = 1.665, lower-flap length = 2.36cm

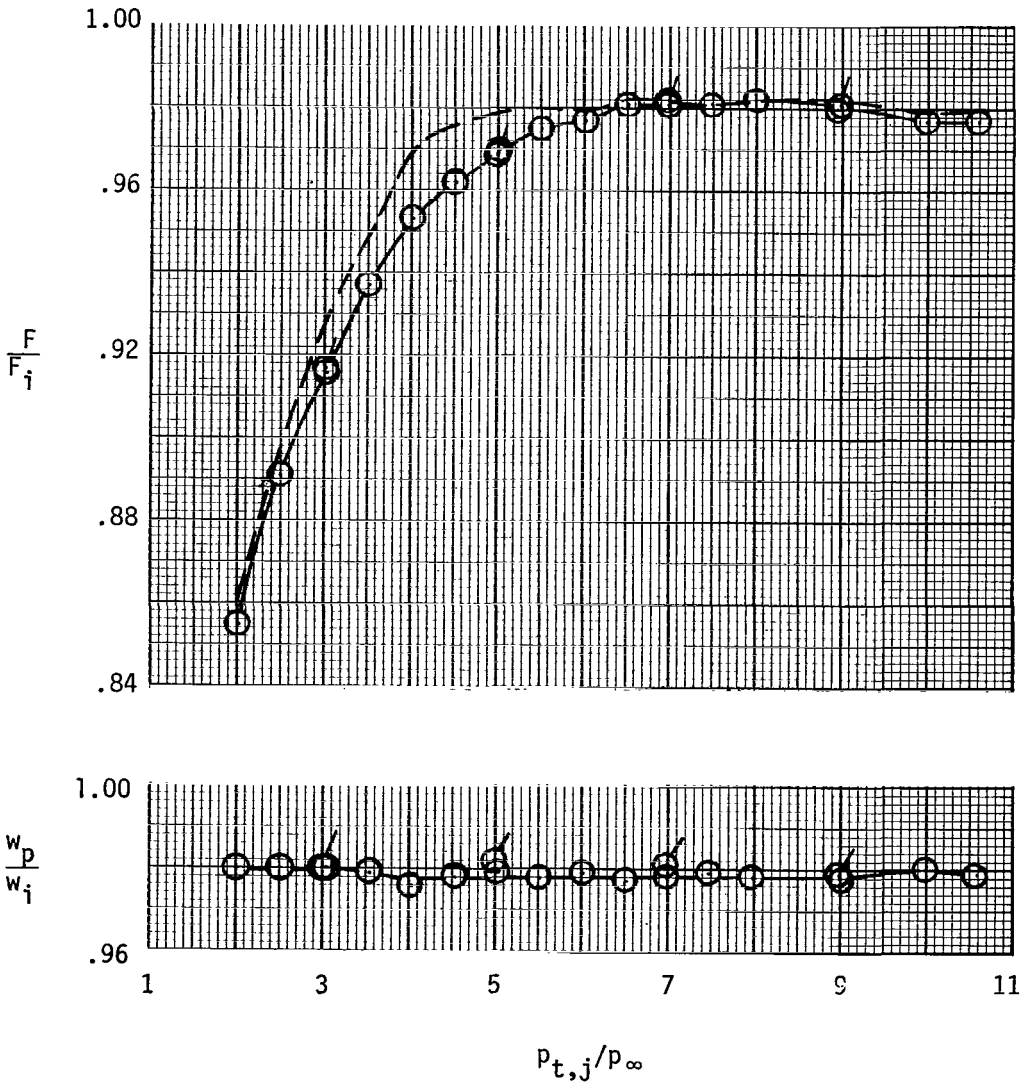

(c) Configuration F3.

Figure 8.- Continued.

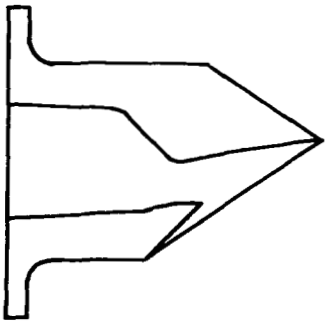

$(A_e/A_t)_i$ = 1.091, $(A_e/A_t)_e$ = 1.476, lower-flap length = 1.09cm

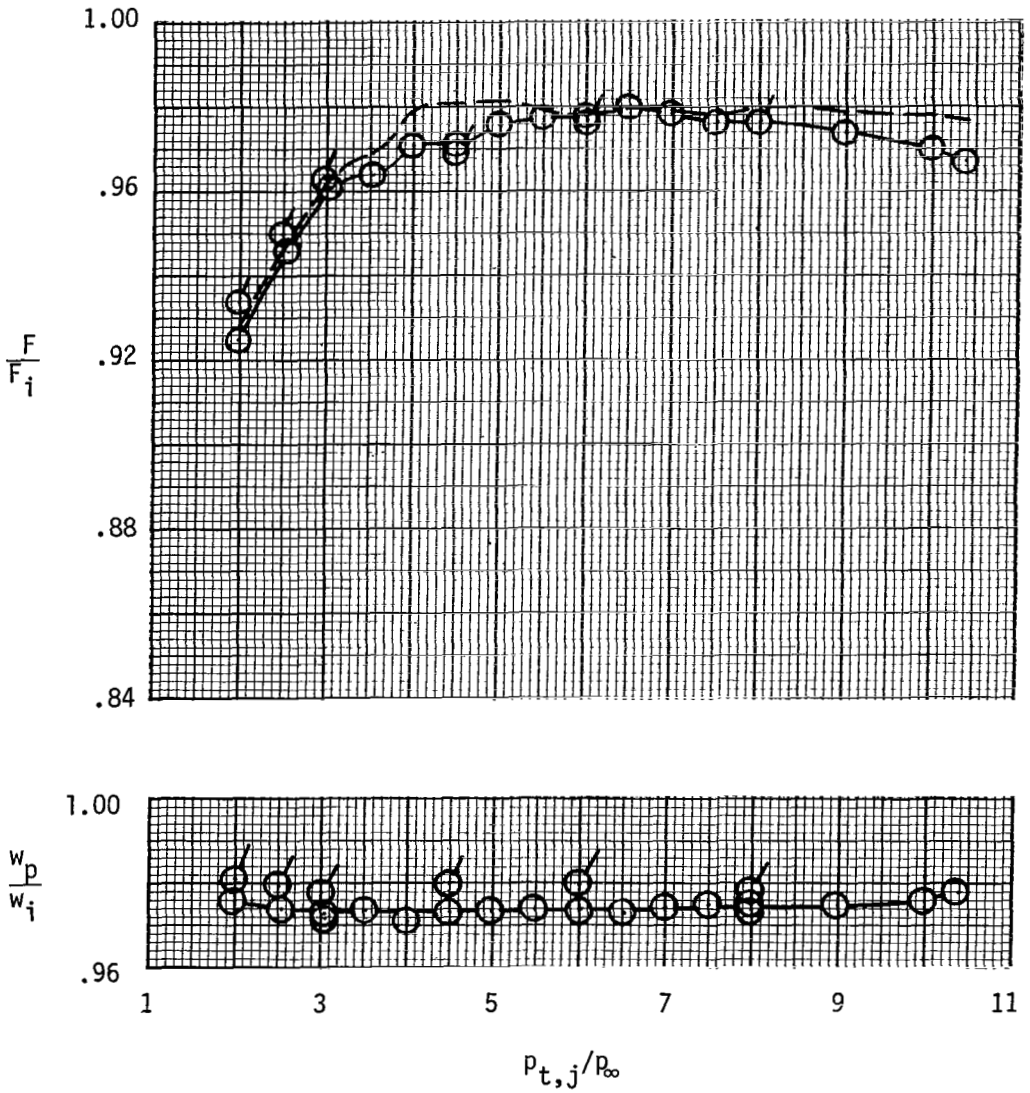

(d) Configuration F4.

Figure 8.- Continued.

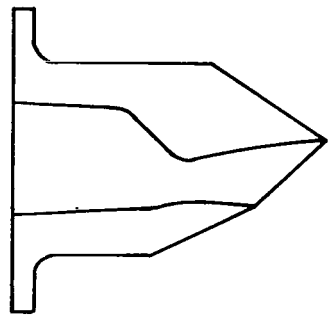

$(A_e/A_t)_i$ = 1.389, $(A_e/A_t)_e$ = 1.558, lower-flap length = 4.01cm

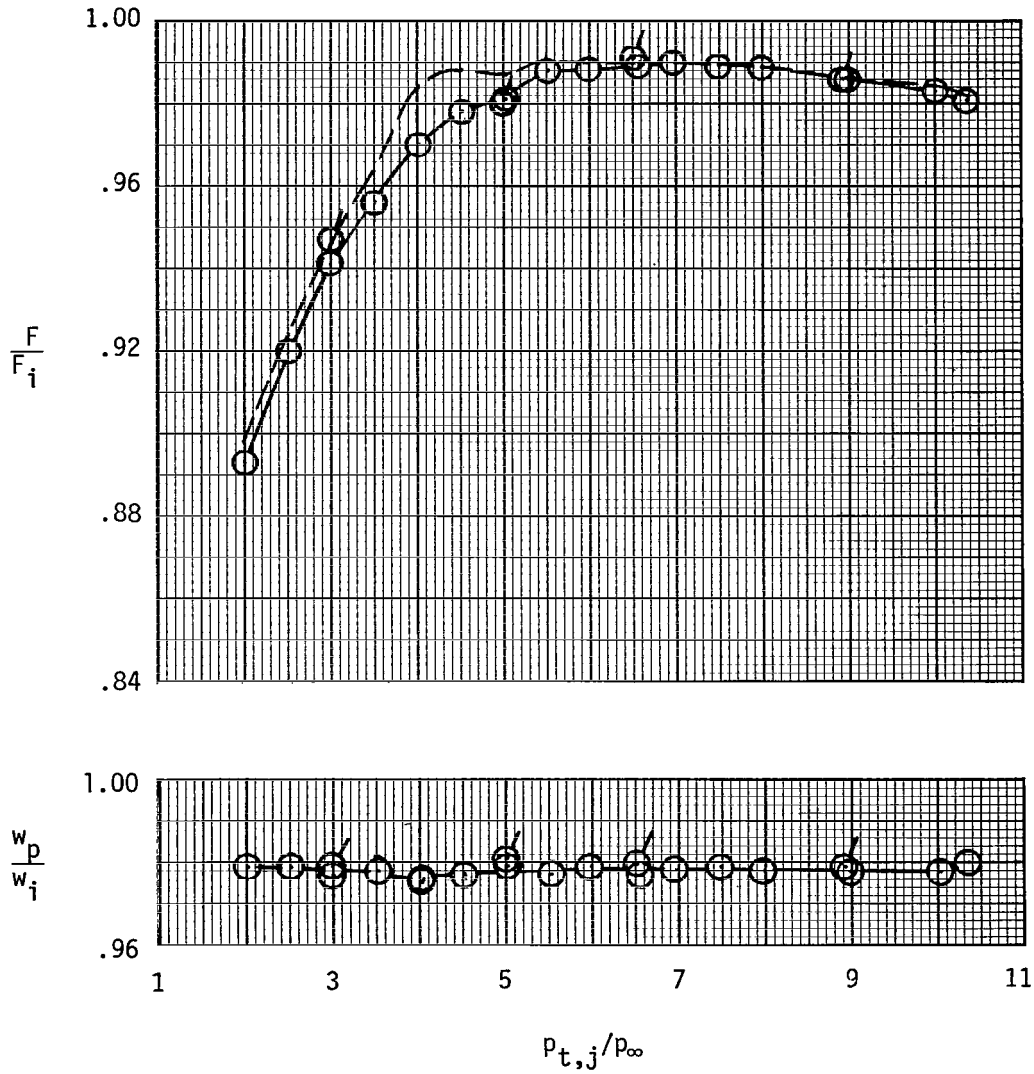

(e) Configuration F5.

Figure 8.- Continued.

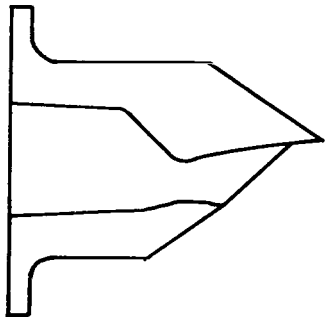

$(A_e/A_t)_i$ = 1.215, $(A_e/A_t)_e$ = 1.510, lower-flap length = 2.36cm

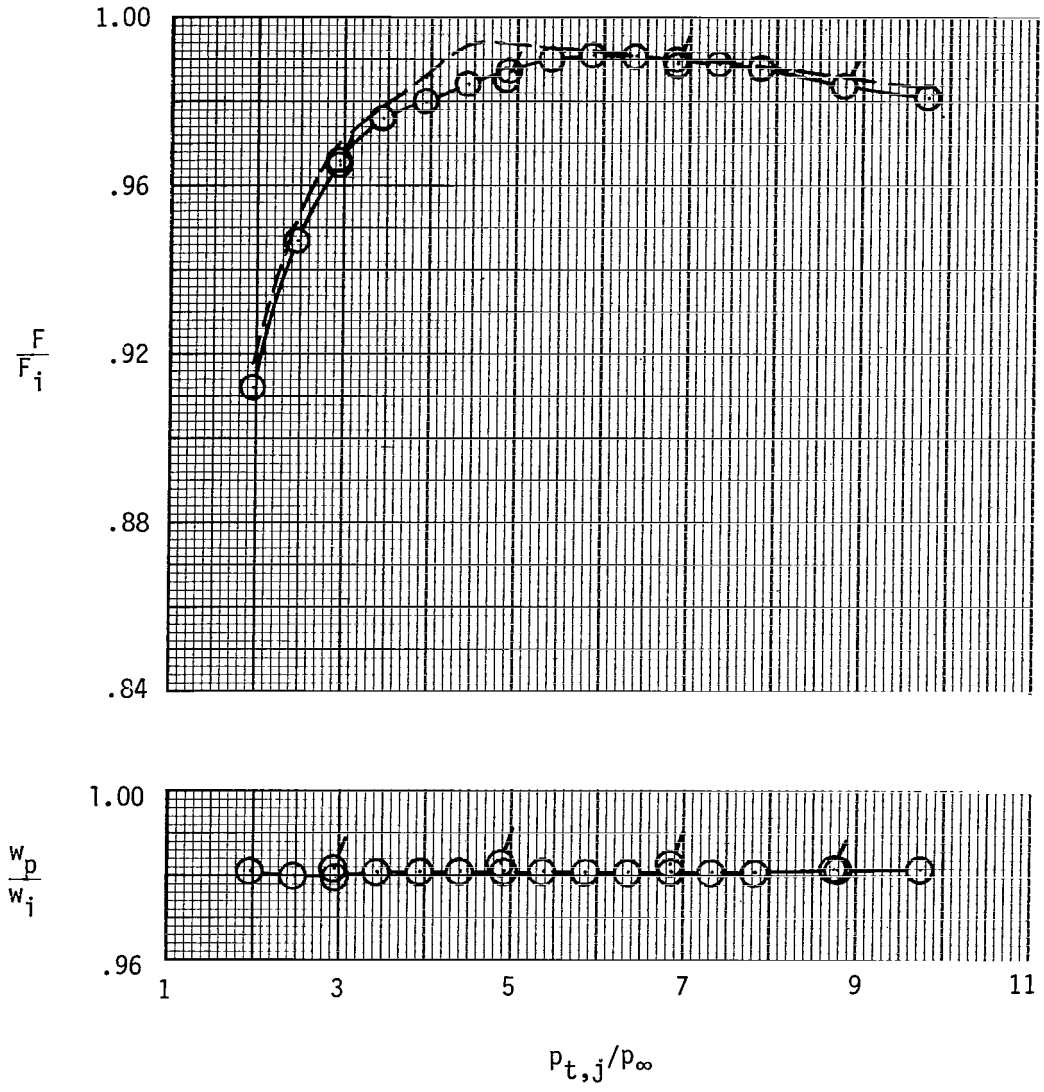

(f) Configuration F6.

Figure 8.- Concluded.

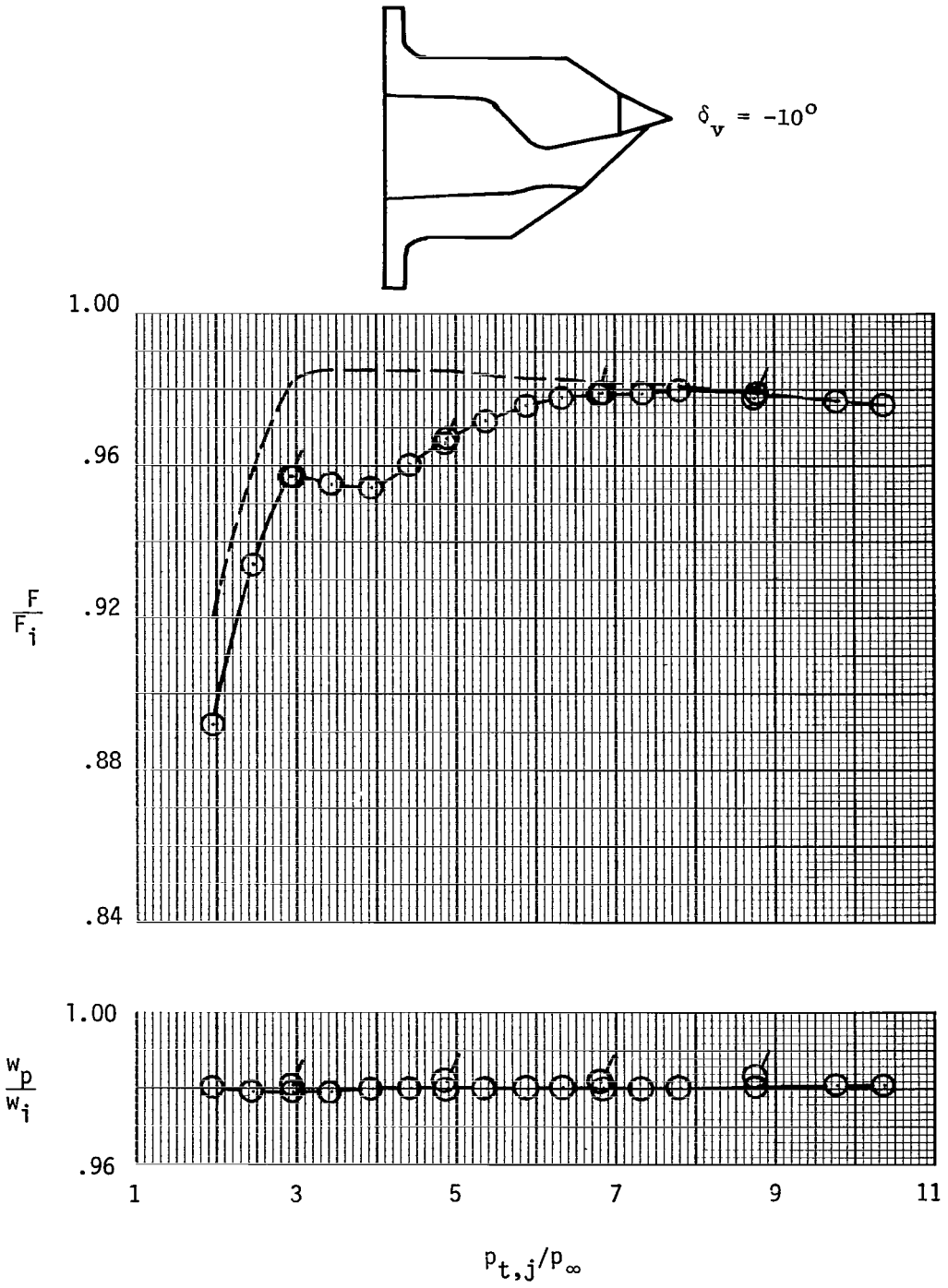

(a) Configuration VF1(-10).

Figure 9.- Variation of nozzle thrust ratio and discharge coefficient with nozzle pressure ratio for single expansion-ramp nozzles utilizing short upper aft flap for thrust vectoring. Baseline (δ_v = 0°) nozzle shown as configuration F6 in figure 8(f). Flagged symbols indicate data taken as nozzle pressure ratio was decreasing. Dashed line indicates values of resultant thrust ratio F_r/F_i.

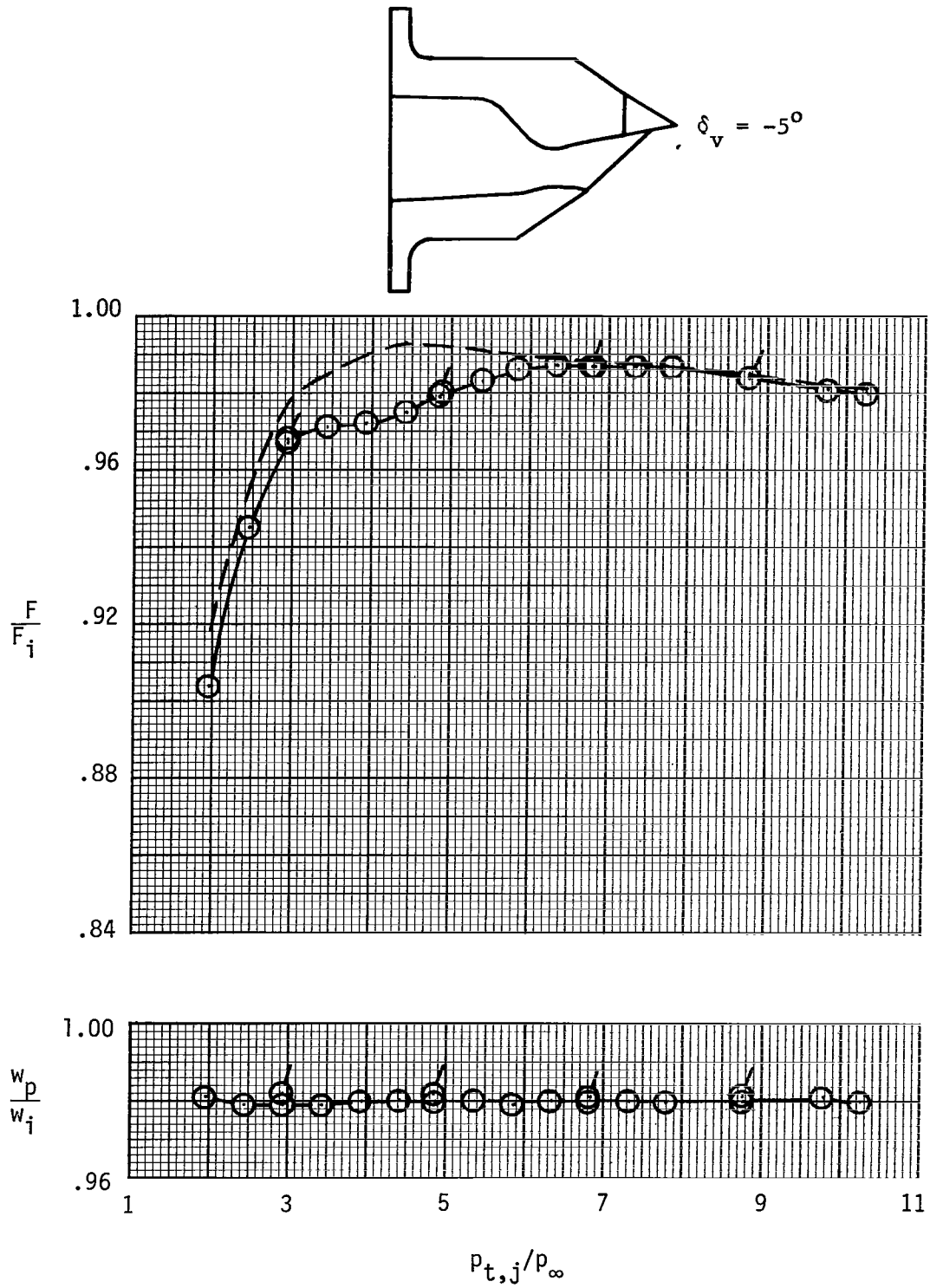

(b) Configuration VF1(-5).

Figure 9.- Continued.

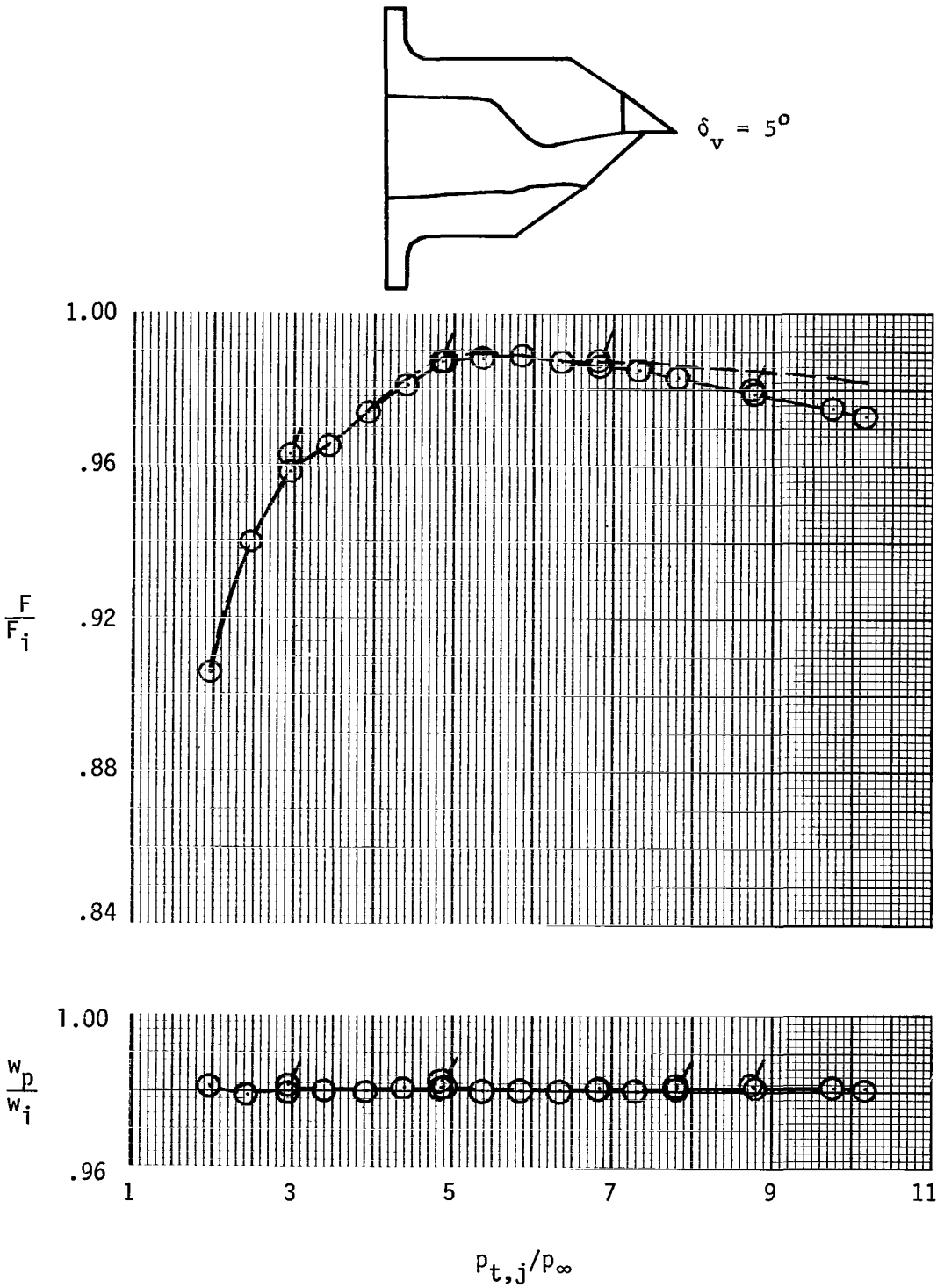

(c) Configuration VF1(5).

Figure 9.- Continued.

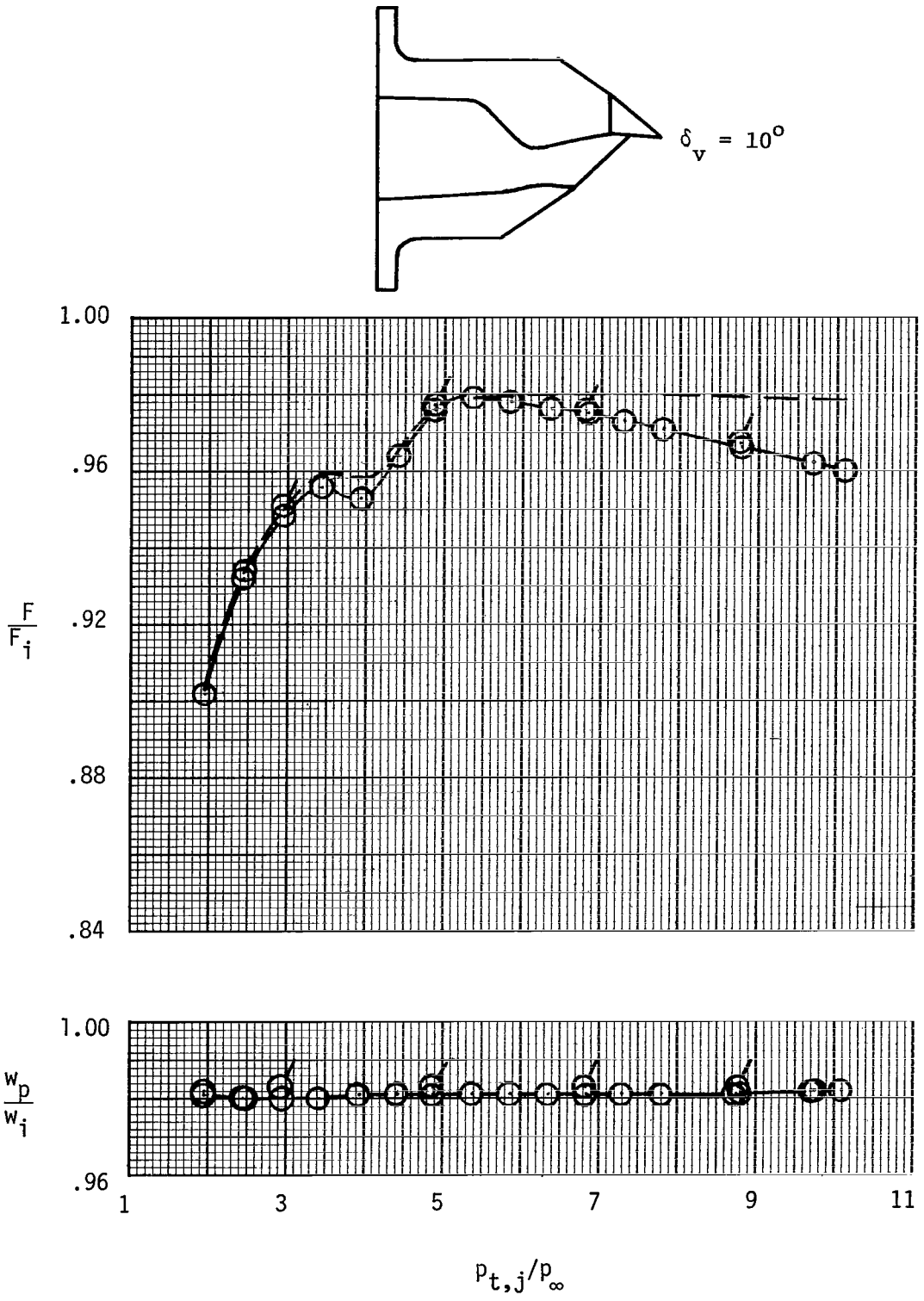

(d) Configuration VF1(10).

Figure 9.- Continued.

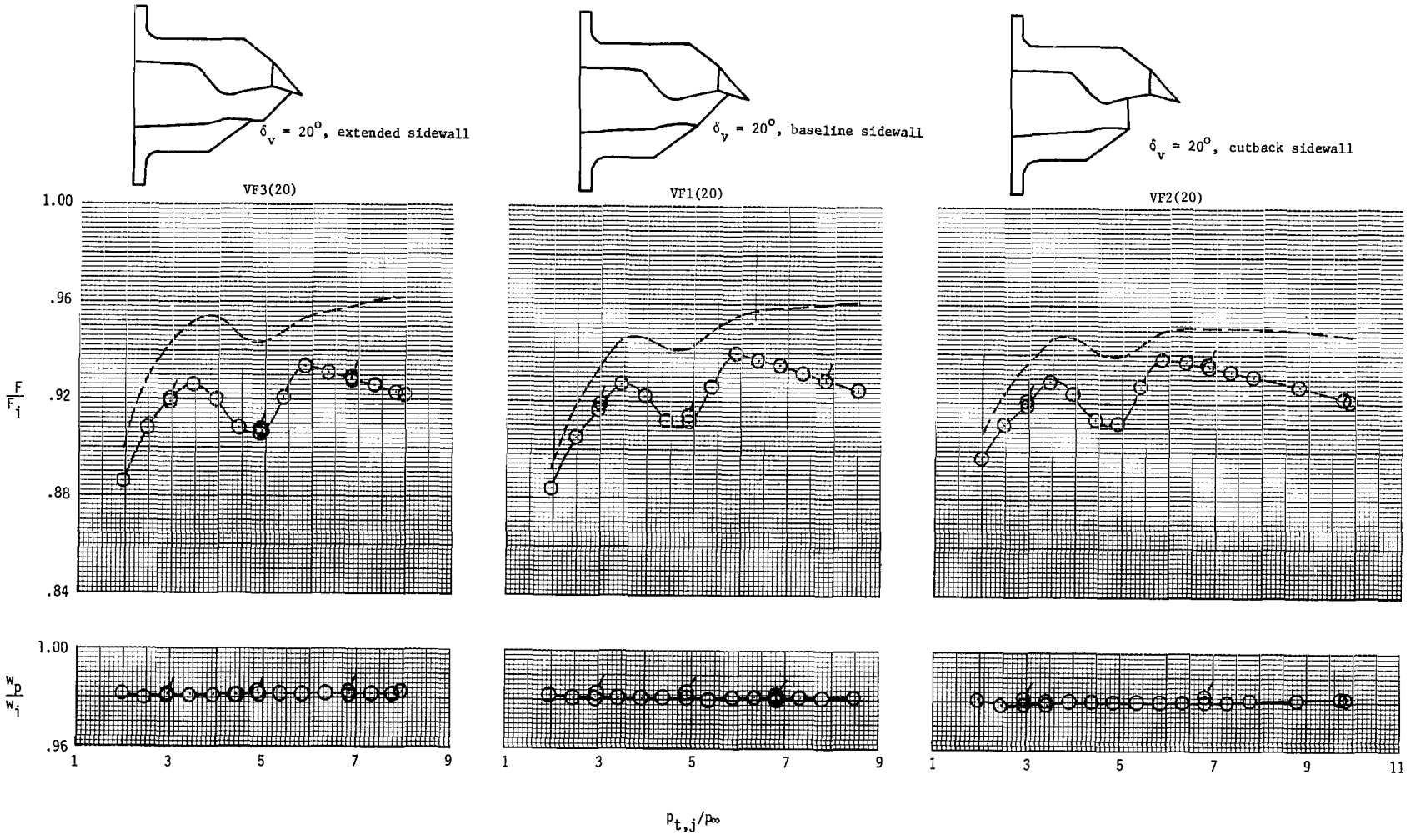

(e) Configurations VF1(20), VF2(20), and VF3(20).

Figure 9.- Concluded.

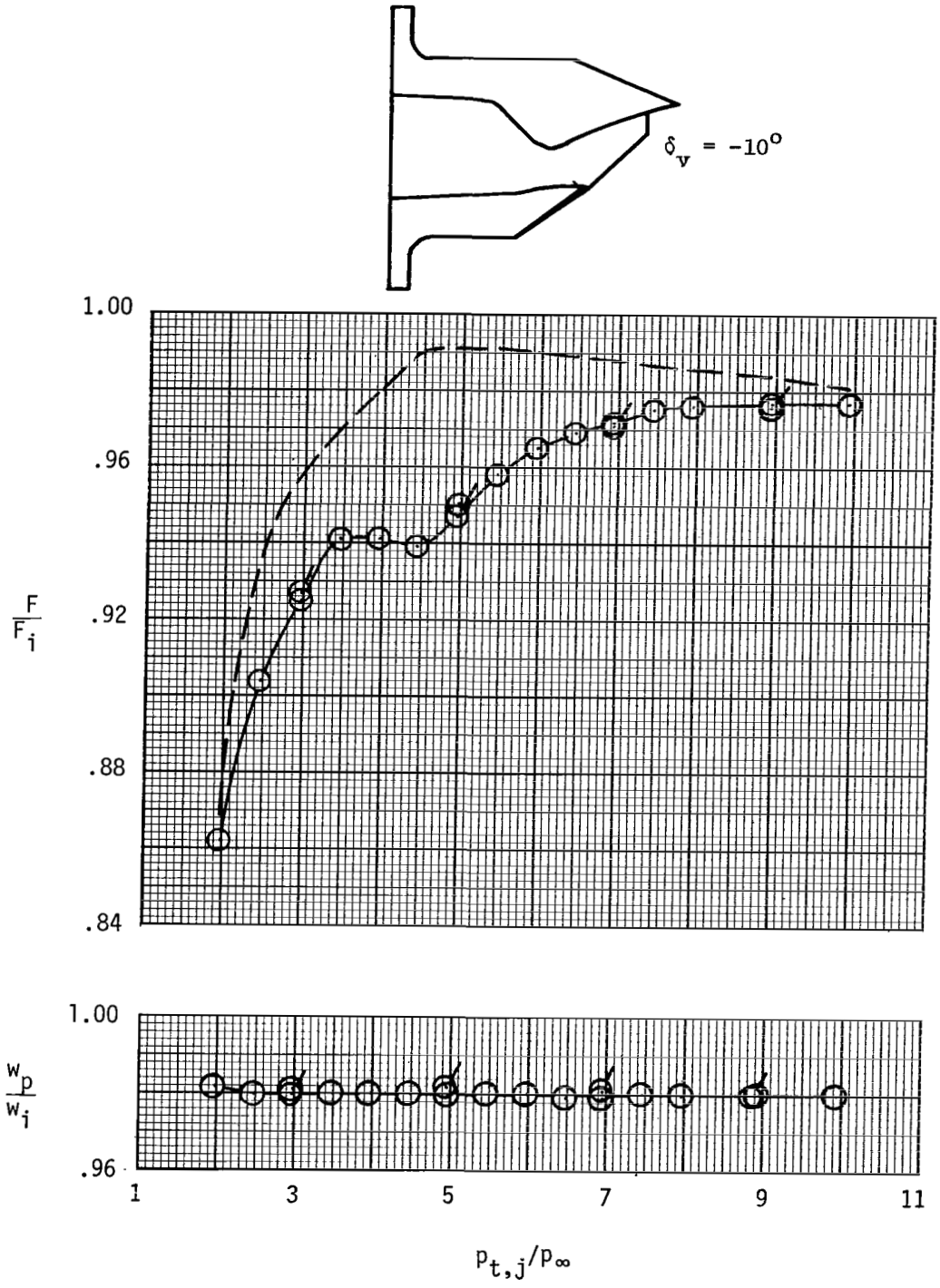

(a) Configuration V1(-10).

Figure 10.- Variation of nozzle thrust ratio and discharge coefficient with nozzle pressure ratio for single expansion-ramp nozzles utilizing upper and lower flaps for thrust vectoring. Baseline ($\delta_v = 0°$) nozzle shown as configuration F6 in figure 8(f). Flagged symbols indicate data taken as nozzle pressure ratio was decreasing. Dashed line indicates values of resultant thrust ratio F_r/F_i.

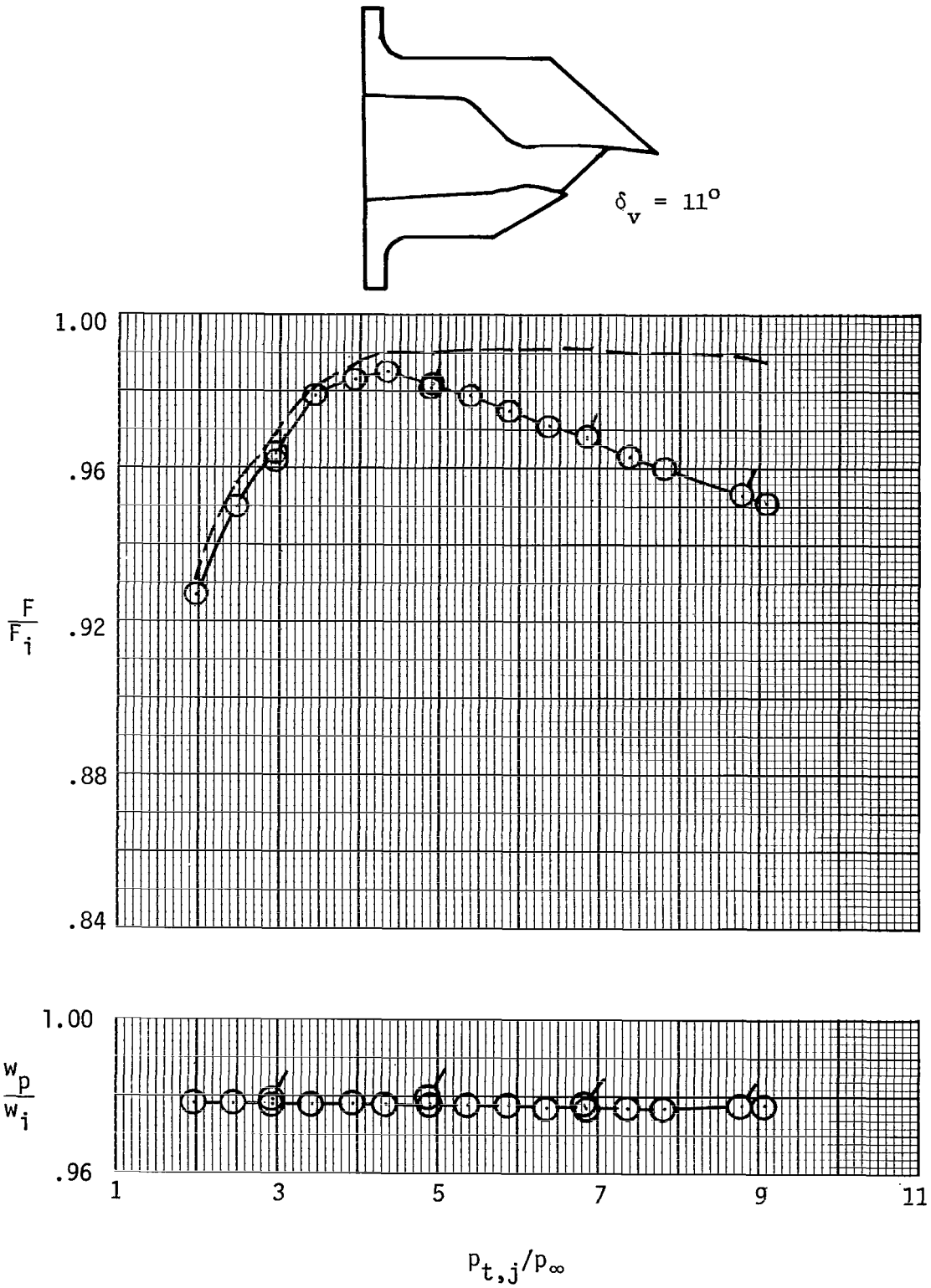

(b) Configuration V1(11).

Figure 10.- Continued.

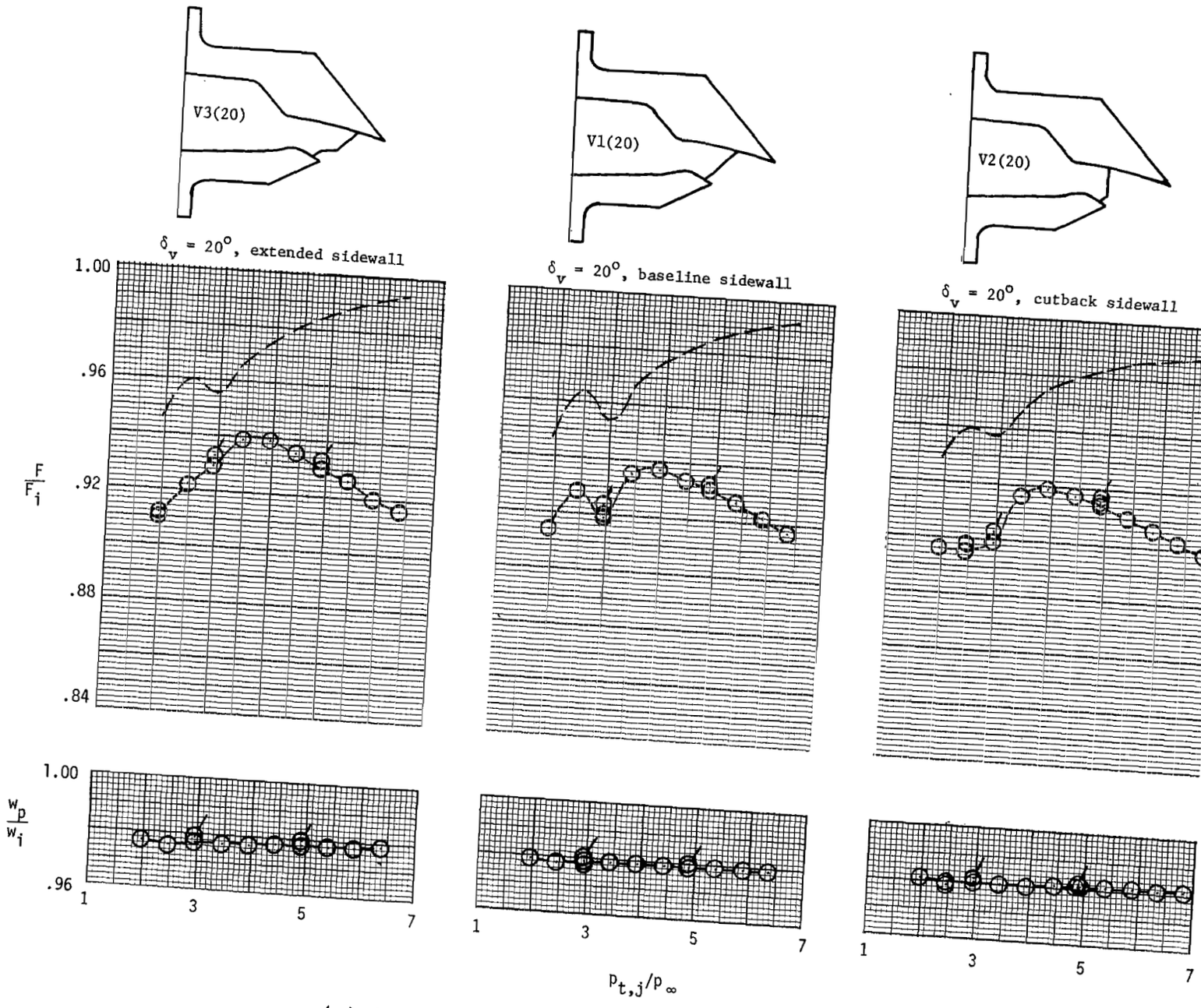

(c) Configurations V1(20), V2(20), and V3(20).

Figure 10.- Concluded.

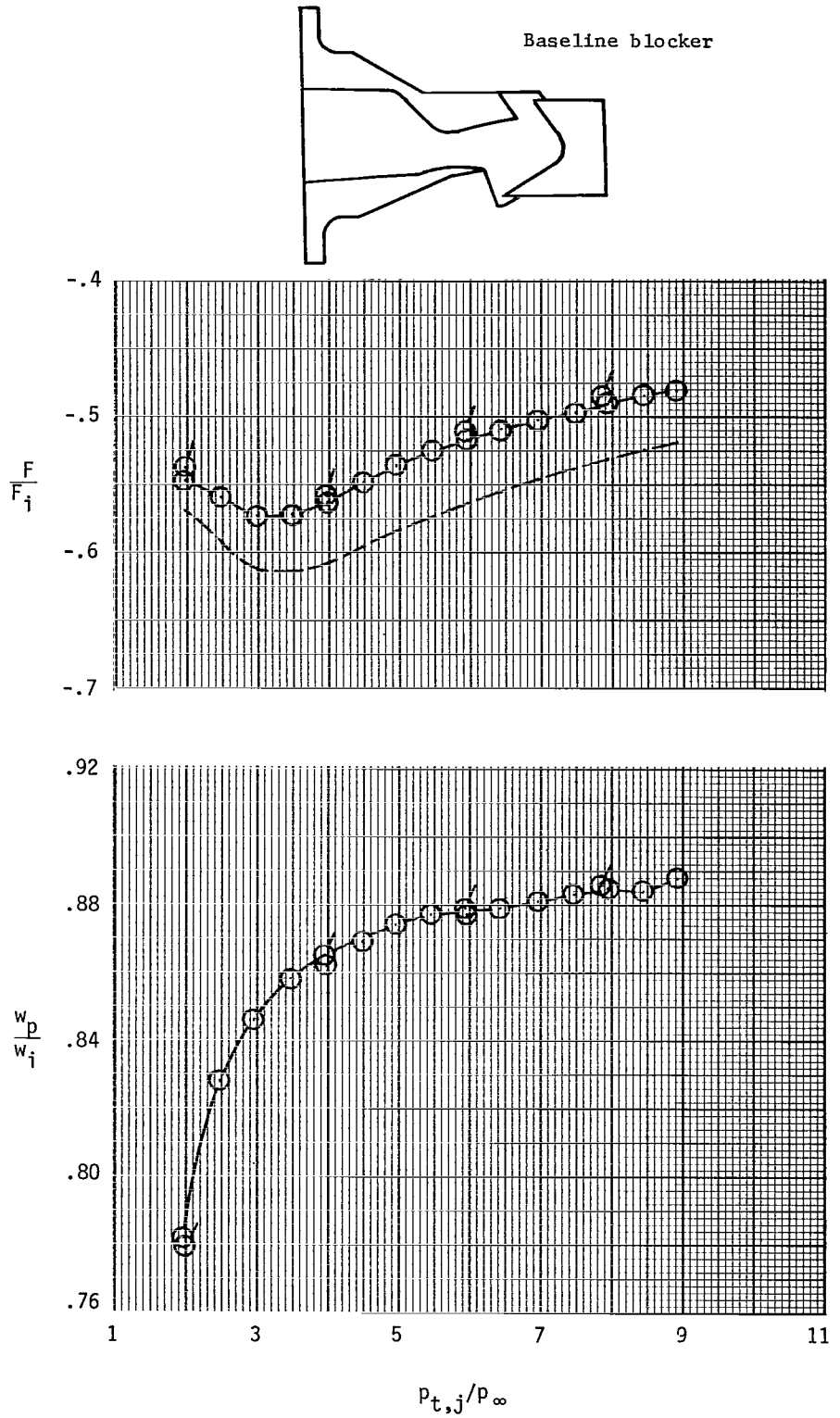

(a) Configuration R1.

Figure 11.- Variation of nozzle thrust ratio and discharge coefficient with nozzle pressure ratio for reversed-thrust single expansion-ramp nozzles. Flagged symbols indicate data taken as nozzle pressure ratio was decreasing. Dashed line indicates values of resultant thrust ratio F_r/F_i.

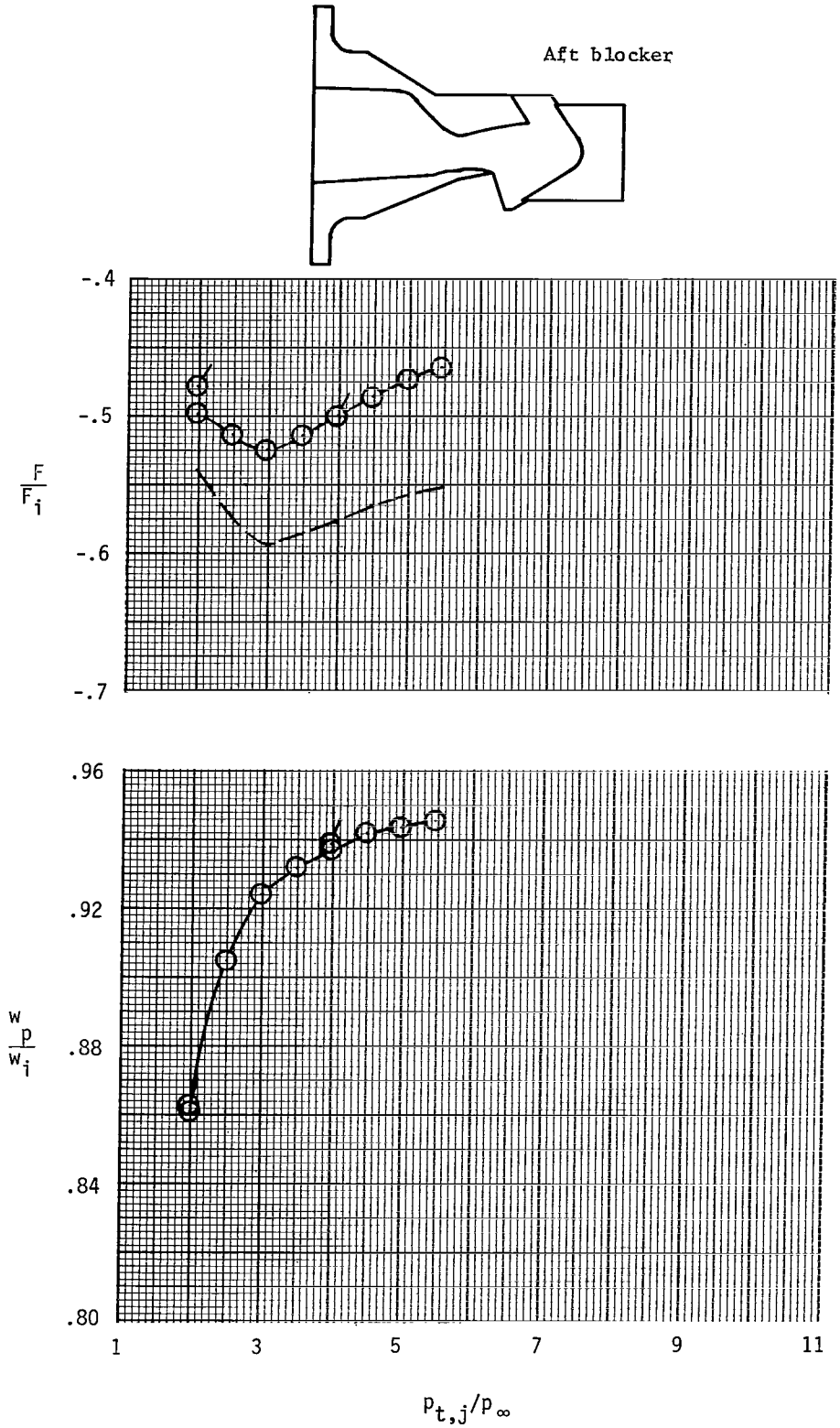

(b) Configuration R2.

Figure 11.- Continued.

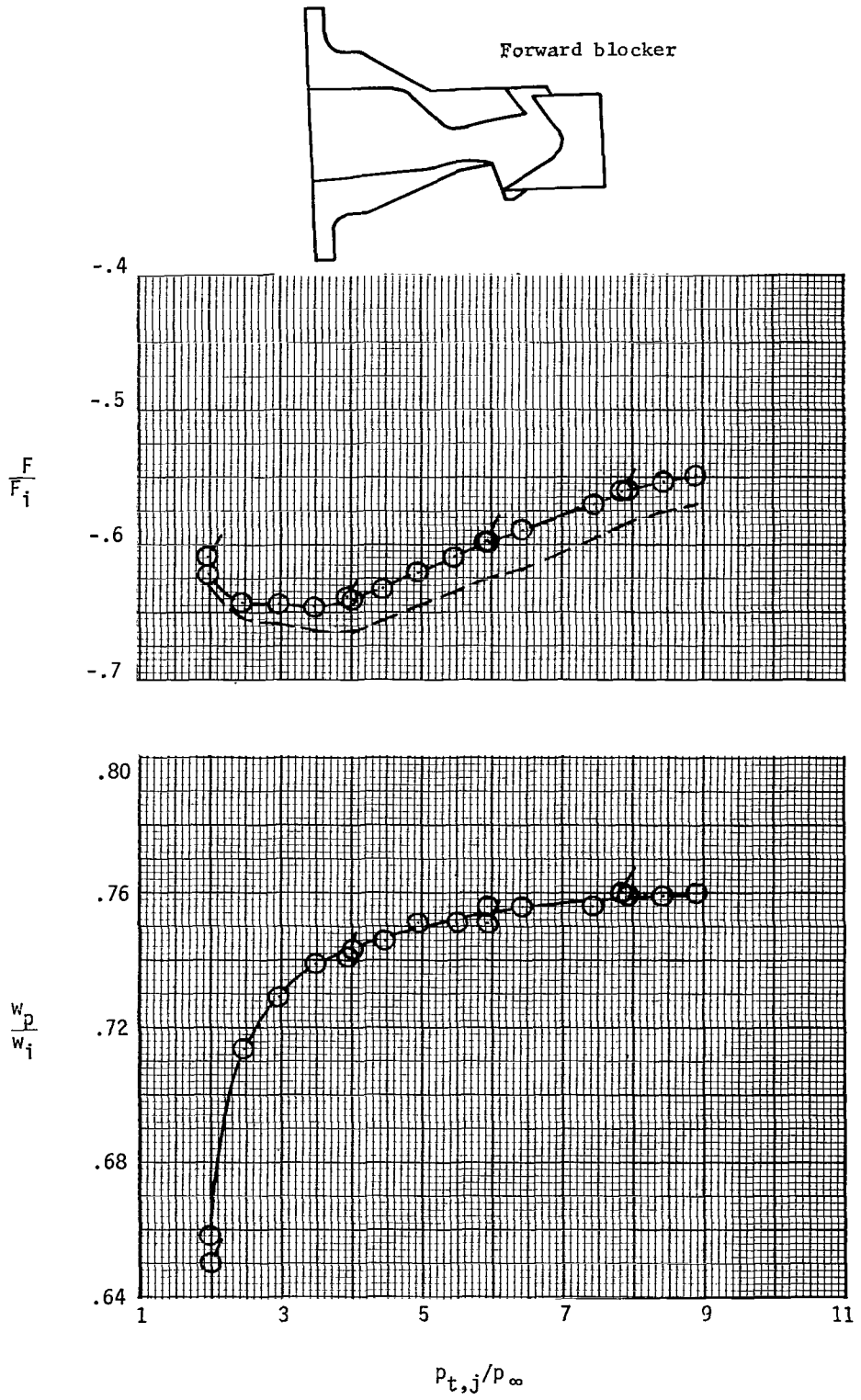

(c) Configuration R3.

Figure 11.- Continued.

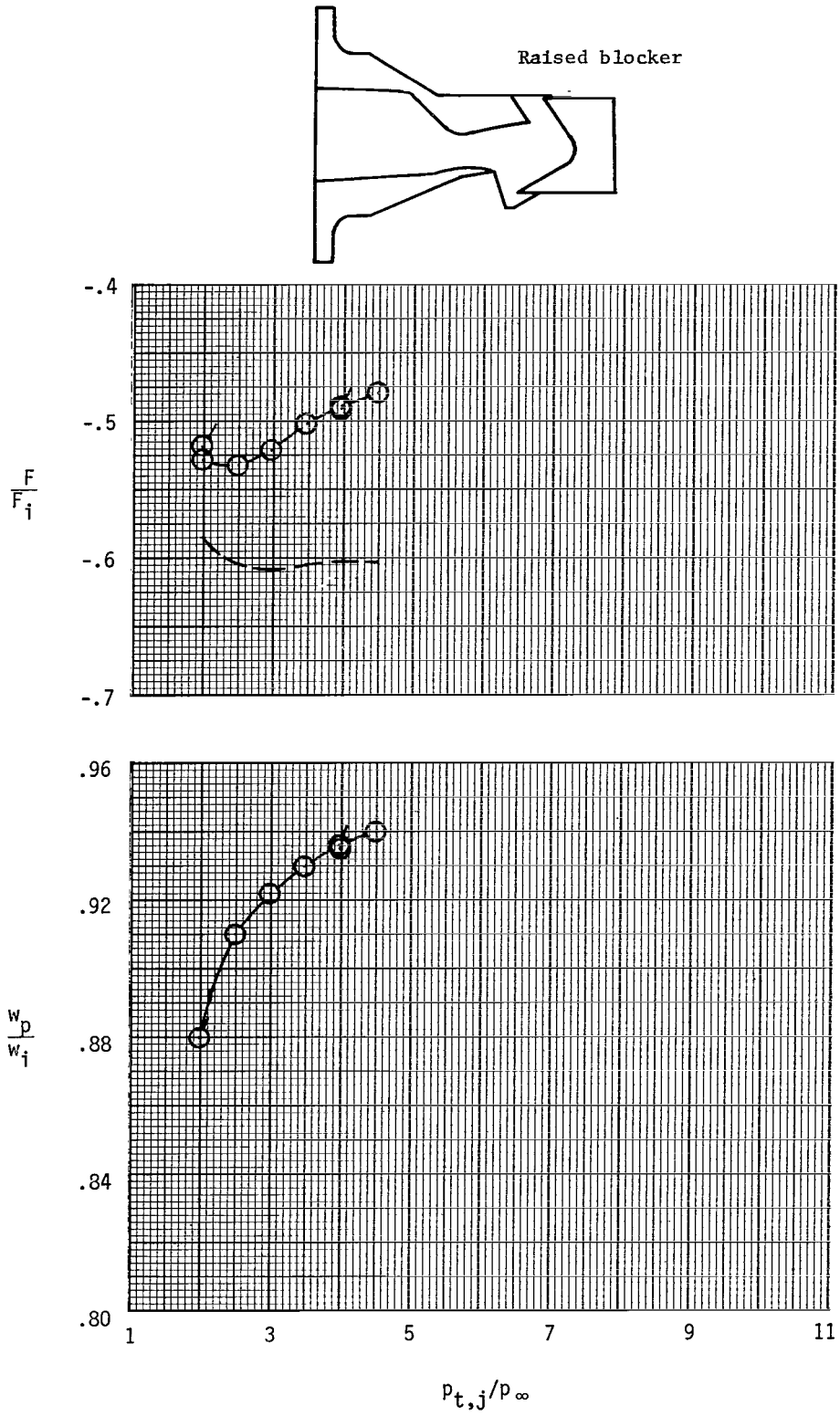

(d) Configuration R4.

Figure 11.- Continued.

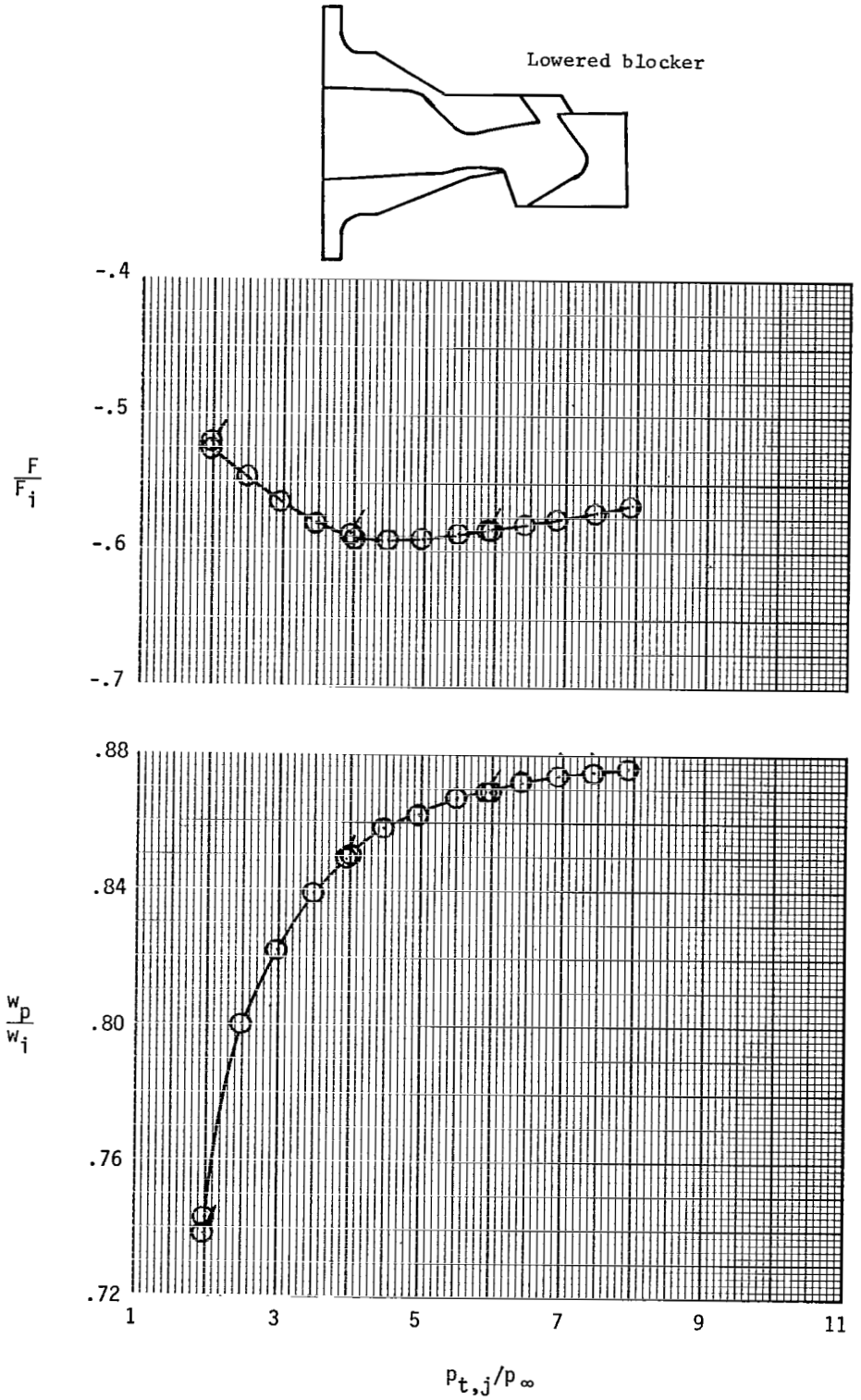

(e) Configuration R5.

Figure 11.- Concluded.

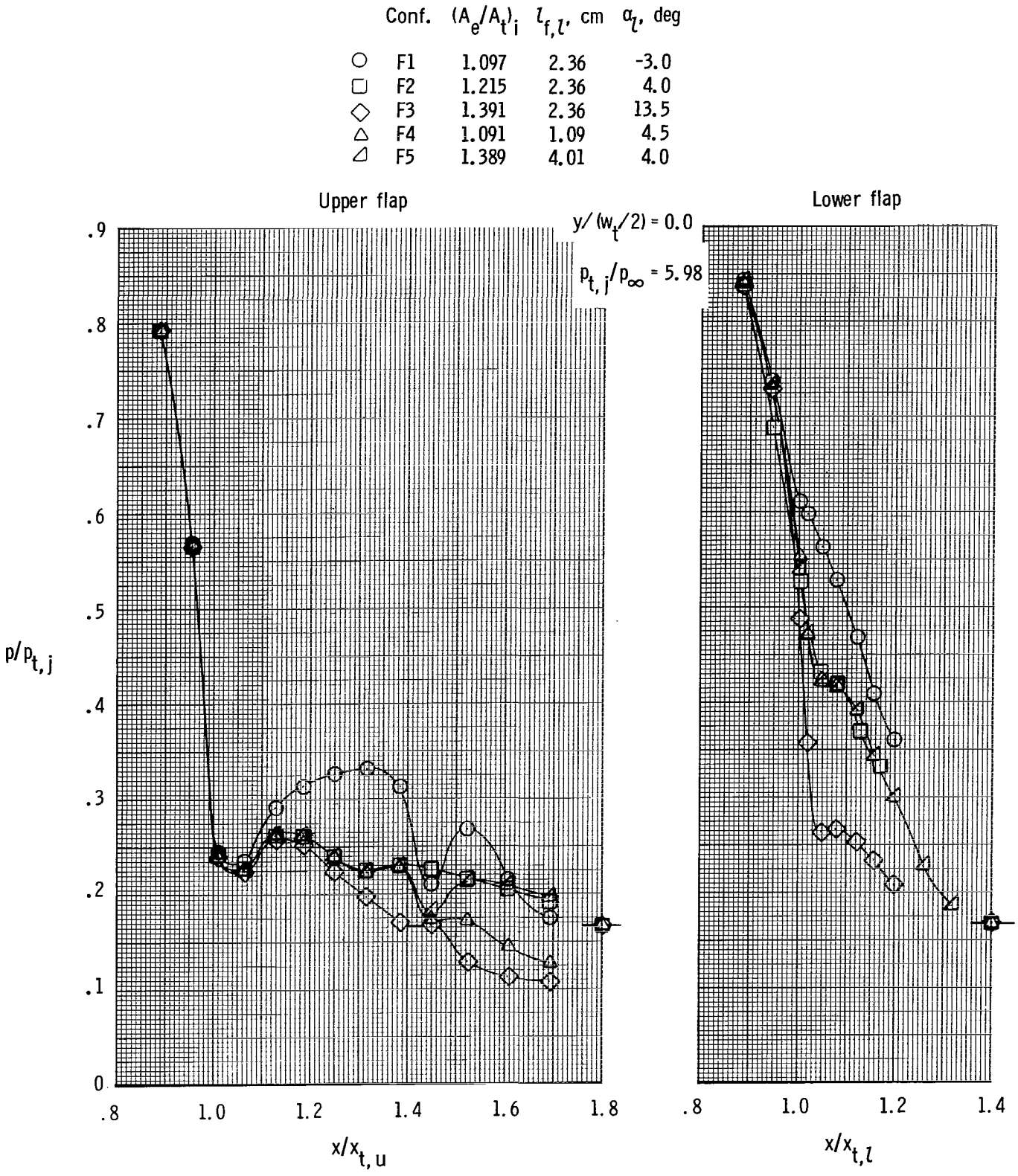

Figure 12.- Effect of nozzle internal geometry on nozzle internal static-pressure distributions. Isolated symbols with tick marks indicate values of $p_\infty/p_{t,j}$.

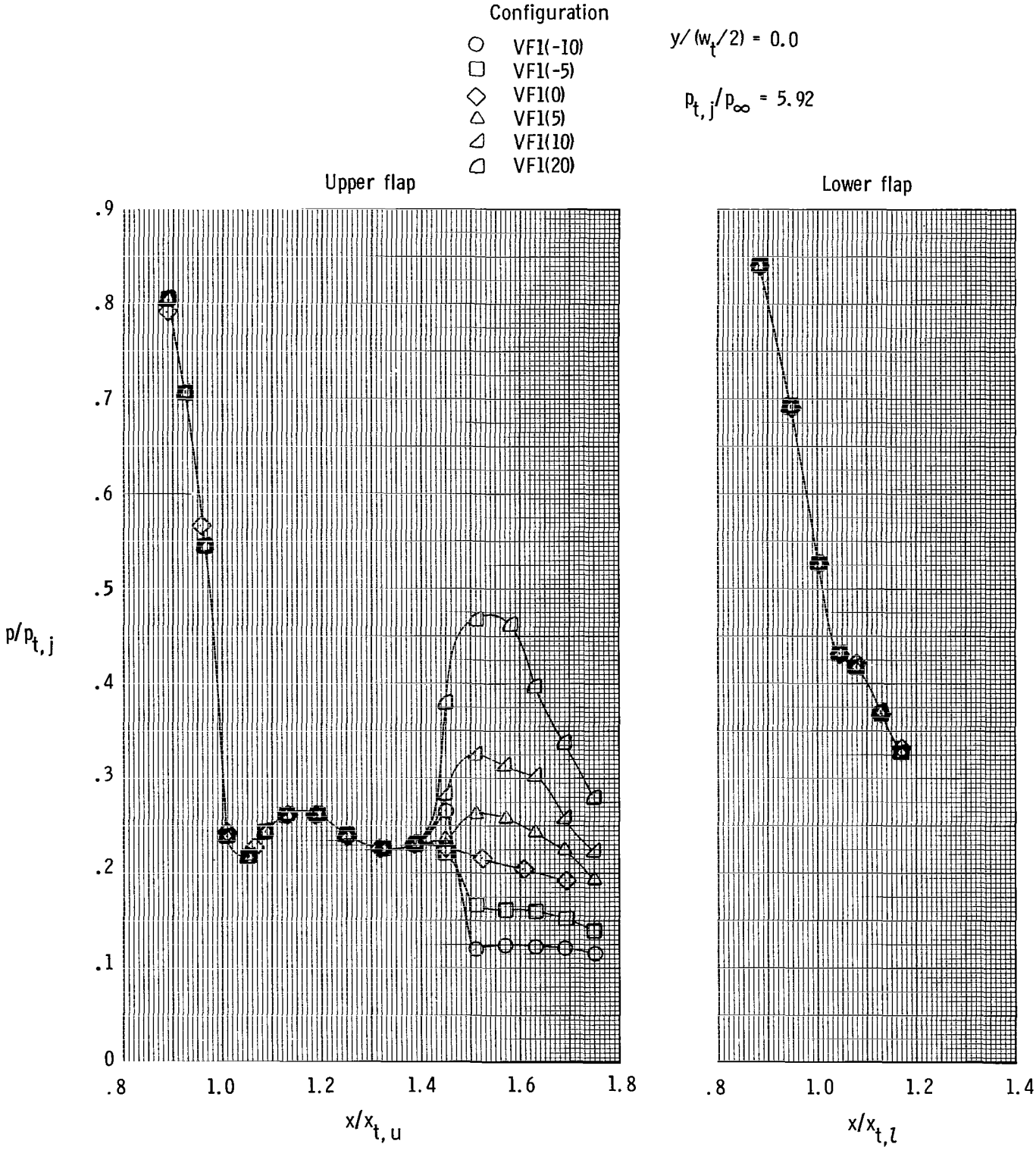

(a) Vectored upper-flap configurations.

Figure 13.- Effect of thrust vectoring on nozzle internal static-pressure distributions.

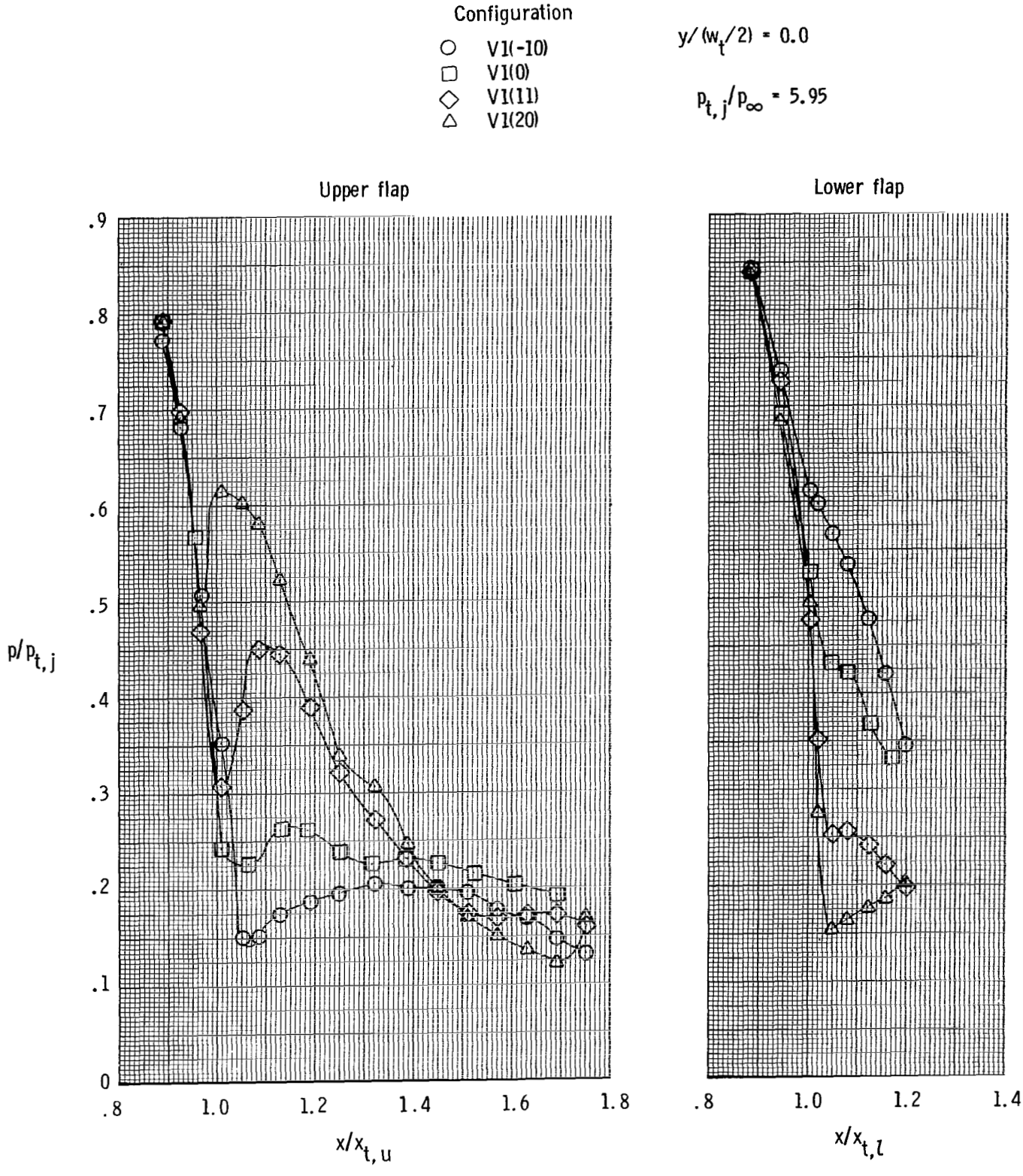

(b) Vectored upper- and lower-flap configurations.

Figure 13.- Concluded.

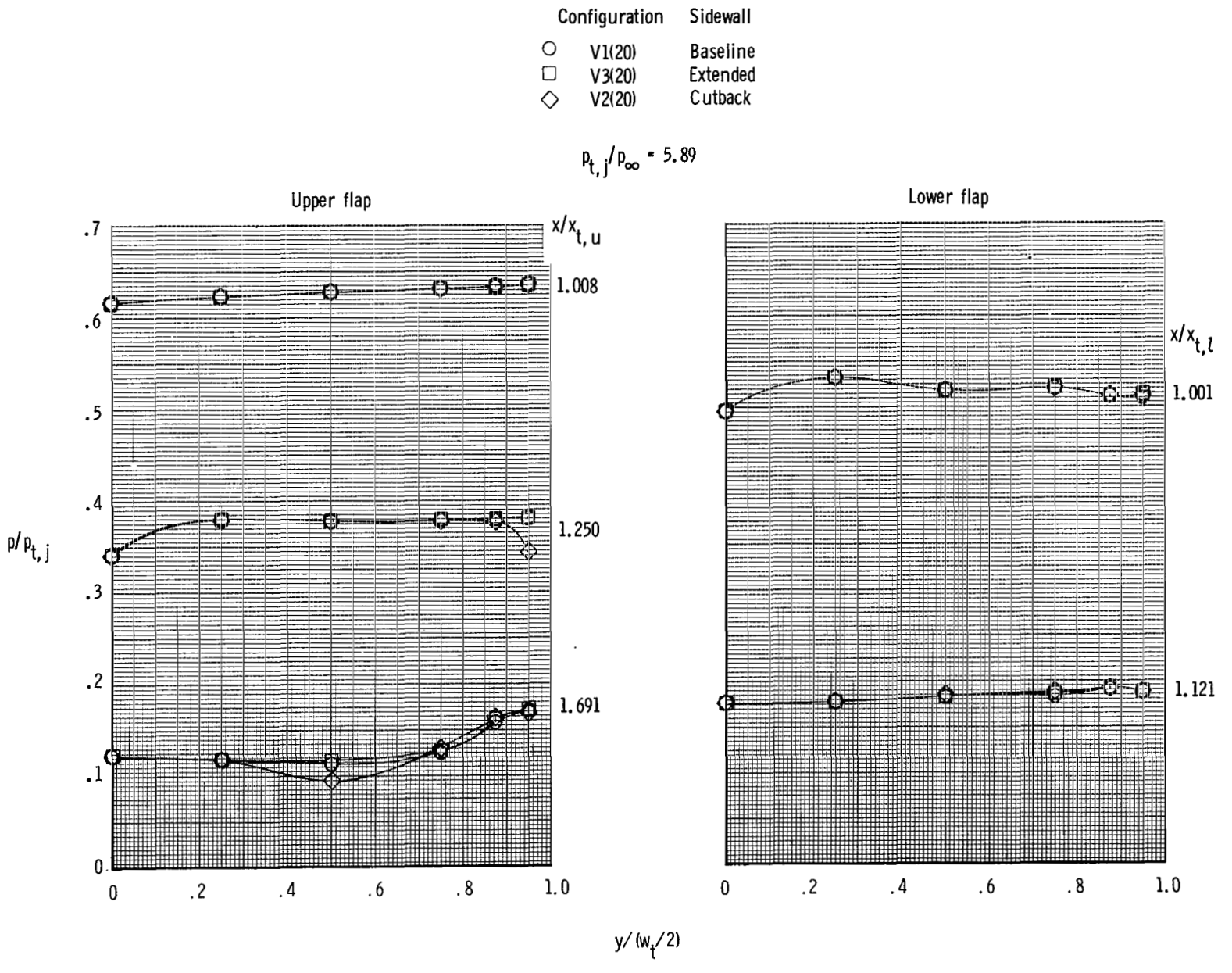

Figure 14.- Effect of sidewall geometry on vectored-thrust nozzle internal static-pressure distributions.

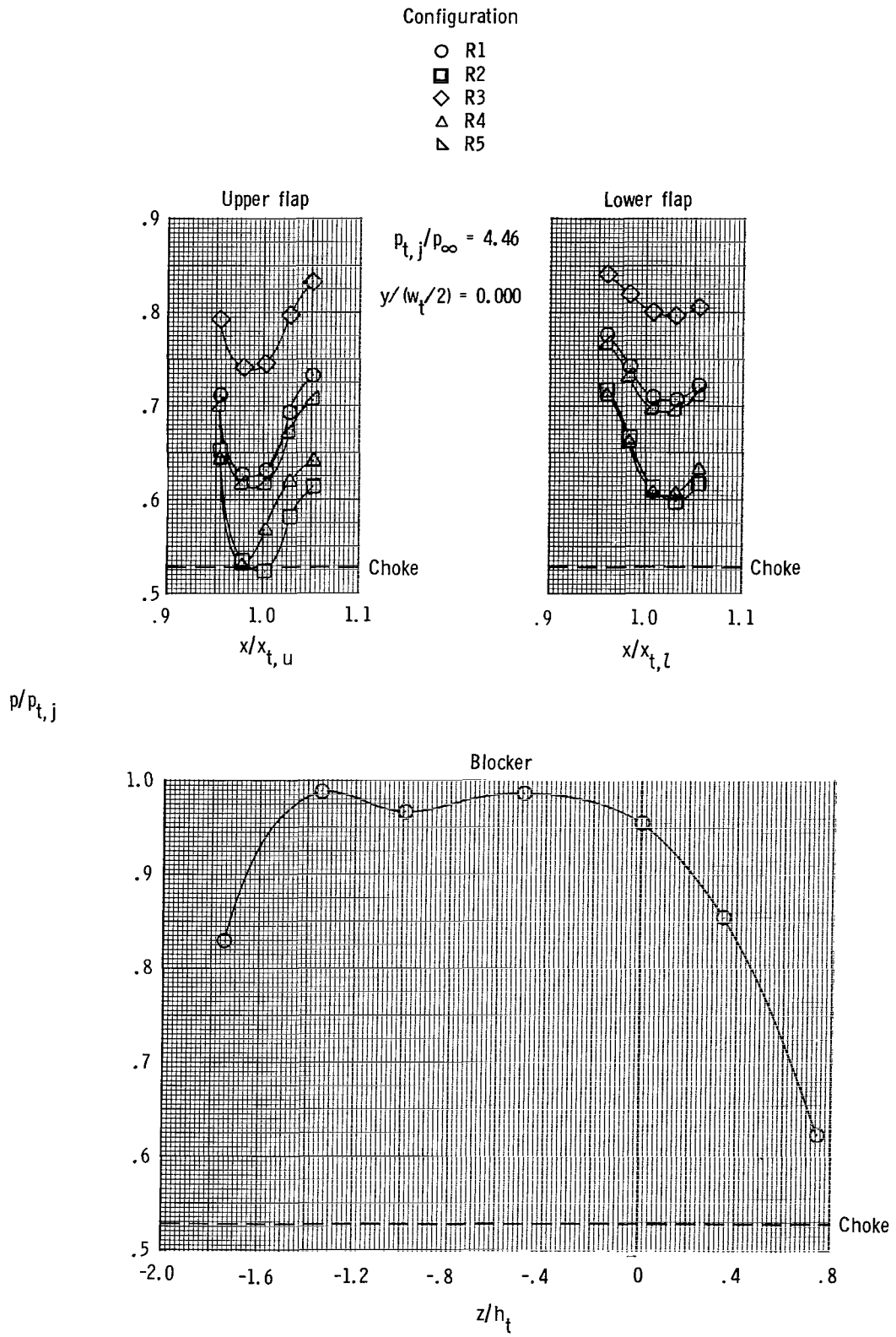

Figure 15.- Effect of thrust reversing on nozzle internal static-pressure distributions.

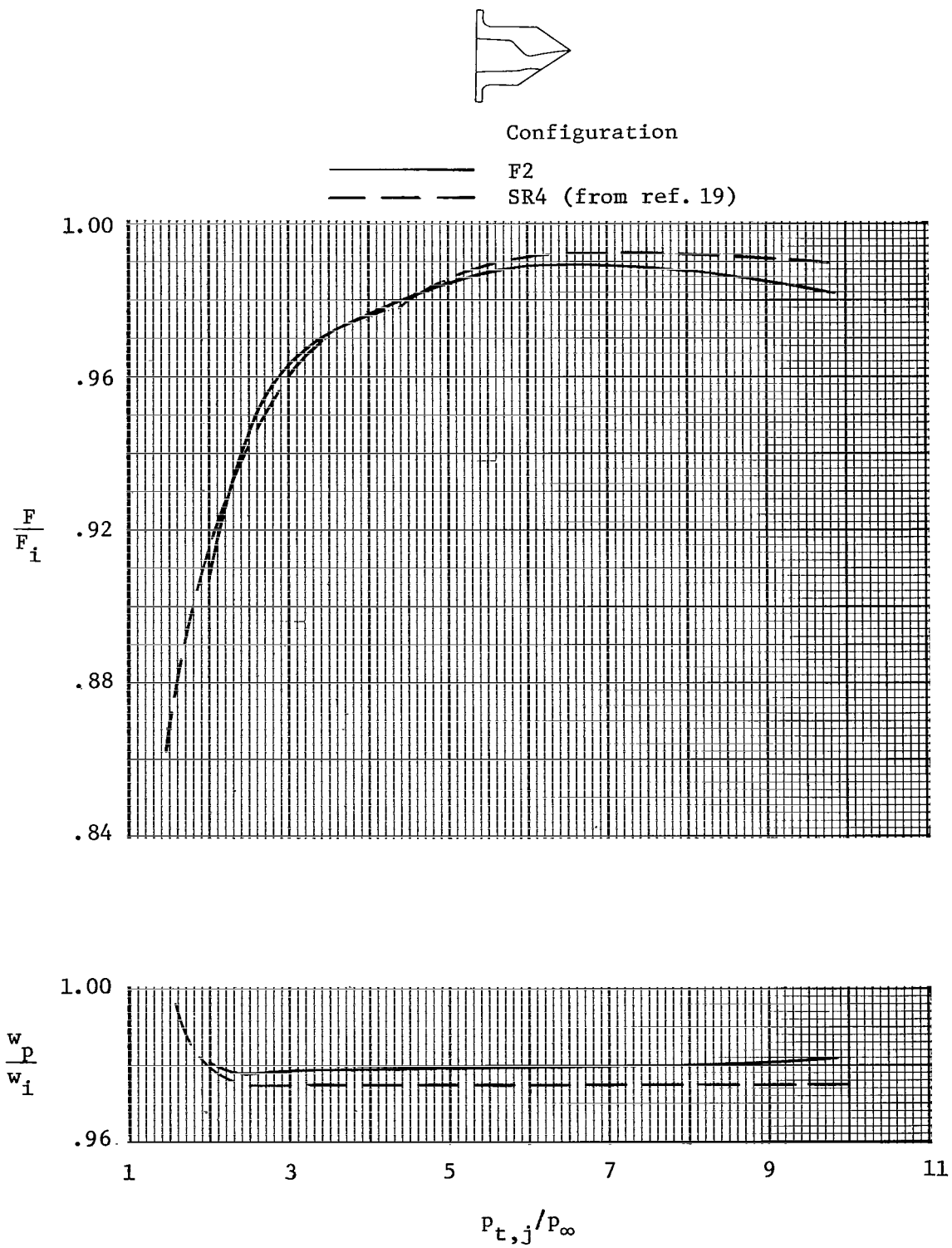

Figure 16.- Comparison of data from current investigation with data from reference 19.

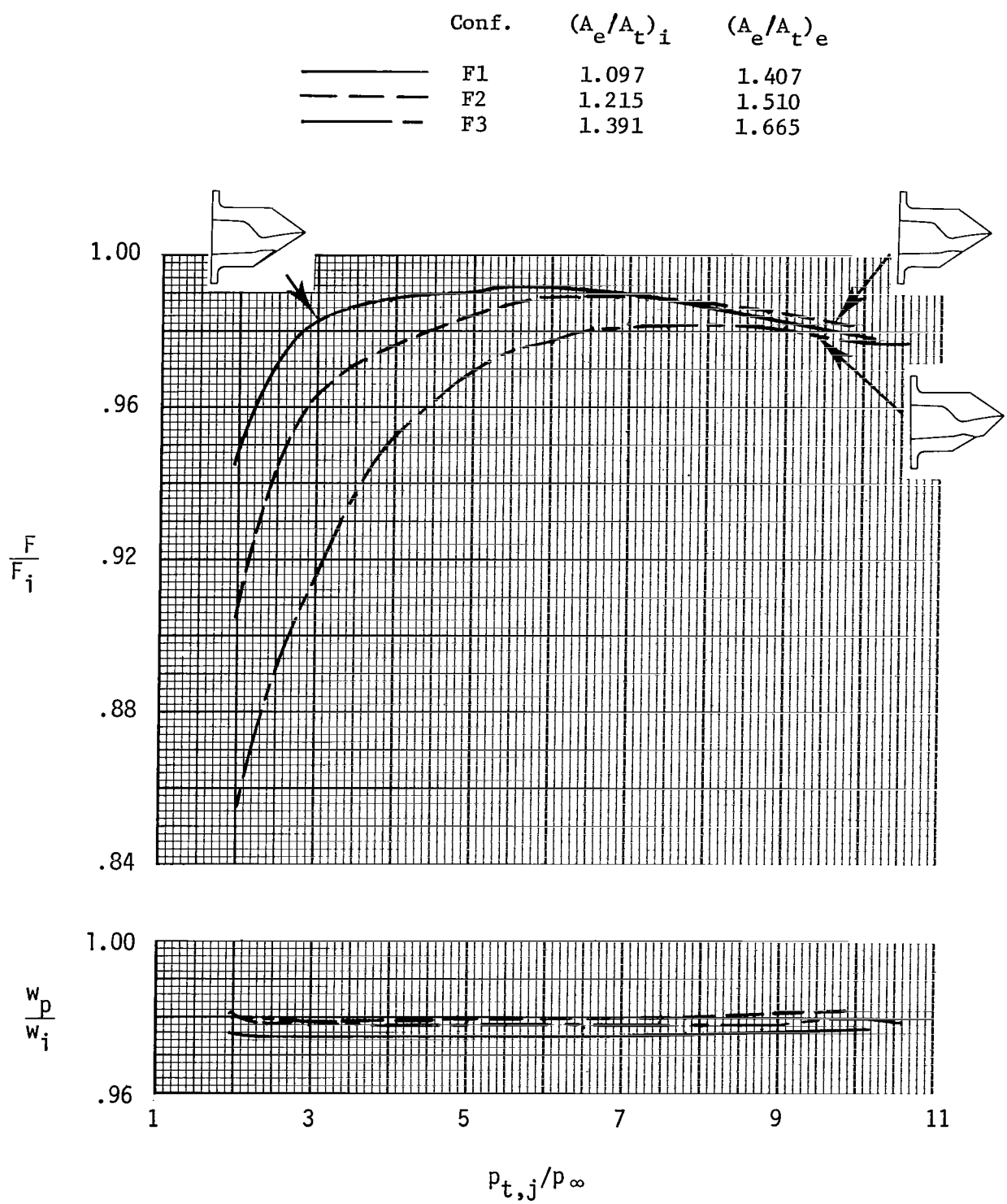

Figure 17.- Effect of expansion ratio (lower-flap position) on cruise-nozzle internal performance.

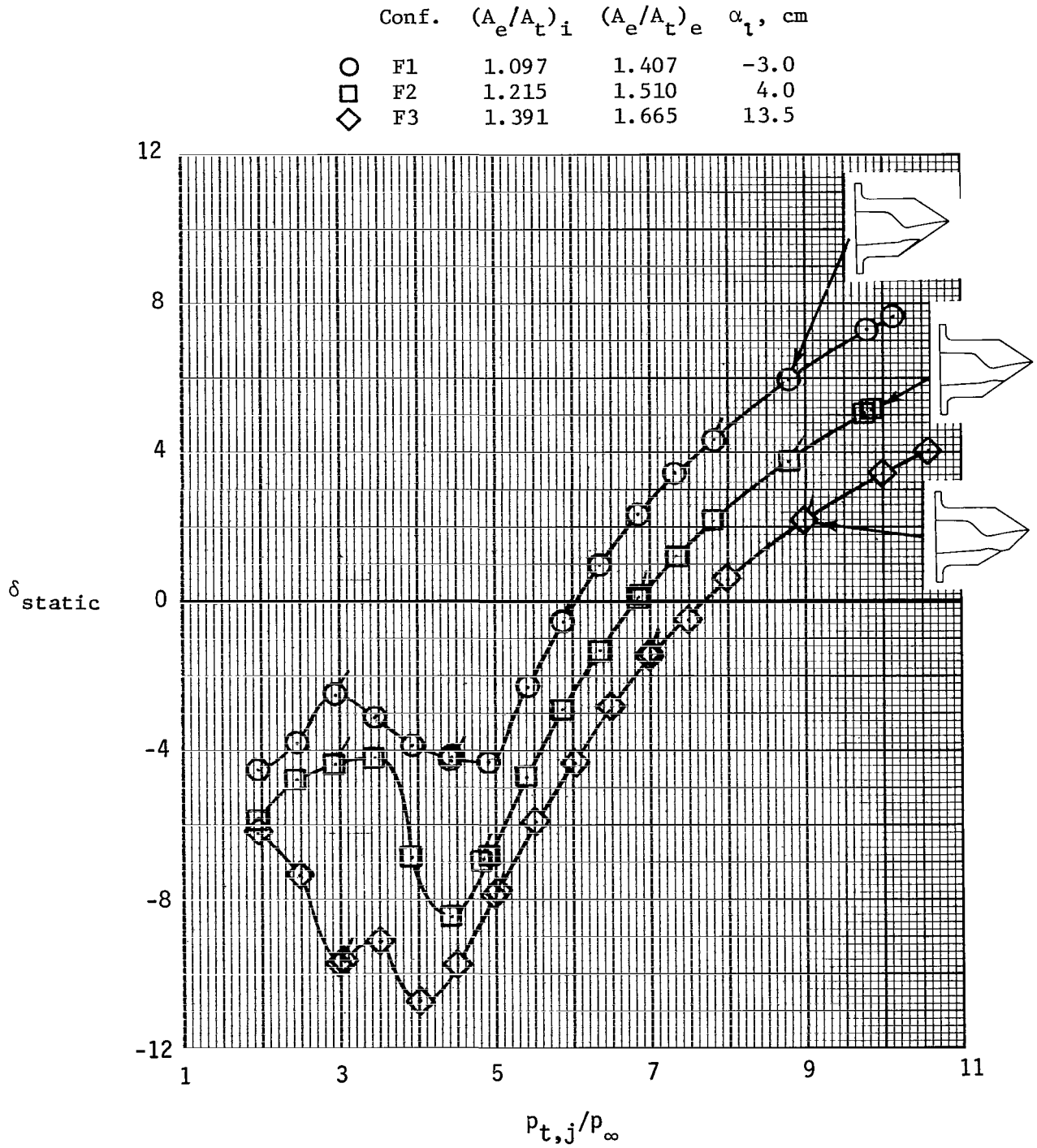

Figure 18.- Effect of expansion ratio (lower-flap position) on resultant thrust-vector angle. Flagged symbols indicate data taken as nozzle pressure ratio was decreasing. $l_{f,l}$ = 2.36 cm.

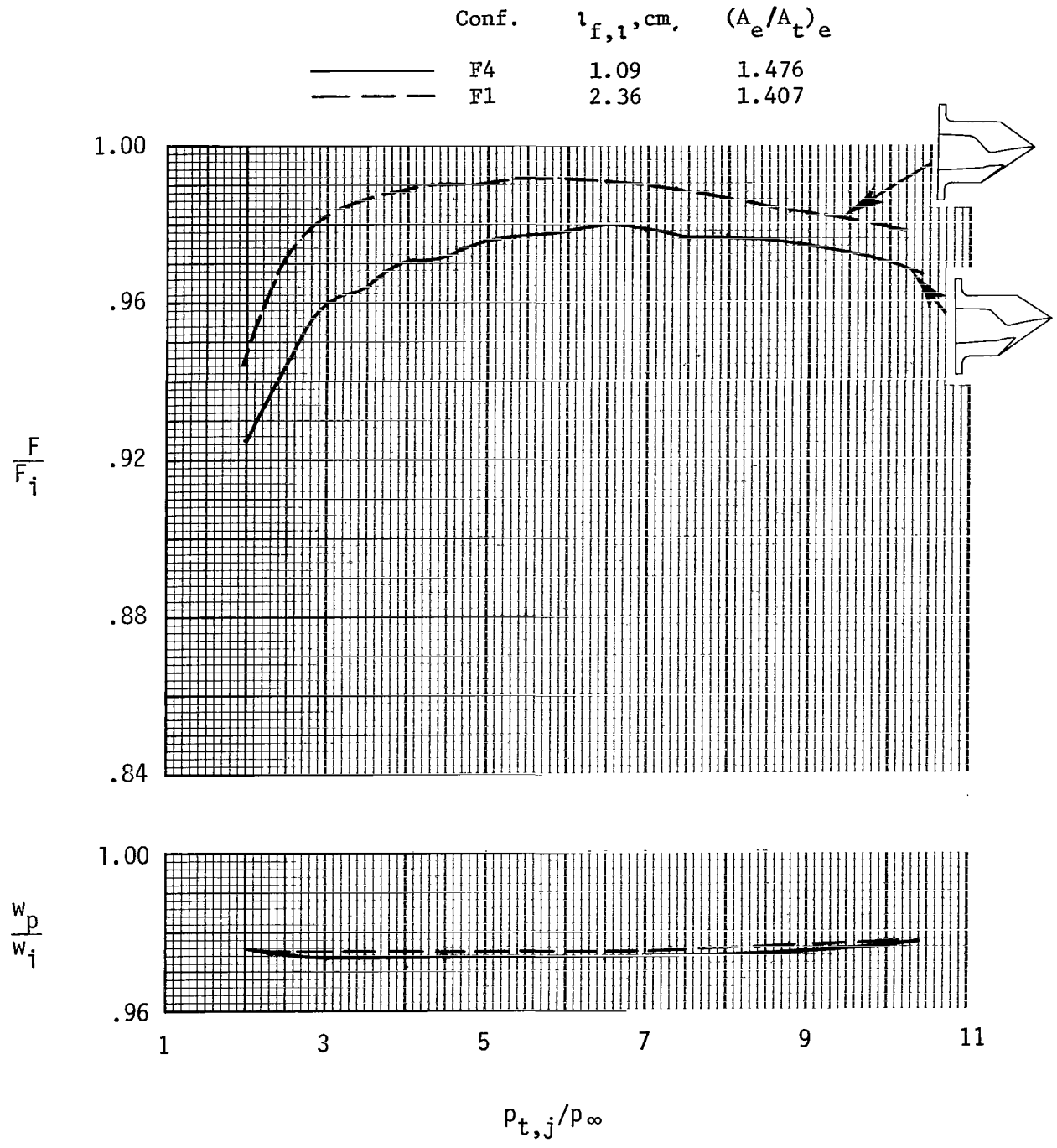

(a) $(A_e/A_t)_i = 1.1$.

Figure 19.- Effect of lower-flap length on cruise-nozzle internal performance.

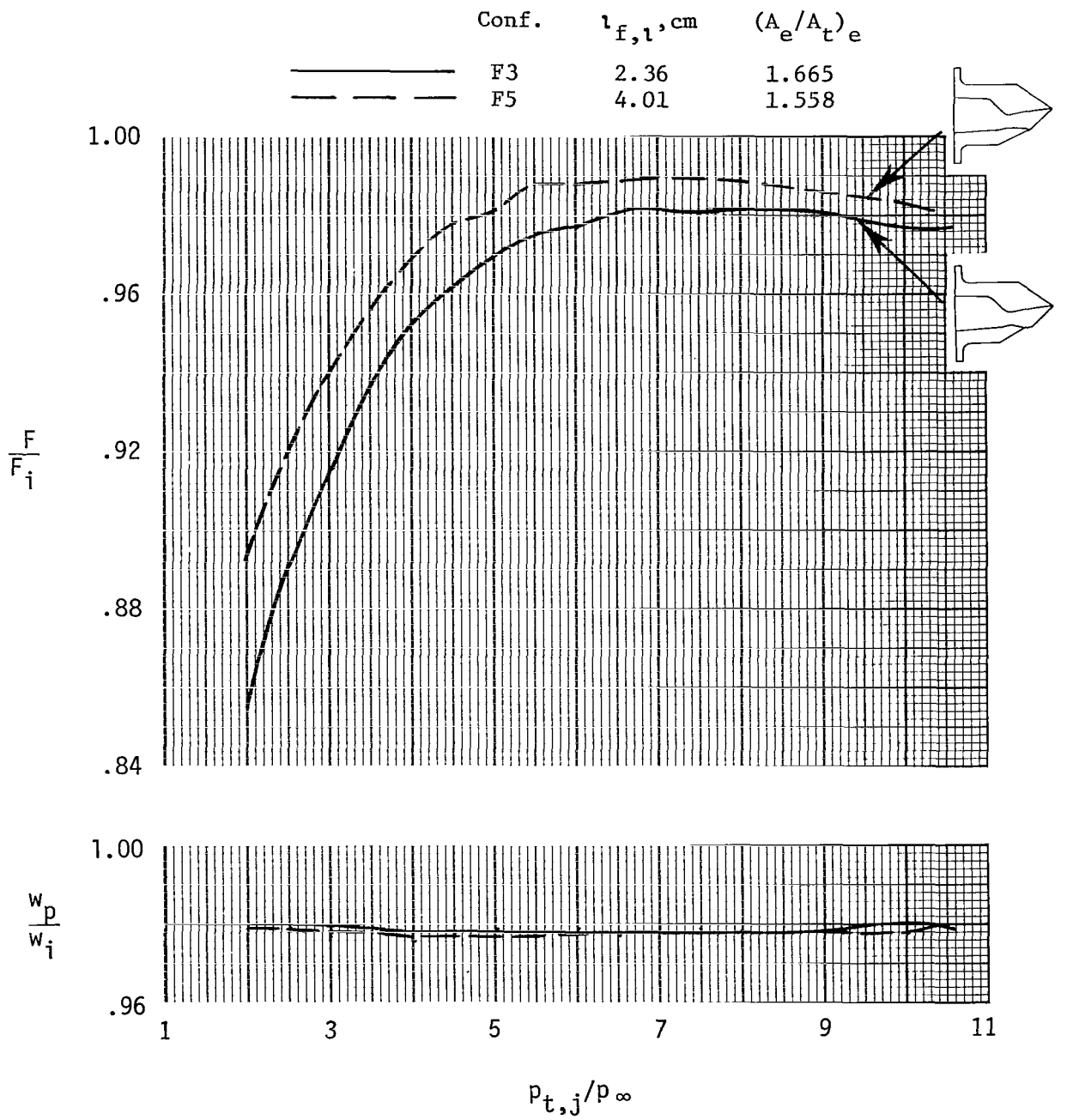

(b) $(A_e/A_t)_i = 1.39$.

Figure 19.- Concluded.

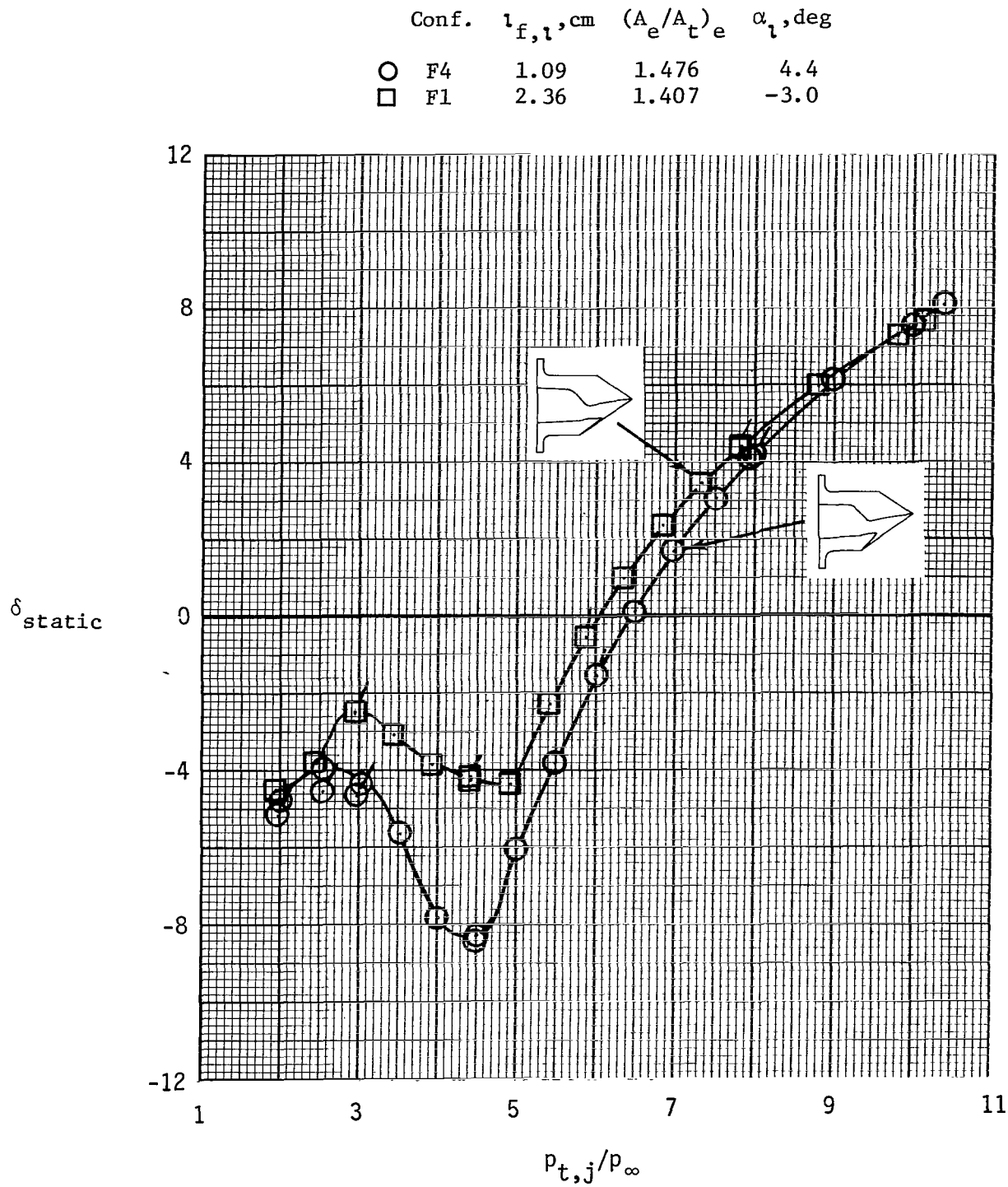

(a) $(A_e/A_t)_i = 1.1$.

Figure 20.- Effect of lower-flap length on resultant thrust-vector angle. Flagged symbols indicate data taken as nozzle pressure ratio was decreasing.

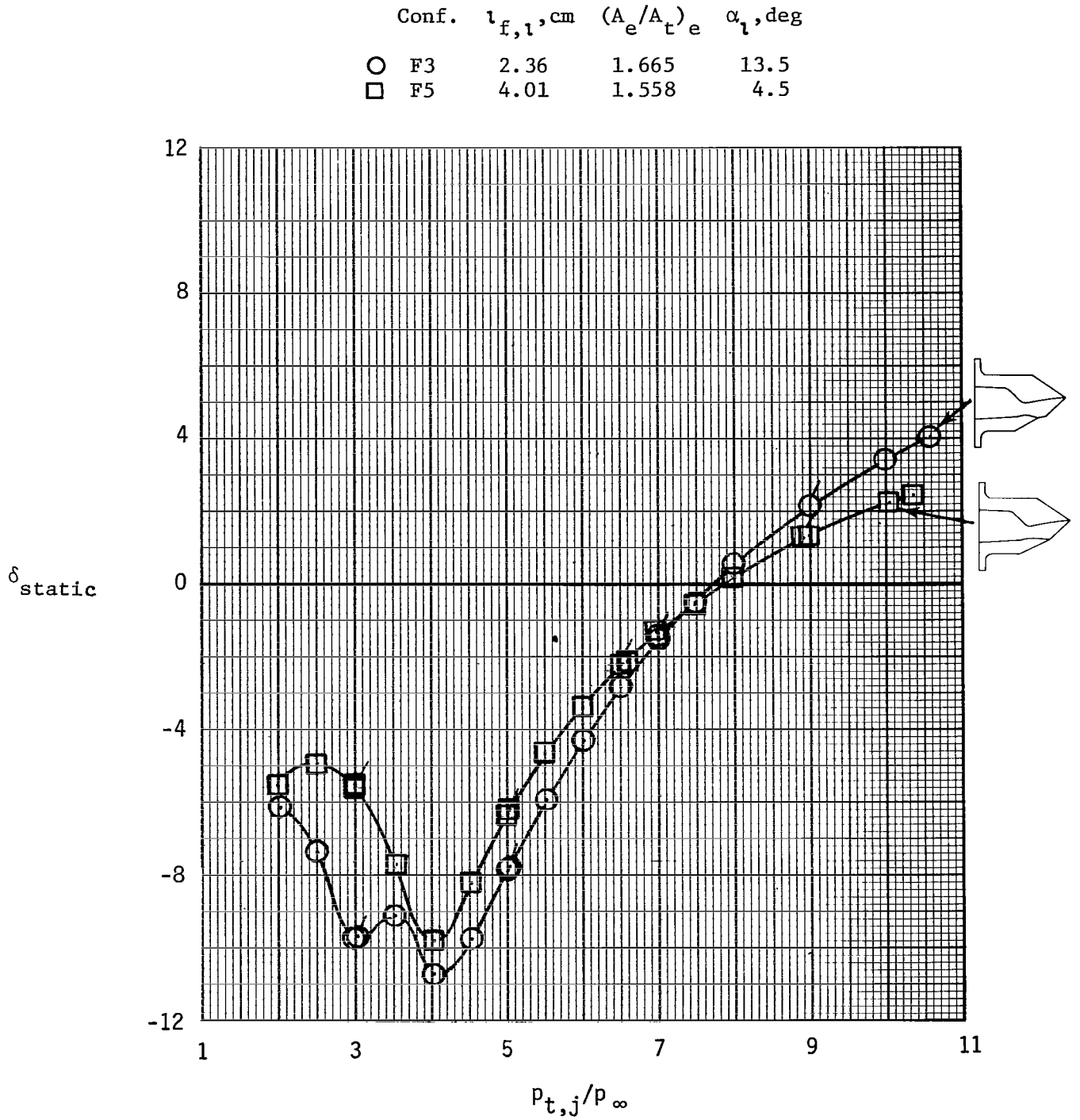

(b) $(A_e/A_t)_i = 1.39$.

Figure 20.- Concluded.

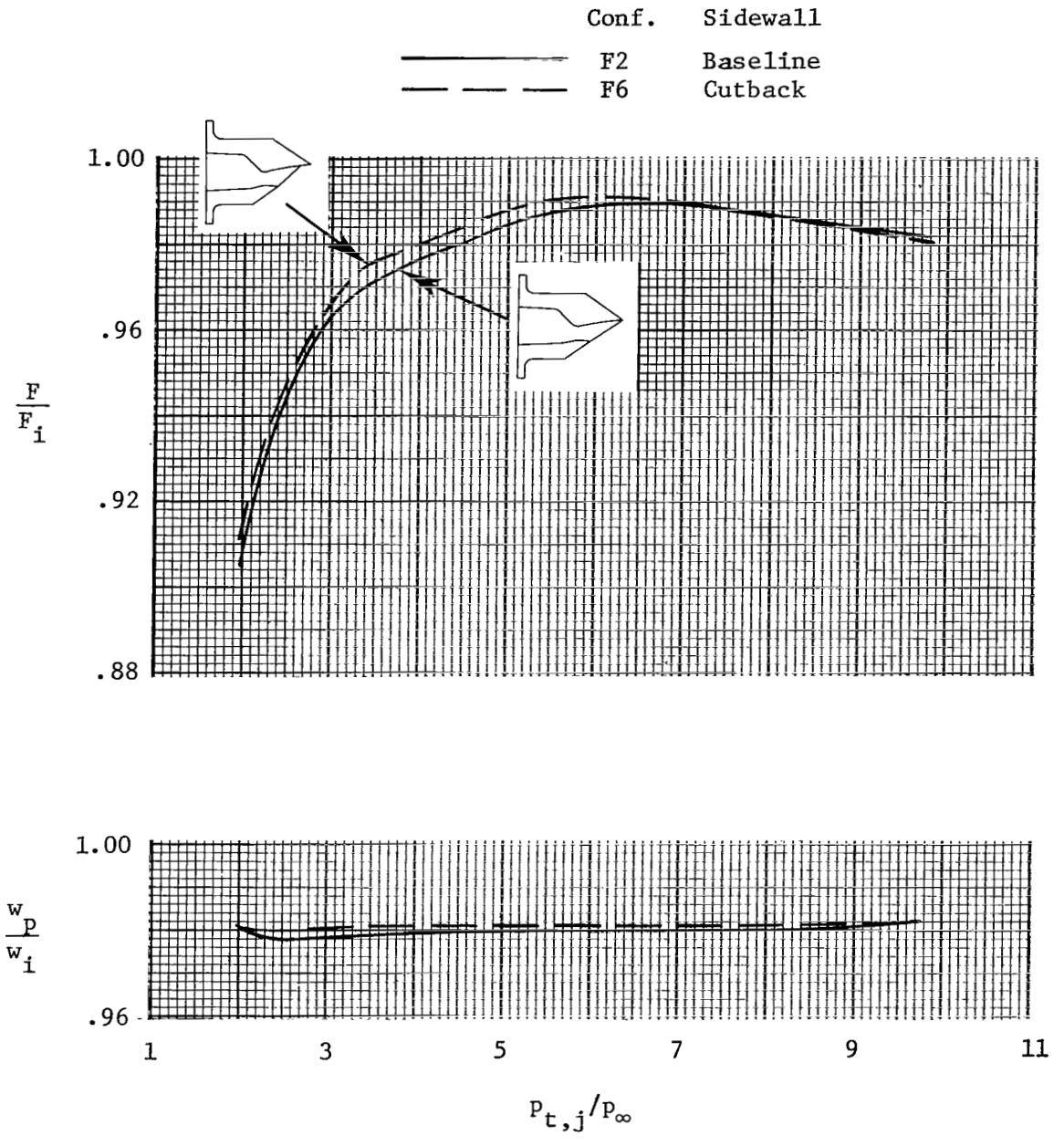

Figure 21.- Effect of sidewall length on cruise-nozzle internal performance. $(A_e/A_t)_i = 1.215$; $(A_e/A_t)_e = 1.510$.

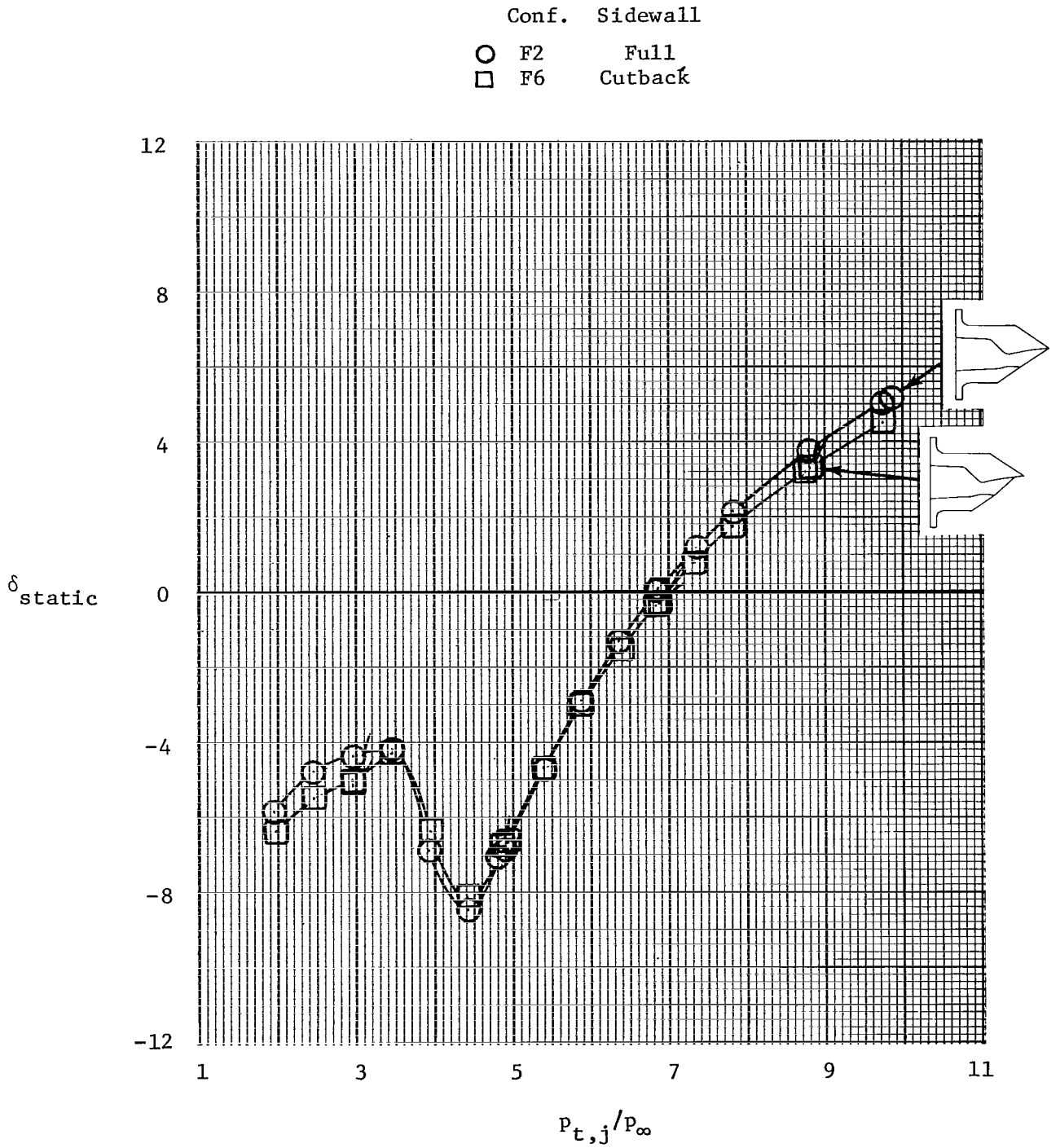

Figure 22.- Effect of sidewall length on resultant thrust-vector angle. Flagged symbols indicate data taken as nozzle pressure ratio was decreasing. $(A_e/A_t)_i = 1.215$; $(A_e/A_t)_e = 1.510$; $l_{f,l} = 2.36$ cm.

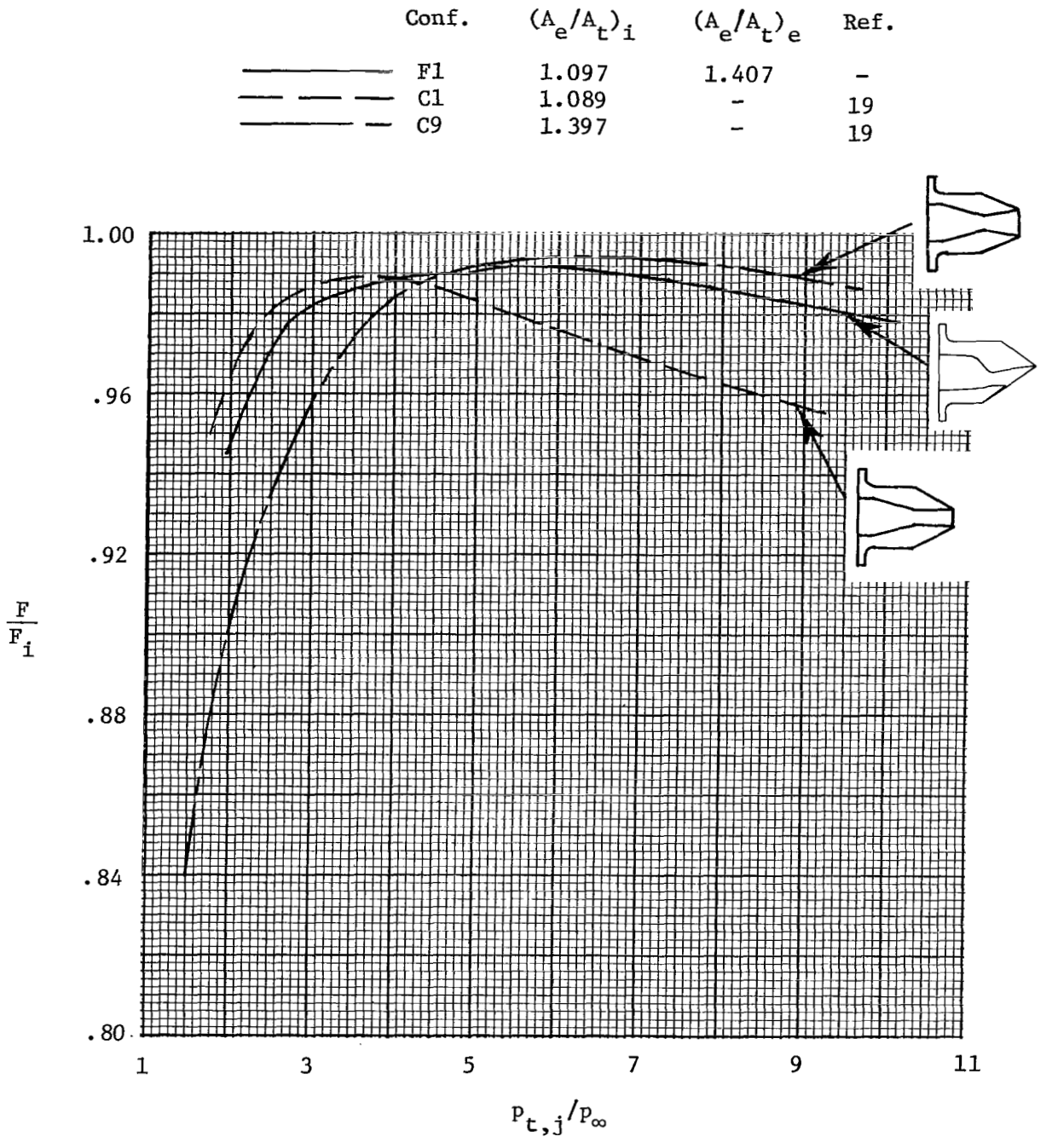

Figure 23.- Comparison of single expansion-ramp nozzle internal performance with nonaxisymmetric convergent-divergent nozzle internal performance.

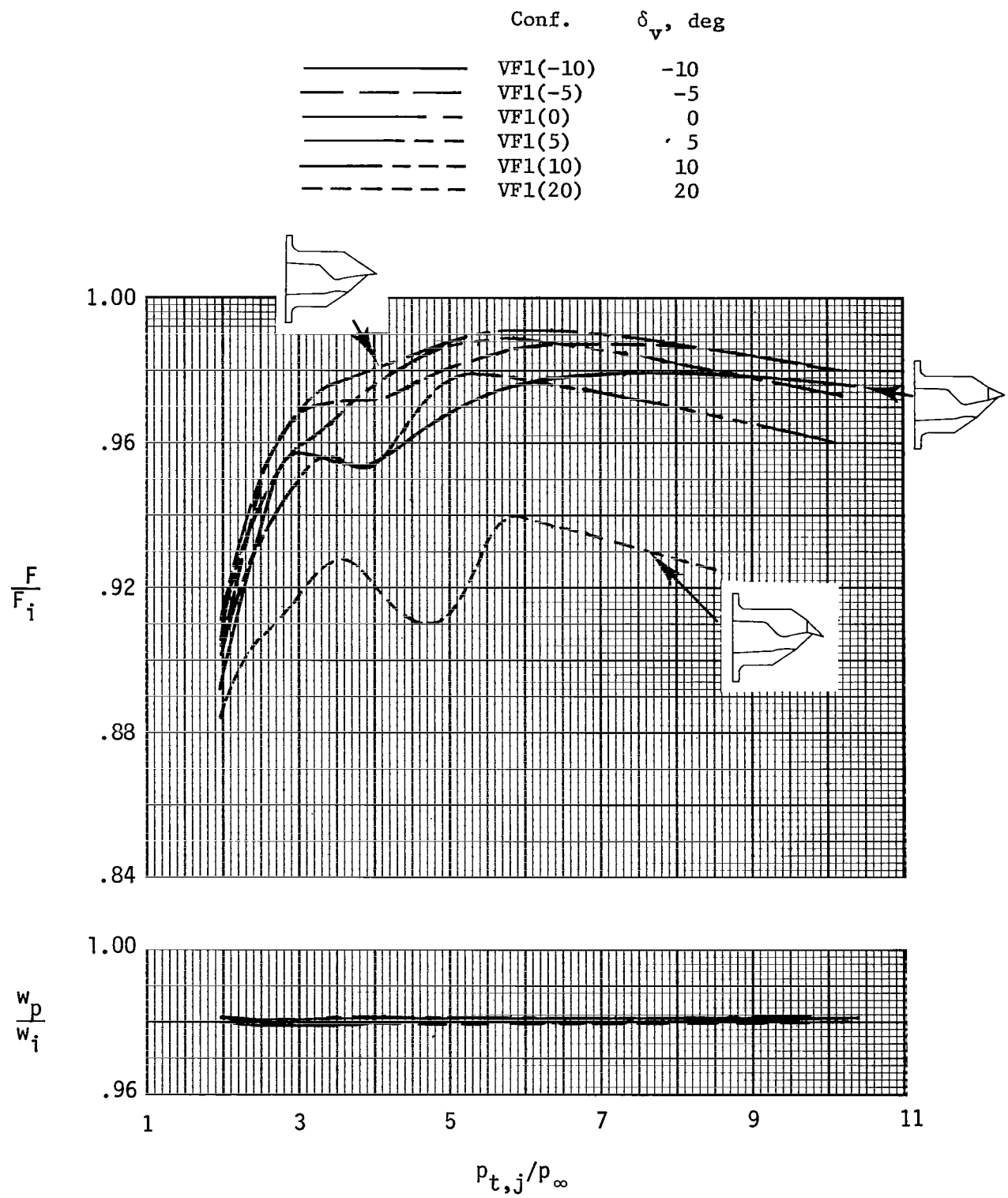

Figure 24.- Effect of upper, aft-flap vectoring on nozzle internal performance.

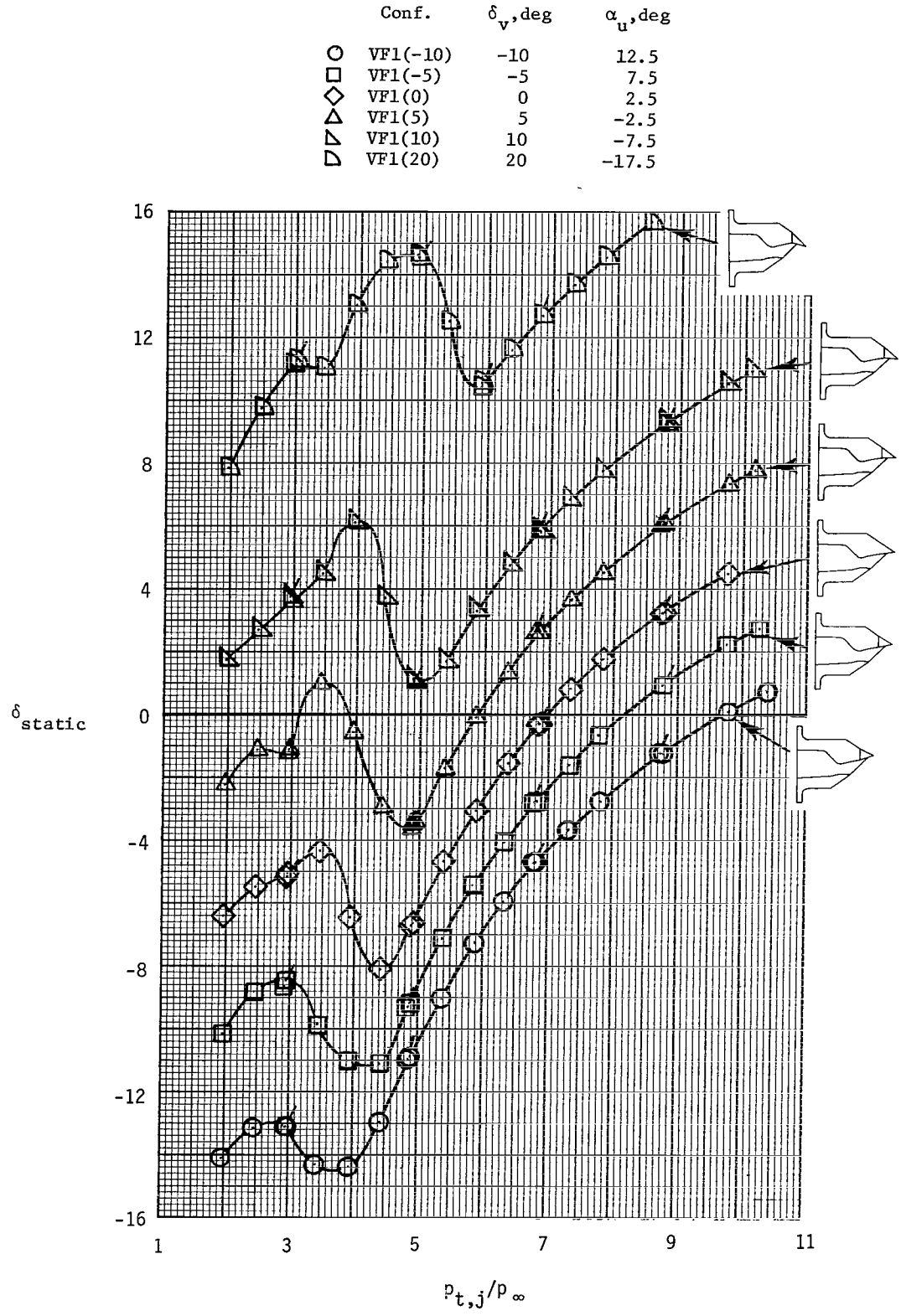

Figure 25.- Effect of upper, aft-flap vector angle on resultant thrust-vector angle. Flagged symbols indicate data taken as nozzle pressure ratio was decreasing.

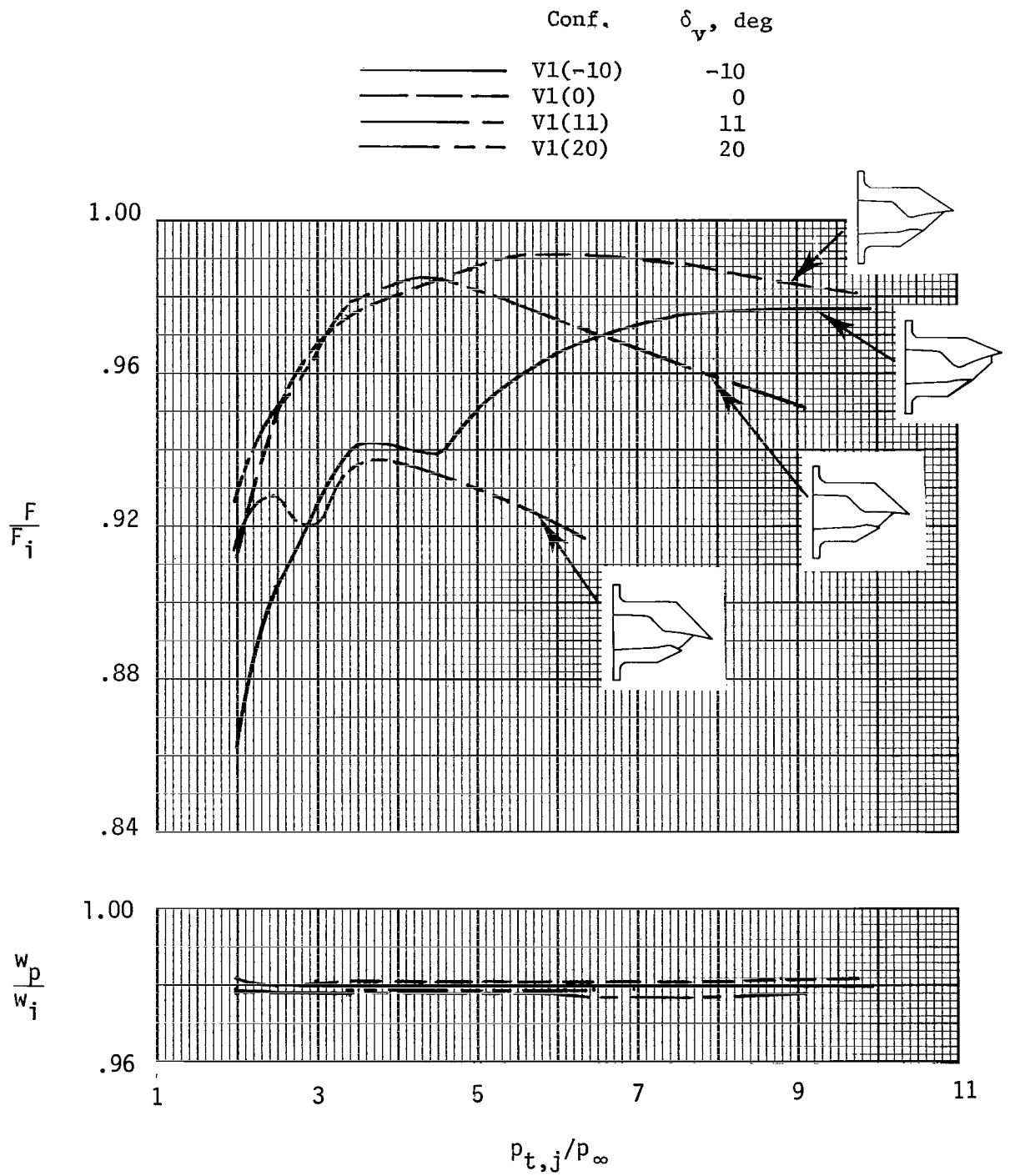

Figure 26.- Effect of upper- and lower-flap vectoring on nozzle internal performance.

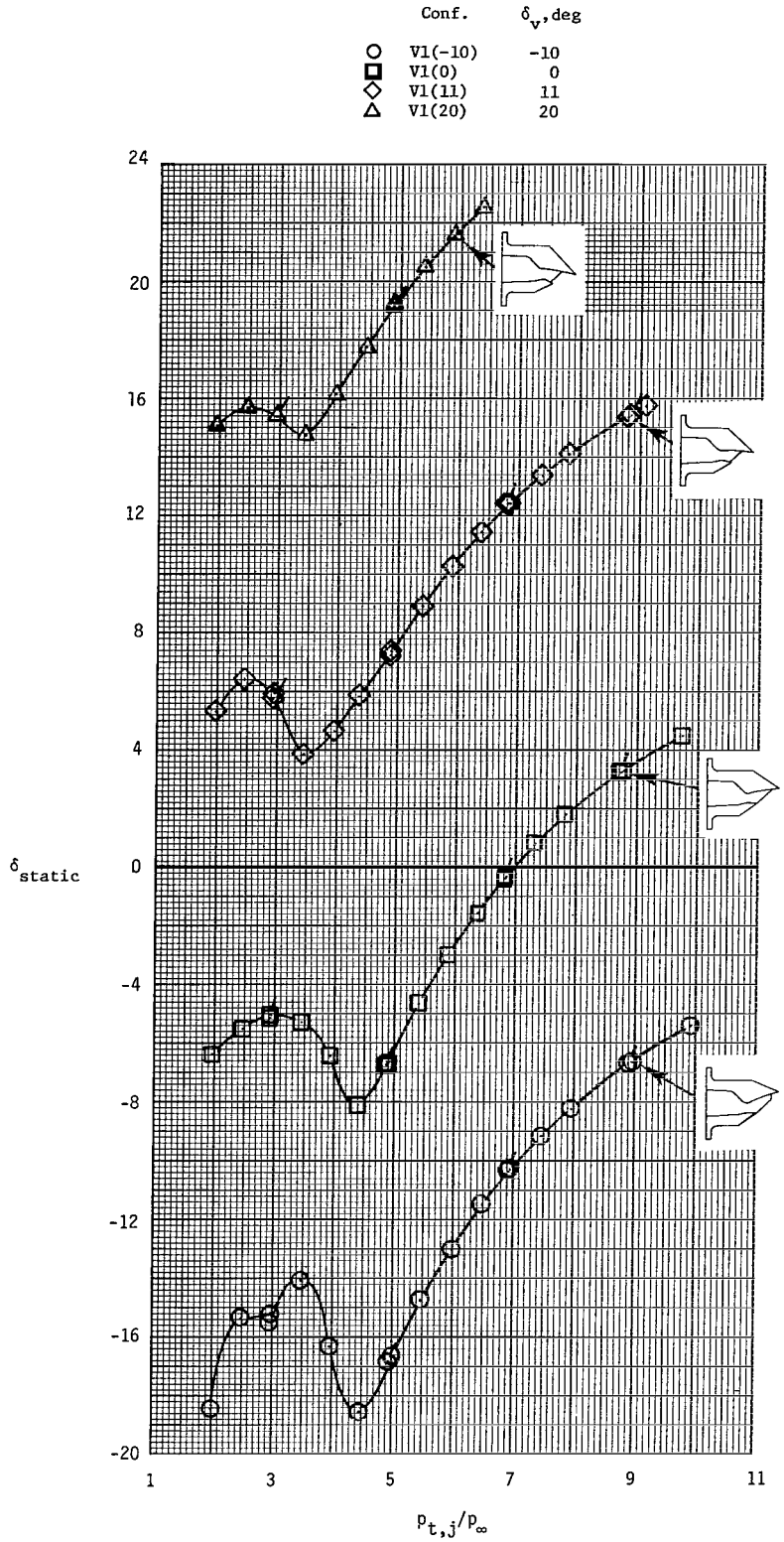

Figure 27.- Effect of vectored upper and lower flaps on resultant thrust-vector angle. Flagged symbols indicate data taken as nozzle pressure ratio was decreasing.

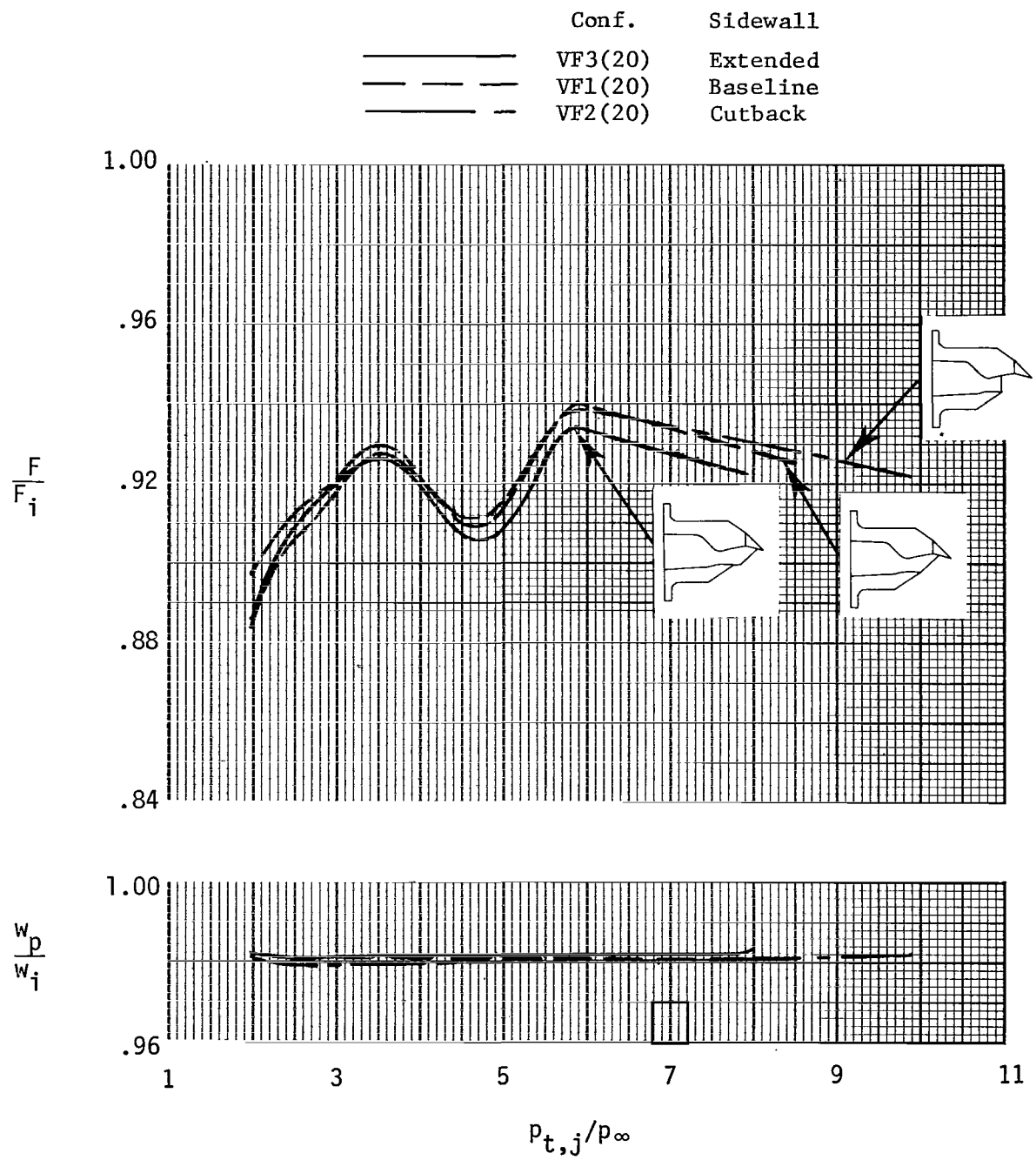

(a) Upper, aft-flap thrust vectoring.

Figure 28.- Effect of sidewall geometry on vectored-nozzle internal performance.

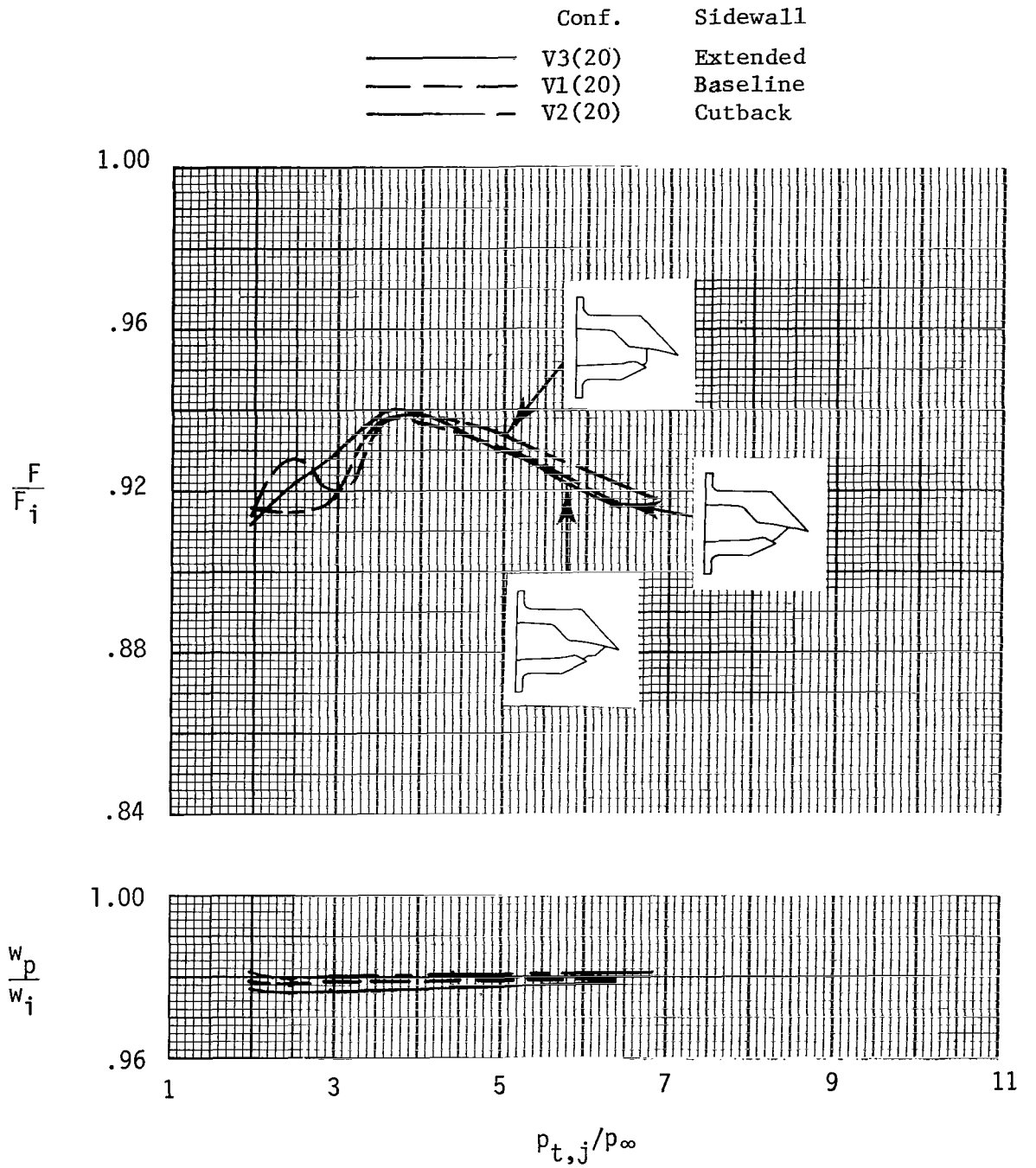

(b) Upper- and lower-flap thrust vectoring.

Figure 28.- Concluded.

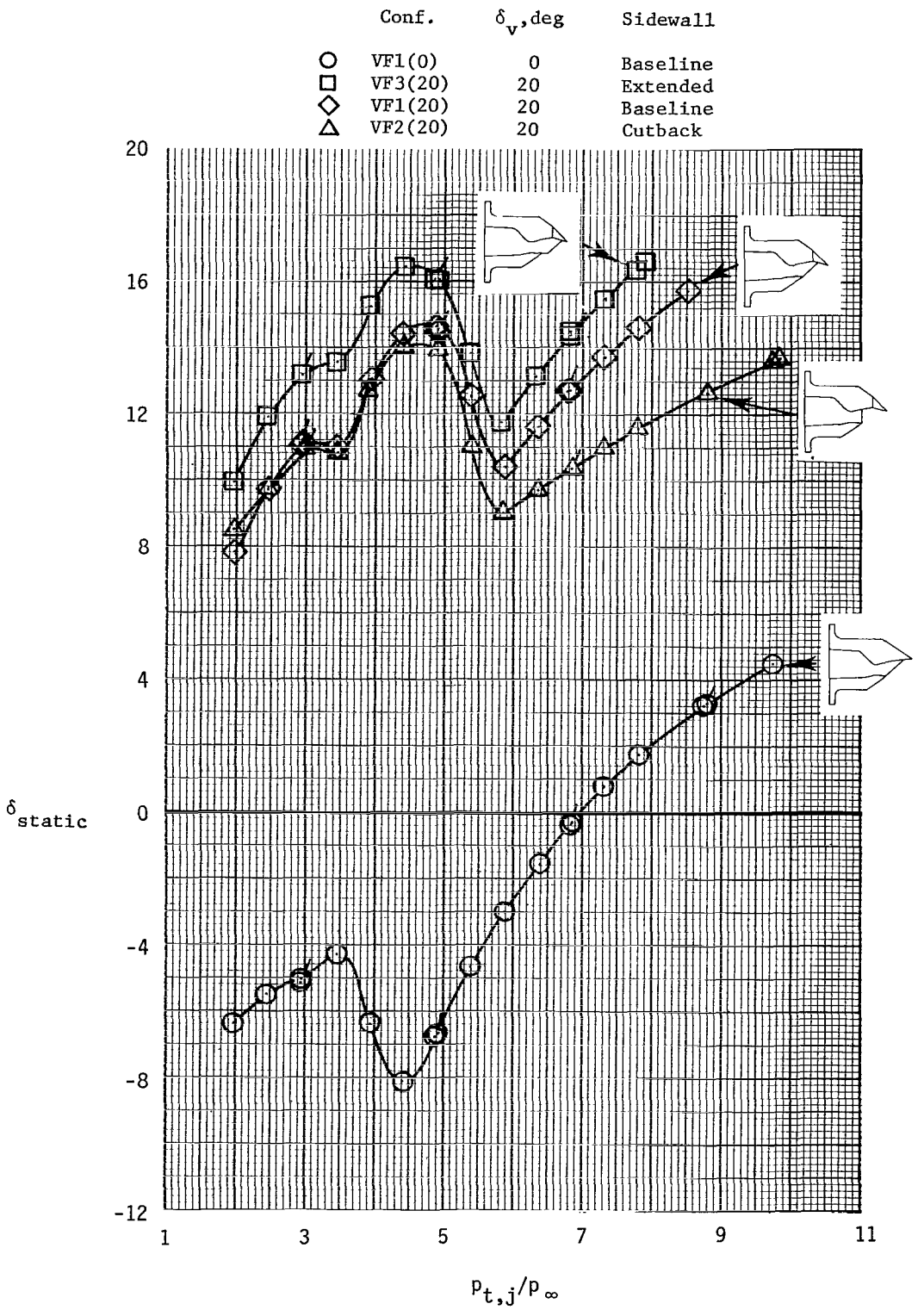

(a) Vectored upper-flap configurations.

Figure 29.- Effect of sidewall geometry on resultant thrust-vector angle. Flagged symbols indicate data taken as nozzle pressure ratio was decreasing.

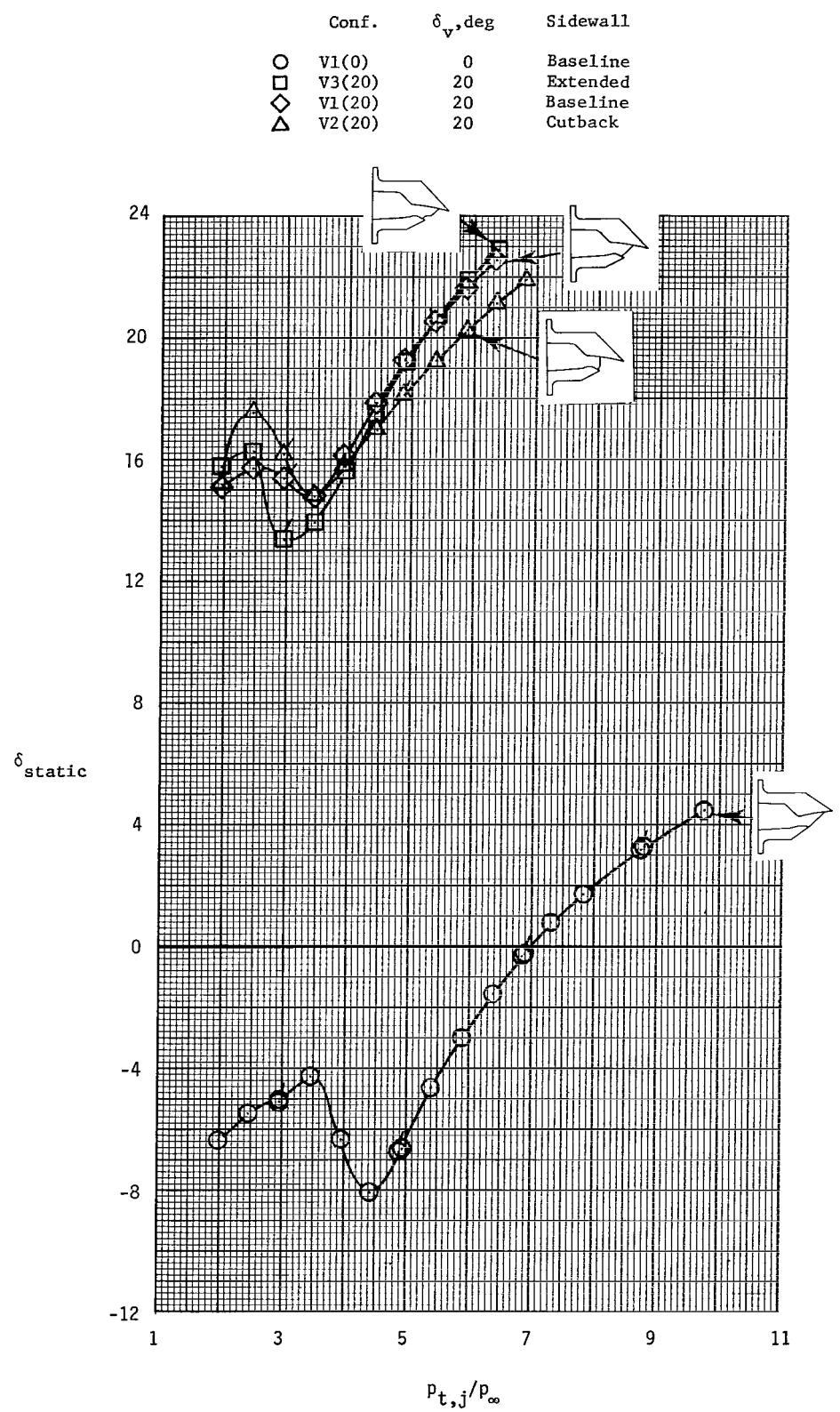

(b) Vectored upper- and lower-flap configurations.

Figure 29.- Concluded.

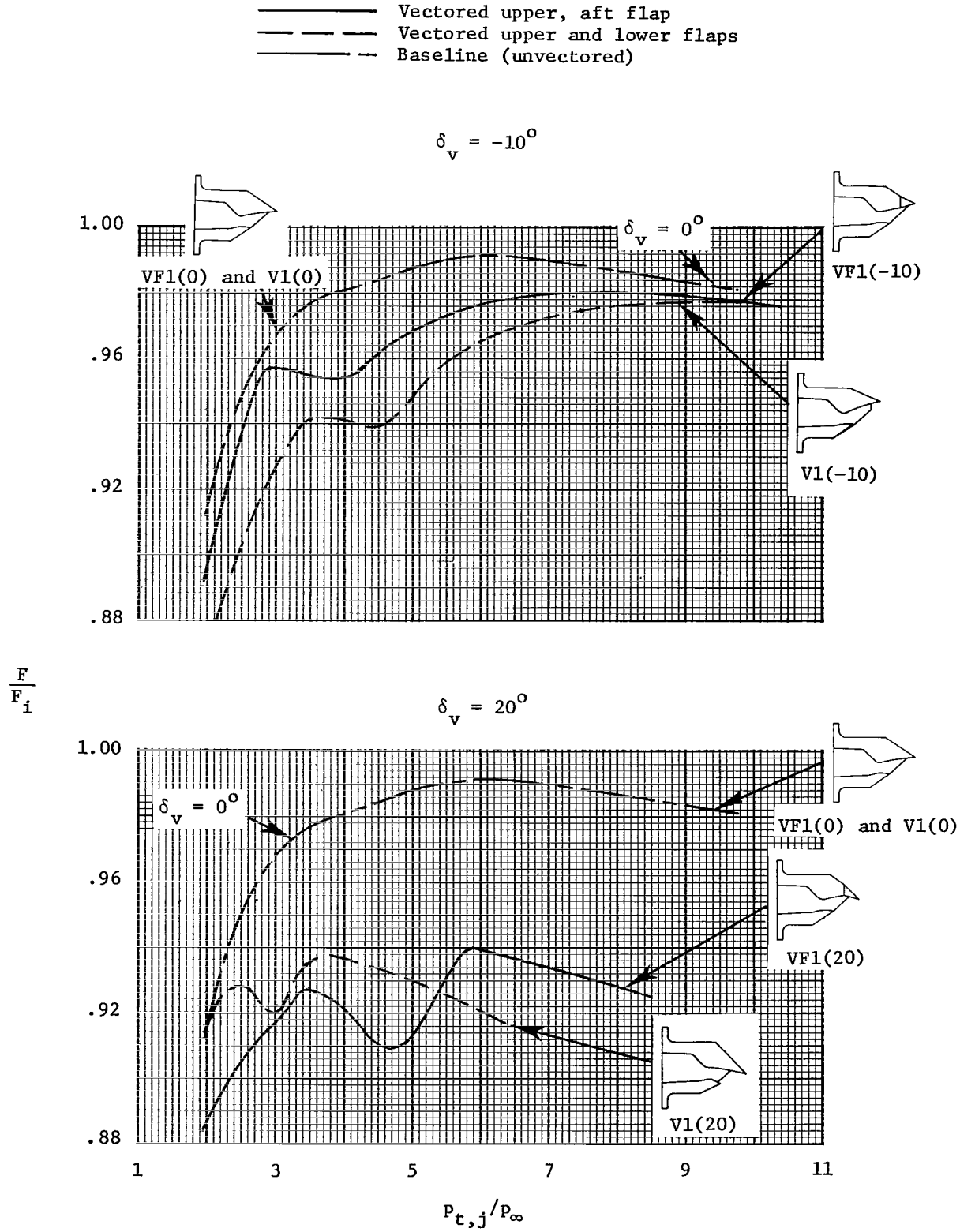

(a) Thrust ratio.

Figure 30.- Effect of vectored-thrust concept on nozzle thrust ratio.

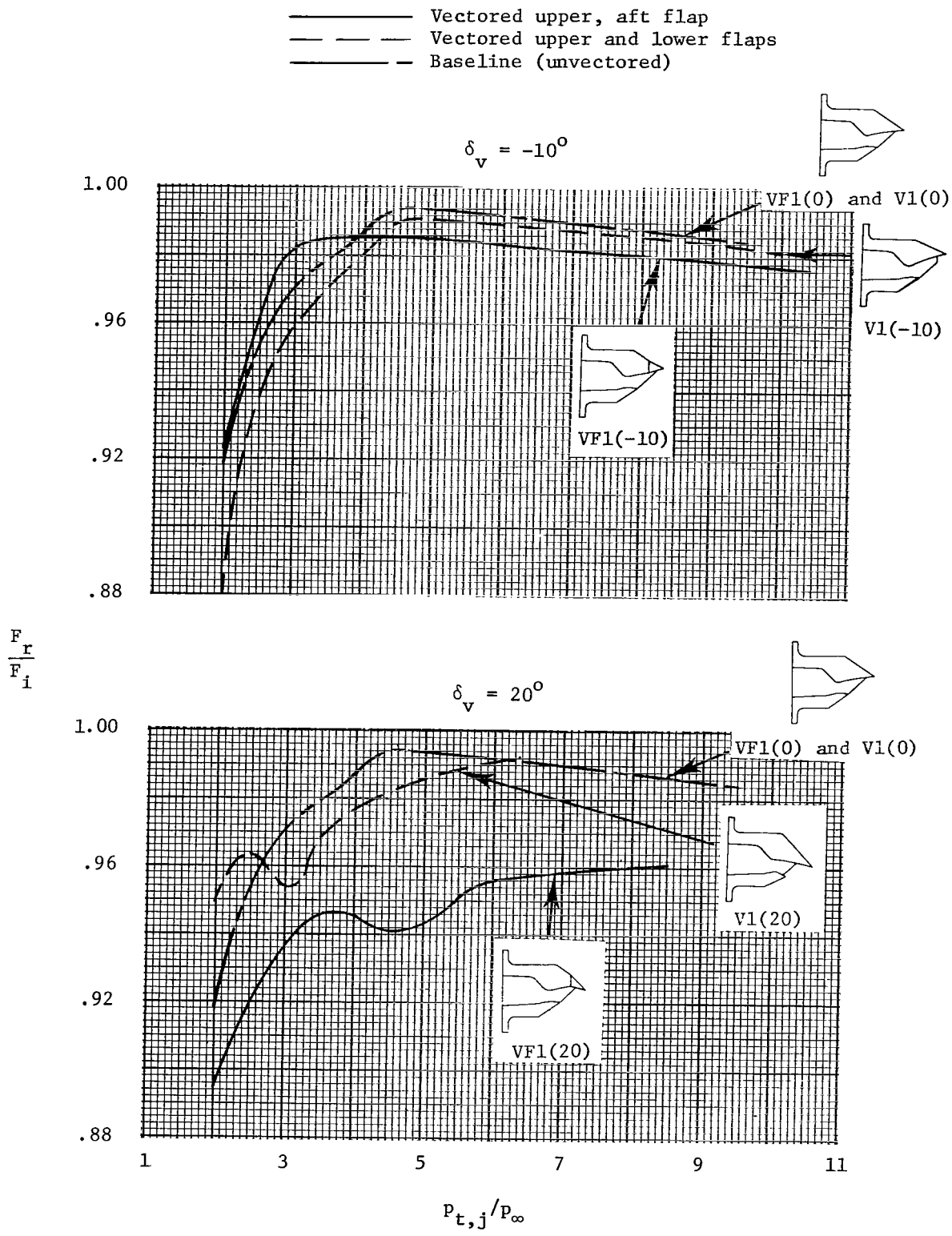

(b) Resultant thrust ratio.

Figure 30.- Concluded.

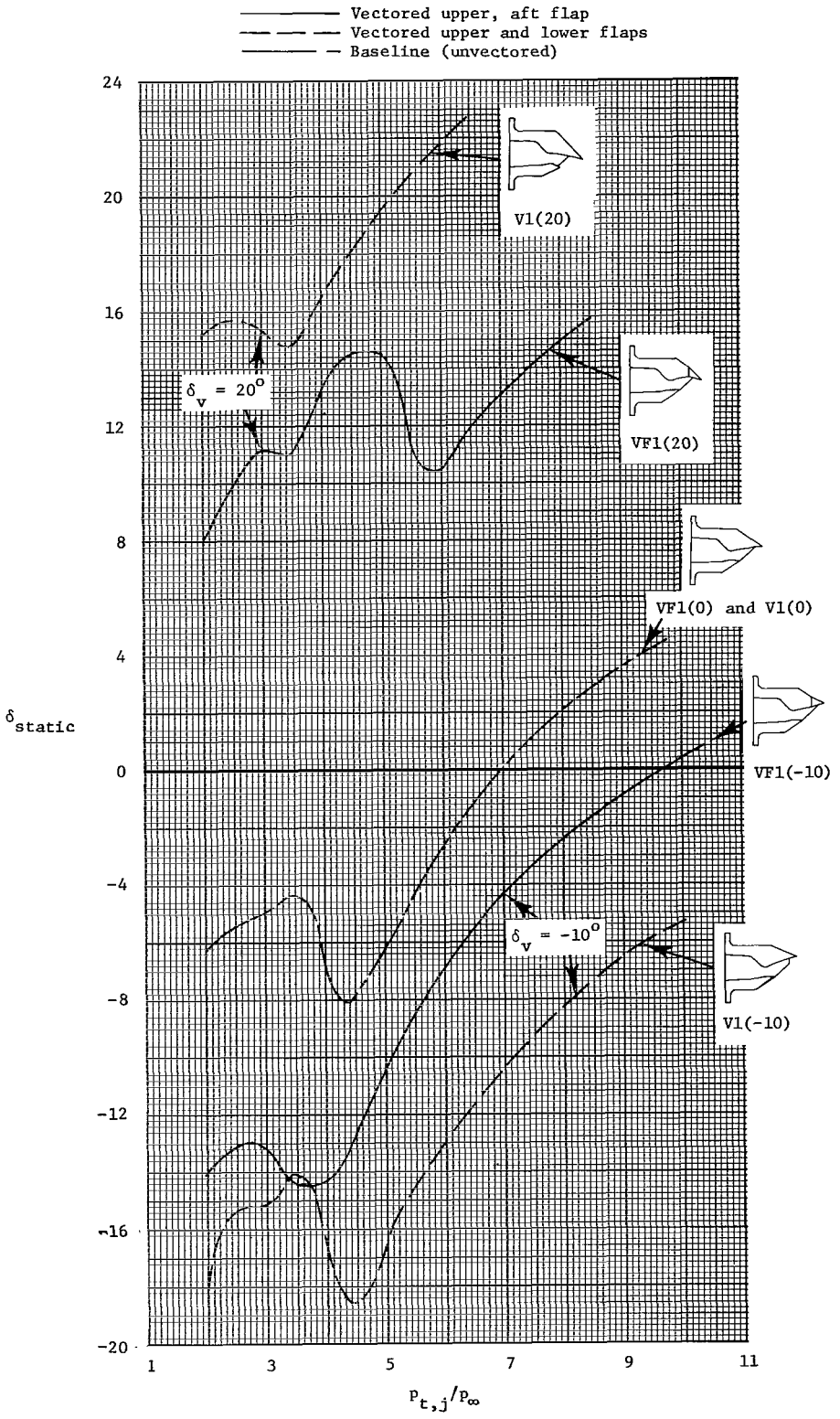

Figure 31.- Effect of vectored-thrust concept on resultant thrust-vector angle.

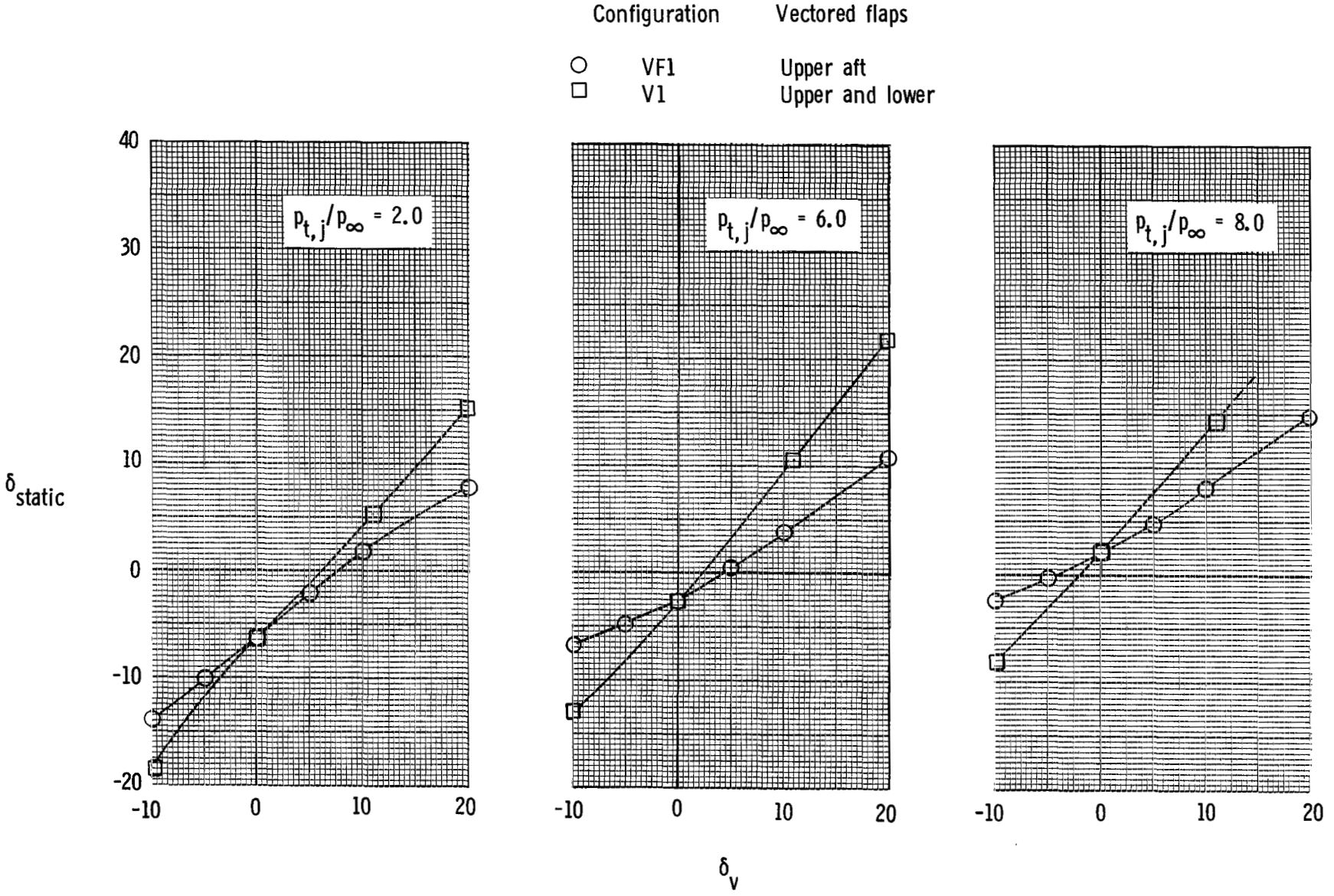

Figure 32.- Effect of thrust-vectoring concept on resultant thrust-vector angle.

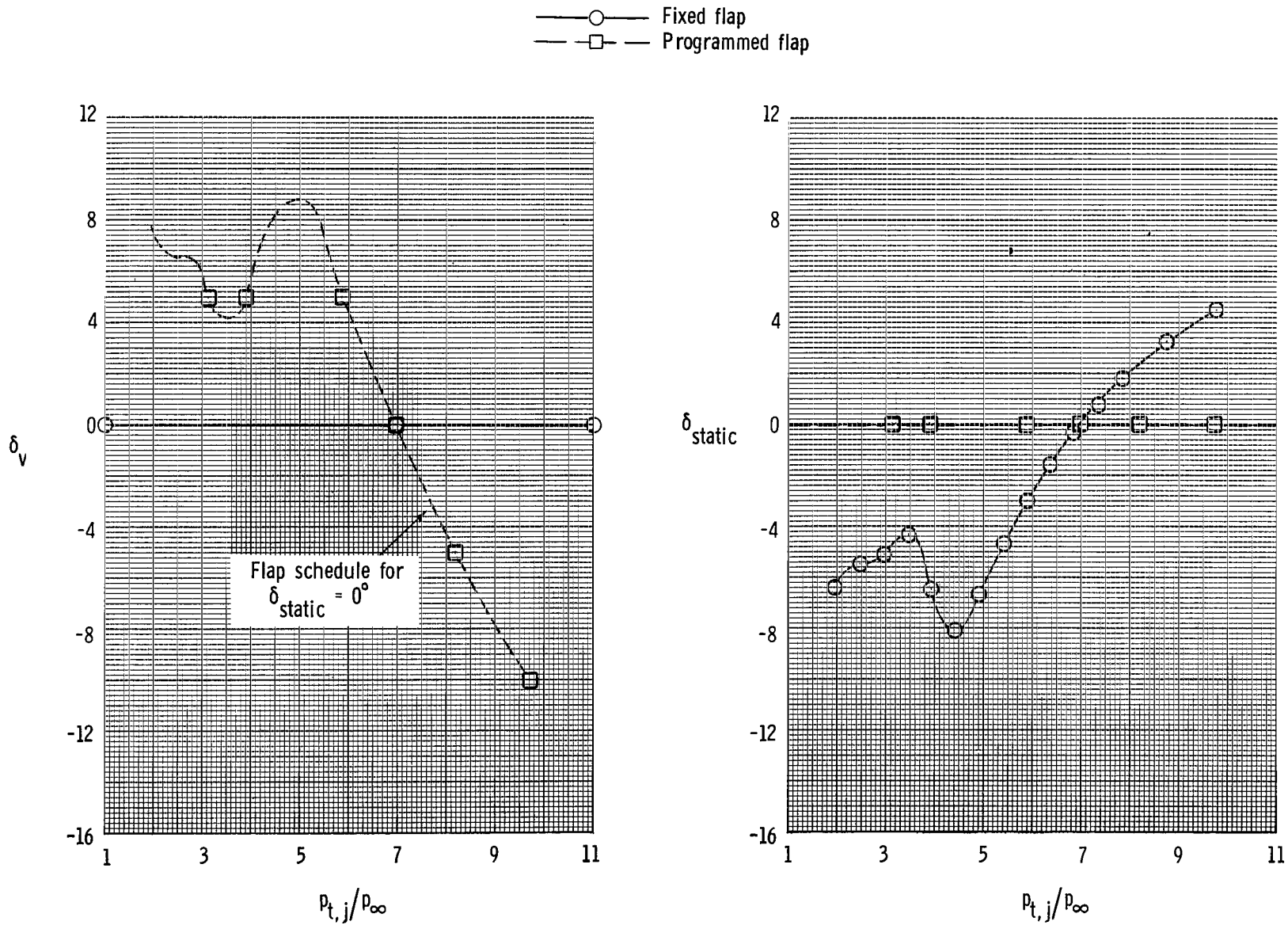

(a) δ_v and δ_{static}.

Figure 33.- Effect of programmed vector flap on vector angles and internal performance. Configuration VF1 - (upper aft-flap vectoring).

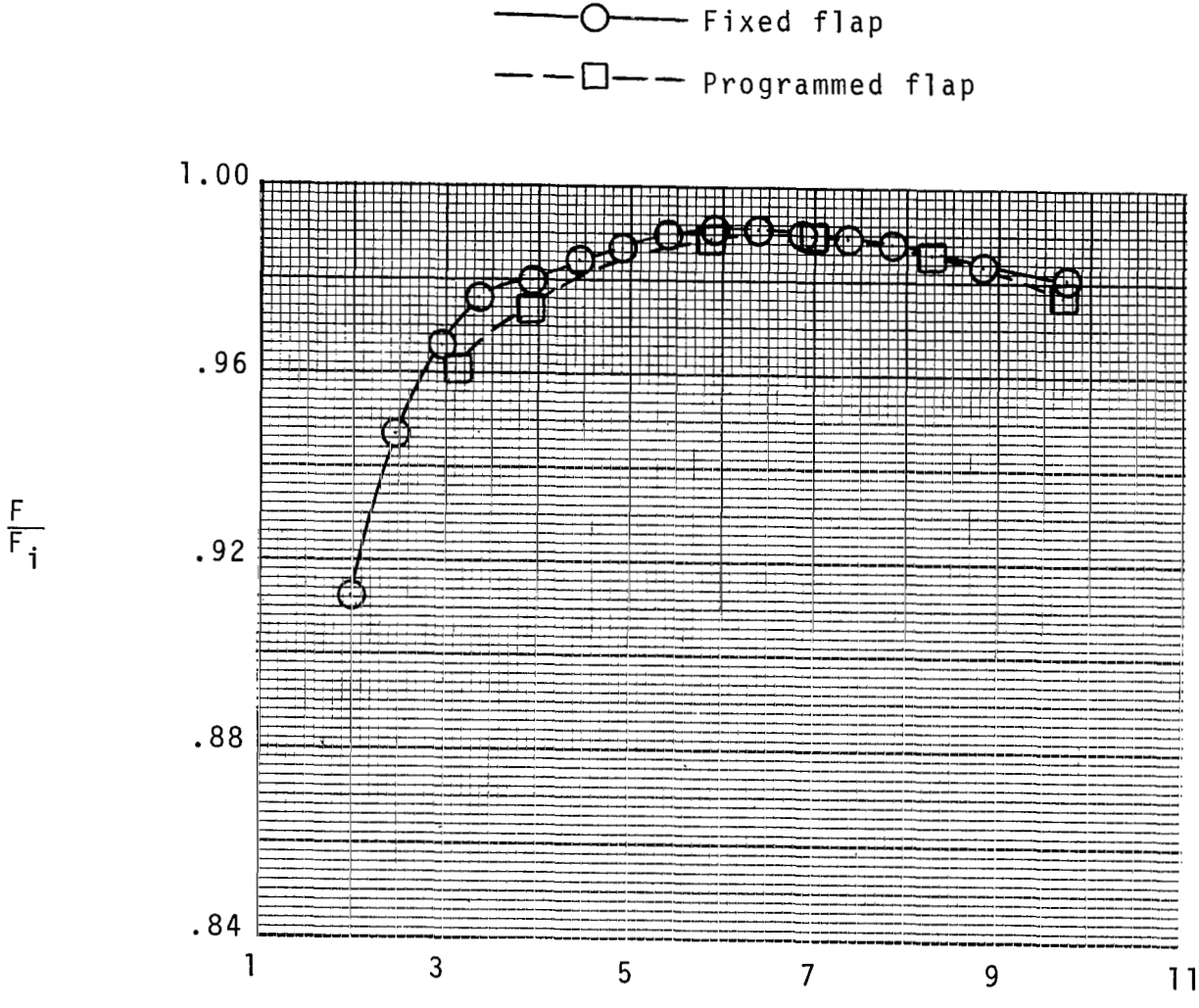

(b) F/F_i.

Figure 33.- Concluded.

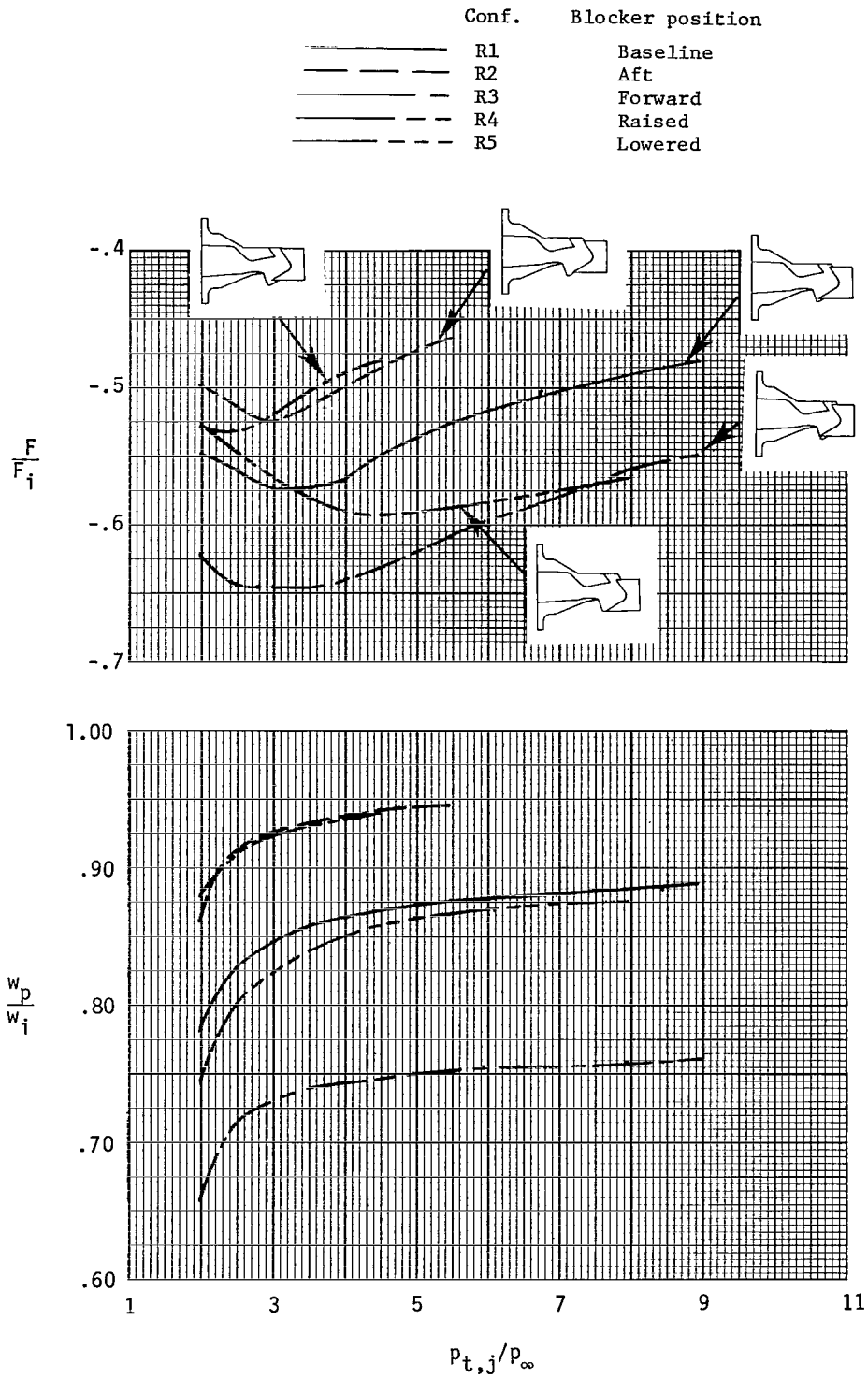

Figure 34.- Effect of exhaust-flow blocker position on reversed-thrust nozzle internal performance.

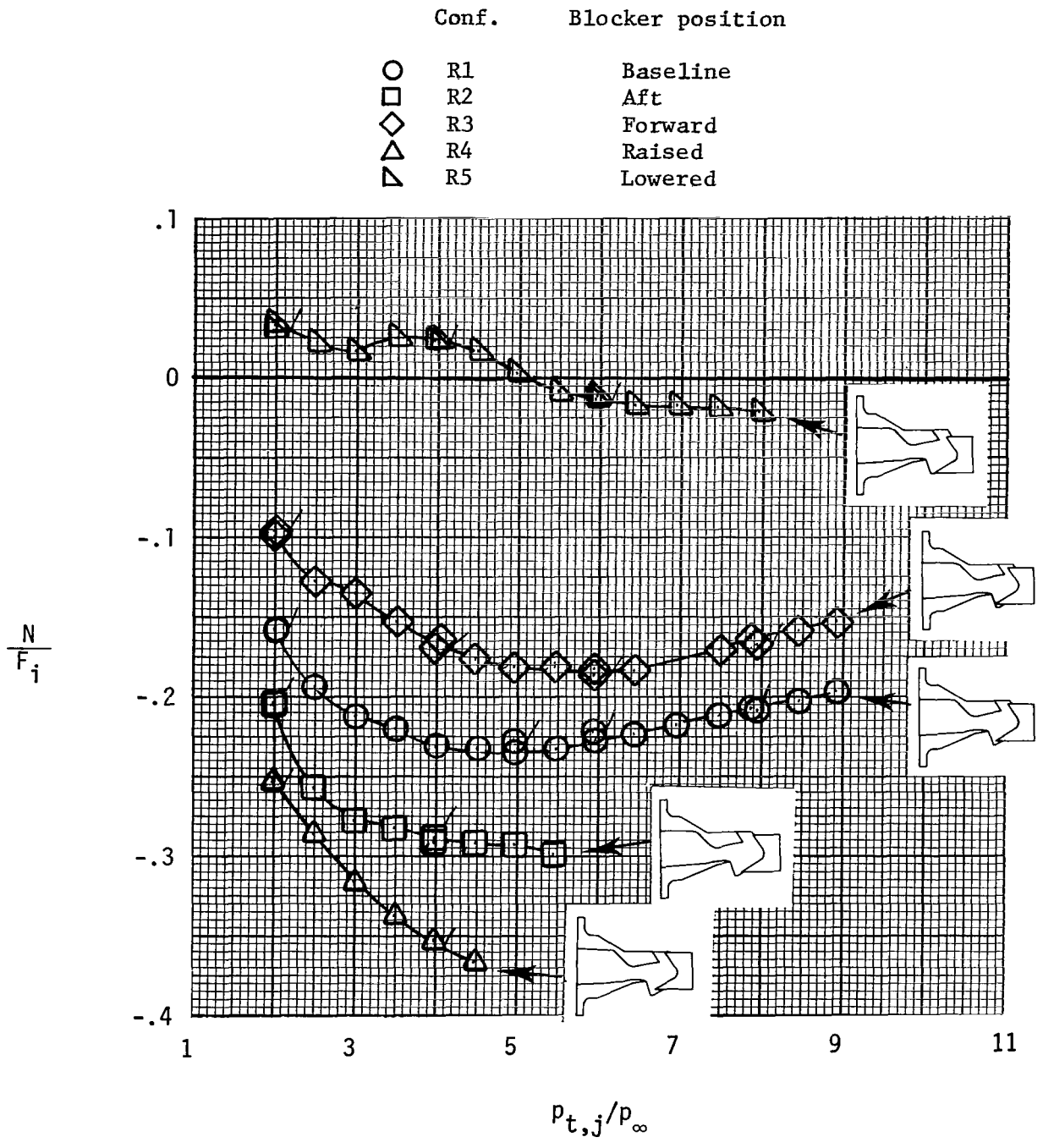

Figure 35.- Effect of exhaust-flow blocker position on measured normal force. Flagged symbols indicate data taken as nozzle pressure ratio was decreasing.

1. Report No.	2. Government Accession No.	3. Recipient's Catalog No.
NASA TP-1962		

4. Title and Subtitle

STATIC INTERNAL PERFORMANCE OF SINGLE EXPANSION-RAMP NOZZLES WITH THRUST VECTORING AND REVERSING

5. Report Date: March 1982

6. Performing Organization Code: 505-32-13-01

7. Author(s)

Richard J. Re and Bobby L. Berrier

8. Performing Organization Report No.: L-14902

9. Performing Organization Name and Address

NASA Langley Research Center
Hampton, VA 23665

10. Work Unit No.

11. Contract or Grant No.

12. Sponsoring Agency Name and Address

National Aeronautics and Space Administration
Washington, DC 20546

13. Type of Report and Period Covered: Technical Paper

14. Sponsoring Agency Code

15. Supplementary Notes

16. Abstract

An investigation has been conducted at static conditions (wind-off) in the static-test facility of the Langley 16-Foot Transonic Tunnel. The effects of geometric design parameters on the internal performance of nonaxisymmetric single expansion-ramp nozzles were investigated at nozzle pressure ratios up to approximately 10. Forward-flight (cruise), vectored-thrust, and reversed-thrust nozzle operating modes were investigated.

17. Key Words (Suggested by Author(s))	18. Distribution Statement
Nonaxisymmetric nozzles Internal performance Single expansion-ramp nozzles Thrust vectoring Thrust reversing	Unclassified - Unlimited Subject Category 02

19. Security Classif. (of this report)	20. Security Classif. (of this page)	21. No. of Pages	22. Price
Unclassified	Unclassified	141	A07

For sale by the National Technical Information Service, Springfield, Virginia 22161

NASA-Langley, 1982

National Aeronautics and Space Administration

Washington, D.C.
20546

Official Business
Penalty for Private Use, $300

THIRD-CLASS BULK RATE

Postage and Fees Paid
National Aeronautics and
Space Administration
NASA-451

1 1 1U,A, 081262 S00903S
DEPT OF THE AIR FORCE
AF WEAPONS LABORATORY
ATTN: TECHNICAL LIBRARY (SUL)
KIRTLAND AFB N. M. 87117

NASA

POSTMASTER: If Undeliverable (Section 158 Postal Manual) Do Not Return